Swansea University
Prifysgol Abertawe

The Development of High-Performance Packaging Steels

Sean Michael Bennett, MEng materials science and engineering

Submitted to Swansea University in fulfilment of the requirements for the degree of Doctor of Engineering

Swansea University

2024

Summary (abstract)

The aim of this work is to create a new packaging grade of high strength steel for can-end applications. This new grade must have a yield strength of 650-750MPa, with a total elongation value of at-least 5% in all directions after double reduction rolling. The higher yield strength is required for downgauging, as well as being capable of withstanding the pressures in the retort process, while the ductility is required to form the rivet on the end to attach the ring pull to.

The methods used to achieve this involved varying typical packaging alloying elements (such as silicon, phosphorous, and nitrogen), and simulating annealing cycles using a Gleeble 3500 heating simulator where annealing parameters (such as heating rate, soak temperature, and cooling rate), were changed. The purpose of these methods was to promote strengthening via solid solution strengthening, and/or via ferrite grain refinement, and/or secondary phase strengthening.

Mechanical properties were assessed using a tensile tester and hardness tester, and microstructures were analysed using optical microscopy and software to obtain statistical information regarding grain size.

It was found that when subjected to the commercial annealing cycle a high nitrogen containing chemistry achieved the desired mechanical properties outlined in the project aims. This is likely due to the solid solution strengthening effect of the large amounts of solute nitrogen.

Intercritical annealing at 850°C does not lead to generation of secondary phase in the steel chemistries assessed in this body of work, and sometimes decreased the strength in some chemistries.

Removal of the slow cool section from simulated intercritical annealing cycles led to negligible changes in Vickers hardness value as well as no microstructural changes either.

It was found that packaging steels do not undergo significant amounts of grain refinement when an ultra-rapid heating rate of 200°C/s was used, nor when a 1,000°C/s heating rate was used.

Declarations and statements

This work has not been previously accepted in substance for any degree and is not being concurrently submitted in candidature for any degree.

This thesis is the results of my own investigations, except where otherwise stated and that sources are acknowledges by footnotes giving explicit references and that a bibliography is appended.

I give consent for this thesis to be made available online in the university's Open Access Repository and for inter-library loan, and for the title and summary to be made available to outside organisations (unless a bar is in place).

The university's ethical procedures have been followed and, where appropriate, that ethical approval has been granted.

Signed:

Date:

11th April 2024

Table of Contents

Acknowledgements

This body of work would not have been possible without the involvement of several people, from those who birthed the idea for this project, to those who offered their advice, guidance, and assistance along the project's life.

Firstly, I would like to thank Dr Edward Span (Tata Steel Netherlands) and Dr David Warren (M2A Swansea University) for interviewing me for this research position. I give thanks to my academic supervisor Professor Cameron Pleydell-Pearce, an inspiration and whose wealth of experience and knowledge in the field of materials science and engineering has helped shaped what this project became and offered recommendations on how to overcome various obstacles encountered in this project. I want to thank Dr. Mark Coleman for his help and chats on the fundamentals of steel during the annealing process.

Probably the most important people in this project's life are the industrial supervisors and contacts i.e., Jérémy Vian (Steel and Metals Institute, Singleton campus), Nigel Jenks and Jack Vaughan (Tata Steel Trostre Steelworks). Without their knowledge, words of advice and encouragement, and drive to organise activities, this project would have taken a different turn. Additionally, I want to thank Peter Evans and Geraint Gladwyn for their contributions to this project namely taking the time out from their own work to conduct the temper rolling and ageing of samples.

I want to apologise to my mum for not doing a degree in something easier for her to understand (she tells people I design bridges instead). I thank her for her patience.

1. Introduction

Modern “tin cans” as we know them today utilise sheet steel for the bodies and lids (otherwise known as can ends). The practice of using sheet steel dates to 1810 when a patent (no 3372) was awarded by king George III to Englishman Peter Durand for this invention of preserving food using tin cans made from iron sheets dipped in molten tin (Cavendish Corporation Staff, 2003). Although the practice of food preservation was invented prior to 1810, it was Peter Durant who exclusively used tin cans as the vessel for food preservation. Using Peter Durant’s patent, Englishmen Bryan Donkin and John Hall opened the first commercial canning factory using tin cans in Bermondsey, England 1812.

Tin cans in this period were laboriously made by pounding iron into flat sheets which were then dipped in molten tin to prevent the iron from rusting. These sheets were then cut into rectangles and circles with the rectangles bent around a cylindrical mould to form the can body, and the circles soldered on top to form the lid. At the time, a skilled can maker could make up to sixty tin cans per day. Nowadays, millions of steel cans are made a year in the UK alone, thanks to today’s modern practices (The Can: Canmakers UK, 2024).

Steel packaging is used as the vessel for a wide range of products such as food, anti-perspirant, and paint containers. Packaging steel faces competitions within the packaging market from other materials such as plastic, glass, and aluminium. However, steel offers numerous benefits over some of these other materials such as being 100% recyclable without loss in mechanical properties (compared to plastic), is more resistant to breaking if dropped (compared to glass) and is an inherently stronger material (compared to aluminium). The innovation in can making procedures over the years has allowed steel cans (bodies and ends) to become thinner (Column: The delicious history of the tin can) without detrimental impact on performance.

The sponsor company of this project (Tata Steel UK) is facing difficulties with its competitors (i.e., ArcelorMittal and Rasselstein) who can make steel can ends which are thinner, have higher strengths, and have suitable elongation values (A50) of at

least 5%. Steel can ends come in two styles, i.e., plain end, and easy-open end. The plain can-end requires a can opening tool to gain access to the content, and the easy-open can-end has a ring pull system attached to the can-end allowing access to the contents without the need for a specialist tool. See Figure 1.1 for examples of both styles of can-ends.

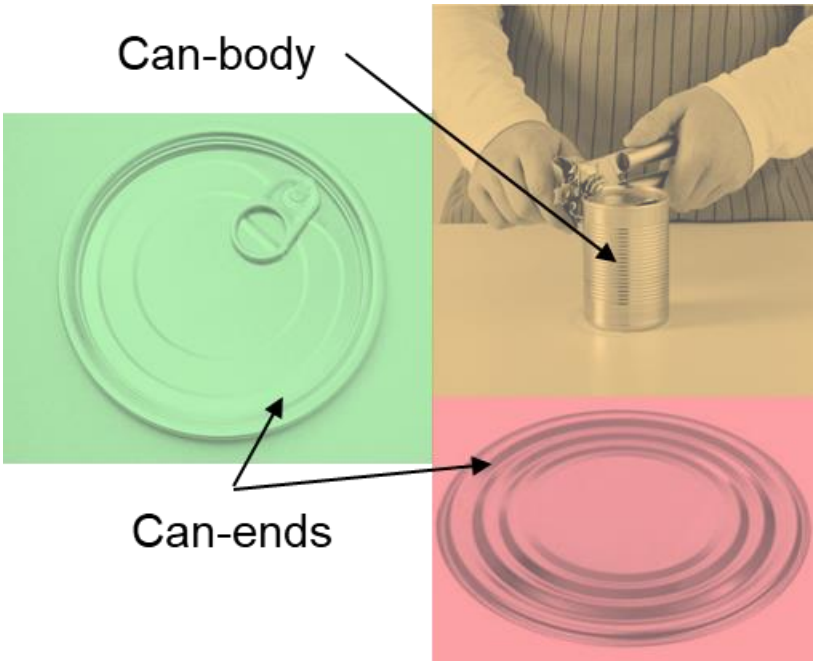

Figure 1.1. Can-body (top right), easy-open can-end (left), and plain can-end (bottom right).

The recent trend sees steel can ends becoming thinner, exhibiting greater mechanical properties, whilst maintaining a suitable elongation value of at least 5% after a secondary cold reduction procedure has been conducted. Can-ends (which this project has focussed on) differ to can bodies (see Figure 1.1, top right image) in several ways because of the different properties required from either part. For example, the mechanical properties of can-ends generally exhibit higher strengths with lower elongation (as measured in a tensile test), whereas for can-bodies it is generally the opposite.

Currently, the sponsor company does not have a product to match their competitors, and if they do not have one soon, will potentially lose their existing customers to their competitors. Therefore, the need to produce a steel grade for can end applications that matches or surpasses Tata Steel's competitors is required.

1.1. Aims and objectives

This is where this project comes in. A new method will need to be figured out that allows the manufacture of can ends that are equal or superior to the competitors' products in terms of mechanical properties, without infringing on patented technologies/processes. The desired mechanical properties are:

- Yield strength equal to 650-750 MPa
- Total elongation equal to at-least 5% in all directions after a double cold-reduction procedure has been applied.

To achieve these properties, it was decided that the composition, and later stages of steel manufacturing (i.e., the annealing stage and onwards) parameters were tested. In addition to the properties mentioned above, it was desirable but not critical to the project, to yield a final product with a gauge <0.2mm.

If can ends of equal properties to the competitors can be made, this will allow Tata Steel Europe to remain competitive with its rivals. If superior properties are achieved, this could give Tata Steel Europe a competitive advantage and result in a greater market share.

1.2. Thesis structure

This thesis is structured so that you will first be introduced to the relevant background information regarding packaging steel for can-end applications such as the manufacturing processing routes, the relevant manufacturing parameters and how they influence mechanical properties, as well as compositional elements and their role on mechanical properties. Then you will be presented with the literature review, where an investigation was conducted looking into the research that has already been done into this problem (or for a similar one), to draw conclusions on what options can be exploited to achieve the aims of this project. You will then be presented with a methodology chapter which introduces the key materials and methods used

throughout this work. The subsequent chapters detail the individual technical experiments that were conducted following the options presented in the literature review. These technical chapters detail the experimental parameters tested, findings/results obtained, and end with discussions and conclusions. The final chapter summarises all the technical chapter conclusions and offers final recommendations.

1.3. Tin plate grades

For clarification, a tinplate grade refers to the chemistry of a steel sheet. In its uncoated form, packaging steel is referred to as black plate. When coated, with either tin/chromium/chromium oxide, it is then referred to as coated steel. The tinplate grades made by Tata steel packaging are defined by European standards and "in house" nomenclature that define certain tempers between the European standards.

Current standards are:

1. BS EN 10202: 1990: Cold Reduced Electrolytic Chromium/Chromium Oxide Coated Steel ECCS
2. BS EN 10203: 1991: Cold Reduced Electrolytic Tinplate
3. BS EN 10205: 1992: Cold Reduced Black plate in coil form to produce tinplate or electrolytic chromium/chromium oxide coated steel
4. BS EN 10079: 1993: Definition of steel products 50 Tin mill products – including tinplate, black plate, and chromium/chromium oxide (ECCS) coated

National standards and their supporting documents are being replaced by European Standards for steel products.

Tinplate grades are placed into two distinct classes, as defined by the European standards. Single reduced tempers are classified by a T number (e.g., T 50), and double reduced tempers are classified by a DR number (e.g., DR 550). The number associated with single reduced tempers refers to the average HR 30 Tm value for aged samples. The number associated with the double reduced tempers refers to the

average 0.2% proof stress value, for aged samples also. The European standard also gives an indication of what HR 30Tm values are to be expected for double reduced material. The overall properties of any temper will differ depending on which of the two annealing routes (batch annealing or continuous annealing) is used. Table 1.3.1 lists the tinplate tempers, their general definitions and usage, of current products offered by Tata steel packaging. Other classifications not produced by Tata steel packaging are included for completeness.

For the purposes of this project, it is assumed that the coating operation does not considerably change the mechanical properties, so coatings as a method for strengthening steel will not be looked at.

Table 1.3.1. Temper classification of grades manufactured by Tata Steel UK, with property requirements and information regarding typical usage for each temper.

Temper Classification		HR 30 Tm Hardness Aim		Average 0.2% Proof Stress			
Current	**Former**	**Nominal**	**Range for sample average**	**Nominal N/mm^2**	**Permitted Range N/mm^2**	**Formability**	**Typical Usage**
T 50	T 1	52 maximum				Extra deep drawing	Deep drawn container
T 52	T 2	52	+/- 4			Deep drawing	DWI cans & deep drawn cont.
T 55[1]		55	+/- 4			General purpose	Specialty packaging
T 56[1]		56	+/- 4			General purpose	DWI cans
T 57	T 3	57	+/- 4			General purpose	Paint lids. Bodies and aerosols
T 61	T 4	61	+/- 4			General increased stiffness	Crowns, paint can bodies, catering packs

[1] These tempers are not designated in the European standards, and their properties have been found by extrapolating current specifications.

Tin plate grades

T 65	T 5	65	+/- 4			Resists buckling	For stiff ends and bodies
T 67[1]		67	+/- 4			Very stiff	Beer & beverage can ends
DR 520[1]		72	+/- 3	520	+/- 70	Double Reduced	Round can bodies & ends
DR 550	DR 8	73	+/- 3	550	+/- 70	Double Reduced	Round can bodies & ends
DR 580[1]		74	+/- 3	580	+/- 70	Double Reduced	Round can bodies & ends
DR 600[1]		75	+/- 3	600	+/- 70	Double Reduced	Round can bodies & ends
DR 620	DR 9	76	+/- 3	620	+/- 70	Double Reduced	Round can bodies & ends
DR 660	DR 9M	77	+/- 3	660	+/- 70	Double Reduced	Beer & beverage can ends

1.4. Important mechanical properties

Below is a list of all mechanical testing and properties that are currently or could be measured for tinplate steel for can-end applications.

1.4.1. Vickers microhardness test

The Vickers microhardness test is a standard measurement used to determine whether single reduced tinplate conforms to what is desired. It can use smaller applied loads ranging from 1-1000g. Vickers microhardness test is easy to conduct, inexpensive, and is a quick measurement to perform.

1.4.2. Tensile test

The tensile test measures more mechanical properties compared to the Vickers hardness test and provides a more overall description of the mechanical behaviour of steel when subjected to a tensile stress. However, this test takes longer to perform and requires samples to be in the shape of dogbones. There are numerous dogbone geometries that are used worldwide, but Tata steel packaging uses the JIS5 style dogbone.

1.4.3. Proof stress

In other steel products such as DP600 steel for automotive applications, continuous yielding behaviour is seen in stress-strain curves .This is where upon yielding, there will be a gradual elastic-plastic transition. This is usually because of the relatively larger amounts of secondary cold work reductions applied them. In these cases, the 0.2% proof stress is taken.

However, high strength steel for can end applications tends to not exhibit continuous yielding behaviour. Instead, it typically exhibits an upper and a lower yield point, in what is termed the *yield point phenomenon*, whereby continuous deformation fluctuates around a constant value of stress. Subsequently, stress begins to rise again after a certain amount of strain has occurred in the steel sample. Therefore, for steels displaying this effect the yield strength is taken as the average stress value correlated to the lower yield point. The yield point phenomenon is present in high strength packaging grade steels in the as-annealed condition, and to a lesser extent the double-reduced condition (due to the relatively lower amount of secondary cold reduction applied post-annealing). Additionally, if a steel has been aged (e.g., 200°C for 20 minutes) it also displays this yield point phenomenon.

However, given that the 0.2% proof stress value usually always aligns with and is identical to the lower yield point value, the proof stress value will be measured and used in this body of work.

1.4.4. Ultimate tensile strength

Ultimate tensile strength is the maximum stress a steel can withstand when being pulled or stretched before undergoing necking and eventual breaking (or breaking as soon as tensile strength is reached as seen in brittle materials). It is shown by the maximum value in an engineering stress-strain curve.

Both hardness and tensile strength are measures of a materials resistance to plastic deformation. Therefore, they are roughly proportional to one another. It is often said

that the ultimate tensile strength of high strength packaging steel is approximately three times greater than the hardness value.

1.4.5. Total elongation

The total elongation value is the total amount of strain steel undergoes before it fractures and is expressed as percent elongation. It is found on a tensile test curve by the final strain value at fracture. It is important for steel can ends to have a total elongation value (A50) of at least 5% in all directions. This is so the can end has enough ductility to allow a ring-pull system to be installed for easy opening, and to bend without fracturing when being opened.

Percent elongation is calculated using formula 1 below:

$$\%EL = \left(\frac{l_f - l_0}{l_0}\right) x\ 100 \qquad \text{Equation 1}$$

Elongation values are reported as either an A50% or A80% elongation value, which refer to the gauge length of the tensile specimen (50mm for A50% elongation value, 80mm for A80% elongation value). Tata steel packaging tend to quote the total elongation value as A50% due to the common practice of using JIS5 type tensile specimens which have a 50mm gauge length. Generally, as hardness and ultimate tensile strength increase, elongation decreases.

1.4.6. Property variability

It is worthwhile mentioning here that measured material properties such as lower yield point, 0.2% proof stress, tensile strength, total elongation etc. will be a little different each time even if the same type of steel being tested, highly accurate equipment is used, and a highly controlled test procedure is used. This is because there will always be variability in the data from specimens of the same material. This variability originates from several factors, from human/operator bias during testing, test method, variations in specimen fabrication, apparatus calibration, inhomogeneities in same lot of material, slight compositional differences from lot to lot.

Even though there will be variability, it is preferred for a "typical" value to be given for a property. Therefore, it is normal to give the average $\overline{x}$ value in this case. The average value is calculated by summing the measurements and then dividing by the total number of measurements (see formula 2):

$$\overline{x} = \frac{\sum_{i=1}^{n} x_i}{n} \qquad \text{Equation 2}$$

Where n is the total number of measurements and x_i is the value of a distinct measurement. In certain cases, it is required to give the magnitude of scatter. A popular way to measure this magnitude is the standard deviation 's', given by formula 3:

$$s = \left[\frac{\sum_{i=1}^{n}(x_i - \overline{x})^2}{n-1}\right]^{1/2} \qquad \text{Equation 3}$$

The larger the value of standard deviation, the larger the magnitude of scatter in the data there is. Ideally, as low a standard deviation as possible is desirable. It should be recognised and accepted that scatter or variability in the data is inevitable, but at the same time efforts to minimise scatter should be done.

1.5. Forming operations

1.5.1. Can end making

Can ends are made by stamping out circular pieces from a steel coil. For plain can ends this is where the operation stops.

1.5.2. Ring pull can end making

For can ends with a ring pull tab, a rivet is used to fasten the pull tab to the can end.

1.6. Can making methods

1.6.1. Can making methods

There are two types of can available today, namely the three-piece can and the two-piece can. There is one procedure used to make three-piece cans called *three-piece can manufacture*. There are two procedures used to make two-piece cans, called *draw and redraw*, and *drawing and wall ironing*.

The can ends are made by pressing circular blanks from a sheet of steel to give a circular blank with a folded rim all around the edge. A sealing compound is later placed into this folded rim to so that an airtight seal is made when the can end is attached to the body.

1.6.2. Three-piece can manufacture

Three-piece cans consist of three separate components, the can body and two ends (which form the base and lid). These cans are made by rolling pre-lacquered rectangular blanks into a cylindrical shape and then electrically welding the ends of a sheet of tinplate to form the cylindrical body of the can. Afterwards, a can end is attached to one end to form the base of the can and having one open end to allow the filling of contents. After the can is filled, another can end is attached to close the can and sealing the contents inside.

1.6.3. Two-piece can manufacture

Two-piece cans consist of two components, the base/body, which is now one part, and the can end which forms the lid. The base/body is made using either two procedures, the *draw and redraw* procedure, or the *drawing and wall ironing* procedure. Which procedure is used depends on the application of the can because the draw and redraw procedure yields a can whereby the height is less than the diameter (as seen in food containers such as tuna fish), whereas and the drawing and wall ironing procedure yields a can with a height that is greater than the diameter (making it suitable for beverages).

1.6.4. Draw and redraw procedure

Both procedures start off by punching a circular blank from a steel sheet and pressing the blank using a circular die to achieve the walls. The thickness of the wall and base is the same here and this is where the draw and redraw procedure ends.

1.6.5. Drawing and wall ironing (DWI)

The drawing and wall ironing extends this procedure further by pressing the redrawn can through a series of dies each with incrementally smaller diameters thinning the can walls to achieve a greater height.

1.6.6. Production of tinplate

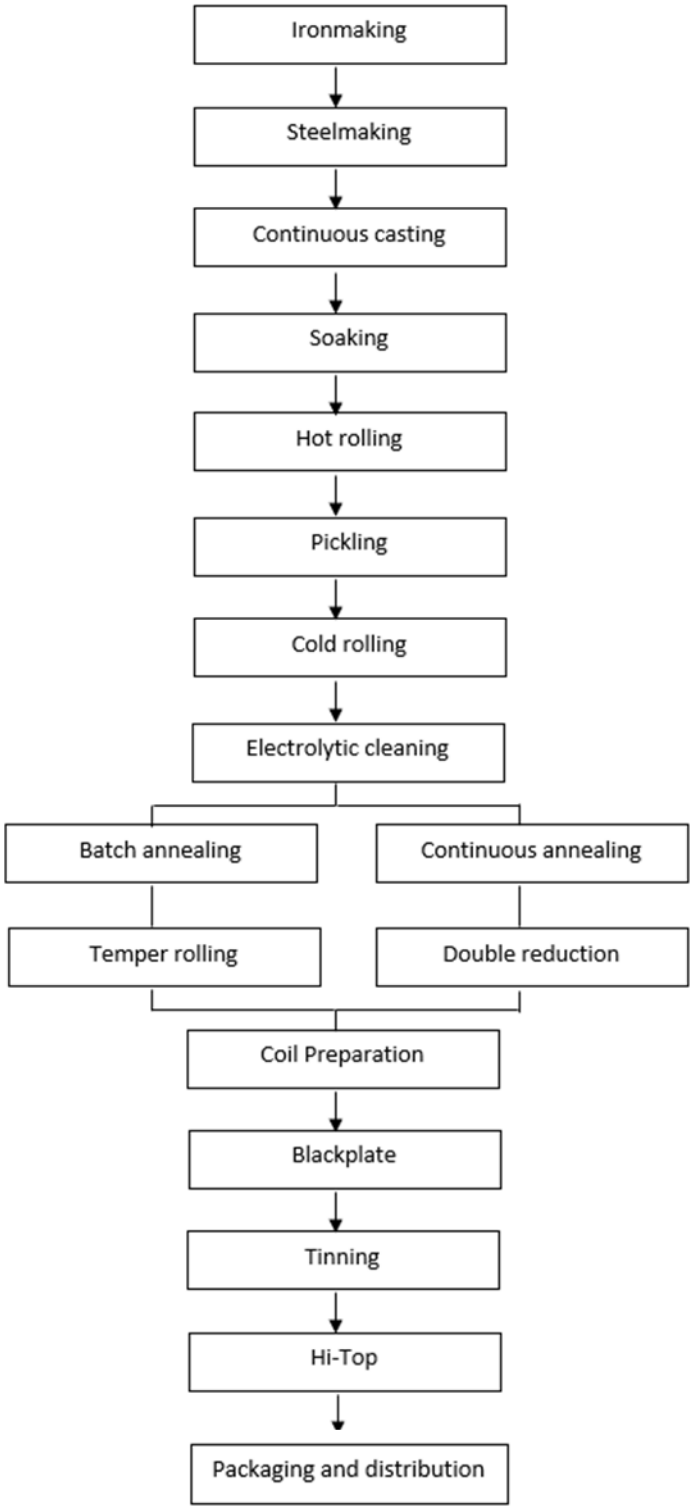

Figure 1.6.1. Schematic of the step-by-step process to making steel for easy-open can end applications.

1.7. Chemistry

The following sections talk about elements that are commonly found in packaging grade steels and their effects on the mechanical properties and how they influence the mechanical properties.

1.7.1. Carbon

1.7.1.1. What is carbon, and its effect on mechanical properties

Carbon is very important for steel used for can-end applications because it is a cheap addition to add to steel that can increase the yield and tensile strengths (albeit at the loss of some ductility). Carbon increases the strengths via **two** main mechanisms, solid solution strengthening and/or precipitation strengthening.

1.7.1.2. Solid solution strengthening

Firstly (and probably most importantly), carbon is a potent solid solution strengthening element. If the carbon is dissolved in steel and remains in its free form, that is when it is not bonded to other elements to form a compound (e.g. Fe_3C), but rather sits in the interstitial spaces within the iron matrix (e.g. body centred cubic ferrite matrix) it increases the yield strength of steel by coefficient of **5544 N/mm^2** per **1 wt %** according to (PICKERING, 1978). However, carbon has very limited solubility **in ferrite** (a maximum of **0.025wt%C** at **723°C**, and 0.008wt%C at room temperature), therefore other sources, such as (Ren and Liu, 2019), empirically give the solid solution strengthening coefficient of carbon as **4570 N/mm^2** when the solid-solved carbon content in ferrite is taken as **0.01wt%C**. This makes the solid solution strengthening effect of carbon in ferrite equivalent to **45.7 N/mm^2** (0.01wt%C x 4570N/mm^2 = 45.70 N/mm^2).

The maximum amount of carbon that can be dissolved in the iron matrix depends on the iron phase and temperature. For the γ-austenite phase it is **2.06wt%C** at **1147°C**. For the **α-ferrite phase**, maximum carbon contents are reported to be either as low as **0.022wt%C** at **727°C** (Callister, 1991) or as high as **0.035wt%C** at 732°C (Wright, 2011), which decreases to 0.008wt%C at room temperature. Therefore,

depending on the ratio of phases present at room temperature, total carbon contents that exceed these solubility values will result in the carbon atoms precipitating out to form carbon-containing precipitates (e.g., Fe_3C, TiC, AlC etc.).

1.7.1.3. Precipitation strengthening

Secondly, carbon can increase the strength of steel via **precipitation strengthening**. This is where the carbon atoms bond with other alloying elements to form a compound that precipitates out of the matrix. Examples of common carbon-containing precipitates found in packaging grade steel are cementite (Fe_3C), titanium carbide (TiC), aluminium carbide (AlC). Carbon-containing precipitates are also known as carbides.

Carbides can increase the strength of packaging grade steel via several processes such as grain refining and interacting with dislocations. It is important to note that if carbon precipitation occurs, it is taken out of solid solution. Therefore, the strengthening associated with solid solution is reduced.

1.7.1.4. Grain refinement due to carbides

Some carbides can improve strength values. For example, Titanium carbide (TiC) can increase strength by restricting the grain growth that occurs at high temperatures (for example 980-1220°C) seen during the hot-rolling stage. This restricted grain growth results in a more refined grain size at room temperature, which according to the Hall-Petch relationship, a smaller grain size equates to an increase in strength. This precipitate works to restrict grain size by precipitating at the grain boundaries (referred to as **inter-granular** precipitation) which cause them to remain stable and more resistant to grain growth.

1.7.1.5. Dislocation motion inhibition due to carbides

Precipitates that do not form at the grain boundaries, but instead within the grains (referred to as **intra-granular** precipitation) increase strength by acting as barriers to dislocation movement. When a certain amount of stress is applied to steel, dislocations are generated which will propagate through the steel if the correct amount of stress is being supplied. These propagating dislocations can be halted

when they encounter a precipitate within the grain and can result in a pile up of dislocations behind the precipitate. This pile up of dislocations requires a greater stress than before to get them to propagate again. Thus, the precipitate has increased the strength of steel by inhibiting dislocation motion.

1.7.1.6. How is carbon added to steel

Steel is defined as an iron-carbon alloy that contains up to 2.06wt%C. Iron-carbon alloys containing more than **2.06wt%C** (i.e., 2-3.5wt%C) are called cast-irons or pig-irons.

Carbon is introduced to steel in the blast furnace when sintered iron ores (containing iron oxides) react with additions of coke (rich in carbon). Following a carbothermic reduction reaction, iron oxides are reduced to metallic iron resulting in a liquid iron containing more than **4wt%C**. To reduce this level of carbon, the **liquid iron** is then treated with oxygen in the basic oxygen steel (BOS) making vessel, where oxygen is blown into the liquid steel for it to react with the carbon to form either carbon monoxide (CO) or carbon dioxide (CO_2). This process sis continued until the desired carbon content is achieved. **Liquid steel** is now produced with a carbon content in the region of **0.02-0.06wt%C**. However, it now contains approximately 0.03wt% oxygen which is removed via additions of aluminium, silicon, or a combination of both which react with the oxygen to form alumina (Al_2O_3) or Silica (SiO_2). Alumina or Silica then separate to the slag at the top of the melt, leaving a liquid steel with the required composition with an oxygen content of 0.005wt%, at 1600°C.

1.7.1.7. Typical quantities of carbon found in packaging steel

Typical carbon contents in high-strength steel used for can ends are in the region of around **0.065-0.08wt%C**. These contents allow for enough ductility (as shown by the total elongation in an engineering stress-strain curve) after a double reduction procedure has been conducted. Carbon increases the yield and tensile strength whilst simultaneously decreases the ductility. So, if carbon contents greater than 0.065-0.08wt%C are used, the steel sheet will have a higher yield and tensile strength and a reduced ductility prior to the double reduction procedure. If a double reduction procedure is performed on this steel, the yield and tensile strength will increase

further, but the ductility will reduced, resulting in a very brittle steel with a total elongation value below 5% in all directions, a value too low for can end applications. A can end must have a total elongation value of at least 5% in all directions after double reduction procedure to ensure a nice bending of the can-end as it is opened via the easy-pull tab.

On the other hand, carbon contents below the range **0.065-0.08wt%C** will result in a more ductile steel but will be softer and weaker steel (lower yield and tensile strength). Steel containing these kinds of mechanical properties make them less suitable for can-end applications but good for can body applications where a greater ductility is required for redraw and wall-ironing purposes.

1.8. Nitrogen

Nitrogen, like carbon, is another powerful solid solution strengthening element. It can exist in dissolved form (otherwise known as free nitrogen) in the iron lattice, or as a precipitate (otherwise known as a nitride).

In ferrite-pearlite steels, free nitrogen has the potential to increase **yield** strength by **5544 N/mm^2** per 1wt% according to (PICKERING, 1978) or **2918 N/mm^2** per 1wt%N according to empirical equations created by (Ren and Liu, 2019). On the other hand, nitrides can increase the strength further via grain refinement, and by acting as barriers to dislocation motion. However, the solid solution strengthening increase associated with free nitrogen is greater than strengthening due to precipitation.

1.8.1. How is nitrogen added to steel

Nitrogen can be added to steel in two ways, in upstream stages during the casting stage, and in the annealing stage after cold reduction, via nitriding.

The limitation of adding nitrogen in the casting stage is that there is a maximum amount you can have before the solubility limit of nitrogen in the solid form of steel (as opposed to the liquid form which can accommodate more dissolved nitrogen) is exceeded leading to issues such as trapped nitrogen gas which results in porosity issues. Therefore, this is the benefit of adding nitrogen in later stages via the

nitriding process because nitrogen contents can be increased without facing the casting issues mentioned previously.

1.8.2. Precipitates of nitrogen

Nitrogen under the right conditions will form precipitates with Titanium (TiN) and aluminium (AlN).

Like carbon, if nitrides form then nitrogen is taken out of solid solution and so the solid solution strength benefits associated free nitrogen will be decreased. It is important in packaging grade steel that the precipitation of nitrogen is suppressed because the solid solution strength benefits of nitrogen is greater than the strength increase due to precipitation hardening.

AlN will start precipitating at temperatures below 1200-1250°C. Therefore, for complete dissolution of AlN, the temperature of the steel will need to be higher than 1150-1300°C. These high temperatures are seen during the hot-rolling stage, and typical slab reheating temperatures are around 1200-1250°C. According to (Hudd Hudd and Llewellyn, 1998) slab reheating temperatures of around 1200-1250°C will cause the aluminium and nitrogen to remain in solid solution and will normally remain in solution after the completion of hot-rolling.

In applications where you want AlN to precipitate out, it is recommended after the hot-rolling stage to have a high coiling temperature of 710°C. This temperature means the tightly wound coil has high thermal mass and therefore takes a relatively longer time to cool, affording the opportunity for the precipitation of aluminium nitride. The slower the cooling rate and higher the coiling temperature, the higher the volume fraction of AlN.

1.8.3. How to increase free nitrogen content in steel

Therefore, in applications where you do not want AlN to precipitate out (like in can-ends so to exploit the solid solution strengthening of nitrogen) there are several things you can do.

Firstly, you can try to suppress the reaction of aluminium and nitrogen. This is done by having a high cooling rate of 80°C/s (as later seen in the hot rolling procedure for

the six lab casts used in this body of work) at the exit of the run-out table (finish roll out temperature = 950°C, cooling (in) = 910°C) to a low coiling temperature of 560°C (Hudd Hudd and Llewellyn, 1998) or 590°C (as seen in hot rolling procedure for the six lab casts). In doing so, aluminium and nitrogen are not afforded the adequate time to form deleterious amounts of aluminium nitrides. In other words, the reaction of aluminium and nitrogen is suppressed, and nitrogen remains in solid solution form (see left-hand side of below equation).

$$2Al+N_2 \rightarrow 2AlN \qquad \text{Equation 4}$$

Secondly, if the goal is to have as much nitrogen in solid solution as possible, it is logical to think that removing all aluminium from the steel composition will help this. However, this would create other issues because aluminium is used as a deoxidiser to bring the levels of oxygen (introduced in the basic oxygen steelmaking process) down to 10-100ppm range. Therefore, aluminium must be present. Steels with aluminium for this purpose are termed aluminium-killed steels.

If aluminium is present and does bond with the nitrogen, we could get around this by reducing the ratio of aluminium to nitrogen to levels that provide just enough of the deoxidizing effect of aluminium whilst simultaneously increasing the ratio of nitrogen to aluminium. This will reduce the likelihood of nitrogen bonding with aluminium, and therefore, there will be more free/unbound nitrogen after the aluminium has bonded to as much nitrogen as it can. However, as mentioned already, there is a limit to the amount of nitrogen you can have as there is a maximum solubility of nitrogen in austenite and ferrite, with maximum solubilities being different for the two phases.

Perhaps a combination of increasing the ratio of nitrogen to aluminium and using the mentioned coiling parameters would be best.

1.9. Phosphorous

After carbon and nitrogen, phosphorous is the next strongest solid solution strengthening element to add to steel and increases **yield** strength by **678 N/mm^2 per 1wt%** when in solid solution (PICKERING, 1978) in **ferrite-pearlite** steel.

1.9.1. Phosphorous in multi-phase steel

However, in low-carbon multi-phase steels containing ferrite with retained austenite, bainite and or martensite, (Chen, Era and Shimizu, 1989) showed that when compared to phosphorous free samples, phosphorous has been shown to **decrease yield strength**, but significantly **increases** the **ultimate tensile** strength. This was due to phosphorus role in increasing the amount of retained austenite, **especially in the presence of 0.5wt% silicon**, which later transformed to secondary phases bainite and martensite. In Si-free steels, **retained austenite** amounts increased from approximately **1%** to approximately **4%** as P increased from 0.006wt%P to 0.204wt%P. In the presence of **0.5wt%Si**, austenite increased from **9.5% to 13.6%**. The low-carbon steel samples used in this study had a base chemistry of 0.15%C-0.5%Si-1.5%Mn with phosphorous contents of 0.006wt%, 0.068wt% and 0.204wt%, and had been cold rolled, intercritical annealed, and isothermally held in a temperature range of bainitic transformation followed by air cooling.

Relative to phosphorous free samples, adding **0.006wt%P** decreased yield strength by **-42MPa** (but tensile strength increased by **98MPa**), and adding **0.204wt%P** decreased yield strength by **-11MPa** (but increased tensile strength by **274MPa**). The more phosphorus that is added, the smaller the reduction in yield strength and greater the tensile strength increases. Tensile strengths increased linearly with phosphorus additions. The slight reductions in **yield** strength were said to possibly be attributed to the:

> "Large amount of retained austenite since stress induced transformation of the retained austenite could trigger flow in the ferrite which is surrounded by retained austenite at a lower stress than would otherwise be possible" (Rigsbee and Vander Arend, 1979; Narasimha-rao, Bangaru and Sachdev, 1982)

To explain the trend of increasing **tensile** strength with phosphorus content,

> "The higher ultimate tensile strength in P-containing steels over that of P-free steel is also considered to be due to the strengthening of the ferrite matrix by the transformation of retained austenite during tensile deformation" to secondary phase.

The samples showed good mechanical properties when phosphorus levels were 0.07wt%P. **yield** strength of **approximately 480MPa tensile** strength of **730MPa** and maximum uniform and **total** elongations of approximately **30% and 35%** respectively. Uniform and total elongations and combination of tensile strength vs ductility (TS x T-El) had maximum values at 0.07wt%P. It is implied that steel for easy-open end applications must have a total elongation (A50) of more than 35% in its as-annealed state (prior to double-reduction).

Based on the study by (Chen, Era and Shimizu, 1989), phosphorus contents in packaging steel should be kept **below 0.07wt%P**. to minimise loss in yield strength, whilst achieving best possible combination of tensile strength vs total elongation. Based on the packaging grades of steel produced in Port Talbot steelworks, Phosphorus is kept to a maximum level of **0.02wt%P**.

It was mentioned that a total amount of secondary phases generated in these samples were 20-25% volume. However, they did not exactly specify what phases they were. Also, for the six casts in this body of work, a much smaller amount of total secondary phase volume fraction is expected due to having almost half the amount of carbon (0.08wt%C).

1.9.2. How phosphorus increases the amount of retained austenite

The mechanism behind why phosphorus helps retain austenite is said to be because phosphorus is an effective element for solid solution hardening, which enhances the matrix constraint affecting the transformation of austenite to bainite and martensite, and thus might be a cause of the retention of austenite. (Chen, Era and Shimizu, 1989)

1.10. Manganese

When dissolved in solid solution, the effect on yield strength of manganese due to solid solution strengthening effect is an increase of 32.3N/mm^2, and the effect on tensile strength is 27.7N/mm^2 in 0.25C-1.5Mn ferrite-pearlite steels, according to (PICKERING, 1978).

It is added to provide additional solid solution strengthening when dissolved carbon and/or nitrogen are low, i.e., they have been taken out of solution and are in precipitate form.

The six steel sheet chemistries in this body of work have manganese levels between 0.374wt% to 0.568wt%. Therefore, based on the solid solution strength coefficients by (PICKERING, 1978), these levels should increase yield strength between 12-18MPa in strength, and tensile strength between 10-16MPa.

1.10.1. Manganese precipitates

Manganese bonds with sulphur to form globular shaped manganese sulphides MnS. Three types of MnS exist, type I, type II, and type III.

Type I exist is silicon-killed steels that contain no aluminium. Because my chemistries contain aluminium, this type will be ignored as they will not form in my samples.

Type II are dendritic structured that form a thin chain-like distribution of discrete particles at grain boundaries. These being to appear when aluminium levels are equal to 0.005wt%Al.

Type III appear alongside type II when aluminium levels are between 0.01-0.03wt%Al. If aluminium levels are approximately 0.04wt%Al, this type is practically assured to be the only type to be present. Because my samples contain aluminium levels between 0.011-0.022wt%Al, I would expect a mixture of type II and III MnS to be present.

It is important that MnS have a globular morphology because if they are stretched out during hot-rolling and become elongated in the rolling direction (termed

manganese stringers), they effectively become a crack in the coil becoming an initiation site for cracking during further mechanical processing (e.g., cold rolling, temper rolling).

1.10.2. Manganese effect on transformation temperatures

Manganese is an austenite stabiliser because it decreases the Ac1, Ac3, Bs and Ms temperatures. The coefficients of these reductions are -14, -7, -69 and -36 respectively.

$$\boldsymbol{Ac_1} = 742 - 29(C) - 14(Mn) + 13(Si) + 16(Cr) - 17(Ni) - 16(Mo) + 45(V) + 36(Cu)$$ Equation 5

$$\boldsymbol{Ac_3} = 925 - 219\left(\sqrt{C}\right) - 7(Mn) + 39(Si) - 16(Ni) + 13(Mo) + 97(V)$$ Equation 6

$$\boldsymbol{B_s} = 771 - 231.5(C) - 69(Mn) - 23(Si) - 58.5(Cr) - 31(Ni) - 55(Mo) - 41(V)$$ Equation 7

$$\boldsymbol{M_s} = 541 - 401(C) - 36(Mn) - 10.5(Si) - 14(Cr) - 18(Ni) - 17(Mo)$$ Equation 8

1.11. Silicon

Silicon in solid solution form increases yield and tensile strength by 83.2N/mm^2 per 1wt%. It is added to augment strength (via solid solution) of steel that has been strengthened via bake-hardening. Silicon increases the Ac1 and Ac3 temperatures by coefficients of +13 and +39 respectively. However, it reduces the Bs and Ms temperatures by coefficients of -23 and -10.5 respectively.

Silicon tends to inhibit carbide precipitation, resulting in carbon atoms remaining dissolved in the matrix. Therefore, during bainite transformation, austenite can become enriched in carbon which stabilises it resulting in a greater final volume fraction of bainite or martensite. Furthermore, because silicon helps carbon remain in

solution, it provides additional hardenability to ensure formation of martensite in dual-phase steels. Si, Mn and Ni all have beneficial contribution to the formation of retained austenite, with silicon being the most effective at doing this.

1.11.1. Limits of silicon

If silicon levels are too high, problems with brittleness and cracking can occur during cold rolling. In packaging steel for easy-open ends, silicon levels are aimed to be zero, with a maximum of 0.0250wt%Si.

1.12. Sulphur

Sulphides (s^{2-}) can negatively impact mechanical properties such as impact bending, hole expansion operations due to formations of non-metallic inclusions. As a result, sulphur levels are usually kept below 0.05wt%S. The negative impacts associated with sulphur are counteracted by additions of manganese so manganese sulphides form.

1.13. Titanium

Titanium does not dissolve in iron, so solid solution effects are negligible. However, it can form a precipitate with carbon and/or nitrogen to form titanium carbide (TiC), titanium nitride (TiN), or titanium carbonitride (TiCN).

Titanium carbide and titanium nitride both increase the strength of steel via precipitation strengthening as both precipitates are grain refiners. For example, during the hot-rolling stage at temperature 1200°C there will be some TiC that is dissolved and some that remains undissolved. This undissolved precipitate of TiC restricts the austenite grain size by pinning the austenite grain boundary. a restricted austenite grain size will result in a finer ferrite grain size on cooling.

Titanium carbides and titanium nitride will precipitate in temperature ranges between 1150-1300°C. Therefore, at temperature below this range they will precipitate and result in carbon and nitrogen being taken out of solution. In cold rolled strip, TiC mainly acts to maintain strength increase due to ferrite grain refinement during recrystallisation. During annealing, TiC coarsens causing the precipitation

strengthening effect to decrease but maintain the small ferrite grain size. TiC/TiN precipitate at the interface of austenite-ferrite grain boundaries. Therefore, strength of cold rolled material is lower than parent hot-band material.

The magnitude of grain refining and interphase precipitation depends on:

Type of elements (Nb, V, Ti → weaker)

- Amount of element
- Base composition
- Soaking temperature
- Coiling temperature
- Cooling rate to ambient

During hot-rolling, solute titanium retards austenite grain growth during successive hot-roll passes due to an effect called ‘solute drag’. As a result, austenite grain size will be smaller because of this.

1.14. Processing

1.14.1. Ironmaking

The procedure to make double-reduced packaging grade steel in an industrial setting involves many stages. The first stage is the ironmaking stage. This involves mixing sintered iron ores (containing iron oxides) with coke (carbon rich) inside a blast furnace and heating up to approximately 1500°C. At this temperature, a carbothermic reduction reaction takes place whereby the metal oxide (e.g., Fe_2O_3) is reduced by the carbon (which is acting as the reducing agent). Although multiple reactions are happening, a simplified equation of this reaction is written below:

$$2Fe_2O_3 + 3C \rightarrow 4Fe + 3CO_2 \qquad \text{Equation 9}$$

Once the carbothermic reduction reaction is complete, carbon dioxide gas is produced as well as liquid metallic iron containing a carbon concentration more than 4wt%C. Iron containing more than 2wt%C is referred to as cast iron/pig iron, therefore the carbon concentration needs to be 2wt%C or less to become steel. Therefore, to make steel molten iron is transferred from the blast furnace via a rat

hole into a waiting torpedo to be transported to a basic oxygen steel (BOS) making vessel.

1.14.2.Steelmaking

Inside the basic oxygen steel (BOS) making vessel oxygen gas is pumped into the liquid iron through the bottom where the oxygen reacts with carbon to form more carbon monoxide or carbon dioxide gas which bubbles to the top. At the end of this operation, the liquid iron now has a carbon concentration of approximately between 0.02-0.06wt%C. because its total carbon composition is now below 2wt%C, it is now referred to as steel.

However, this liquid steel now contains dissolved oxygen levels of approximately 0.03wt%O_2. Oxygen needs to be removed from the steel because oxygen can create dangerous carbon monoxide boil in the ladle during the casting stage, can react with carbon during solidification and form carbon monoxide gas and cause inner defects such as blowholes, which if in abundance or large enough size, can originate defects in the rolled product (Madias, Moreno and Genzano, 2015). Furthermore, high oxygen levels can create harmful oxide inclusions in the steel product.

Therefore, oxygen levels are decreased via deoxidisation using additions of aluminium, silicon, or a combination of both. This is because aluminium and silicon have high affinity for oxygen and will react to form oxides alumina (Al_2O_3) or silica (SiO2). These oxides then float to the top of the boil where they get absorbed by the slag. However, because these oxides can be small, for example 0.05mm, the upward movement of them to the slag can be slow. Therefore, a combination of deoxidisers is used which create larger oxides that float more easily. Furthermore, stirring the melt with argon, as well as applying an electromagnetic field can be used to facilitate more upwards lift of the oxides (Nutting, Wondris and Wente, 2019).

After deoxidisation, the liquid steel is at a temperature around 1600-1700°C, and oxygen levels have been decreased from around 0.03wt%O_2 to around 0.005wt%O_2. Typical composition of steel at 1600-1700°C is shown in Table 2.

Table 1.14.1. Typical chemistry of liquid steel for high strength can end applications.

Element	**Amount (wt%)**
Oxygen	0.005
Carbon	0.03-0.06
Nitrogen	0.002-0.005
Manganese	0.15-0.3
Silicon	<0.01
Sulphur	<0.01
Phosphorous	<0.01
Aluminium	0.03-0.07

The basic oxygen steelmaking (BOS) process can produce up to 300 tonnes of liquid steel at a time and can take up to 40 minutes.

After the deoxidation step, the liquid steel is poured into a steel ladle (referred to as tapping) with a basic refractory lining. In here the liquid steel is further refined and alloying materials are added to give the steel desired mechanical properties required by the customer. Note, alloying elements added at this stage are most likely to remain in solution form due to the high temperature, i.e., they will not form precipitates.

Examples of alloying materials used are phosphorous, silicon, and manganese, which are added to increase yield strength via substitutional solid solutions strengthening. For example, adding 0.01wt%P increases yield between 7-10MPa, adding 0.1wt%Si increases yield by 10MPa, and adding 0.1wt%Mn increases yield by 3.5MPa.

Substitutional solid solution is when solute atoms (i.e., phosphorous, silicon, manganese etc.) replace or substitute atoms in the solvent metal e.g., phosphorus

replaces an iron atom in the iron lattice. For substitution to occur, there are four factors that determine the ability for a solute atom to dissolve in a metal solvent:

1. **Atomic size factor**. The solute atom size needs to have a radii difference of less than ±15% compared to the solvent atom. A radii difference larger than ±15% will result in the substantial lattice distortions and a new phase will form instead.
2. **Crystal structure**. If solute and solvent atoms share the same crystal structure, then appreciable amounts of solute will dissolve in the solvent.
3. **Electronegativity**. The smaller the difference in electronegativity of the solute and solvent atoms are to one another, the greater the likelihood that they will form a substitutional solid solution. If the difference is considerably greater, the increase in likelihood the solute and solvent atoms will form an intermetallic compound instead.
4. **Valences**. A metal will have more inclination to dissolve another metal of higher valency than one of a lower valency.

Other elements can be added, such as carbon and nitrogen, which also increase the yield strength but via interstitial solid solution strengthening. This is where the solute atoms (i.e., carbon and nitrogen atoms) sit within the iron lattice (in between the empty spaces of iron atoms) and place strain on the iron lattice. The extent to which interstitial atoms will dissolve in iron depends on many factors:

1. **Phase of iron**. Face-centred cubic austenite phase iron can accommodate more carbon atoms compared to body-centred cubic ferrite phase. The maximum solubility of carbon in austenite is 2.14wt%C at 1147°C, compared to ferrite 0.022wt% at 727°C. The reason why FCC iron can accommodate more carbon atoms is because the FCC interstitial positions are much larger, therefore the strain imparted on the iron lattice by the carbon interstitials is much lower.
2. **Size of interstitial**. The smaller the interstitial, the likelier it will fit within the iron lattice.

By adding 0.01wt%C, yield strength is increased by 5MPa, and by adding 0.001wt%N increases yield strength by 5MPa. As mentioned previously, precipitates

such as TiCN increase the strength via precipitation hardening and by restricting grain growth from occurring during processing, resulting in a smaller final grain size.

1.14.3. Continuous casting and slabbing

After the steelmaking process, the liquid steel (of required composition) is then poured from the ladle, via tundish, into an oscillating water-cooled copper mould that is around 900mm deep. Upon contact with the mould, the liquid steel undergoes rapid solidification, emerging from the mould at a speed of 0.9-1.0m/min, producing a solidified slab of typical dimensions 250mm thickness x 0.6-2m width x 8-10m length.

1.14.4. Reheating

After slabs are formed, they are then reheated to temperature approximately 1200°C to soften the slab in preparation for further thickness reduction during the hot-rolling stage.

One tonne of steel requires a theoretical heat input of 0.8GJ. However, due to the frequent and necessary opening and closing of the furnace doors, the actual heat input is closer to 1.4GJ/tonne. If the steel slab has a total carbon composition between 0.03-0.06wt%C, and the reheat temperature is 1200°C, the steel will be in its austenite FCC phase during reheating, as well as throughout the hot-rolling stage over temperature range 1200 to 900°C.

The six lab cast steel chemistries in this body of work have A3 temperature of 860-915°C (according to JMatPro®), therefore the hot-rolling stage occurs only in the FCC austenite phase.

1.14.5. Rough rolling

Rough rolling is employed to shape the slab a bit better and reduce thickness from 230-250mm down to 70-90mm in either a reversing mill or in a tandem mill. During this operation, the temperature drops from approximately 1200°C to 1000°C.

1.14.6.Hot rolling

The slab enters the hot-roll stage at approximately 1000°C with the metallurgy consisting of equiaxed austenite grains. The slab undergoes further compression by rolling. This results in the equiaxed austenite grains becoming stressed, deformed, and elongated in direction of rolling each time the slab passes through a set of rollers. In between sets of rollers, grain nucleation, dynamic recrystallisation, and grain growth occurs.

If grain boundary precipitates (such as titanium carbides) are present and have begun precipitating at austenite grain boundaries, then recrystallisation is delayed until precipitation is complete. This will cause grain growth recovery to be slowed down resulting in a pancaked shaped grain which enter the next rolling stand and rolling force increases.

Each subsequent set of rollers have a smaller roll gap resulting in more reduction in slab thickness. At the end of hot rolling, the slab is now 70mm thick.

1.14.7.Coil box or delay table

After hot rolling, the sheet is held as a coil in a coil box or as a long bar of steel on a delay table to wait for adjustments of roll gaps, roll forces, and drive speeds on the finishing mill (matter of seconds).

Coil box helps retain heat, and permit reversal of ends of bar to entry of finishing mill, thus facilitating temperature homogenisation within the bar.

1.14.8.Finishing mills

After adjustments of roll gaps, roll forces, and drive speeds on the finishing mill have been completed, the steel from the coil box or delay table enters at approximately 1000°C, first through descaling box, then roller set number 1. Each subsequent set of seven rollers (referred to as stands) has a smaller roll gap to further reduce the thickness of the steel plate.

The steel plate emerges from the finishing mill at a speed of 10-20m/s (referred to as exit speed), at 900°C with a thickness of around 1.5-10mm, and a length of 100m.

1.15. Cooling on run out table (ROT)

The strip enters the run-out table at 900°C (referred to as run out table enter temperature), still in its FCC austenite phase, with an initial speed of approximately 10m/s that accelerates to top speed of 20m/s as it proceeds. Water sprays from top, and water jets from bottom, to reduce temperature of strip to range of 500-740°C.

Partial transformation of austenite to ferrite takes place if temperature is reduced to one between the Ar1 and Ar3 transformation temperatures of the steel. This is inside the austenite-ferrite phase range roughly between 727-850°C (exact values are dependent on composition and cooling rate). The microstructure will consist of austenite and ferrite phases.

Full transformation of austenite to ferrite will occur if temperature is decreased below the Ar1 temperature of the steel (e.g., ~727°C) to above the bainite (Bs) and martensite (Ms) start temperatures. Where the microstructure will consist of ferrite phase.

Partial or full transformation of austenite to ferrite will always result in the ferrite grains having a smaller size than the parent austenite that has been hot rolled.

1.15.1. Effects of finishing temperature

The effect of finishing temperature is very important due to its influence on the phase transformation, grain size, and formation of precipitates. To produce a stronger packaging grade steel to be used in easy-open can-ends, a phase transformation, a small grain size, and suppression of precipitation would be beneficial as they can increase the strength.

1.15.2. Effect of ferrite grain size

For example, if the finishing temperature at the end of the hot rolling stage is well above Ar3, for example 1200°C, then the austenite grain size will be larger because of the faster rate of diffusion of the iron atoms. This will result in the final ferrite grain size being larger also.

If finishing temperature is just above Ar3, for example 950°C, then austenite grain size will be smaller due to slower rate of diffusion of iron atoms. The resulting ferrite grain size will be smaller.

At even lower finishing temperatures so that some deformed austenite was unable to fully recrystallise, transformation occurs from a mixture of deformed and recrystallised austenite which results in ferrite having a mixed grain size.

Finally, at even lower temperatures so that all of the austenite is unable to recrystallise, transformation takes place from deformed austenite resulting in a ferritic microstructure within ‘tubes’ of prior austenite.

In parallel to hot deformation, precipitation of TiC or NbC can occur within deformed austenite grains, and upon transformation of deformed austenite to ferrite, ferrite grains will be within ‘tubes’ of prior austenite, but with precipitates throughout microstructure.

1.15.3.Effect of coiling temperature

After cooling on the run-out table, the sheet is then coiled. The coiling temperature refers to the temperature which the sheet is cooled down to when coiling begins. The effect of coiling temperature and cooling rate is important as it affects the final grain size of the product, and the likelihood of precipitation (e.g., carbides and nitrides) occurring.

For example, if the sheet is cooled from ~900°C down to coiling temperatures 700-750°C (requires very little water on the run-out table), then transformation from austenite to ferrite will occur. Partial transformation will occur at the upper temperature range (i.e., 750°C) as some austenite will remain due to 750°C being above the Ar1 temperature for most packaging steels. However, as the coil slowly cools to room temperature this untransformed austenite will eventually transform to ferrite. Full transformation will occur at the lower end (i.e., 700°C) as this is temperature is below the Ar1 transformation temperature for most packaging steel grades. However, cooling to 700-750°C, the ferrite grain size will continue to grow whilst the coil slowly cools down to room temperature. Also, excess carbon

precipitates out of the ferrite as cementite (Fe_3C) which then coarsens because of the higher temperature granting carbon a higher diffusion rate. Excess carbon precipitates out because ferrite (body-centred cubic crystal structure) has a much smaller solubility limit than the face-centred cubic austenite. Furthermore, precipitation of nitrides, titanium nitride (TiN) and aluminium nitride (AlN) occurs in the ferrite grains.

If the sheet is cooled from ~900°C down to coiling temperature 550-600°C (requires more water to be used on the run-out table) then ferrite has little time to grow (as coil slowly cools to room temperature) due to the iron atoms having a smaller diffusion rate. As a result, the final ferrite grain size will be smaller. Furthermore, whilst excess carbon still precipitates to form cementite (Fe_3C), it is much finer due the smaller amount of time it has to coarsen as the coil cools to room temperature. Additionally, due to the rapid cooling rate used, precipitation of aluminium nitride has been suppressed. Therefore, Aluminium and nitrogen atoms remain in solid solution.

If the sheet on the run-out table is cooled to a coiling temperature of 350-450°C (plentiful amounts of water used), then transformation of austenite to ferrite has been suppressed due to the very fast cooling rate. Instead, austenite transforms to bainite, cementite (Fe_3C) remains finely dispersed, and aluminium nitride (AlN) has been totally suppressed.

1.15.4. Interrupted cooling

The cooling procedures above describe a straightforward uninterrupted cooling from runout table temperature to coiling temperature. On the other hand, it is possible to cool to a midway temperature in between the runout table and coiling temperatures. This is referred to as an interrupted cooling regime. It works by initially slow cooling to, and held briefly, at a temperature above the bainitic (Bs) and martensitic (Ms) start temperatures (approximately >600°C) to allow some of the austenite to transform to ferrite. After holding at this temperature briefly, the sheet is rapidly cooled to temperature range 350-450°C to transform the residual austenite to bainite. This cooling regime is not seen in the packaging industry.

1.16. Important hot rolling parameters for packaging grade steel for easy-open ends applications

Table 1.16.1 summarises the important hot-rolling parameters for packaging grade steel used in easy-open end applications. It is also the hot rolling history of the six casts provided by the sponsor company.

Table 1.16.1. Important hot-rolling parameters for high-strength packaging steel applications.

parameter	**Desired level(s)**	**Notes.**
Reheat temperature	1250°C	
Rough rolling/milling	30mm gauge x 120mm width	
Reheated temperature	1220°C	To completely austenitise the material
Reheat time	40 minutes	
Further reduction	2.0mm gauge (~80% of material, 3.0mm gauge (~20% of material)	Reduction in four steps, 30mm→20mm→10mm→4mm→2mm (~80% of material); 30mm→20mm→5mm→3mm (~20% of material)
Hot rolling finishing temperature - FRT(in)	980±30°C	
transport	3s	
Hot rolling finishing	950±30°C	

temperature - FRT(out)		
Run-out table temperature/ cooling (in)	910±30°C	
Run-out table rate to coiling temperature	-80°C	
Run-out table temperature/ cooling (out)/ coiling temperature	590°C±20°C	Because cooled from 910°C to 590°C, it is presumed aluminium nitrides will not be present. Therefore, no grain refining effect (grain strengthening), but solid solution strengthening.
Cold rolling	2.0mm→0.2mm gauge (for the 80% material)	No cold rolling applied to the 3.0mm gauge (other ~20% material)
Cut all material for HDAS test	250mm long, full width	

1.17. Pickling of strip products

During hot rolling, the steel surface is exposed to atmospheric gasses. These gasses oxidise the surface of the steel causing a scale to build up. This scale is removed via the process of pickling. This involves immersing the steel in a 7%wo sulphuric acid (H_2SO_4) or hydrochloric acid (HCl) solution in water at 70-90°C. Pickling can be enhanced using ultrasonic baths. The result is a clean and scale free steel coil weighing approximately 30 tonnes. For applications using hot rolled coils (automotive, shipbuilding, bridgebuilding etc.), here the coil is ready for sale. The hot rolled market represent 30% of the total production for a major UK strip

producer, equivalent to 7 million tonnes of hot rolled strip product output for said producer.

1.18. Cold rolling

Typically, pickled hot rolled products are cold rolled by 50-70% reduction in 5 stand, 4 high rolling mills to 0.7-1.5mm thickness for strip applications such as motor cars and domestic applications. However, for tinplate applications (i.e., packaging, food, aerosol container, easy-open ends), the reduction is much more, by 85-90% reduction to 0.15-0.30mm.

Cold rolling results in ferrite microstructures that are elongated in the direction of rolling. As a result, the steel at the end of cold rolling exhibits anisotropic properties when measured 45° and 90° to the rolling direction in a tensile test, due to the anisotropic distribution of the plastic strain of cold rolling.

Importantly, the strength of cold rolled steel is much higher than that of its parent hot-rolled material. This sharp increase in strength is due to work hardening causing an increase in the dislocation density within the material. However, ductility of the steel becomes very poor.

To recover some ductility, the steel is then subjected to an annealing process.

1.19. Annealing

There are two choices of annealing processes to use in packaging steel. Batch annealing and continuous annealing.

1.19.1.Batch annealing

Batch annealing is very good at recovering a lot of ductility and formability in the steel which makes it the suitable annealing process to prepare steel for drawn and redrawn (DRD) or drawn and wall ironed (DWI) products. DRD and DWI products are used in the can bodies. Batch annealing consists of stacking three to four coils in a furnace and enclosing them with a seal, with an atmosphere consisting of 95% N_2 + 5%H_2, or 100% H_2 getting pumped into the furnace to prevent oxidation of the coils, while the furnace is being heated by a mixture of natural/ coke oven gas. However, the batch annealing process can up to ten days from start to finish due to the slower heating rates (20-30°C per hour), longer holding times at soak temperatures (6-24hours at 650-710°C), and slow cooling rates used (slow furnace cooling). See Figure 1.19.1 for a schematic of the batch annealing process.

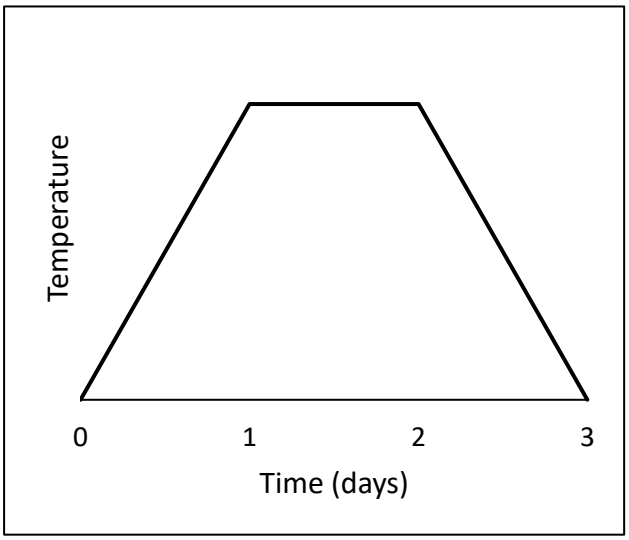

Figure 1.19.1. Schematic of the batch annealing process.

Furthermore, whilst ductility and formability are recovered to a desired level (due to the replacement of heavily cold rolled ferrite grains with equiaxed ones via recovery and recrystallisation processes), the yield and ultimate tensile strengths are too low for easy-open can end applications. This is because the slower heating rates, longer soak times and higher soak temperature results in a larger ferrite grain size.

Therefore, batch annealing is not used to manufacture easy open can ends and will not be considered as an annealing process in this project.

1.20. Overview of the continuous annealing for easy-open end applications

On the other hand, the continuous annealing process is much faster, taking between 6minutes (if line speed of 200mpm is used) and up to 6 minutes (if line speed is set to 450mpm) in total (i.e., the heating, soak, rapid cooling, and over aging steps). The process includes welding several cold rolled coils end to end, cleaning them, then feeding into a continuous annealing furnace consisting of pre-heat, anneal/soak, rapid cool, and over ageing sections (see Figure 1.20.1).

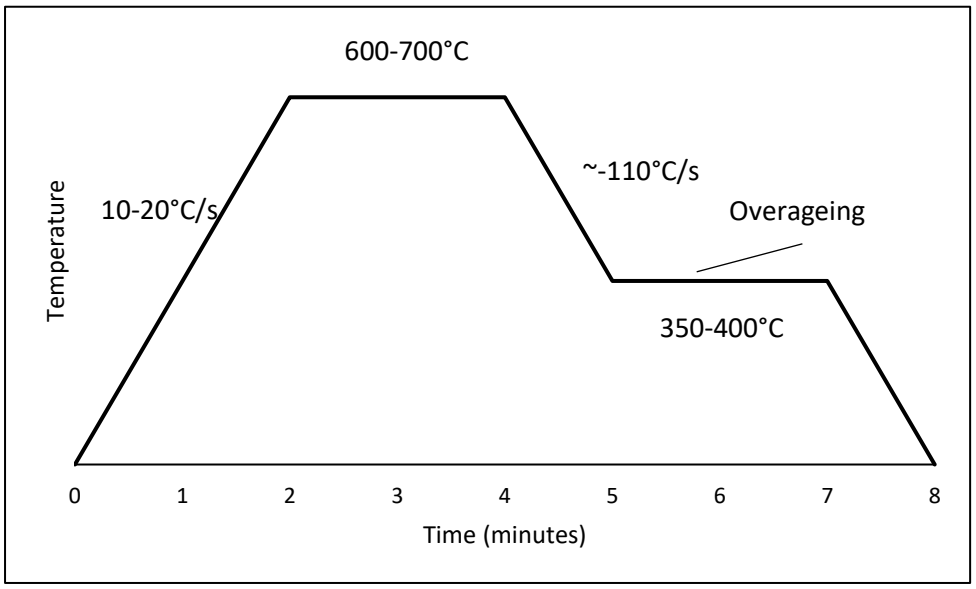

Figure 1.20.1. Schematic of the continuous annealing process.

In continuous annealing, the line speed is set to a specific speed in the range of 200-450mpm, for example if 450 metres per minute is used, the welded coils travel through each section of the line at 450mpm. Therefore, setting the line speed fixes the heating rate, soak temperature, and the overall annealing time.

In the continuous annealing process for packaging grade steel, heating rates are greater (approximately 8.2-18.5°C/s), cooling rates are greater (approximately 48.9-110°C/s), soak times are shorter (approximately 53-120 seconds), yet recrystallisation must take place and recrystallised grains must grow to a sufficient size so that continuous annealed steel has sufficient amount of formability (implied that an elongation value of ~35% is required in as-annealed condition for high strength easy-open can ends). As with the batch annealing process, the rates of recovery and recrystallisation are dependent on heating rate and soak temperature. The coil dwells in the soak section at 615-670°C, for a long enough time for total recrystallisation to occur.

After the soak section, the coil is subjected to a slow cool from around 635°C to around 600°C at a cooling rate of around 7°C/s, followed by a rapid cool using high pressure air cooling (cooling rate of around 110°C/s) to approximately 400°C (or 320°C) before entering the overaging section, where the coil is held at a temperature of 400°C for 60-135s to precipitate excess solute atoms such as carbon and nitrogen. Upon exiting the overaging section, the coil is air cooled to room temperature at cooling rate of around 37.5°C/s. Compared to the batch annealing process, continuous annealing results in a finer ferrite grain size which is desirable for producing a higher strength steel for easy-open ends.

According to (Abe and Satoh, 1990), Continuous annealing has the following advantages:

- More homogeneous mechanical properties along the length and width of coils compared to batch annealed coils.
- Can reach higher soak temperatures and thus allows for greater product development.

1.21. Important parameters in the continuous annealing process

Important parameters to consider during the continuous annealing process for easy open ends are the:

1.21.1. heating rate

In general, a slow heating rate of say 1°C/s will allow plenty of time for deformed ferrite grains to grow (after recovery and recrystallisation have occurred), resulting in a larger ferrite grain size. According to the Hall-Petch relationship, an increase in ferrite grain size will lower yield and tensile strength (whilst increasing the ductility). On the other hand, a high heating rate, such as 18.5°C/s (used in Trostre for easy-open end application steel), increases the yield and tensile strength of steel. This is for several reasons. Firstly, a high heating rate shortens the time it takes for steel to reach the soak temperature, therefore the overall time the steel is at temperatures that enable growth to occur is reduced, thus grain growth is minimised, and grain size is smaller.

To clarify, we want to avoid a large ferrite grain size for easy-open ends and aim for a grain size of around 5µm for the as-annealed condition (and 2.7µm for the 5% double reduced condition).

Secondly, heating rate influences the recrystallisation start and finish temperatures. If heating rate is high enough, it can increase the recrystallisation start and finish temperatures. If heating rate is high enough it can increase the recrystallisation start and finish temperatures to above the Ac1 transformation temperature. The influence of heating rate on recrystallisation start and finish temperatures can be exploited for our gain. For example, a lot of research has shown how ultra-rapid heating rates (heating rate above 200°C/s) to intercritical soak temperatures has resulted in a refined microstructure.

There are many terms for this technique; rapid annealing, ultra-rapid annealing, flash annealing etc. but essentially all meaning using heating rates much higher than conventional heating rates as used in continuous annealing.

1.21.2. soak temperature.

The soak temperature is very important because it determines whether processes have the required activation energies to occur. Processes such as:

- recovery
- recrystallisation
- grain growth
- Secondary phase formation
- formation of precipitates/dissolution of precipitates.

Soak temperatures below the Ac1 temperature (i.e., below ~723°C) are referred to as sub-critical annealing. Soak temperatures above the Ac1 and below the Ac3 temperatures are referred to as inter-critical annealing.

1.21.3. cooling rate

Firstly, the cooling rate is important because it determines whether elements in solution (e.g., titanium and nitrogen) stay in solution during the transition from soak section to over aging section. If heating is too slow, then elements you want to stay in solution (i.e., nitrogen) can bond with other elements (e.g., titanium) to form a precipitate (e.g., titanium nitride) thereby negating the strengthening effect (i.e., solid solution strengthening) of nitrogen in solid solution form. When continuously annealing packaging grade steel for easy-open end applications, we want a high enough cooling rate, i.e., a minimum of -48.9°C/s that prevents the bonding of nitrogen to other elements it wants to bond with.

Secondly, the cooling rate determines what secondary phases will be formed and their volume fractions when cooling from a soak temperature above the Ac1 transformation temperature. On quenching, austenite formed during intercritical annealing (soak temperature between Ac1 and Ac3 temperatures) transforms to the secondary phase, and maybe some retained austenite.

The volume fraction of secondary phase is dependent on the volume fraction of austenite generated during the soak stage. The volume of austenite generated during the soak stage is dependent on the carbon content and soak temperature.

To achieve a high-strength packaging grade steel that is stronger than the current grades Trostre makes, heat treatments that produce a secondary phase in the final microstructure should be attempted and tested. However, the Continuous Annealing Production Line (CAPL) in Trostre steelworks currently has a section whereby the steel is subjected to a conventional gas jet cooling (a slow cool section) after the soak stage and prior to the high gas jet cooling (rapid cooling stage).

1.21.4. Overageing stage overview

The overageing stage follows the soak stage and precedes the final cooling to ambient temperature. Its purpose is to reduce solute carbon levels by taking supersaturated solutions and induce carbon precipitation via precipitation of Fe_3C carbide (cementite). The consequence of this is the annealed steel is more resistant to ageing, and no longer susceptible to strain ageing. This reduces the yield and tensile strengths but increases ductility of steel.

1.21.4.1. Overage temperature

The over aging temperature determines whether excess solute atoms such as carbon and nitrogen precipitate, by ensuring they have enough energy to overcome barriers that prevent them from precipitating. If the over aging temperature is too low, excess carbon and nitrogen will not precipitate. In easy-open end can applications, we want to keep as much carbon and nitrogen in solid solution as possible to exploit their solid solution strengthening effects, and strain aging.

When a large amount of carbon in solution is present in annealed steel, the steel is prone to ageing even at ambient temperatures. Aging is when solute carbon diffuses through steel and surrounds dislocations, resulting in the reduction of the ductility of steel, but increase in yield and tensile strengths. During the continuous annealing stage, rapid cooling ensures solute carbon remains in solution. Therefore, it seems logical that for easy-open ends, the removal of the overageing stage can increase the

yield and tensile strength, at the expense of ductility. However, removal of the overageing step is not possible with the Trostre annealing line. The alternative is to use as low an overageing temperature as possible, with 300-340°C being the lowest possible range (400°C is what Trostre uses for high strength easy-open end steel).

1.21.4.2. over ageing time

Over aging time is important because it determines how much excess carbon and nitrogen will precipitate. The longer the overageing time, the more excess carbon and nitrogen that will precipitate out. In steel for easy-open can end applications, an overageing time of 60-135s (depending on the line speed) is typically used.

1.21.4.3. Ageing process

The over ageing step in continuous annealing induces the process called *ageing*. Ageing is when dissolved interstitial atoms such as carbon and nitrogen diffuse through the lattice (e.g., ferrite, bainite, martensite etc.) and precipitate at dislocations (natural or generated), forming an atmosphere of carbon, nitrogen, carbides, nitrides. Natural dislocations are those present in the microstructure from the casting stage, and artificial dislocations are those generated when steel has been strained, i.e., through cold rolling, skin passing, double reduction etc.

When solute atoms have precipitated at dislocations, strength increases and ductility decreases. This is because dislocation movement is impinged. As a result, a greater tensile force is required to initiate dislocation movement again and is shown in a tensile test as an increase in yield and tensile strength.

Ageing occurs naturally when steel is left at ambient temperatures. Moreover, it can occur artificially when steel enters the over ageing section of the continuous annealing line. Ageing can also be induced via a procedure known as bake hardening, a procedure typically seen in low carbon automotive steel for car body applications, whereby strained (cold rolled) steel is subjected to a heat treatment consisting of 180°C soak for around 20 minutes. Bake hardening positively exploits

strain ageing and is like the retort process used to sterilise food in closed cans which similarly uses temperatures of 200°C for a period of 20 minutes.

An additional effect of ageing is that it produces a yield point elongation (YPE) in the tensile test curve of an aged steel, and the tensile curve is characterised as having a lower and upper yield point. When a steel exhibits a YPE, both lower and upper yield points are quoted.

This YPE is present after the continuous annealing process (due to the over ageing section) but is removed when work is done to the coil, such as double reduction (as seen in steel for easy-open ends). This is why temper rolling (usually 0.5-2% strain or strain exceeding luders strain) is the final step used on single reduced packaging steel used in other applications.

Because ageing involves the diffusion of solute carbon and nitrogen atoms and the presence of dislocations, the strength increase due to ageing can be enhanced if the amounts of solute carbon and nitrogen are increased, so that more solute carbon and nitrogen can precipitate on dislocations. High amounts of solution carbon and nitrogen originates when high cooling rates and low coiling temperatures are used at the end of the hot rolling process, to prevent carbon and nitrogen from combining with their precipitate forming elements. Furthermore, solute carbon and solute nitrogen can be kept high if high cooling rates are used after intercritical annealing at around 850°C or more is used during the soak stage in continuous annealing. Like the high cooling used at the end of hot rolling, high cooling after soaking will prevent carbon and nitrogen from combining with precipitate forming elements and keep in solution. Additionally, greater amounts of carbon and nitrogen can be used in the base composition in addition to what was mentioned above. However, the base composition of carbon and nitrogen in packaging steel for easy-open ends is already at its maximum allowable numbers, and increases are unlikely.

Although ductility is reduced when ageing occurs, it has been shown to increase the strength yield strength by ~50MPa. It has been stated from an industrial contact that steel for easy-open ends must have a minimum total elongation of **3% ductility** (because of the rivet required to attach the ring pull to) for a **550MPa strength steel**. Therefore, as long as the ductility loss due to ageing does not result in total elongation dropping below 3%, it should be fine.

The yield strength of continuous annealed packaging grade steel can be as low as 330MPa (when single reduced), and as high as 620MPa (when double-reduced). Although it should be mentioned that competitors are making products with higher yield strength values and with smaller tolerance ranges.

1.22. How to alter continuous annealing process parameters

1.22.1. Heating rate

Conventionally, the heating rate can be altered by increasing the temperature of the heating section, where heating rates are in the region of 10-20°C/s. A method to achieve higher heating rates would be to attach an induction coil heating system in the heating section where the coil passes through the inside the of the coil. In doing so, the heating can be increased up to 1800°C/s . However, Tata steel Trostre do not currently use an induction coil heating system.

1.22.2. Soak temperature

The soak temperature is controlled by the amount of natural /coke oven gas is being burned. Current design limits the maximum soak temperature of the continuous annealing line in Trostre is approximately 650°C.

1.22.3. Cooling rate

In Tata steel Trostre, the cooling rate can be altered by opening or closing banks of jet cooling air in the cooling section. By opening banks (up to a total of three banks) the cooling air is split between multiple banks resulting in a lower air pressure passing over the steel coil, and thus a lower heating rate is achieved. On the other hand, by closing all air cooling banks besides one, forces the air through one

opening. This results in a higher air pressure passing over the surface of the strip, and therefore a higher cooling rate is achieved.

1.23. Skin passing, temper rolling and double reduction

Skin passing, temper rolling, and double reduction are the final steps taken in cold rolled steel strip for easy-open ends and take place after annealing has been conducted. They all work on the principle of applying different degrees of cold deformation to annealed steel strip using rollers.

1.23.1. Skin passing

Skin passing is when an extremely small amount of cold deformation is applied via a set of rolls to an annealed strip of steel. It is mainly used as a flattening process to ensure the surface of the steel strip is flat. It is not a process applied to easy-open ends.

1.23.2. Temper rolling and double reduction

Like skin passing, temper rolling, and double reduction are cold deformation procedures applied to annealed strip to give flatness, but involve greater amounts of cold reduction, 0.8-1.5% for temper rolling, and up to 38% for double reduction. However, for high strength steels used for easy-open end applications, double reduction is the only cold deformation procedure used. Typical double reductions are in the region of around 12-13% for TH620- 3364 grade, and 28% for TH62N, 346x grade. The amount of double reduction to apply is dependent on the mechanical properties of the steel in its as-annealed condition, as it changes the microstructural and texture properties of the annealed steel strip, affecting its ductility. Double reduction is necessary to obtain smaller strip thickness.

1.23.3. Effect of double reduction on yield point elongation (YPE)

Furthermore, double reduction (and temper rolling) is used to remove the yield point/ yield point elongation (YPE) seen in the tensile test curve of annealed steel. It does this by changing the yielding behaviour from discontinuous to continuous. Tensile testing of strip in its annealed condition results in the formation of visible Lüders bands on the surface of the tensile test sample. In practical terms, if this steel in its annealed condition was used in easy-open ends, upon stamping to give the strengthening ridges seen in can-ends, or opening of the can, such discontinuous yielding would occur as soon as the elastic strain is exceeded, and plastic straining occurs. As a result, an effect like Lüders bands would occur as undulations or ripples on the surface of the can-end. These undulations/ripples are referred to as 'stretcher-strain marks' which adversely affect the appearance of the can-end. By removing the yield point/yield point elongation (YPE), removes these stretcher-strain marks.

1.23.4. Effect of double reduction on grain orientation

Furthermore, like cold rolling, double reduction effects the orientation of grains by elongating them in the direction of rolling. This causes anisotropic behaviour. However, the magnitude of this elongation and anisotropy is less than that seen in cold rolling.

1.23.5. Advantages of double reduction

The advantages to using double reduction are:

- **It increases yield and tensile strength**. Because double reduction is a form of cold working, it must be remembered whilst it increases strength, it simultaneously decreases ductility. Therefore, it is important that the steel strip must have an elongation value (A50) of at least 5% in all-directions after a double reduction procedure.
- **Permits further gauge reduction**. This means that more can ends can be obtained per coil.

- **Removes the yield point/ yield point elongation**. Changes the yielding behaviour from discontinuous to continuous.
- **Reduce the susceptibility of lattice atoms to slip**. Double reduction produces new dislocations into the material, where upon meeting other dislocations reduces the ability of dislocation movement. They create distortion in the lattice structure. Overall, a stronger steel is produced, with a greater yield strength and ultimate tensile strength. It is important to note that increasing the amount of reduction incrementally does not translate to the same increment magnitude to the yield and ultimate strengths. For example, as cold reduction is increases, the rate of strengths increase reduces.

1.24. Blackplate

After double reduction sheet has been conducted, the strip can be coiled. At this stage, the material is termed as black plate.

1.25. Tin plating, chrome plating

Afterwards the coil then has a tin, or a chrome coating applied to it to prevent oxidation of the can.

1.26. Lacquer/Polymer coating

After the metallic coating has been applied, the interior surfaces of the can have a polymer coating applied to provide a barrier in between the contents (e.g., food and drink) and the tin/chrome coating.

For the purposes of this project, it is assumed that the coating (tin/chrome or polymer) has no significant impact on the mechanical properties of can-ends.

1.27. Packing and delivering

Finished steel strip coils are delivered to customers for shaping into can bodies or stamping into can ends. The can bodies are filled with product and can ends are attached.

1.28. Retorting process

1.28.1. What is it?

Once the cans are filled (with either raw or cooked food) and ends are attached to form a hermetically sealed (airtight) container, the sealed cans are placed in a pressure cooker, then subjected to the retorting process. The retorting process is used to reliably sterilise the can contents (low acid foods) via the application of heat to prevent spoilage and extend the shelf life, enabling the can contents to remain safe and wholesome up to many years at room temperature without the use of additives or preservatives. Spoilage is prevented because the heat kills commonly occurring microorganisms such as Clostridium botulinum.

The retort process varies but the typical industrial retort process in food canning **is 200°C for 20 minutes**. This temperature is used to reliably ensure that low heat resistance microorganisms (ones that becomes inactivated when exposed to temperatures 75-95°C), and the more heat resistant bacterial spores (inactivated at temperatures between 110-150°C) are killed (Teixeira, 2009).

It is important the can end can has high enough strength to withstand the pressures experienced throughout the retort process, whilst still being easy to open, and enough ductility to undergo seaming and rivet forming operations.

1.28.2. Why is the retort process important to consider in this project?

The retort process is the final heat treatment process the easy-open end will undergo. As mentioned previously, like bake hardening, it consists of a 200°C soak for 20

minutes and will modify the deformation behaviour of the can end by changing it from continuous deformation to discontinuous deformation.

Therefore, to give an accurate representation of these lab casted steel samples will behave to the actual consumer, the samples used in this body of work should be heat treated at 200°C for 20 minutes after having been double reduced.

1.29. Closing remarks

The performance of tinplate/chrome plate is dependent on several factors such as the base composition, casting method, hot-rolling and cold rolling procedures used, annealing parameters utilised, amount of temper rolling/double-reduction used. For the purposes of time and material resources, this project will focus on the annealing and double reduction stages to see how parameters within these stages can be modified to bring about the creation of a higher strength steel for easy-open can ends applications.

2. Literature review

2.1. Ultra-rapid annealing (URA)

Annealing of cold worked low carbon steel is done to improve the microstructural and mechanical properties, as well as facilitating the conditions to enable a second application of cold rolling, i.e., double reduction, to reduce the gauge further, and further improve mechanical properties.

A lot of research on severely deformed (via equal channel angular pressing, high pressure torsion, or constrained groove pressing) low carbon steel has been conducted but have used conventional heating rates (e.g. 5°C/s) (Shin *et al.*, 2000), (Park and Shin, 2002), (Ivanisenko *et al.*, 2003), (Khodabakhshi and Kazeminezhad, 2011).

2.2. Problem with conventional heat rates

However, conventional heating rates are a problem when trying to produce a refined microstructure because no grain refinement occurs. This is because the slow heating rates allow plenty of time for deformed ferrite grains to form recrystallised grains and just allows thermal stability of **severely** deformed grains.

2.3. What is ultra-rapid annealing (URA)

However, ultra-rapid annealing (URA), a process whereby heating rates greater than those seen in conventional annealing are employed, can be used to refine the microstructure of severely deformed low-carbon steel. Currently, the research into URA of **severely deformed** low carbon steel is relatively limited. Also, research into URA of **cold rolled** low carbon steel is limited.

2.4. Benefit of ultra-rapid annealing (URA)

2.4.1. in severely deformed material

The final grain size is influenced by the condition of recrystallisation, which itself is influenced by heating rate. A high heating rate has been shown to enable recrystallisation to occur with a high nucleation rate and increased kinetics (Wang *et al.*, 2011), (Gorelik, 1981).

2.4.2. In deformed (cold-rolled) materials

On the other hand, in **deformed** steels (e.g., 70% cold reduction), conventional heating rates (0.1-10°C/s) has shown recrystallisation to start and finish before the Ac1 transformation temperature is reached. This leads to a fully recrystallised microstructure, but not a refined one.

However, heating rates above conventional (like in ultra-rapid annealing), increase the ferrite recrystallisation temperature to higher temperatures near or above the Ac1 transformation temperature (Gorelik, 1981), (Massardier *et al.*, 2010a), (Muljono, Ferry and Dunne, 2001), (Xu *et al.*, 2014a), (Li *et al.*, 2013), (Azizi-Alizamini, Militzer and Poole, 2011), (Zheng and Raabe, 2013), (Stockemer, Vanden Brande and Brande, 2003). This retardation effect increases with higher heating rates to such an extent that if heating rate is high enough, can delay the recrystallisation temperature to intercritical temperature ranges (between Ac1 and Ac3 transformation temperatures), that produces a **stronger interaction** between recrystallization and transformation of eutectoid ferrite to austenite (Huang, Poole and Militzer, 2004), (Li *et al.*, 2013), (Azizi-Alizamini, Militzer and Poole, 2011), (Zheng and Raabe, 2013).

If recrystallisation temperature has been retarded to **near** the **Ac1**, this creates a scenario where deformed non-recrystallized ferrite grains can be present as transformation begins during the intercritical temperature range (Chowdhury, Pereloma and Santos, 2008). Therefore, the activation of recrystallisation and transformation occurs with both processes interacting with each other, and the kinetics of recrystallisation is influenced by this interaction (Lesch *et al.*, 2007), (Lesch *et al.*, 2006), (Karmakar, Ghosh and Chakrabarti, 2013).

2.4.3. URA effects on recrystallisation

This interaction is important and leads to a more refined microstructure due to recrystallisation kinetics being increased in intercritical temperature ranges when compared to subcritical (below Ac1) temperature ranges (Karmakar, Ghosh and Chakrabarti, 2013), (Chbihi, Barbier and Germain, 2014).

2.4.4. URA effect on transformation

Aside from recrystallisation kinetics, transformation kinetics are also accelerated when URA within intercritical temperature ranges. Transformation kinetics are:

- Shown to **increase with heating rate** (Meng, Li and Zheng, 2014).
- Shown to increase when there is an **interaction between recrystallization and transformation** (Xu *et al.*, 2014b), (Li *et al.*, 2013), (Zheng and Raabe, 2013), (Meng, Li and Zheng, 2014), (Mohanty, Girina and Fonstein, 2011).
- Affected by the **condition of recrystallisation state of ferrite during transformation**. Presence of deformed non-recrystallized ferrite in the intercritical range accelerates rate of austenite transformation (Zheng and Raabe, 2013; Xu *et al.*, 2014a), (Peranio *et al.*, 2010; Mohanty, Girina and Fonstein, 2011; Karmakar, Ghosh and Chakrabarti, 2013; Chbihi, Barbier and Germain, 2014).

All three conditions described above are possible with URA to intercritical temperature range of **severely deformed** low carbon steel.

However, it has been mentioned (Lesch *et al.*, 2007), (Lesch *et al.*, 2006), that grain refining of deformed steel during URA is not possible for all compositions, particularly ones that contain **microalloying elements** that **influence** the **interaction behaviour** (i.e. titanium and niobium) which may inhibit grain refinement.

However, the compositions of the lab casted grades in this body of work do not contain microalloying element niobium, so interaction between recrystallisation and transformation should not be negatively affected, thus not inhibiting further grain refinement. However, five of six lab casted chemistries contain relatively small

quantities of titanium in amounts 0.01-0.02wt%Ti so could influence the interaction behaviour but could be a negligible effect. Additionally, tensile results in work (Lesch *et al.*, 2007) showed that HSLA grades (containing titanium and niobium) gave highest proof stress (Rp0.2) values of samples used in that study, i.e. **508** and **537**MPa. Although, these values are still below the target value for Rp0.2 (650-750MPa) in this project, those samples were **not subjected to a double reduction procedure**.

2.4.5. Role of carbides in grain refinement during intercritical annealing using ultra rapid heating rates

The role of carbides in grain refinement during intercritical URA has been discussed by (Massardier *et al.*, 2010a). At intercritical ranges there is competition between coarsening of primary ferrite grains and austenite formation. Carbides have been identified in having a role in inhibiting primary ferrite grain coarsening. This effect allows maximum refinement of final microstructure to occur. Given the simulated low coiling temperatures of the six lab casted samples in this body of work, it is presumed that carbides are not present during the beginning of simulated CAPL annealing cycles, and it is unknown if they will form during the ~51s soak time.

2.5. Gaps in URA literature

Wide soak temperatures (sub-critical & intercritical) and looking at both microstructural and mechanical properties

Published work (Ferry, Muljono and Dunne, 2001; Stockemer, Vanden Brande and Brande, 2003; Álvarez *et al.*, 2005; Massardier *et al.*, 2010a; Azizi-Alizamini, Militzer and Poole, 2011) looking at URA of deformed low-carbon steel strip is limited in that it either does **not** look at **wide soak temperature ranges** that include both **sub-critical** and **intercritical**, or simultaneously studying the effect on **microstructure** and **mechanical** properties.

90% reduced material

Furthermore, the effect of **strain** and **consequent stored strain energy** during URA is little discussed but is a big influence on grain refinement (Mohanty, Girina and Fonstein, 2011; Karmakar, Ghosh and Chakrabarti, 2013; Chbihi, Barbier and Germain, 2014). When the amount of stored strain energy is increased (due to greater amounts of deformation), the **barrier** to **energy** for **austenite nucleation** is **decreased** (Peranio *et al.*, 2010), which **accelerates** both **recrystallisation and austenite transformation kinetics**. However, the work mentioned in (Peranio *et al.*, 2010; Mohanty, Girina and Fonstein, 2011; Karmakar, Ghosh and Chakrabarti, 2013; Chbihi, Barbier and Germain, 2014) looks at cold rolled **deformed** steel samples that have been reduced in ranges 50-80% to thicknesses 1.75mm, 1.2mm. and 0.7mm respectively. High-strength packaging steels for can-end applications undergo cold reductions greater than 80%, typically around 90% reductions. The lab-casted material in this body of work has undergone cold reductions of **90%** (from 2mm to 0.2mm).

Packaging grade steel chemistry

Additionally, the literature I have seen uses automotive HSLA chemistries seen in applications for deep drawability. I have not seen any literature that uses high strength steel packaging grades for can end applications. Additionally, I have not seen samples that use the exact chemistries in my inventory, either they are similar but contain different quantities of elements (e.g. three times the manganese content – (Lesch, Álvarez and Bleck, 2007) or contain elements not present in my samples such as niobium, chromium (Lesch, Álvarez and Bleck, 2007)(Álvarez *et al.*, 2005) (Massardier *et al.*, 2010b) respectively.

Microstructural and mechanical properties after over ageing and double reduction

I have not seen published results of microstructure and mechanical properties after over ageing and double reduction has been performed.

Gaps in literature summary

To summarise, I have not seen published results including all below:

- URA on packaging grade steel **compositions**
- Microstructural and mechanical properties of (packaging grade) steels after **over ageing** (400°C for 50s) AND **double reduction** AND **ageing** (200°C for 20 minutes) have been performed.

Example of literature looking at ultra-rapid annealing (URA) to sub-critical and intercritical temperatures in severely deformed low-carbon steel.

A URA study (M. A. Mostafaei and Kazeminezhad, 2016) looking at effects of different heating rates (0.3°C/s, 75-1800°C/s) to soak temperatures 250-910°C has been done on severely deformed (via 2 passes of **constrained groove pressing (CGP)**, low carbon steel with chemistry 0.05 C, 0.2 Mn, 0.011 P, 0.007 S, 0.055 Al, 0.04 Ni (All in %wt.) in the form of sheet.

Findings include conventional and subcritical URA cannot lead to a fully refined microstructure (or a microstructure as refined as one annealed using higher heating rates to inter-critical temperatures), it was mentioned that this was due to recrystallisation **starting and finishing prior** to the **Ac1** temperature being **reached** (for samples conventionally heated to an intercritical temperature range), and a **shifting** of the **start** and **finish recrystallisation temperatures** to **intercritical** temperatures (for the subcritical URA tests).

Why does URA increase hardness in intercritical soak temperature annealing?

Furthermore, URA using a 200°C/s heating rate to **little above the Ac1** temperature (i.e., 730°C) causes **fully recrystallized** microstructure. This was because of the interaction of between recrystallization and transformation. This interaction occurs because **dispersed austenite** phases generated in the intercritical temperature range **provide preferred sites** for **eutectic ferrite** (formed below Ac1) **recrystallisation** and **pin** the refined recrystallized ferrite to **prevent** it from **coarsening** (see Figure 2.1 for a schematic of the microstructure evolution during Ultra-Rapid Annealing). URA to higher intercritical temperature led to formation of larger fraction of austenite which led to fine second type ferrite (α_2) generating during cooling. Figure 2.2 shows the relationships between the mechanisms involved during inter-critical annealing using a rapid heating rate.

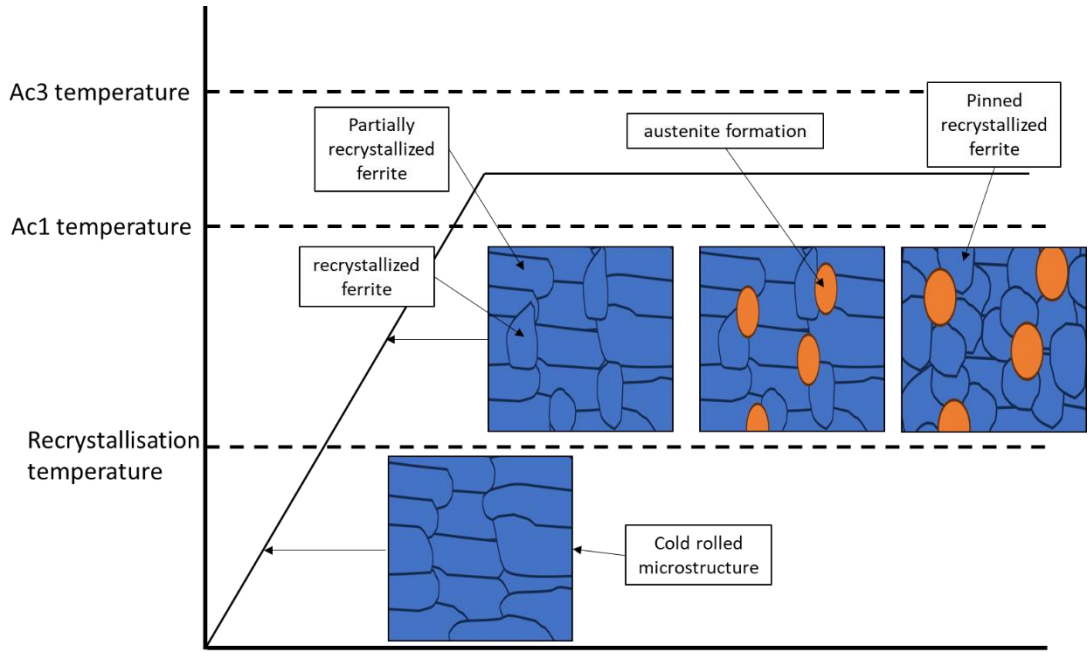

Figure 2.1. Evolution of fully refined microstructure of steel during Ultra-Rapid Annealing (URA).

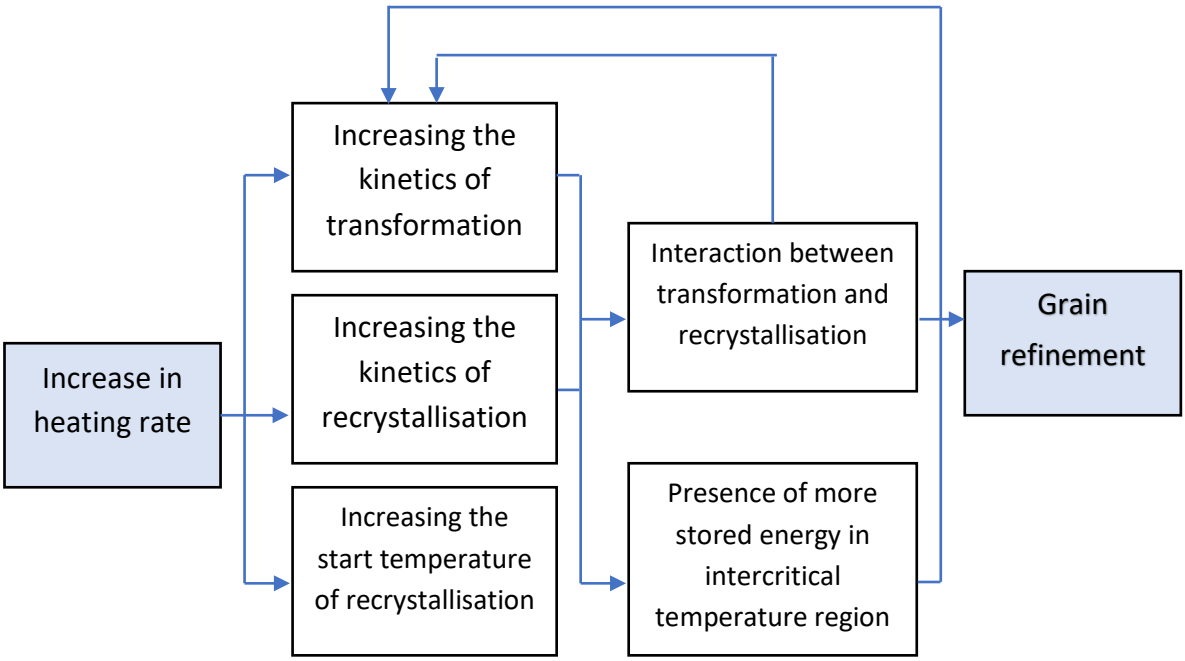

Figure 2.2. Relationships between the mechanisms involved in ultra-rapid annealing (URA) of low carbon steel.

URA has been shown to increase hardness values of low carbon steel during as soak temperature was increased during subcritical annealing (M. A. Mostafaei and Kazeminezhad, 2016) see Figure 2.3. For example, hardness increased from ~175 HV30kg (at ~450°C) to 225.3 HV30kg (at 660°C). This contrasts the effect seen in the same study, when conventionally heating rate (0.3°C/s) to sub-critical temperatures saw a reduction in hardness with temperature, to values the same as hot-rolled and normalised material (pre constrained groove pressing).

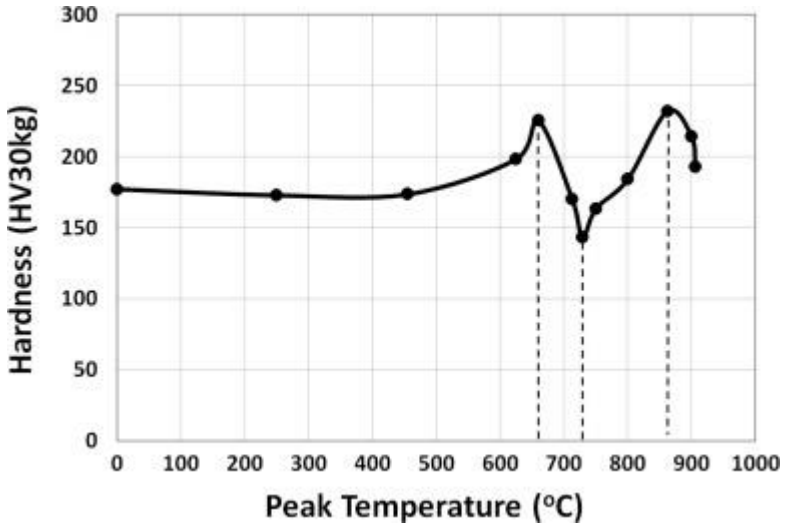

Figure 2.3. Hardness variation during URA of 2 passes CGPed steel with the heating rate of 200 °C/s.(M. A. Mostafaei and Kazeminezhad, 2016)

Why does URA increase hardness in sub-critical soak temperature annealing?

The reason why URA increases hardness in **subcritical** temperatures is said to be due to **insufficient time** for formation of **carbides**, resulting in a greater amount of carbon remaining in solid **solution** in the matrix (Massardier *et al.*, 2010a).

The hardness then **decreased** with temperatures **around Ac1** because of **accelerated recrystallization**, from **225.3 HV30kg** (at 660°C) to a **minimum** of **~140 HV30kg** (at **730°C**). However, hardness increased again to a maximum of **232.0 HV30kg** at **870°C** in higher intercritical temperatures because of formation of **harder phases** (carbide, martensite and bainite) upon cooling of austenite.

Summary of URA effects on mechanical properties

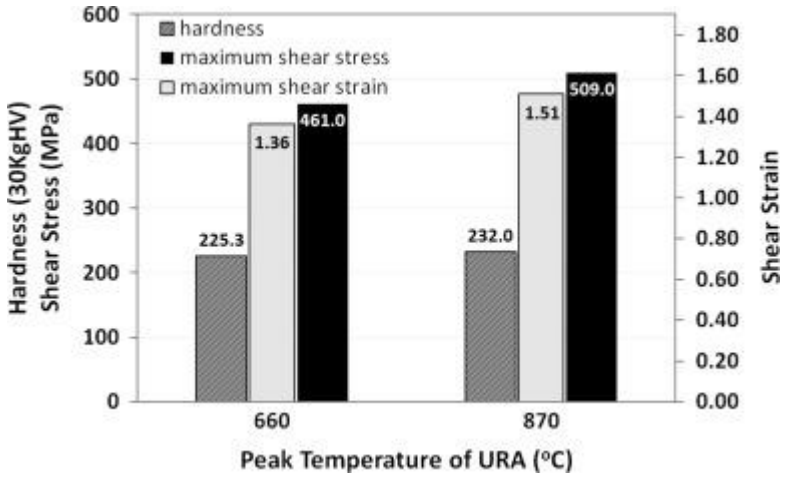

Figure 2.4. Comparison of hardness, strength and ductility between the samples ultra-rapidly annealed by 200 °C/s up to the temperatures of 660 °C and 870 °C (M.A. Mostafaei and Kazeminezhad, 2016).

URA to **intercritical** gave better **hardness**, maximum **shear strength** and maximum **shear strain** (both criterion of strength and ductility respectively) than those URA to subcritical, when measured via hardness tester and shear punch test (see Figure 2.4). In general, URA (heating rate=200°C/s) to soak temperature 870°C, as opposed to soaking at temperature 660°C, has resulted in an increase of **6.7** 30HV, **48 MPa**, and **0.15** for hardness, maximum shear stress and maximum shear strain, respectively.

From literature (What is the shear strength of mild steel?, 2022), maximum shear stress is typically **1.73x less** than tensile stress. Therefore, the above results for maximum shear stress translates as approximately **797.53 MPa UTS** (461*1.73) when soak temperature 660°C was used, and **880.57 MPa UTS** (509*1.73) when soak temperature 870°C was used.

Why will I use 200°C/s as my heating rate?

A comprehensive study looking at effects of different heating rates 75-1800°C/s, rapidly cooled and conventionally (0.2°C/s heating rate) to same soak temps was studied. (M. A. Mostafaei and Kazeminezhad, 2016) and found a 200C/s heating rate to be the best compromise because the Ac1 temperature is not significantly affected by this rapid heating rate. For example, the ferrite recrystallization temperature is not pushed above the Ac1 temperature making it feasible for recrystallisation to occur during sub-critical annealing. Furthermore, although recrystallisation does start

before the eutectic ferrite to austenite transformation initiates, it is not completed when transformation starts for inter-critical annealing. Therefore, an interaction of the two processes (recrystallisation and transformation) still occurs. Therefore, in this body of work, a heating rate of 200C/s will be used.

How my research will differ (the novel aspects)

However, the above work (M.A. Mostafaei and Kazeminezhad, 2016) used samples that contains around **0.04wt% nickel**. My samples do not contain nickel, and so the influence nickel has will not be present in my samples. Ni is known to stabilise austenite phase by moving the tip of the nose of a CCT curve to the right, thus decreasing the bainite start temperature of formation (Fox and Mattes, 1990).

Also, samples have been severely deformed via **constrained groove pressing (CGP)** whereas my samples have been cold rolled by 90% to give a gauge reduction from 2.0mm to 0.2mm.

Furthermore, research using the exact compositions and amounts of each element seen in my six samples has not been seen or used. For example, research either uses samples containing higher manganese contents, or do not include elements present in my samples.

3. Methods and Experimental Procedures

This chapter details the materials and experimental procedures used in each technical chapter of this thesis. Information on the processing history of the materials, the equipment and auxiliary software used, what data was collected and information on how the data was processed to give relevant information is provided.

3.1. Processing history of laboratory compositions 1-6.

Lab-casted alloys 1-6 were casted into ingots using a laboratory Vacuum Induction Melter (VIM) at the Research & Development laboratory of Tata Steel Ijmuiden Steelworks. These steel ingots, with chemistries given in **Table *3.1*. Table showing the compositions of lab cast alloys 1-6.**Table 3.1, were reheated up to 1250°C and rough milled to 30mm gauge x 120mm width. The resulting slabs were reheated up to 1220°C for at least 40 minutes and further reduced in four rolling passes (30mm → 20mm → 10mm → 4mm → 2mm) to 2.0mm gauge. After the rolling reductions had been completed, the hot-rolled sheets entered the Front Run-out Table (FRT(in)) at 980°C (±30°C), transported for 3 seconds, and left the Front Run-out Table (FRT(out)) at 950°C (±30°C). Cooling began (Cooling(in)) at 910°C at a rate of 80°C/s, to a coiling temperature of 590°C ±20°C (Cooling(out)). All material was cold rolled to an aim target of 0.2mm (i.e., 90% reduction), cut into A4 sized sheets, and then shipped to Swansea University, Bay campus. These materials were used in chapter numbers 4-8 (i.e., technical chapters 1-5).

Table 3.1. Table showing the compositions of lab cast alloys 1-6.

Sample	C	Mn	Al	Si	S	P	Ti	N	Fe
Alloy 1	0.0780	0.4710	0.0110	0.0090	0.0010	0.0010	0	0.0109	Bal.
Alloy 2	0.0820	0.3740	0.0220	0.4760	0.0008	0.0540	0.0010	0.0100	Bal.
Alloy 3	0.0790	0.4130	0.0180	0.4750	0.0010	0.0280	0.0010	0.0102	Bal.
Alloy 4	0.0810	0.4890	0.0180	0.2350	0.0009	0.0560	0.0010	0.0106	Bal.
Alloy 5	0.080	0.4980	0.0180	0.2410	0.0004	0.0940	0.0020	0.0100	Bal.
Alloy 6	0.0790	0.568	0.0160	0.2140	0.0010	0.0860	0.0010	0.0209	Bal.

Table 3.1 shows the compositions of the lab casted materials used in chapters 4-8 (i.e., technical chapter 1-5). These compositions were made to study the effects of different amounts of Silicon and Phosphorous on the mechanical properties of high strength packaging steel for easy open can-end applications. The high nitrogen content seen in alloy 6 was made by accident but was kept because it was thought to be an interesting composition to study. Elements other than silicon and phosphorous seen in table 3.1 were kept constant, but the slight variation seen is due to random error.

3.2. Processing history of commercial grade 3465

The nitrogenised steel grade 3465 has applications in easy open ends where the thickness of the sheet is 0.18mm and below. This grade was casted, coiled (at an aim temperature of 560°C±20°C), and hot-rolled at Tata Steel Port Talbot Steelworks. The coiling temperature for 3465 is low to prevent formation of aluminium nitrides in the hot strip microstructure. The hot roll band was 2.1mm when it departed Port Talbot Steelworks and underwent an 88% cold reduction to 0.25mm upon arrival at Trostre steelworks. This material was cut into A4 sized sheets, and delivered to Swansea University, Bay campus. This material was used in chapter number 9 (i.e.,

technical chapter 6). See Table 3.2 for the production aim composition values of commercial nitrogenised grade 3465.

Table 3.2. Table showing the chemistry of grade 3465.

Steel	**C**	**Mn**	**Al**	**N**
Nitrogenised	0.065	0.5	0.02	0.0120

During cold rolling, the ferritic microstructure deformed and aligned along the rolling direction. Figure 3.1 shows the initial microstructure of grade 3465 in its cold reduced condition. The cold-rolled microstructure consists of ferrite grains aligned in the rolling direction with a uniform distribution of carbides in the ferrite matrix, as well as areas of remarkably high dislocation density.

Figure 3.1. Optical image of nitrogenised grade 3465, in its transverse orientation, in its cold rolled condition at a magnification of 500x.

3.3. Determination of Ae1 and Ae3 transformation temperatures (JMatPro software)

JMatPro version 10.2 software was used to determine the Ae1 and Ae3 temperatures for laboratory grades 1-6, and for the commercial grade 3465. These temperatures are given in Table 3.3. This software was used to ensure the selected soak temperatures 650 °C (used in chapters 4 and 5) and 635 °C (used in chapter 9) used in the annealing heat treatments were below the Ae1 transformation temperature (sub-critical) for these materials. Furthermore, to check the chosen soak temperatures 850°C (used in chapters 6 and 7), 750 °C and 775 °C (used in chapter 9) were in between the Ae1 and Ae3 transformation temperatures (inter-critical) for these chemistries.

Table 3.3. Table showing the Ae1 and Ae3 transformation temperatures of laboratory alloys 1-6, and commercial grade 3465 as determined by JMatPro software.

Alloy	Ae1 (°C)	Ae3 (°C)
1	710	860
2	724	907
3	721	897
4	716	888
5	717	900
6	713	890
3465	709	863

In addition to obtaining the transformation temperatures for these grades, Temperature-Time-Transformation (TTT) diagrams were produced. For these TTT diagram simulations, a 5µm prior austenite grain size was used for all grades. These diagrams will be shown in relevant chapters.

3.4. Gleeble 3500 Simulated Annealing Procedures

3.4.1. Gleeble 3500 Sample preparation.

The cold rolled materials were sheared (using a benchtop guillotine) into strips of dimensions 210 mm length x 35 mm width x 0.2 mm thickness (for laboratory grades 1-6) or 0.25 mm thickness (for commercial grade 3465). Then, the strips were grinded manually using sandpaper and ethanol to clean the strip surfaces (of oil/dirt etc.) in order to provide an optimal sample contact surface for the Gleeble 3500 jaws to grip onto. Samples were then cleaned and dried using ethanol and blue tissue paper, and had a k-type thermocouple welded in the centre of the strips. The individual thermocouple wires were threaded through a ceramic sheath with two separate channels to prevent the individual thermocouple wires from contacting each other during each test. This ceramic sheath was placed close to the steel strip sample, but with approximately a 5 mm gap between it and the sample. One sample at a time was set up in the Gleeble 3500, and the desired annealing cycle was programmed into the auxiliary computer. See Figure 3.2 for a labelled picture of the Gleeble 3500 internal chamber where samples were subjected to simulated heat treatments.

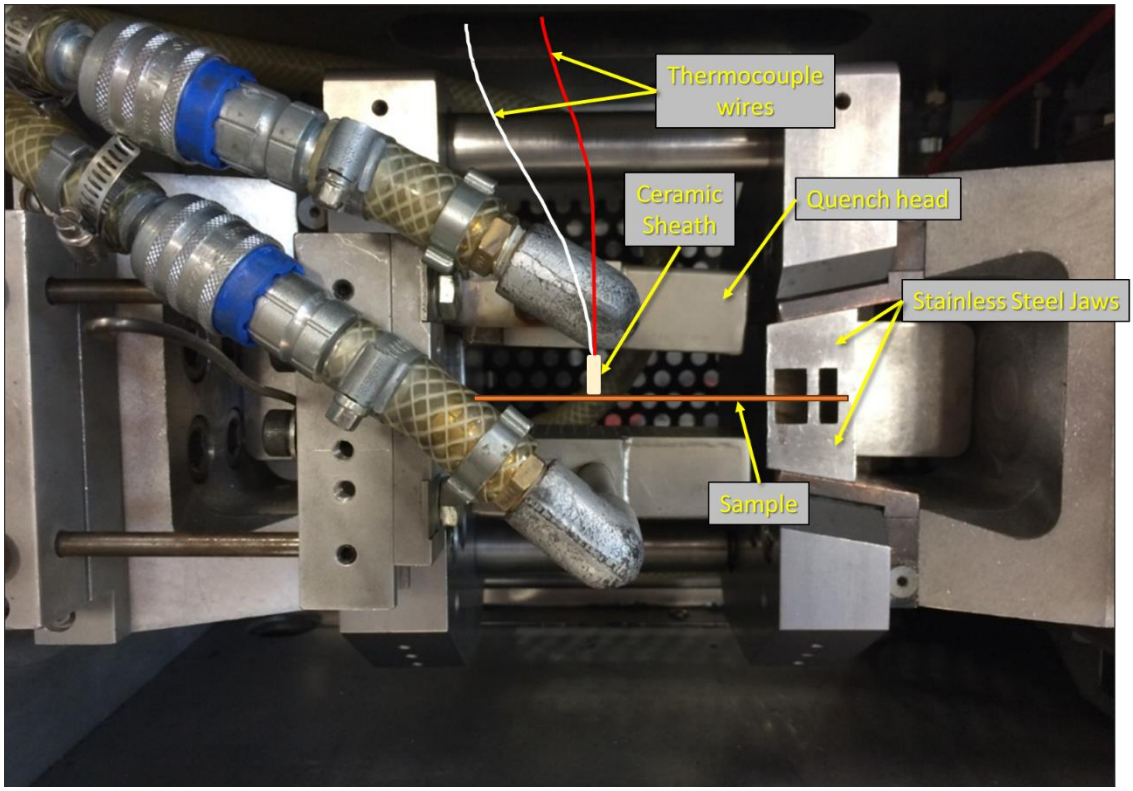

Figure 3.2. A sample set up in the Gleeble 3500 with a k-type thermocouple welded in the centre-middle of the trip surface.

3.4.2. Annealing Cycle Used in Chapter 4 (Technical Chapter 1).

Samples in chapter 4 were subjected to a simulated annealing cycle that mimicked a typical commercial annealing cycle applied to high-strength packaging steel for can-end applications. Using the Gleeble 3500, samples were heat treated using a heating rate of 20°C/s to a soak temperature of 650 °C and held at this temperature for a period of 51 seconds. After 51 seconds had passed, samples were then subjected to a simulated slow cooling stage consisting of cooling the sample at a rate of -5.6 °C/s for 6.25 seconds. Following this, samples were then rapidly cooled at a rate of -300 °C/s using high pressure air quenching, to an overageing temperature of 400°C and held for 56 seconds. After the overageing step, all samples were cooled to room temperature at a rate of 27 °C/s. Figure 3.3 shows the heat treatment cycle applied to the samples in chapter 4.

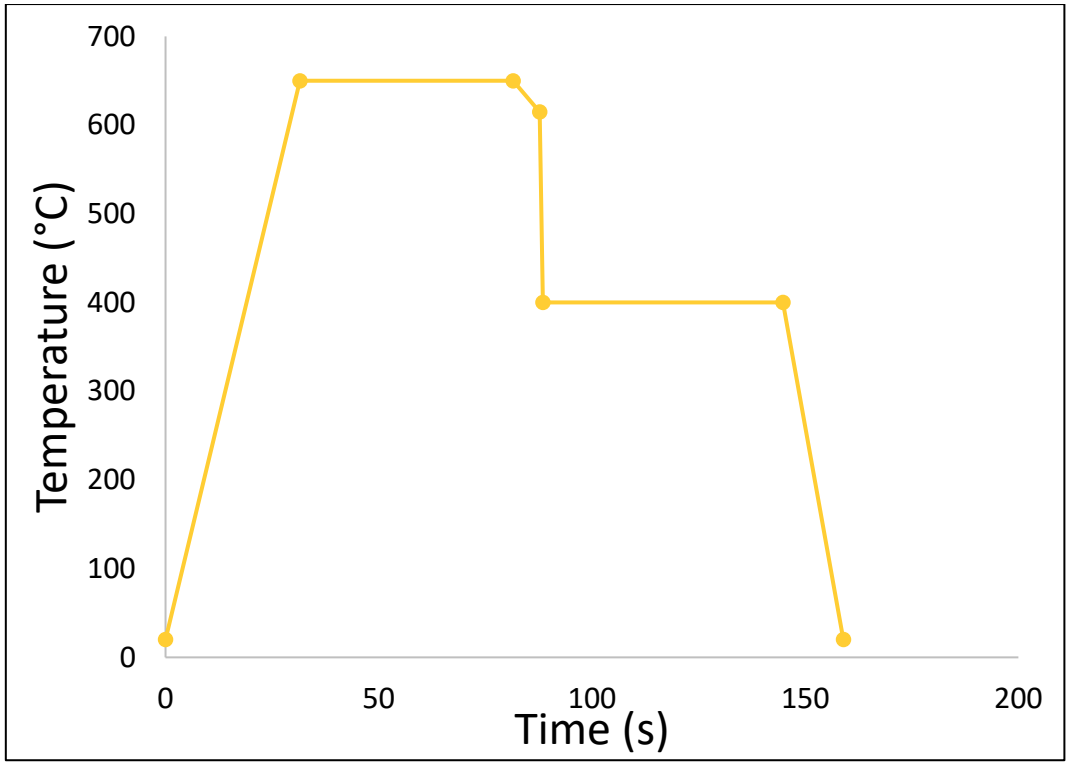

Figure 3.3. The commercial annealing cycle samples in chapter 4 were subjected to.

3.4.3. Annealing Cycle for Chapter 5 (Technical Chapter 2).

In chapter 5 (The effect of flash annealing (200°C/s heating rate) on lab-casted high-strength packaging grade steels for can-end applications) samples underwent a similar simulated annealing cycle as used in chapter 4, but a heating rate of 200 °C/s was used instead. See Figure 3.4 for a schematic of the heat treatment cycle performed on lab grades 1-6 in chapter 5 (grey coloured line).

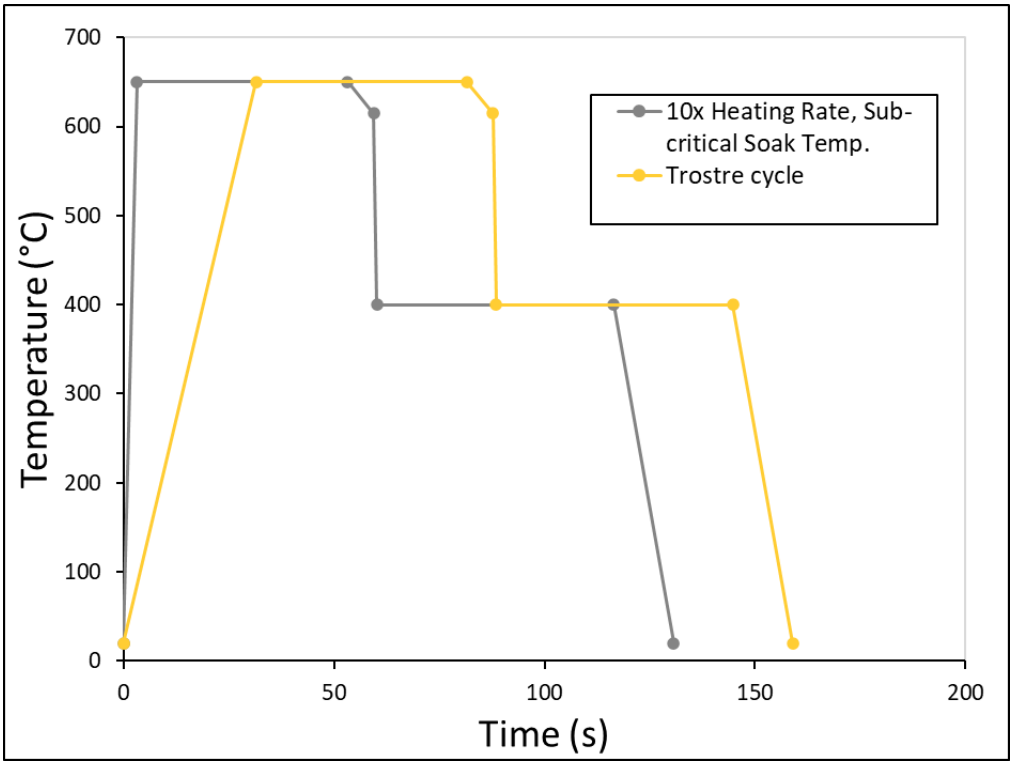

Figure 3.4. The rapid heating rate annealing cycle (grey coloured line) carried out on samples in chapter 5. The commercial annealing cycle (yellow coloured line) used in chapter 4 is shown for reference.

3.4.4. Annealing Cycle for Chapter 6 (Technical Chapter 3).

In chapter 6 (The effect of intercritical soak temperature 850°C on lab-casted high-strength packaging grade steels for can-end applications) samples of lab alloys 1-6 were subjected to a similar simulated annealing cycle as used in chapter 4, but a soak temperature of 850 °C/s was used instead. See Figure 3.5 for a schematic of the heat treatment cycle performed on lab grades 1-6 in chapter 6 (red coloured line).

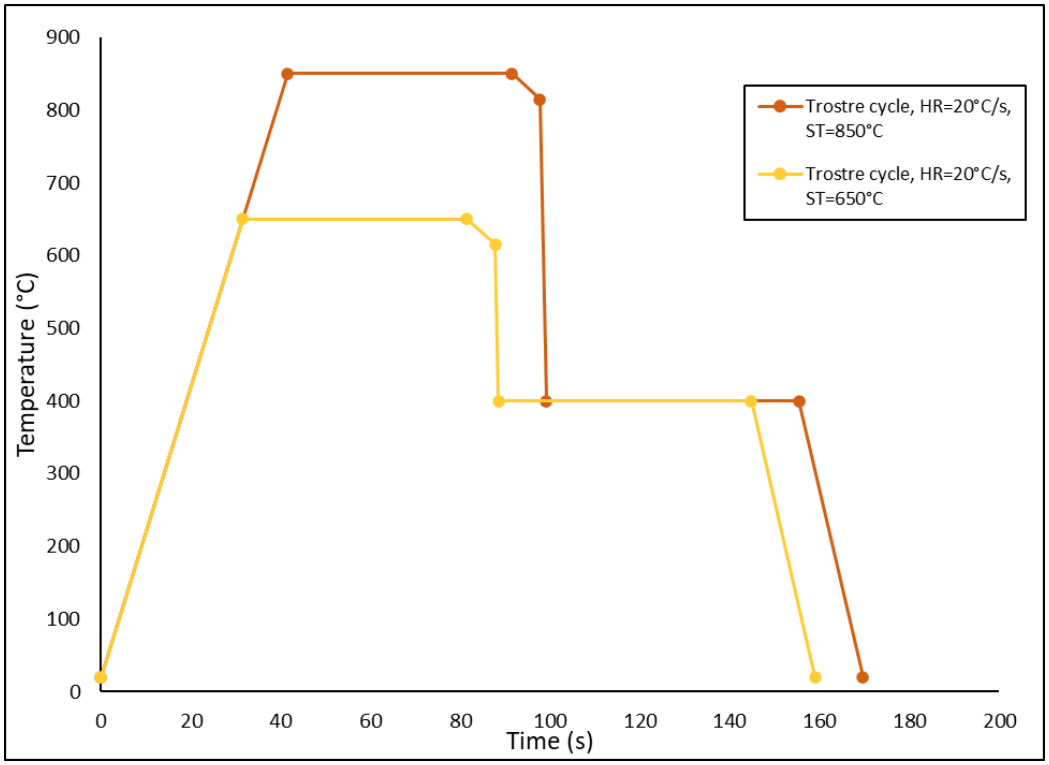

Figure 3.5. The intercritical soak temperature annealing cycle (red coloured line) carried out on samples in chapter 6. The commercial annealing cycle (yellow coloured line) used in chapter 4 is shown for reference.

3.4.5. Annealing Cycle for Chapter 7 (Technical Chapter 4).

In chapter 7 (Technical chapter 4 – The effect of rapid 200°C/s heating rate to intercritical annealing soak temperature 850°C on lab-casted high-strength packaging grade steels for can-end), samples of lab alloys 1-6 were subjected to a simulated annealing cycle that combined the approaches used in chapters 5 and 6, i.e., a 200 °C/s heating rate and an intercritical soak temperature of 850 °C. See Figure 3.6 for a schematic of the annealing cycle performed on lab grades 1-6 in chapter 7 (blue coloured line).

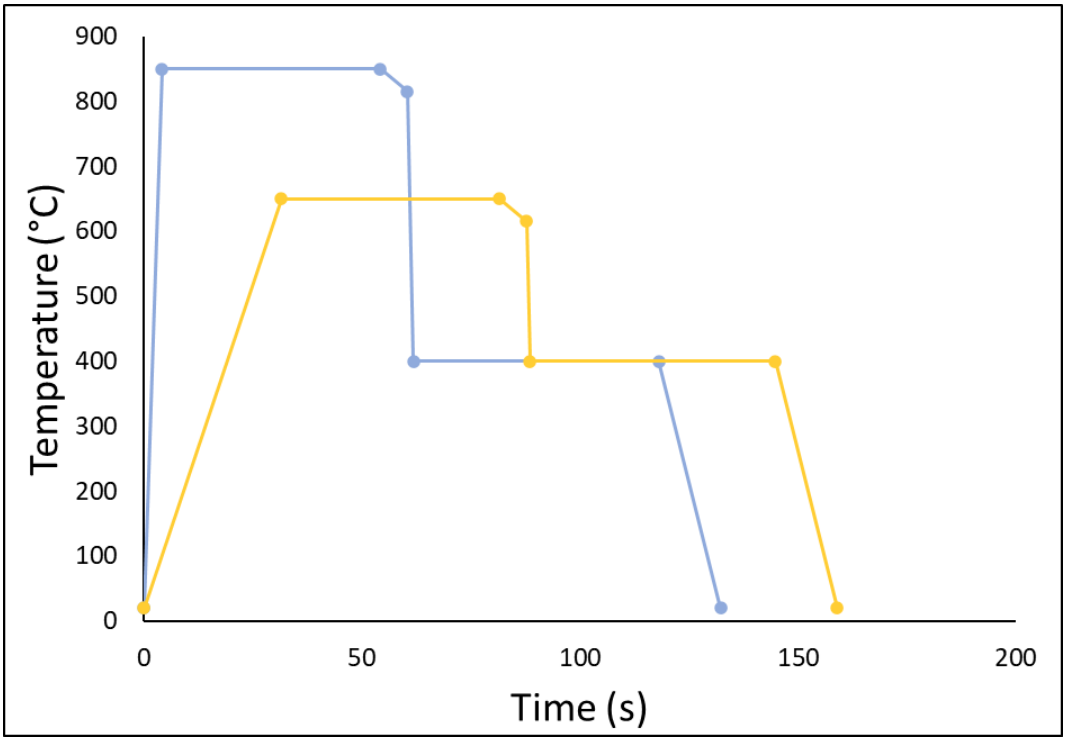

Figure 3.6. The ultra-rapid heating rate and intercritical annealing cycle performed on samples in chapter 7 (blue coloured line). The commercial annealing cycle (yellow coloured line) used in chapter 4 is also shown for reference.

3.4.6. Annealing cycle for chapter 8 (Technical chapter 5).

In chapter 8 (Technical chapter 5 – The effect of removing the slow cool section from Trostre's continuous annealing production line on the microstructural and mechanical properties of packaging grade steel), samples of lab alloys 5 and 6 were subjected to two simulated annealing cycles using a Gleeble®3500 system. One cycle mimicked that used in chapter 6 (intercritical soak temperature of 850 °C), and another that mimicked the cycle used in chapter 7 (rapid heating rate of 200 °C/s to intercritical soak temperature. However, the difference being is that both cycles had their slow cool section removed from the annealing cycle. Therefore, at the end of the soak stage, samples were immediately subjected to a rapid cooling to the overageing stage. See Figure 3.7 for a schematic of the annealing cycles performed on lab grades 5 and 6 in chapter 8 (blue and red coloured lines). After annealing, samples were microstructurally analysed, and hardness tested.

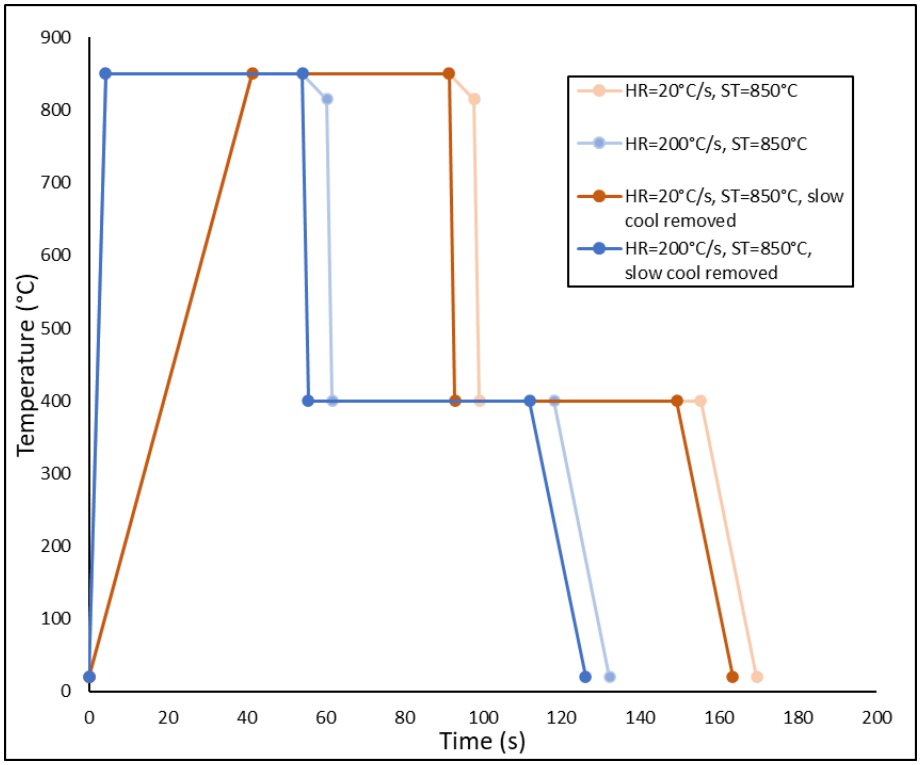

Figure 3.7. The two annealing cycles performed on alloys 5 and 6 in chapter 8 (blue and red coloured lines). The same cycles but with the slow cool sections included are shown for reference (light blue and light red lines).

3.4.7. Annealing cycle for chapter 9 (Technical Chapter 6).

In chapter 9 (Technical Chapter 6 - Effect of rapid heating rates, soak temperatures, and cooling rates on the grain size and mechanical properties of a commercial nitrogenised packaging grade steel for can-end applications (impact activity)), samples of commercial nitrogenised steel grade 3465 were subjected to a number of simulated annealing cycles that looked at the effect of heating rates (i.e. 20 °C/s, 200 °C/s, and 1,000 °C/s), soak temperatures (635 °C, 750 °C, 775 °C, and 850°C), and cooling rates (300 °C/s, 500 °C/s, and 775 °C/s) on the mechanical properties and microstructure. Cooling straight from soak temperature to toom temperature was conducted, meaning no slow cool section and no overageing section was used. See Figure 3.8 for a schematic of the annealing cycles performed on commercial grade 3465 in chapter 9.

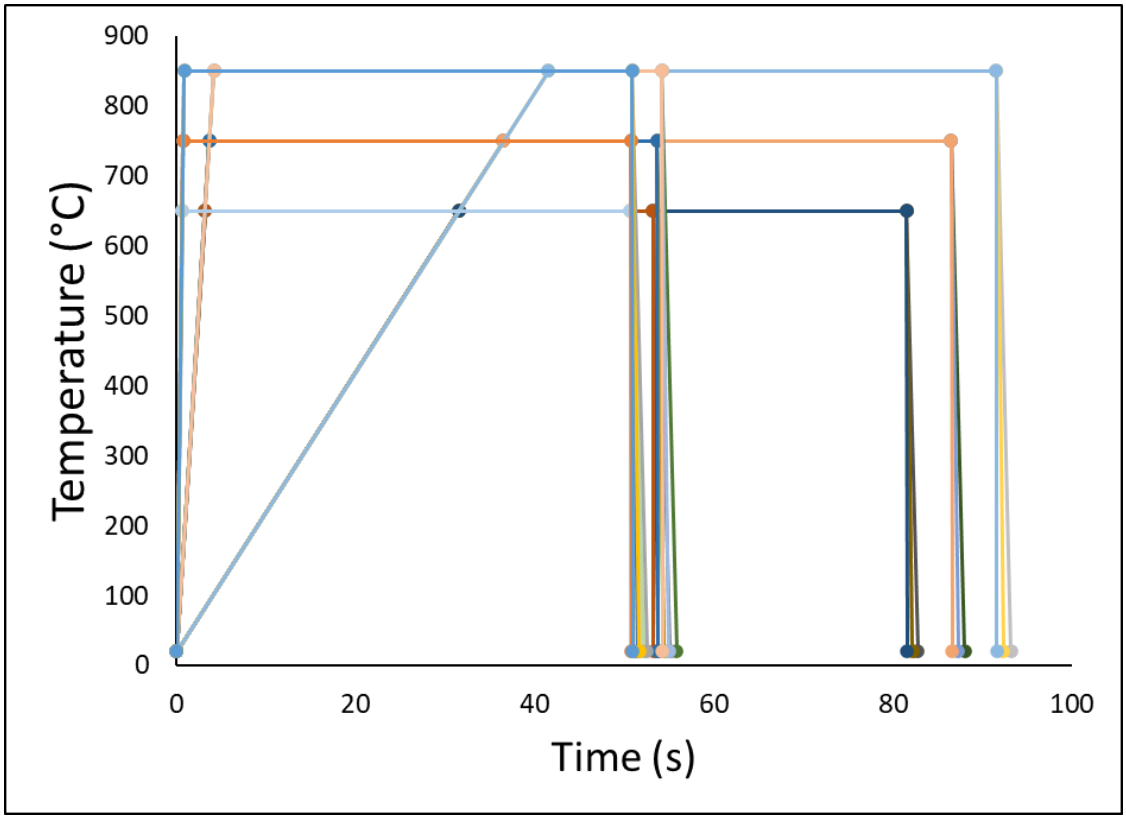

Figure 3.8. The annealing cycles performed on commercial nitrogenised grade 3465 in chapter 9.

The annealing simulations consisted of heating rates (Rh) being 20°C/s; 200°C/s; and 1,000°C/s, the holding time (ta) equal to 50s at annealing temperature (Ts) of 635°C; 750°C and 850°C, the cooling rates (Rc) consisting of 300°C/s, 500°C/s, and 750°C/s. The annealing parameters were varied to determine their impact upon secondary phase generation. The steel samples were annealed using a Gleeble 3500 thermo-mechanical simulator which is based on induction heating with cooling carried out by air gas jets blown on both sides of the steel sheets. This simulator allowed samples (210m length and 35mm width) to be heated with precise control (±1°C) thanks to the use of type K-thermocouples. The microstructures of the annealed samples were characterised through optical microscopy to assess the evolution of grain size/shape after annealing, to determine the mean grain size of the steels, and identifying the presence of secondary phase.

This chapter 9 (technical chapter 6) consisted of two sections, phase 1 and phase 2.

3.5. Phase 1 – Effect of Rapid Heating Rates on the Ferrite Grain Size.

These tests were conducted to determine which heating rate would give the smallest ferrite grain size. In knowing this, the total number of experiments could be reduced. The three heating rates chosen were 20°C/s, 200°C/s, and 1000°C/s. Soak temperatures 635°C and 850°C (for a soak time of 51seconds) were used as it was presumed that ultra-rapid heating rates would have difference consequences on grain size at temperatures above and below the Ac1 transformation temperature. Finally, cooling rate was fixed at -300°C/s. The heat treatments are given in Table 3.4, and graphically shown in Figure 3.9.

Table 3.4. Heating rates and soak temperatures used in Phase 1.

Heating rate (°C/s)	**Soak temperature (°C/s)**
20	635
200	635
1,000	635
20	850
200	850
1,000	850

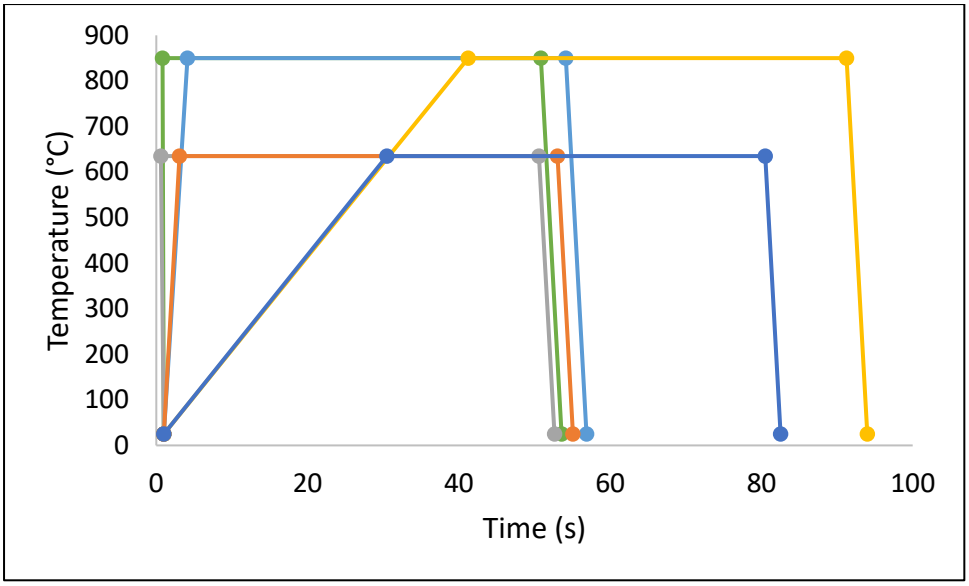

Figure 3.9. Schematic showing the heat treatment profiles performed to determine heating rate that yields smallest ferrite grain size.

3.6. Phase 2 – Effect of annealing soak temperature and cooling rate

3.6.1. Alloy casting, hot-rolling, and cold rolling procedures

Commercial packaging grade steel 3465 in cold rolled condition was used in this section of work, and is the same material used in the previous section (Phase 1- Effect of Rapid Heating Rates on the Ferrite Grain Size). The chemistry, hot-rolling, and cold rolling procedures are the same. For reminding purposes, the chemistry of the steel is given in Table 3.5 below:

Table 3.5. Table showing the chemistry of grade 3465.

Steel	C	Mn	Al	N
Nitrogenised	0.065	0.5	0.02	0.0120

3.6.2. Annealing cycles performed

The heating rate was fixed at **200°C/s** because this was found to be the level that achieves a smaller ferrite grain size (see previous chapter ‘Effect of Rapid Heating Rates on the Ferrite Grain Size’).

Samples were heated to three soak temperatures:

- 635°C
- 750°C
- 775°C

Samples were held at these soak temperatures for 50s, and then cooled to room temperature using the following cooling rates:

- 300°C/s
- 500°C/s
- 775°C/s

Cooling straight from soak temperature to room temperature was conducted, meaning no slow cool section and no over ageing section will be used. This is like how the competitor ArcelorMittal is speculated to manufacture their high-strength steel on their continuous annealing line (CAL) setup.

635°C is the soak temperature that is used when commercially making grade 3465. This temperature is subcritical (<Ac1), and its cold rolled grains will recrystallise at this temperature when 20°C/s heating rate is used. The effect of greater soak temperatures on properties such as yield strength and break elongation can be compared to it.

750°C is above the Ac1 temperature (709°C) so that austenite can form which will later be transformed to a secondary phase martensite and increase yield strength via secondary phase hardening, upon cooling. At 750°C it is predicted (according to a single point equilibrium calculation performed on Thermocalc) that austenite volume fraction will be 0.11605.

Similarly, the 775°C soak temperature is expected to be formed at 775°C is 0.143322. This larger volume fraction of secondary phase is presumed to increase strength properties but also decrease total strain to failure, to a larger extent when compared to samples annealed at soak temperature 750°C, as measured via tensile tests. Soak temperatures above 775°C are not possible with the Trostre steelworks CAPL, and not thinkable in a near future. Inter-critical temperatures 750°C and 775°C soak temperature might give some shorter-term steer on a potential way forward for the company towards achieving a stronger grade of steel without having to use a different steel chemistry.

A cooling rate of 300°C/s is Trostre's maximum cooling rate. Therefore, will be used as a baseline and the effect of higher cooling rates will be compared to it.

Cooling rates 500°C/s and 750°C/s were chosen to try and generate secondary phase martensite., and to see how different cooling rates effect the resulting volume fraction of secondary phase. Martensite is a harder phase than ferrite, pearlite, and bainite, and so the magnitude of martensite's effect on mechanical properties will be compared to the baseline conditions.

See Figure 3.10 for a schematic of the annealing cycles performed in Phase 2.

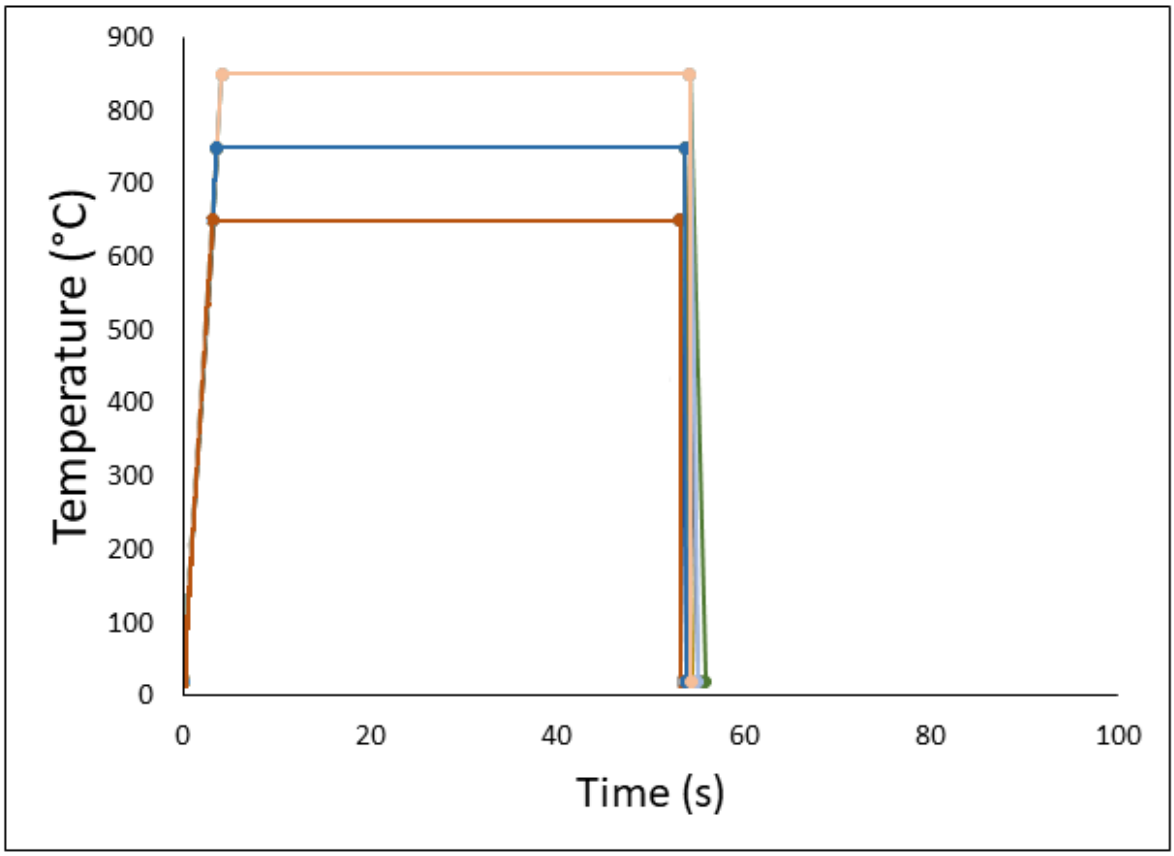

Figure 3.10. Graph showing the heat treatments performed in Phase 2.

Unfortunately, for all annealing heat treatments cycles performed in all of these chapters, the HNx gas atmosphere used on the continuous annealing production line was not replicated, because of equipment limitations. This meant that samples (particularly ones annealed at soak temperature 850°C) developed an oxide layer. However, this layer was removed prior to further work such as when microscopy and tensile testing were conducted.

3.7. Temper rolling and aging

Where stated in the experimental chapters below, samples of annealed alloys 1-6 and commercial nitrogenised grade 3465 were subjected to a 5% temper rolling procedure using an industrial cold rolling mill located in Tata Steelworks in Llanwern. This procedure was conducted by first scribing a 40mm length line along

the rolling direction of the sample and then subjecting each sample to multiple cold roll passes until the scribe length increased by 5%, i.e., until a 42mm length was achieved.

Following temper rolling, an ageing procedure was performed that consisted of heating all temper rolled samples to a temperature of 200°C for 20 minutes using a laboratory box furnace. This ageing procedure was carried out because it is recommended in the EN10202 packaging food standard. This ageing treatment is carried out because it replicates the industrial cooking process canned food undergoes for cooking/sterilisation. This ageing procedure also has the effect of reducing the amount of ageing that occurs in continuously annealed low carbon steels.

3.8. Tensile testing

For all tests, a Tinius Olsen tensile tester with a 5KN load cell was used to conduct the tensile tests, with a ‘XSight ONE’ video extensometer used to measure strain. Tensile specimens were grinded using P800 griding paper prior to testing to remove the oxide layer and enable reliable strain measurements. Samples tested included those in their as-annealed, and 5% temper rolled and aged conditions. Two repeats of each sample were tested. ASTM 25 geometry tensile specimens were used because the gauge length and some of the tab is well within the homogeneous heating zone exhibited on each sample during Gleeble heat treatments. ASTM 25 tensile specimens were also used because it was found that samples that were initially tensile tested using the JIS5 style tensile specimens often exhibited failure towards the radius of the tensile specimens (where temperature during a test was lower than the target), rather than in the middle. See Table 3.6 for information regarding the differences in dimensions of JIS5 and ASTM 25 tensile pieces.

Table 3.6. Table showing the differences in critical tensile test piece dimensions for ASTM25 and JIS5 style tensile specimens.

	Parallel length/mm	Gauge length/mm	Gauge width/mm	Grip width/mm	Shoulder radius/mm	Length ratio	Slender ratio	Width ratio	
	Lc	Lo	W	B	r	Lo/Lc	Lo/W	W/B	(Lc-2W)/Lo
JIS5	60	50	25	30	25	0.83	2	0.83	0.2
ASTM25	32	25	6	10	6	0.78	4.2	0.6	0.8

All samples were aged in a furnace at 200°C for 20 minutes prior to tensile specimen machining. Where mentioned, samples were studied in their **as-annealed condition** and their **5% temper rolled condition**. This will allow the effect of 5% temper rolling to be examined as well.

3.8.1. Tensile test parameters

Tensile test strain rate parameters are given in

Table 3.7. Depending on whether samples were subjected to a 5% temper rolling procedure, slightly different tensile test parameters were used. For example, for samples tensile tested in their as-annealed condition, tensile test strain rates described in column labelled ‘Single reduced continuously annealed’ were used. On the other hand, samples that were tensile tested after having a 5% temper rolling procedure applied were subjected to tensile test strain rates described in column labelled ‘Double-reduced’. Where V1 refers to the strain rate up to the yield point, V2 refers to the strain rate between yield point and ultimate tensile strength, and V3 refers to the strain rate applied after the ultimate tensile strength was reached, until sample failure. These are the tensile test procedures that Tata Steel Trostre

steelworks use when testing their materials in the as-annealed condition, or after when a secondary cold reduction procedure has been applied.

Table 3.7. Table showing the tensile test parameters used in testing samples in their as-annealed condition (Single reduced continuous annealed) and their temper rolled condition (Double-reduced).

	Single reduced continuously annealed	Double-reduced
V1	0.00015sec^{-1} (0.288mm/min)	0.00015sec^{-1} (0.288mm/min)
V2	0.0045sec^{-1} (8.64mm/min)	0.00075sec^{-1} (1.44mm/min)
V3	0.006sec^{-1} (11.52mm/min)	0.00075sec-1 (1.44mm/min)

3.9. Microstructural characterisation

Microstructural characterisation and hardness tests were conducted on 10mm x 10mm area cut from the middle-centre of each heat-treated sample (the area where thermocouples were attached to) and prepped for microscopy and hardness measurements using standard metallographic preparation techniques and etched in 5% Nital solution to reveal the microstructure. All microscopy work was conducted on the transverse direction of the strip, as information regarding grain size distribution can be determined.

3.10. Sample Preparation for Microstructural Characterisation using Standard Metallographic Preparation Techniques

3.10.1. Hot Mounting, Grinding, Polishing, and Etching

As mentioned above, a 10x10 mm area sample was cut from the middle-centre section of each heat-treated sample using a benchtop guillotine. Each sample was mounted using a stainless-steel mounting clip and placed into a Struers CitoPress-15 hot mounting machine chamber and filled with conductive Bakelite powder. Samples were then heated under pressure at a temperature of 180 °C for four minutes. Samples were mounted in the hot mounting chamber using a stainless-steel clip to ensure the transverse cross-sectional area would be visible when grinding/polishing occurred.

Samples were then subjected to a grinding and polishing procedure to remove layers of Bakelite material to reveal the sample, and to gradually produce a clean, flat, and polished sample surface. Samples were grinded using Silicon Carbide papers of incremental grit sizes P180, P280, P400, and P800 using an automatic grinding machine, with a rotational speed of ~250 rpm. Water was used as the lubricant.

After the grinding stage was complete and sample surfaces were satisfactory, polishing was commenced using a diamond lubricant, and diamond polishing suspensions beginning with 9 µ grit size, and then 6, 3 and finally a 1 µm diamond polishing grit size. For samples analysed in the SEM (for high magnification imaging / EDS technique), a final polishing stage using colloidal silicate abrasive was used. In between different stages of polishing grit sizes, samples were washed using a soap detergent and running water, then coated with ethanol before blow drying with a handheld dryer.

To reveal the microstructure for optical microstructure analysis, mounted samples were then etched using a 5% concentration of Nital acid etchant. This procedure consisted of filling a shallow glass petri dish with 5% concentration Nital acid, and dipping the polished face well into the acid ensuring it does not touch the bottom of the glass dish. Polished sample faces would remain submerged in the acid for a period of 5 seconds, before it was washed taken out and rinsed with ethanol and dried using compressed nitrogen gas. This procedure was repeated until a satisfactory etched sample was obtained. See Figure for an example of a polished sample.

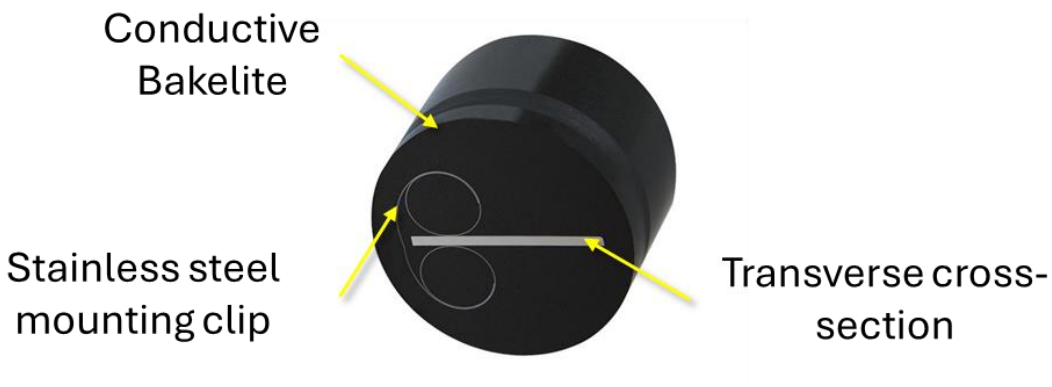

Figure 3.11. Example of a polished mounted sample.

3.11. Optical microscopy

Optical microscopy was carried out using a Zeiss Observer z1m optical light microscope located at Swansea University, Bay campus. Three images would be taken per sample along the length from the left, middle and right side, at 50x magnification (see Figure). All microscopy images were conducted on samples in their as-annealed condition.

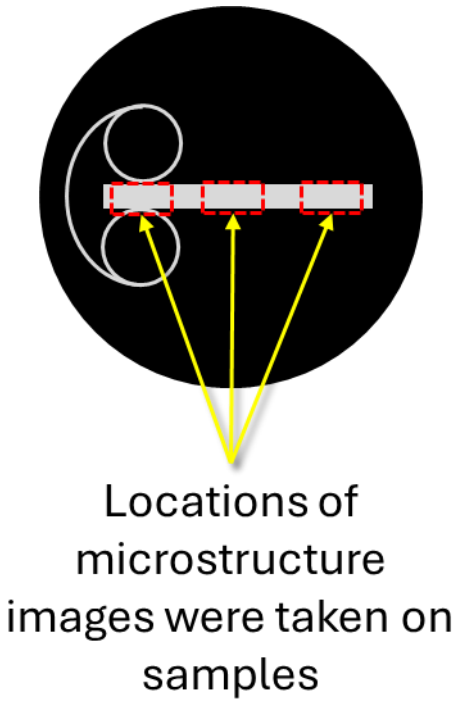

Figure 3.12. Locations optical microstructure images were taken.

3.12. Grain size analysis method

The planimetric method was used to determine grain size information on each sample such as the average and modal grain sizes, and information on the grain size distribution. The planimetric technique for grain size analysis was conducted using the inbuilt software (called 'Zen core v2.7') on a Zeiss Observer z1m optical light microscope located at Swansea University, Bay campus, within the AIM department. Five microstructure images were taken on the transverse direction of each sample, in their as-annealed condition, at 50x magnification to obtain the required number of grains for the technique as recommended in the grain size analysis standard ASTM E 112-13.

By default, the 'Zen core v2.7' software outputs a report that presents each samples grain size in ASTM number format. However, this format is not very familiar, or clearly understood in industry. Therefore, the macro behind the software for the planimetric method was modified so that the area of each grain in a sample would be measured in micrometre squared (μm^2). In addition to area, a parameter called 'Area Bound Unscaled ($pixel^2$)' associated with each grain area measurement was measured. Some ~13,000 grain size areas (and Area Bound Unscaled ($pixel^2$)) per sample were then exported to Microsoft Excel, where each individual grain result was filtered so that each area measurement that has an associated Area Bound Unscaled value below 10 were discarded. This was done because the resolution of this technique (optical microscopy) was being approached, and pixels of ≤10 were most likely noise and not actual grains. Therefore, confidence that pixels of ≤10 were actually grains was low. After these results were discarded, this left approximately ~6,000 grains for analysis.

The area (μm^2) of the filtered grains was then converted to Equivalent Circle Diameter (μm^2) using the equation described in Equation *10* below:

$$Circle\ Equivalent\ Diameter\ = 2 * \sqrt{\frac{Area}{\pi}} \qquad \text{Equation 10}$$

The circle equivalent diameter values were then rounded to the nearest whole number e.g., 1, 2, 3 …etc., and the sum of each equivalent circle diameter was counted. The total number of grains were counted, so that the proportion of each grain size could be determined. The proportion of grain sizes in each sample was determined by dividing the number of grains of a particular diameter, e.g., 1µm, and then dividing it by the total number of grains in the sample, then multiplying by 100. Table 3.8 shows an example of how the distribution of grain sizes of a sample was determined.

Table 3.8. An example of how the distribution of grain sizes within each sample was determined.

	Count	Equivalent Circle Diameter	Proportion
	0	0-1	0
	4	1	0
	356	2	18
	555	3	28
	404	4	20
	275	5	14
	175	6	9
	106	7	5
	65	8	3
	35	9	2
	22	10	1
	10	11	1
	5	12	0
	2	13	0
	3	14	0
	1	15	0
total	2014		

The Proportion (y-axis) was plotted against Equivalent Circle Diameter (x-axis) to produce a distribution curve like that shown in Figure .

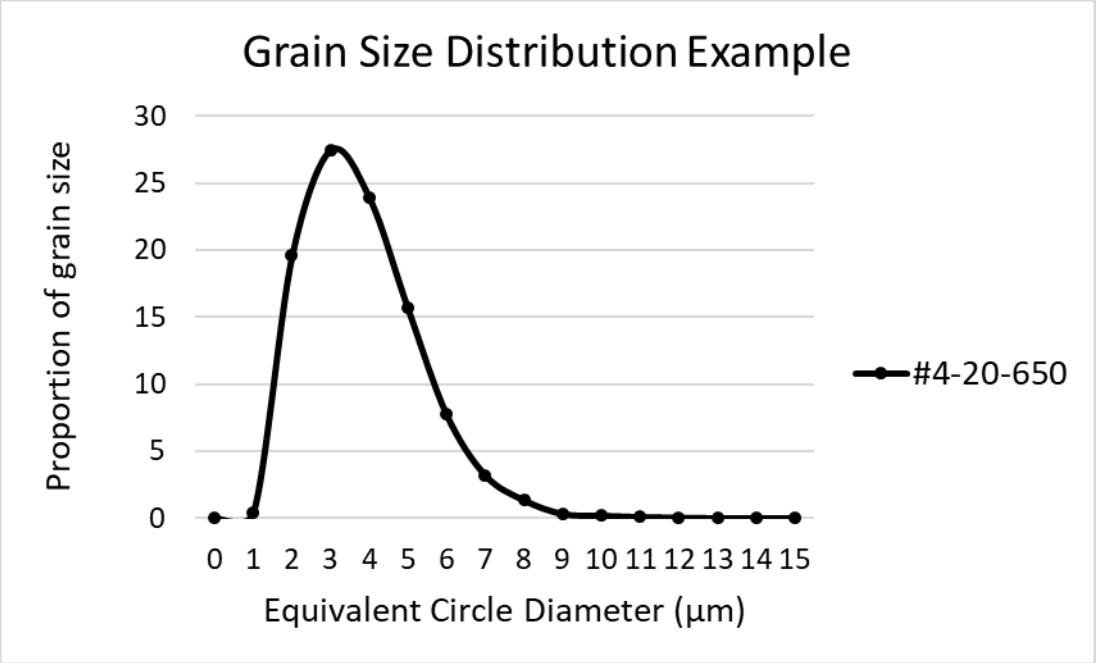

Figure 3.13. An example of distribution of grain sizes in an annealed sample.

3.13. Scanning Electron Microscopy (SEM)

A Zeiss Evo Scanning Electron Microscope was used to provide high magnification microstructural images a selection of samples, and to carry out Energy Dispersive Spectroscopy (EDS) using the Aztec software. As mentioned in section in section 3.81 (Hot Mounting, Grinding, Polishing, and Etching), samples for Scanning Electron Microscopy (SEM) imaging were subjected to a final polishing procedure utilizing colloidal silicate abrasive. After polishing with colloidal silicate, samples were cleaned with ethanol and blow dried to remove any residues or contaminants that could interfere with SEM imaging. Furthermore, samples were subjected to a plasma cleaning procedure for two minutes, prior to being inserted into the SEM. When using the SEM, parameters for working distance, beam current, electron beam energy were around 13 mm, 250 pA, and 13 kV respectively. All samples were analysed in imaged and analysed in their as-annealed condition.

3.14. Vickers Hardness Testing

Vickers hardness testing was carried out on mounted, polished, and etched samples prepared as described in section 3.81 (Hot Mounting, Grinding, Polishing, and Etching). Samples were analysed using an automatic Vickers hardness testing machine, whereby a line of 10 measurements were recorded to give a statistically relevant value of hardness per sample (See Figure). Due to the thin nature of the material studied, a low-test load of 100 gf for a dwell of 10 seconds was used to ensure the indenter tip fitted within the material and well away from the sample edge (so as not to have the results influenced by the Bakelite). Furthermore, a measurement spacing of 1.5mm between each measurement was used to ensure each result was not influenced by the strained field generated by the previous measurement.

After all measurements were conducted on a sample, each indentation was measured again manually (measurements were made automatically by the machine but were manually verified) to ensure the diagonals of the indentation aligned correctly. The calculation of the hardness value was conducted using the inbuilt software of the machine, and results were exported from the machine to be analysed on MS Excel. Unless otherwise stated, all samples were hardness tested in their 5% temper rolled condition.

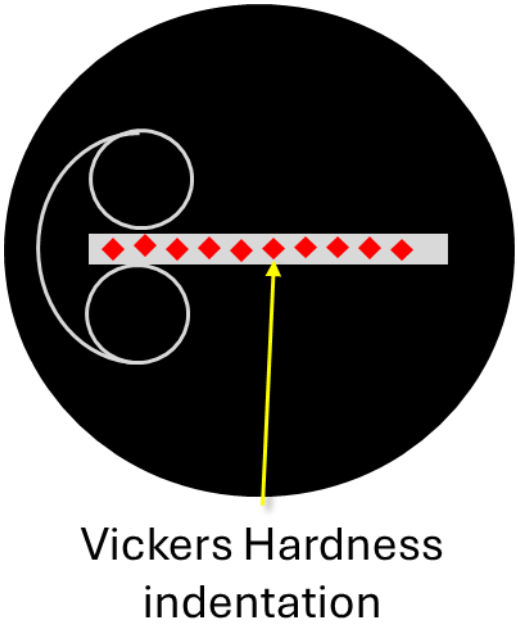

Figure 3.14. Example of sample subjected to Vickers hardness indentations.

4. Technical chapter 1 – The effect of higher levels of silicon, phosphorous, and nitrogen contents after a simulated commercial annealing procedure on high-strength packaging grade steels for can-end applications.

4.1. Purpose of study

To subject six lab-casted packaging grade steels to a simulated commercial annealing procedure, i.e., when a heating rate of 20°C/s, and a soak temperature of 650 °C was used (as shown in Figure 4.1). This cycle simulated the maximum heating rate and soak temperature that the sponsor company can use in their Continuous Annealing Production Line (CAPL), and reflects a typical annealing cycle used on the CAPL for high strength steel for can-end applications. Furthermore, this cycle gave insight into how the mechanical properties would change if chemistry alone (silicon, phosphorous or nitrogen contents) was modified, as seen in the data for alloys 2-6, and whether the target range of 650-750MPa for yield strength could be achieved, whilst maintaining a suitable break elongation value above 5%. Because Alloy 1 exhibited a composition that is similar to the current commercial grade used for high strength packaging steel for easy-open ends, it provided a baseline in which alloys 2-6 can be compared against. In addition, the annealing cycle used in this chapter provided a baseline for subsequent chapters where annealing parameters were changed. Silicon, phosphorous, and nitrogen were specifically chosen because they are known to increase the strength of steel via solid solution strengthening, and are economic alloying additions.

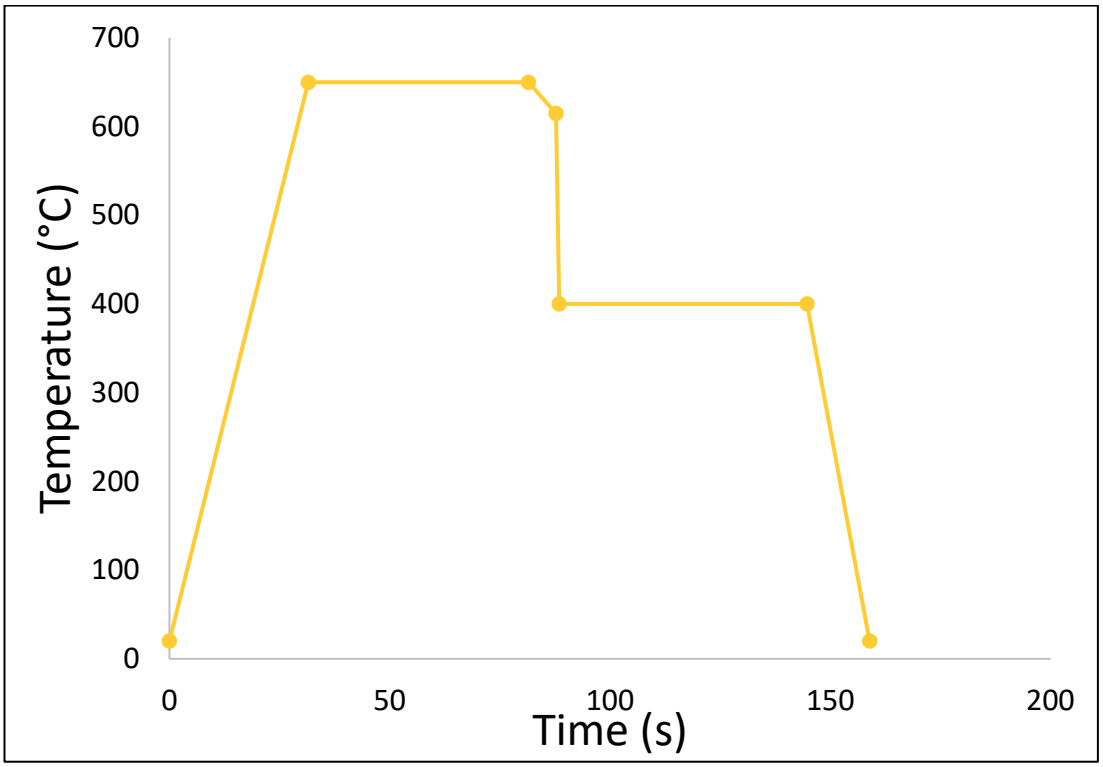

Figure 4.1. The simulated annealing cycle samples in this section were subjected to.

4.2. Advantages/disadvantages of these chemistries

The advantages of silicon are it is known to increase yield strength of steel by 83.2MPa per 1wt% added. Furthermore, Silicon tends to inhibit carbide precipitation resulting in carbon remaining in solid solution. This is good because the solid solution strengthening coefficient of carbon is **4570 N/mm^2** when the solid-solved carbon content in ferrite is taken as **0.01wt%C** (Ren and Liu, 2019). Because the dissolved carbon content is kept high, any austenite phase that forms on intercritical annealing becomes enriched and stabilises, thus increasing the volume fraction of secondary phases upon cooling.

The disadvantages of silicon are it can increase the Ac1 and Ac3 transformation temperatures by factors of 13x and 39x respectively. Furthermore, it can reduce the bainitic and martensitic starts temperatures by a factor of -23x and -10.5x respectively. Therefore, if strengthening were to be achieved by secondary phase

generation, then this could require greater annealing soak temperatures which can add costs to the manufacturing process.

An obvious advantages of Phosphorous is it is the third best element for strengthening steel via solid solution strengthening and is quoted as being able to strengthen ferrite-pearlite steel by 678MPa for every 1wt% added (Hudd Hudd and Llewellyn, 1998). For the amounts of phosphorous seen in these six samples (i.e. 0.028wt%P – 0.094wt%P), the equation found in (Ren and Liu, 2019) predicts the contribution of solid solution strengthening on yield strength due to phosphorus to be between 19-64MPa.

Although Phosphorous increases the tensile strength of steels, it can is said to decrease the yield strength of multi-phase steels (Chen, Era and Shimizu, 1989) . Compared to samples containing no phosphorous, 0.006wt%P decreases yield strength by 42MPa (tensile strength increased by 98MPa), and 0.204wt%P decreased yield strength by 11MPa (tensile strength increased by 274MPa). Therefore, high Phosphorous samples may not lead to higher yield strengths when annealed to intercritical soak temperatures.

The advantage of nitrogen is it is a potent solid solution strengthening element in steel, and can increase the yield strength by **2918 N/mm^2** per 1wt%N according to empirical equations created by (Ren and Liu, 2019). For the nitrogen contents seen in these samples, yield strength is estimated to increase between 46-96MPa due to solid solution strengthening of nitrogen.

The disadvantage of nitrogen is it is difficult to increase the nitrogen content of packaging steels to levels above approximately 0.0130wt%N during conventional steelmaking process. This is because the solubility limit of nitrogen in steel is reached. Therefore, if nitrogen content were to be exceeded here, trapped nitrogen gas can occur leading to porosity problems, and increases the likelihood of nitrogen precipitates forming which are not advantageous for steel designed for can-end application. Therefore, an additional method such as nitriding will need to be utilised. This is where ammonia gas (NH_3) is deposited onto the steel during the annealing process whereby it dissociates into nitrogen gas which diffuses into the steel, thus increasing its nitrogen content above the restricted 0.0130wt% level,

without facing the casting issues of porosity. It is speculated that this is how a rival steelmaking business produces their high strength packaging grade steel.

4.3. Experimental procedure

For information and details regarding the experimental procedures used in this chapter, please refer to Table which will direct you to the relevant sections within the Methods and Experimental Chapter (Chapter 3).

Table 4.1. Where to find information and details on the experimental procedures used in this chapter.

Procedure	Section number
Processing history	3.1
Transformation temperatures	3.3
Annealing heat treatments performed	3.4.2
Temper rolling and Ageing	3.7
Tensile testing parameters	3.8.1
Optical microscopy	3.11
Hardness testing	3.14
Grain Size Analysis	3.12

4.4. Results

4.4.1. Tensile data

The average tensile results of alloys 1-6 in their 5% temper rolled and aged condition are given in Table 4.2. Figure 4.2 shows a bar chart of the average tensile data of alloys 1-6 when annealed using the commercial annealing settings i.e., a heating rate of 20°C/s and soak temperature 650°C. It shows the effect of chemistry on the average Rp0.2 offset yield strength, Ultimate Tensile Strength, and break elongation, with targets for yield strength (650-750MPa) and break elongation (minimum of 5%) shown.

N.B. from here on, 0.2% offset yield strength will be referred to as simply yield strength.

Table 4.2. Table showing the average mechanical properties of alloys 1-6 in their 5% temper rolled condition.

Sample	Heating rate (°C/s)	Soak temperature (°C)	offset yield, 0.2% (MPa)	Tensile strength (MPa)	Break elongation (%)
1-20-650	20	650	467	486	10.2
2-20-650	20	650	554	574	8.1
3-20-650	20	650	430	459	14.7
4-20-650	20	650	481	507	12.6
5-20-650	20	650	522	542	11.3
6-20-650	20	650	658	707	8.2

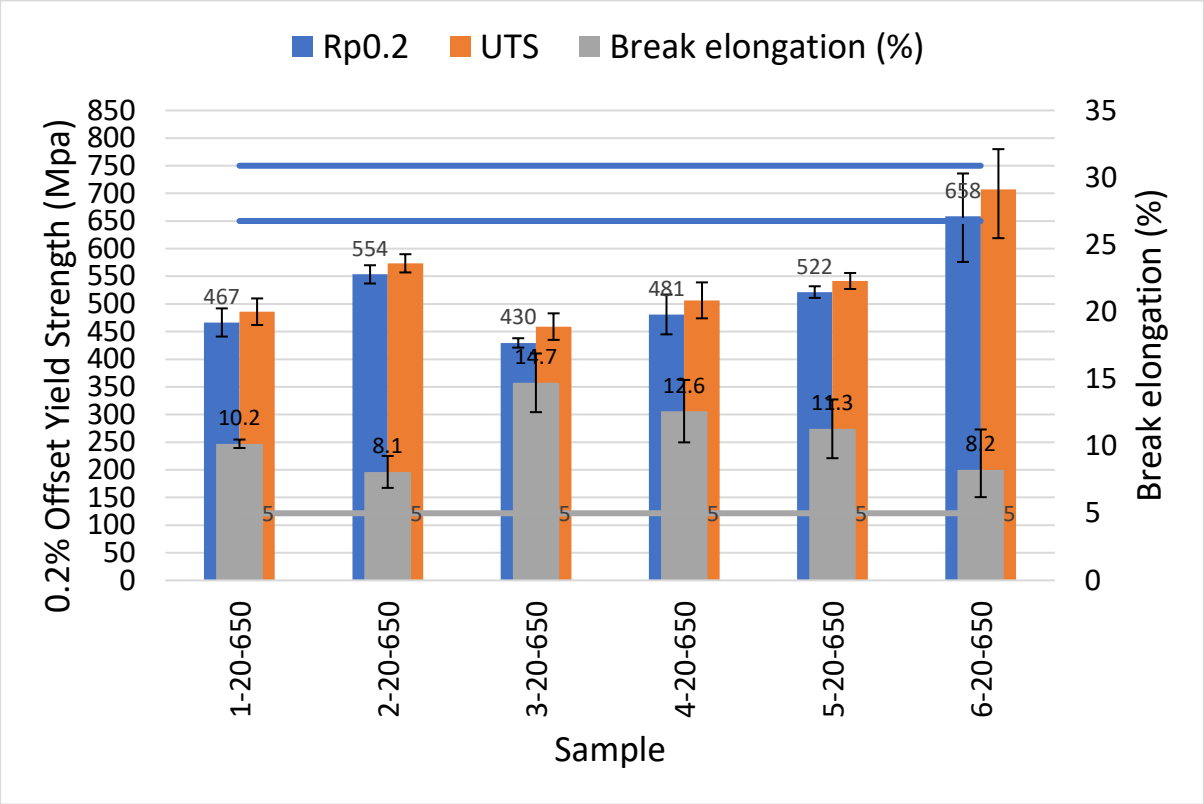

Figure 4.2. Bar chart showing the effect of chemistry during annealing when 20°C/s heating rate and 650°C soak temperature was used, in the 5% temper rolled condition.

Of the six samples tested, only alloy 6 has the required combination of yield strength and break elongation. On average, alloy 6 has the required yield strength (658MPa) and break elongation (8.2%).

4.4.2. Micrographs

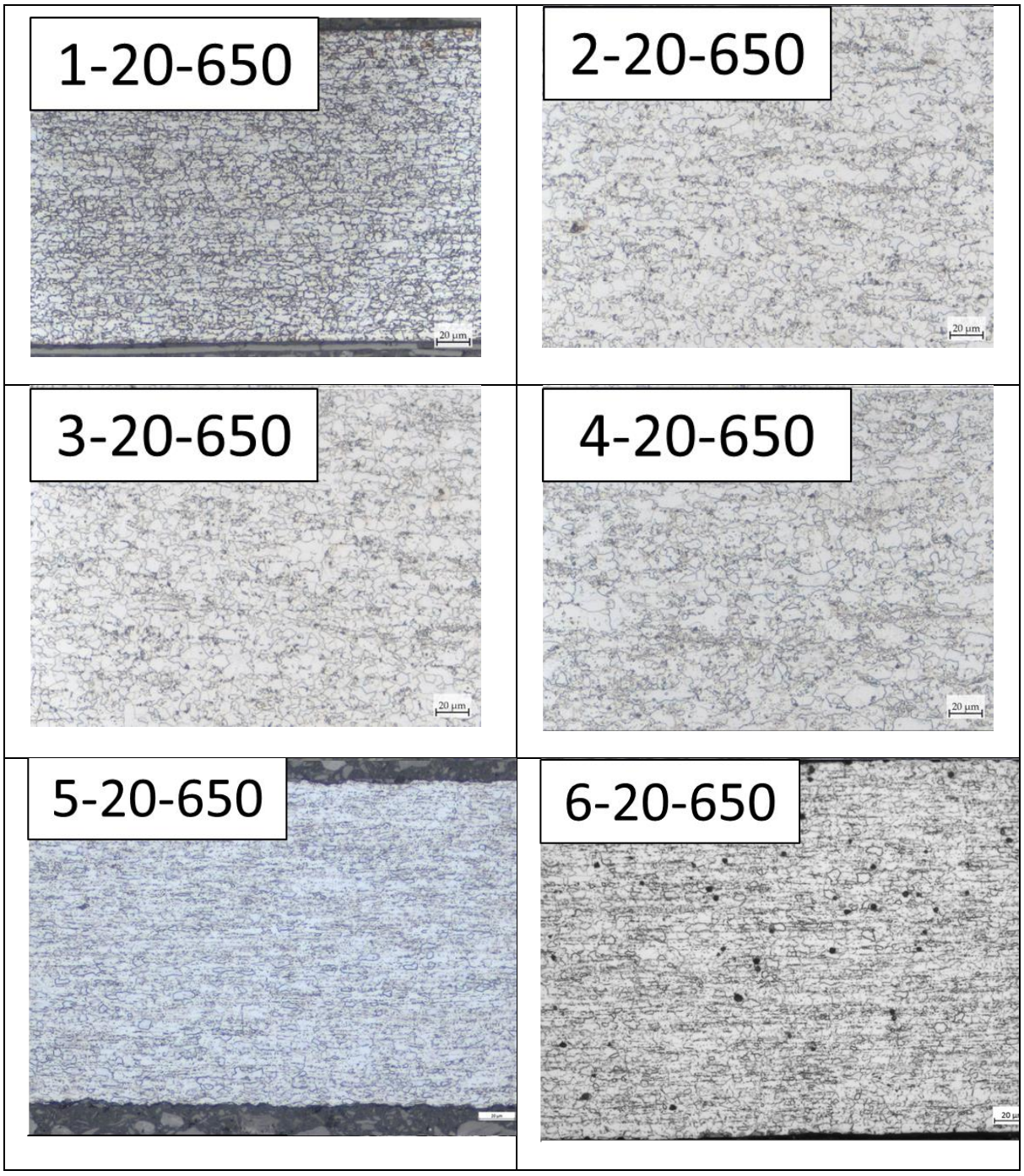

Figure 4.3. Optical microstructures of lab casted alloys 1-6.

Figure 4.3 shows optical microstructures of alloys 1-6 in their as-annealed condition

4.4.3. Grain size distributions

Figure 4.4 and Table 4.3 show the effect of changing silicon, phosphorous and nitrogen contents had on grain size data. The curves all look similar in that they are all positively skewed, meaning that the grain size is mostly small, with a mode of 2µm (for alloys 1-5) and 3µm (for alloy 6), and an average grain size of 5µm for alloy 2, and 4µm for alloys 1, and 3-6. However, there are subtle differences occurring because of increasing silicon, phosphorous, and nitrogen contents as detailed in Table 4.3, which lists statistically relevant data for each alloy.

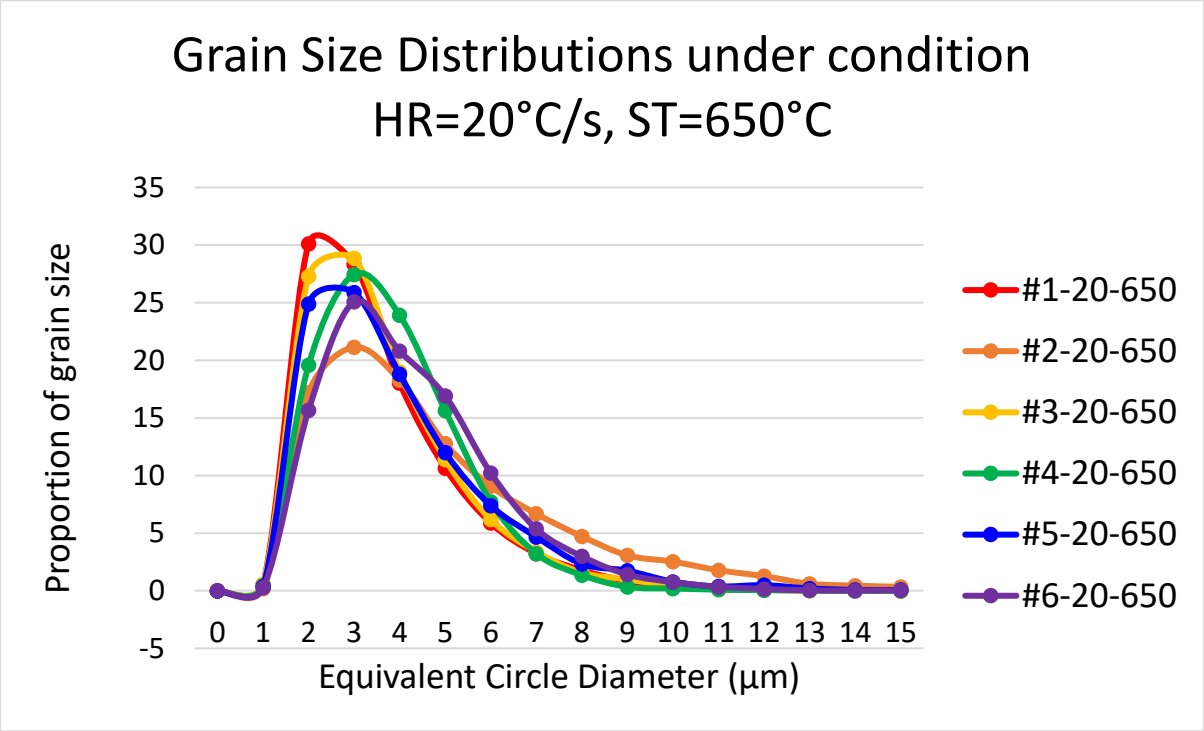

Figure 4.4. The effect of additional silicon, phosphorous and nitrogen contents on the grain size distribution.

In general, the grain size distributions of alloys 2-6 are wider than the base alloy 1. N.B. the reduction in distribution at small grain size 1µm is due to the resolution of the technique being reached.

Table 4.3. Statistical data on grain size of alloys 1-6 when commercial annealing parameters were used.

Annealing condition	*Alloy*	*S.D.*	*Average*	*mode*	*Skew*	*Kurt*
Heating rate = 20°C/s, soak temp. = 650°C	Alloy 1	1.7	3.6	2.0	1.5	2.8
	Alloy 2	2.9	4.9	2.3	1.7	4.4
	Alloy 3	1.7	3.7	2.2	1.5	2.9
	Alloy 4	1.5	3.8	2.4	1.0	1.5
	Alloy 5	2.0	4.0	2.3	1.6	3.9
	Alloy 6	1.8	4.3	2.6	1.2	2.1

4.4.4. Alloys 1&2 (effect additional 0.467wt%Si and 0.053wt%P)

The effect of increasing silicon and phosphorous contents from the reference values of 0.009wt%Si and 0.001wt%P, as seen in alloy 1, to 0.4760wt%Si and 0.0540wt%P, as seen in alloy 2, has increased the average Rp0.2 value from 467MPa to 554MPa (an increase of 87MPa), whilst decreased the average break elongation from 10.2% to 8.1% (a difference of 2.1%).

The effect on grain size distribution is all the statistical data on grain size increases, e.g., the average grain size increased from 3.6µm to 4.9µm. Modal grain size insignificantly changed from 2.0µm to 2.3µm, as did the skewness (from 1.5 to 1.7). Standard deviation increased from 1.7 to 2.9.

4.4.5. Alloys 1&3 (effect additional 0.466wt%Si and 0.0.027wt%P)

However, when the phosphorous content was decreased to a lower amount of 0.0280wt%P (compared to the phosphorus content in alloy 2), the average Rp0.2 value decreased from

467MPa to 430MPa (a reduction of 37MPa), and average break elongation increased from 10.2% to 14.7% (an increase of 4.5%).

Alloys 2 and 3 are similar in chemistry, except that alloy 2 contains 0.0250wt%P more Phosphorous (roughly double that of alloy 3). Alloy 2 has a 1:0.1 ratio of Si and P (0.5000wt%Si, 0.05wt%P), and alloy 3 has a 1:0.05 ratio of Si and P (0.5000wt%Si, 0.0250wt%P). This additional Phosphorus content in alloy 2 is perhaps responsible for the greater 124MPa, and reduction of 6.6% as seen in the 0.2wt% offset yield strength and break elongation respectively.

Furthermore, instead of increasing the phosphorous content to 0.054wt% but instead to 0.028wt%P (as seen in alloy 3), the average grain size increased by a smaller amount from 3.6µm to 3.7 µm, modal grain size increased from 2.0µm to 2.2µm, and skewness and standard deviation did not change.

4.4.6. Alloys 1&4 (effect additional 0.226wt%Si and 0.0.55wt%P)

When silicon levels were increased from 0.009wt%Si to 0.235wt%Si, and phosphorous levels were increased from 0.001wt%P to 0.0560wt%P, the average Rp0.2 increased from 467MPa to 481MPa (a small increase of 14MPa), and average break elongation increased from 10.2% to 12.6% (an increase of 2.4%). However, the strength and elongation values for alloy 1 are within the margins of error for the data of alloy 4.

When silicon and phosphorous levels of 0.235wt%Si and 0.056wt%P were used (as seen in alloy 4) the average grain size insignificantly increased from 3.6µm to 3.8µm, and modal grain size increased from 2.0µm to 2.4µm. Skewness decreased from 1.5 to 1.0, and standard deviation decreased from 1.7 to 1.5.

4.4.7. Alloys 1&5 (effect additional 0.232wt%Si and 0.093wt%P)

When silicon levels were increased from 0.009wt%Si to 0.241wt%Si and phosphorous increased from 0.001wt%P to 0.0940wt%P, the average Rp0.2 increased from 467MPa to

522MPa (an increase of 55MPa), and average break elongation increased from 10.2% to 12.3% (an increase of 2.1%).

Furthermore, average grain size increased from 3.6µm to 4.0µm, modal grain size increased from 2.0µm to 2.3µm, whilst skewness increased from 1.5 to 1.6, and standard deviation increased from 1.7 to 2.0.

Alloys 4 and 5 are chemically similar but alloy 5 contains 0.04wtwt%P more phosphorous. This extra 0.04wt%P is perhaps responsible for increasing the average 0.2% offset yield strength by 41MPa, and decreasing the break elongation by 0.3%, as seen in the tensile results for alloy 5. Here, Phosphorous appears to have insignificant effect on average break elongation (reduction of 0.3%) whereas has a significant effect on break elongation as shown in alloys 3 and 4. Perhaps this is to do with the lower silicon contents in alloys 4 and 5, which are having less negative effect on the break elongation value. The lower silicon values in alloys 4 and 5 could also explain the smaller increase in offset yield strength.

4.4.8. Alloys 1&6 (effect additional 0.205wt%Si and 0.085wt%P)

When silicon, phosphorus, and nitrogen were increased from 0.009wt%Si, 0.001wt%P, and 0.0109wt%N to levels of 0.2140wt%Si, 0.0860wt%P, and 0.0209wt%N, the average Rp0.2 increased from 467MPa to 658MPa (an increase of 191MPa), while break elongation reduced from 10.2% to 8.2% (a reduction of 2%).

Comparing alloy 6 with alloy 5 we can determine that an additional 109ppm of nitrogen increased the RP0.2 value by 136MPa and reduced the break elongation by 4.1%. Furthermore, when total nitrogen content was increased from 0.01 to 0.0209wt%N, average grain size increase from 4.0 to 4.3µm, modal grain size increased from 2.3 to 2.6µm, skewness decreased from 1.5 to 1.2, and standard deviation increased insignificantly from 1.7 to 1.8.

4.4.9. Results Summary

Sample 6-20-650 exhibits the highest average yield strength of 658MPa whilst having an average break elongation of 8.2%, making it a possible solution for the project. This is because the Rp0.2 value is within the strength target range, whilst break elongation is above the minimum target of 5%. However, whilst the heating rate and soak temperature are currently achievable on Trostre's continuous annealing production line, the chemistry, i.e., the nitrogen level, is currently unachievable. Given that the average break elongation value is 8.2%, there is opportunity to apply a greater amount of secondary cold reduction, of say 6 or 7%, to increase the Rp0.2 value, make a thinner sheet, and keep break elongation above 5%.

Sample 2, 20, 650 appears to be a potential next candidate as it has the second highest 0.2% offset yield strength, a chemistry that may be feasible, and a break elongation value above the minimum 5%. However, without chemistry alteration the strength will not match that of alloy 6 or even reach the strength target. The follow up candidate sample is 5-20-650. Although it has an Rp0.2 value that is 32MPa less than alloy 2, it does have a greater break elongation value. If given a double-reduction amount greater than 5%, the strength value will increase to a level closer to the target range. However, although it is possible to subject these samples to a higher level of double reduction, i.e., more than 5%, it could incur the risk of reducing the break elongation values below the minimum 5% value.

It is recommended that future trials involve higher double-reduction amounts of around 7-8% to assess the impact on break elongation.

4.5. Discussion

4.5.1. Predictions

Prior to testing alloys 1-6, some estimations for yield strength at all conditions were made using the following equations for yield strength:

$$\sigma_y = \sigma_0 + \sigma_s + \sigma_g + \sigma_d + \sigma_p$$

$$\sigma_s = 37[Mn] + 83[Si] + 59[Al] + 38[Cu] + 11[Mo] + 33[Ni] - 30[Cr] + 680[P] + 2918[N] + 4570[C] \quad (6)$$

Where:

- σ_0 is the lattice frictional stress (value for low-carbon steel is 53MPa)
- σ_s is solid solution strengthening
- σ_g fine grain strengthening (The value for the k_y constant in the Hall-Petch formula was taken to be 17.4MPa.mm$^{1/2}$)
- σ_d is dislocation strengthening
- σ_p precipitation strengthening. The precipitation strengthening σ_p parameter was excluded because it was assumed that there were no precipitates in these samples based on their hot-rolling history (specifically the simulated high cooling rate to low coil temperature) which made it unlikely for appreciable amounts of precipitates to have formed.

For data regarding fine grain strengthening and dislocation strengthening, alloys 5 and 6 were initially chosen in a trial and subjected to all heat treatments and 5% temper rolled and were tensile tested and had their grain size measured. The grain sizes of alloy 5 were used for the predictions of strength for alloys 1-4 because its chemistry was more similar, and it was assumed the grain sizes of alloys 1-4 wouldn't be largely different to alloy 5. Therefore, the estimations of alloys 1-4 are mostly assessing the impact of the different chemical elements in solid solution.

Alloys 5 and 6 were tensile tested in the as annealed condition and their 5% temper rolled condition to measure and determine the magnitude that 5% temper rolling had on yield strength.

The yield strength predictions are below:

yield strength (σy) estimation

	σy (HR=20°C/s, ST=650°C)	σy (HR=20°C/s, ST=850°C)	σy (HR=200°C/s, ST=650°C)	σy (HR=200°C/s, ST=850°C)
alloy 1	469	421	424	471
alloy 2	539	490	493	540
alloy 3	523	474	477	524
alloy 4	526	477	480	528
alloy 5	552	503	506	554
alloy 6	565	588	515	618

From these yield strength estimations, it is likely that the alloys most likely to give the desired yield strength from most to least likely are:

1. Alloy 6
2. Alloy 5
3. Alloy 2
4. Alloy 4
5. Alloy 3
6. Alloy 1

A drawback to these predictions is these equations are for hot-rolled properties, and give empirical trends, not the solutions. Additionally, there were no equations for predicting break elongation, so there was no way of knowing if ‘promising’ samples had the required minimum 5% break elongation value. Therefore, experimental work was performed to verify yield strengths, and determine the break elongation values.

4.5.2. Effect of higher silicon and phosphorous (alloys 1 & 2)

Comparing the mechanical results of alloy 1 and 2 assesses the impact of increasing silicon and phosphorous contents from 0.009wt%Si and 0.001wt%P (as seen in reference sample alloy 1) to higher levels such as 0.4760wt%Si and 0.054wt%P (as seen in alloy 2) and suggests that there is an insignificant change to average and modal ferrite grain size due to the extra amounts of silicon and phosphorous.

Furthermore, it is also implied that the impact of grain size strengthening is not responsible for the differences in mechanical properties seen in the six alloys as shown in Table 4.3 and Figure 4.4. Therefore, it can be assumed the effect of substitutional and interstitial strengthening is a more likely to be taking place. This is assumption is reinforced when comparing the average and modal grain sizes (Table 4.3), and tensile data (Figure 4.2) of alloys 5 and 6. Both of which have extremely similar grain size characteristics, but the Rp0.2 value of alloy 6 is 208MPa higher. The difference between these two alloys is the nitrogen content, of which alloy 6 contains 175ppm more.

To help justify this, it is worthwhile to look at the predicted strength increases from solid solution alone (see Table 4.4).

Table 4.4. Measured and predicted yield strengths of alloys 1-6.

	Measured Yield strength	Predicted yield strength due to solid solution effects	Effect of grain size effects on yield strength
alloy 1	467	97	254
alloy 2	554	166	253
Difference	**87**	**69**	**1**

As can be seen in Table 4.4, the difference in measured yield strength values between alloys 1 and 2 (87MPa) is more likely the result of solid solution strengthening effects. It is estimated that the greater silicon and phosphorus amounts

in alloy 2 will increase the yield strength by an additional 69MPa. Compare this to the insignificant contribution of grain size effects in the third column.

4.5.3. Effect of high silicon and low phosphorus (alloys 1 & 3)

The tensile result of alloy 3 is unexpected as it was assumed it would have a greater Rp0.2 value and a lower break elongation compared to the reference alloy, due to especially containing 0.466wt% more silicon and 0.027wt% more phosphorous. However, the measured Rp0.2 value of alloy 3 is 37MPa less than that of the reference alloy and has 4.5% more elongation. Using empirical equations developed by (Ren and Liu, 2019), the presence of additional 0.466wt%Si and 0.027wt%P are thought to increase the strength yield by ~39MPa and ~18MPa respectively, giving a combined strength increase of approximately 57MPa. Factoring into account that alloy 3 contains slightly less manganese and nitrogen, it was estimated that alloy 3 would have a yield strength some 53MPa greater than alloy 1 due to solid solution effects alone. Using the measured yield strength of alloy 1, it would be reasonably expected for the yield strength of alloy 3 to be somewhere in the region of 520MPa (i.e., 467MPa+53MPa).

An explanation for the less than expected yield strength and increased break elongation could be because alloy 3 possessed a 0.1µm higher average grain size and a 0.2µm higher modal grain size than alloy 1 (see Table 10). However, according to the Hall-Petch formula, this equates to a small reduction in yield strength of 4MPa (when using average grain size) or 18MPa (when using mode grain size). Therefore, even if mode grain size was used, the calculated reduction on yield strength caused by alloy 3's larger mode grain size falls short of the 37MPa difference to the reference alloy, and leaves 19MPa (i.e., measured difference of 37MPa minus the estimated reduction in yield due to 0.2µm increase in mode grain size 18MPa) unaccounted for. However, this could be the result of converging on measurement error (based on the repeats). The overall larger grain size of alloy 3 may provide an explanation for the increase in break elongation.

It is unlikely that some elements precipitated out of solution (e.g., phosphorous precipitates) because the soak temperature and time were too low for this to have happened. EDS technique was attempted to see if there were any indication if precipitates had formed, but the results showed a homogenous spread of all elements, with the exception of areas of silicon concentrations (see Figure 4.5 and Figure 4.6).

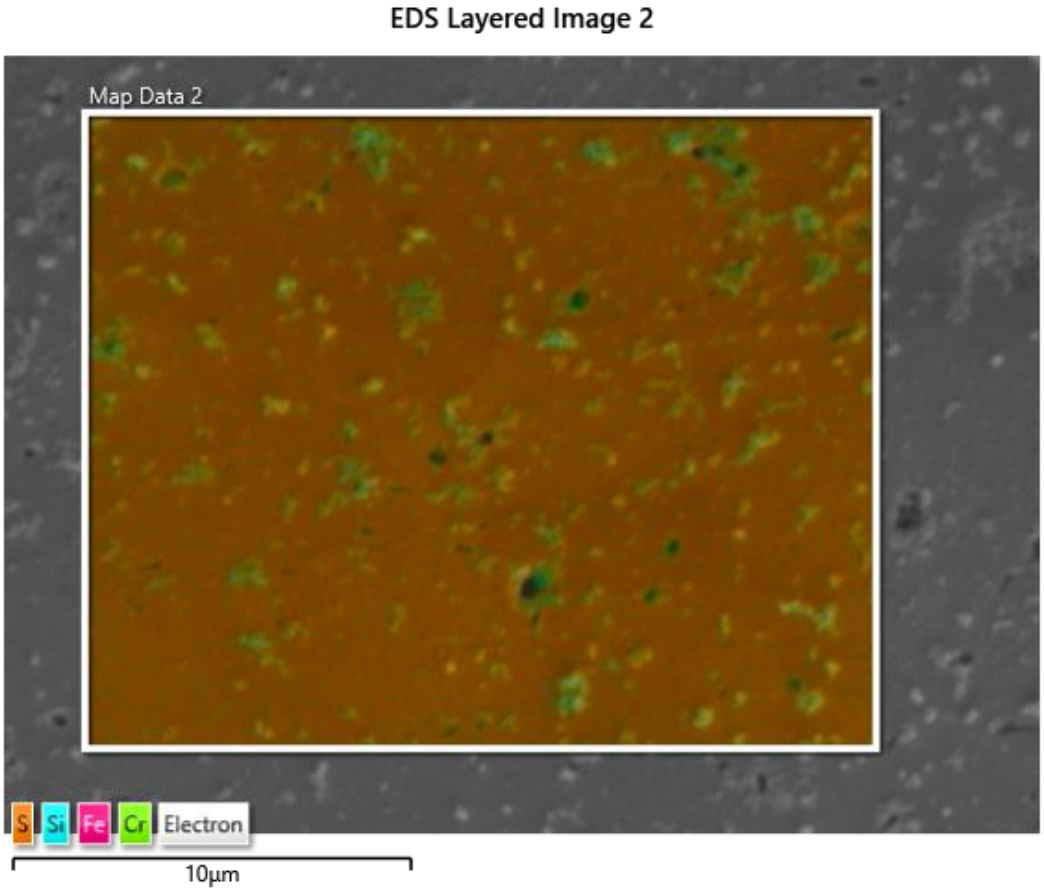

Figure 4.5. EDS image of 3-20-650.

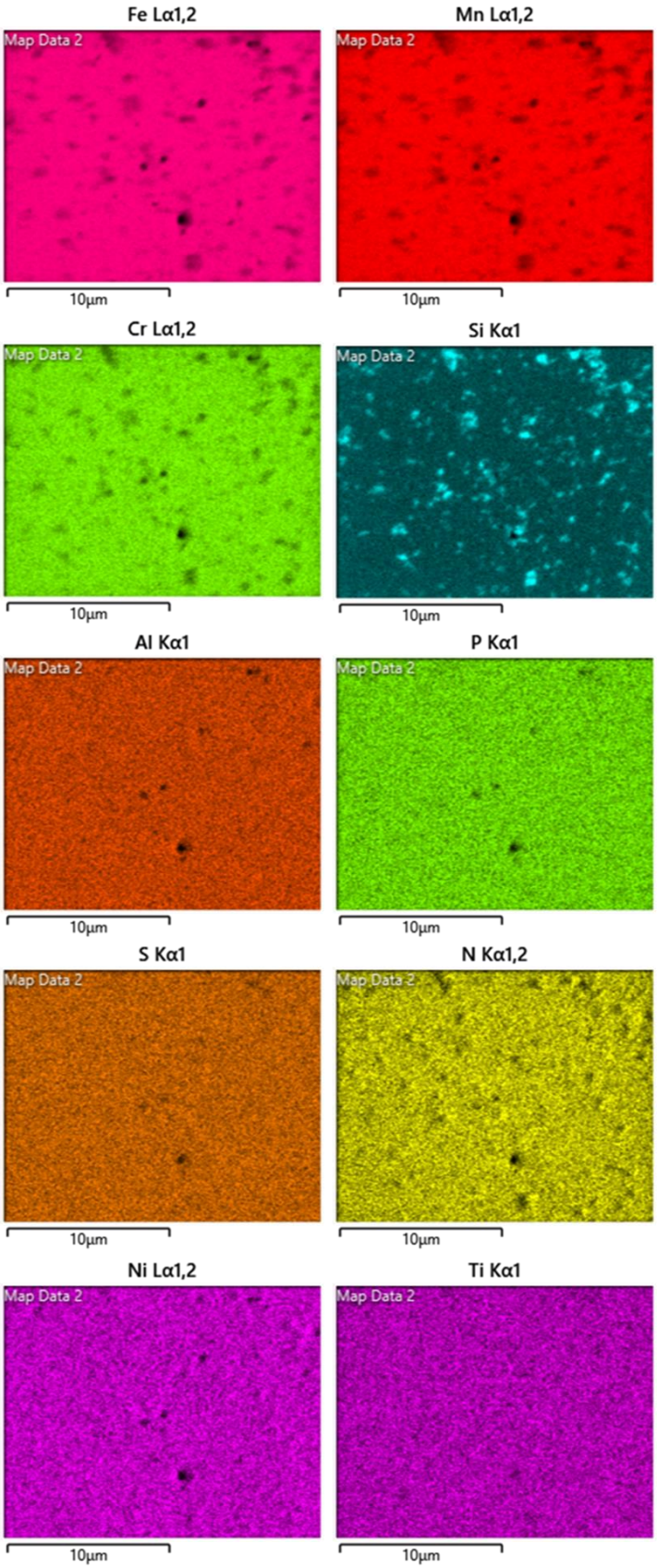

Figure 4.6. EDS maps individual elements.

Another reason for the difference between the estimated (~520MPa) and measured (~430MPa) yield strength of alloy 3 (compared to reference alloy 1), could be due to the lower amounts of manganese and nitrogen. Furthermore, the aluminium and titanium content in alloy 3 is higher which could have contributed to a reduced strength as those elements may have formed precipitates with nitrogen and carbon, at some point in the processing history, thus reducing the solid solution strengthening effect of nitrogen. For example, if we assume at some point in the processing history that the extra 0.007wt%Al and 0.001wt% Ti bonded with the unbound nitrogen and formed aluminium nitride (AlN) and Titanium nitride (TiN), and the resultant precipitates effects were insignificant, this would have removed ~0.008wt%N or 80ppm of nitrogen. This would have reduced the solid solution strengthening effect of nitrogen by 80MPa and thus yield strength by 80MPa, which could account for the 90MPa difference between the estimated and measured yield strength. However, the question of why this didn't happen with the other alloys, and also the EDS technique did not yield any meaningful aluminium/titanium precipitates.

4.5.4. Effect of low silicon and high phosphorous (alloys 1 & 4)

As expected, alloy 4 contained a higher Rp0.2 value than reference alloy 1. Assuming all elements were in solution, and using the Equation 11, it was estimated the yield strength of alloy 4 would have been around 56MPa greater, due to the combined influence of additional 0.226wt%Si and 0.055wt%P, in solution. However, measured tensile results of alloy 4 had an average of 14MPa higher. In addition, alloy 4 was not expected to have a higher break elongation value (+Δ 2.4%) than the reference alloy either.

Equation 11

$$\sigma_s = 37[Mn] + 83[Si] + 59[Al] + 38[Cu] + 11[Mo] + 33[Ni] - 30[Cr] + 680[P] + 2918[N] + 4570[C]$$

Looking at Table 4.3, the average and modal grain size for alloy 4 is 0.2µm and 0.4µm respectively higher compared to the reference alloy. This equates to a

reduction of 8Mpa (when using average grain size) or 34MPa (when using mode grain size) in yield strength. If the mode grain size is solely looked at, this increase in grain size is probably responsible for the less than estimated yield strength value and goes someway in explaining why the Rp0.2 value of alloy 4 was only 14MPa greater than the reference sample. However, this leaves 22-48MPa unaccounted for. The larger mode grain size could also explain the increase in average break elongation.

However, although alloy 4 has a larger average and modal grain size compared to alloy 3, it has a smaller average break elongation. This is likely due to the higher silicon and phosphorous contents in alloy 4.

4.5.5. Effect of phosphorus when silicon is high (alloys 2 &3)

Comparing alloys 2 and 3, we can see that increasing the phosphorus content from 0.0280wt%P to 0.0540wt%P (+Δ0.026wt%P), increases the yield strength by 124MPa and decreases the break elongation value by 6.6%, when silicon levels are relatively high. Therefore, every 19MPa in yield strength gained was matched by a decrease of 1% in break elongation.

Comparing alloys 2 and 3 we can compare the effect of increasing P content again but with higher silicon levels of 0.4750wt%Si. Increasing P from 0.028 to 0.054 (difference of 0.026wt%P) results in a positive skew of the grain size. However, as seen in alloys 2 and 4, the increases in the proportion of grains >5µm are perhaps due to the influence of higher silicon contents. Silicon has been suggested in literature (SHAH *et al.*, 2020) to have a retarding effect on recrystallization (i.e., increasing the recrystallization start temperature) due to a solute drag effect. Furthermore, the increased silicon appears to have made the material more insensitive to processing parameters, perhaps due to the more sluggish recrystallization (Somani *et al.*, 2019). However, the steels in those references are much different with a much higher carbon content.

4.5.6. Effect of phosphorus when silicon is low (alloys 4 and 5)

Comparing alloys 4 and 5, we can see again the effect of increasing phosphorous levels at higher levels from 0.0560wt%P to 0.0940wt%P (+Δ0.038wt%P), when the silicon amounts are approximately half the amount seen in alloys 2 and 3. The average Yield strength increased by an 41MPa, and break elongation decreased by a small 1.3%. Therefore, this implies that yield strength increased by 32MPa for every 1% reduction in break elongation.

4.5.7. Effect of silicon (alloys 2 & 4)

Comparing alloys 2 and 4, we can see the effect of increasing silicon only, from 0.2350wt%Si to 0.4760wt%Si (+Δ0.241wt%Si) caused the average yield strength to increase by 73MPa and reduce the break elongation by 4.5%. Therefore, yield strength increased by 16MPa for every 1% loss in break elongation. As expected, these results show that phosphorous increases the yield strength more than silicon does whilst reducing the break elongation value by a smaller increment. Furthermore, the proportion of smaller grain sizes 2-5µm are reduced while the proportion of larger grain 7-12µm are increased when higher silicon levels are used in alloy 2.

4.5.8. 1&5

As expected, the higher silicon and phosphorus contents in alloy 5 at these conditions have contributed towards a greater yield strength compared to reference alloy 1. However, the accompanying increase in break elongation was unexpected as it is thought it would have decreased. This could be explained by the 0.4µm higher average and 0.3µm higher mode grain sizes of alloy 5 (see Table 10). But these difference in grain sizes are insignificant in the context of measurement error and standard deviation of measurements (standard deviation was around 2).

It was estimated that the yield strength of alloy 5 would be 82MPa higher than the reference alloy 1 due to the combined influence of additional 0.232wt%Si and 0.093wt%P. The effect of a larger average 0.4µm, and a larger modal 0.3µm is estimated have reduced the yield strength by magnitudes of 15MPa (if average grain size used) or 26MPa (if mode grain size is used) respectively. The measured yield

strength of alloy 5 is 55MPa higher than the reference alloy. Comparing this to the estimated 82MPa difference, there is 27MPa unaccounted for. However, the difference of 27MPa between the estimated and measured yield strength could be accounted for by the calculated reduction in yield strength that a larger 0.3 µm mode grain size caused.

A common theme is seen where increasing silicon and phosphorus amounts are increasing the average and mode grain sizes. This is potentially due to the role of silicon in increasing the recrystallisation temperature due to the solute drag effect (Somani *et al.*, 2019; SHAH *et al.*, 2020).

4.5.9. Effect of Phosphorous on grain sizes- (alloys 4 and 5)

Comparing alloys 4 and 5 allows us to see the effect of increasing P content from 0.0560 to 0.0940 wt.% (difference of 0.038wt%P) whilst silicon is at a low concentration of 0.2350wt%Si. It is seen that increasing phosphorous refined the grain sizes by increasing shifting the peak of the grains size distribution towards the left to smaller grain sizes i.e.., 2-3µm size.

4.5.10. 1&6

As expected, Alloy 6 gave the highest average yield strength of these chemistries, with a promising result of 658MPa, whilst having a UTS of 707MPa and a break elongation of 8.2%. This is likely to be a consequence of its higher alloying content of silicon, phosphorous, and especially nitrogen. The 209ppm nitrogen content of alloy 6 is approximately twice that of the reference alloy 1 and is most likely responsible of all the alloying elements for the large increase in yield strength. This is seen by comparing alloy 6 with alloy 5, which differ only by nitrogen content.

However, compared to alloy 5, alloy 6 was estimated to have a yield strength increase in the region of 26MPa ,when estimated using equations by (Ren and Liu, 2019), assuming all elements were in solution. But in reality, the Rp0.2 value was 136MPa higher.

Additionally, the tensile strength is estimated to be 109MPa greater according to statements made in TKS patent WO2016030056. Within this patent it is stated there is a linear relationship between the amount of unbound nitrogen and tensile strength, where tensile strength increases by 1MPa for every extra 1ppm of unbound nitrogen. This patent makes no explicit statement that this relationship applies to yield strength. Because of the extra 109ppm of nitrogen (which is assumed to all be in solution), the tensile strength of alloy 6 should be approximately 109MPa greater than alloy 5. Because the UTS of alloy 5 was 542MPa, this would estimate the tensile strength of alloy 6 in the region of 651MPa.

However, the UTS was 707MPa, which was 56MPa more than estimated. Although this unaccounted 56Mpa is within the margins of error for alloy 6, an explanation could be that alloy 6 had a 0.3µm larger average and mode grain size than alloy 5. This larger grain size is estimated to have reduced the yield strength by 10MPa (if average grain size is used) or 22MPa (if mode grain size is used). Nevertheless, this would still leave 34MPa (56MPa – 22MPa, effect of mode grain size) or 46Mpa (56MPa-10MPa, effect of average grain size) unaccounted for.

As mentioned above about previous chemistries, it was suspected that the actual chemistries of these samples were not as quoted, which could provide an explanation for the large differences in estimated yield strengths for alloys 1-6. To gain more clarity on reasons for this large difference in yield and tensile strength between alloy 5 and 6, all chemistries were analysed using a ‘SPRECTROLAB LACM12’ optical emission spectroscopy (OES) to double check the amounts of elements and that they match the original quoted amounts. Below are the OES measurements for each of the alloys, with each value being an average of four measurements:

Table 4.5. OES determined chemistries of alloys 1-6.

Alloy	C	Mn	Al	Si	S	P	Ti	N	Fe
1	0.0930	0.491	0.0614	0.0110	0.0208	0.0070	0.0000	0.0312	Bal.
2	0.103	0.392	0.0751	0.523	0.0045	0.0683	0.0003	0.0197	Bal.
3	0.111	0.442	0.0578	0.534	0.0089	0.0395	0.0000	0.0339	Bal.
4	0.0899	0.512	0.0744	0.257	0.0029	0.0667	0.0005	0.0164	Bal.
5	0.0901	0.517	0.0547	0.255	0.0031	0.111	0.0008	0.0154	Bal.
6	0.0846	0.587	0.06675	0.2595	0.00435	0.10245	0.0005	>0.035	Bal.

The OES measurements bear strong similarity to the original quoted values apart from the readings for nitrogen, where some values are the maximum measurement capability of the machine[2]. This means the actual nitrogen amounts could have been greater. Therefore, samples had their nitrogen contents measured using an ELTRA machine, with an average of three measurements given. The results of the OES with ELTRA obtained nitrogen results are given in Table 4.6:

Table 4.6. OES determined chemistries with ELTRA obtained nitrogen values.

Alloy	C	Mn	Al	Si	S	P	Ti	N	Fe
1	0.0930	0.491	0.0614	0.0110	0.0208	0.0070	0.0000	0.0111	Bal.
2	0.103	0.392	0.0751	0.523	0.0045	0.0683	0.0003	0.0103	Bal.
3	0.111	0.442	0.0578	0.534	0.0089	0.0395	0.0000	0.0105	Bal.
4	0.0899	0.512	0.0744	0.257	0.0029	0.0667	0.0005	0.0110	Bal.
5	0.0901	0.517	0.0547	0.255	0.0031	0.111	0.0008	0.0108	Bal.
6	0.0846	0.587	0.06675	0.2595	0.00435	0.10245	0.0005	0.0283	Bal.

[2] It was later revealed this machine is not suited for measuring the nitrogen content of thin gauge steel sheet. One given reason was the test penetrates though the material, leaving a hole, and detects nitrogen in the atmosphere.

With these updated values, the actual difference in nitrogen content between alloys 5 and 6 is greater at 175ppm, rather than the previously thought 109ppm. Following the statement made in the TKS patent, this should put the yield and tensile strength of alloy 6 in the region of 697MPa (assuming a similar 1MPa:1ppm relationship) and the UTS at 717MPA. Whilst this suits the UTS value, it puts the estimated yield strength 39MPa higher than the average measured value, which makes the unaccounted yield strength loss greater. Whilst the initial 27MPa using the original chemistry could be accounted for by looking at the 0.3µm increase in average and mode grain size (-10 to 22MPa), there is now an extra 12 MPa unaccounted for (39MPa-27MPa). However, the larger context these values are very small compared to the measurement error.

Although this is within the margin of error for yield strength for alloy 6, a potential explanation is that the unbound nitrogen was removed from solution at some point in the alloys processing history, e.g., in the early hot-rolling stage where the aluminium and titanium could have bonded with unbound nitrogen and formed Aluminium nitrides (AlN) and/or titanium nitrides (TiN). Perhaps this explains the less than estimated yield and tensile strength values for alloy 6 as well as all alloys above.

Additionally, the two aging steps performed on these samples, i.e., the simulated overageing section 400°C for 1 minute during simulated annealing and aging of temper rolled samples 200°C for 20 minutes prior to tensile test, could be why the elongation value of alloy 6 was lower. These two heat treatments and the higher nitrogen content of alloy 6 enabled diffusion of more nitrogen to dislocation cores thus pinning them more.

Within the TKS patent, there was no mention of the relationship between nitrogen content and yield strength and break elongation. Therefore, Figure 4.7 below offers some insight.

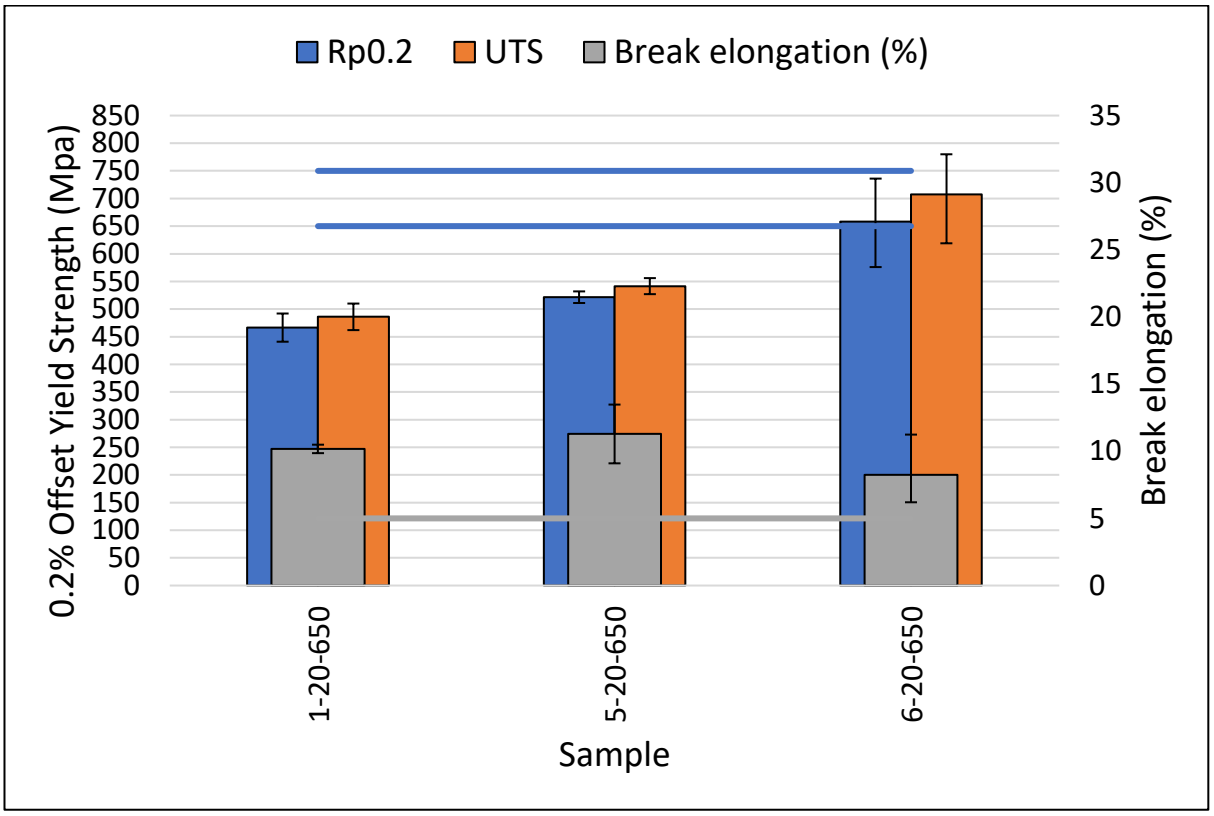

Figure 4.7. Rp0.2 yield strength and break elongation of alloys 5 and 6 (and alloy 1).

Comparing alloys 5 and 6 (see Figure 4.7), we can see that an additional 175ppm of nitrogen has increased the Rp0.2 value by an average of 136MPa and decreased the break elongation by an average of 3.1%. Therefore, it can be said that an increase of 1ppm of nitrogen added in the casting/melting stage, the yield strength increases by ~0.8MPa, and the break elongation reduces by ~0.02%. However, it should be highlighted that the TKS patent describes unbound nitrogen being introduced in two separate stages. One via the melting/casting stage, and another via a secondary process during the annealing stage whereby ammonia gas is dissociated over the steel furnace and free nitrogen dissolves and diffuses into the sheet. All alloys above only had nitrogen introduced in the melting/casting stage offering additional opportunities for precipitation (and associated reduction in free nitrogen) through processing.

4.5.11. Effect of nitrogen on grain size

When comparing the higher nitrogen content of alloy 6 with alloy 5, nitrogen appears to shift the peak towards the larger grain sizes, reducing the proportion of 2µm sized grains by ~9%, reducing the proportion of 3µm sized grains by an insignificant 1% but increasing the proportion of 4, 5, and 6µm sized grains by 2%, 5%, and 3% respectively. Perhaps this is another reason why nitrogen is able to increase the Rp0.2 value whilst not reducing the average break elongation below a suitable 5%.

Overall, the effect of grain size strengthening has had an insignificant/limited impact on the mechanical properties of these six alloys. Therefore, another more potent strengthening mechanism must be responsible for the big differences in mechanical properties.

Furthermore, in terms of optimising the chemistry of alloy 6 so that the average yield strength is halfway between the lower and upper yield strength targets, i.e.,700MPa, it might be advisable that the nitrogen content is reduced by 48ppm to approximately 0.0241wt%N. It could be expected this reduction in nitrogen will have the following benefits:

1. Break elongation is expected to increase, to approximately 7.5%.
2. Enabling a higher double-reduction amount to be performed, say 6 or 7%, which will increase Rp0.2 value (potentially closer to the prior 742MPa).
3. Resulting in a thinner gauge sheet, therefore increasing the area of a steel coil, thus potentially increasing the number of can ends able to be extracted per coil.

It’s important to bear in mind that a thinner gauge due to higher double-reduction will mean more driving force for recrystallisation. This could result in a steel with greater elongation value, but also a lower strength value.

However, there are limiting factors for the adoption of alloy 6 chemistry, particularly its 0.0283wt%N nitrogen content, which are:

- Tata Steel Port Talbot (from which Trostre are supplied with their hot-rolled packaging steel) is limited to only introducing nitrogen into the steel during the melting/casting stage at which 120ppm nitrogen is the maximum they can achieve. Even if it were possible to achieve a higher nitrogen content in the melting/casting stage, it's advised not to go above 160ppm. This is because it increases the likelihood of undesirable defects such as pores and cracks to form, which are oxidised by ambient oxygen, thus leading to coils being scrapped and wasted.
- Trostre do not have an additional secondary procedure in which to introduce and further increase nitrogen in the steel. Such secondary procedures include:
    - **Gas nitriding** in an ammonia atmosphere at a slight over pressure (a method used and patented by competitor Thyssenkrupp).
    - **Bath nitriding** using nitrogenous salt bathing.
    - **Plasma nitriding.**

Sources of error in the results could have been:

- Inaccurate secondary cold rolling applied after annealing, i.e., less than or more than the desired 5% reduction. The secondary cold rolling work was performed externally by technicians using the industrially cold mill.
- The proportion of free nitrogen is unknown and presents a gap in the understanding of the tensile results.

4.6. Conclusions

Six novel lab-casted packaging grade steels for high-strength can end applications were subjected to a simulated annealing cycle that replicated the commercial annealing cycle used by industry for this application. The conclusions of this work are:

- Firstly, it appears that higher additions of silicon, phosphorus, and nitrogen overall encourages grain growth, causes the distribution of grain sizes to become wider, and shift the peak of the distributions to the right towards larger grain sizes, compared to the reference alloy 1. However, these effects

are small and can be insignificant in the context of the Hall-Petch relationship and the contribution of grain size strengthening towards the mechanical properties of these steels.

- Secondly, it was determined that the solid solution strengthening effects of higher alloying amounts of silicon, phosphorous, and nitrogen (as seen in alloys 2-6) are more likely responsible for the difference in tensile properties seen in these grades. In general, higher amounts of silicon, phosphorus, and especially nitrogen result in proof stress and ultimate tensile strength to be greater.
- The high nitrogen chemistry, alloy 6, gave significantly higher proof stress and ultimate tensile strength values compared to the other chemistries, whilst maintaining a suitable elongation value above the 5% minimum. The significantly higher proof stress and ultimate tensile strength values were attributed to the higher nitrogen content whereby it was presumed to contain a greater amount of free nitrogen. Alloy 6 was the only chemistry to give the desired proof stress value within the 650-750MPa range (actual average value was 658MPa) and to maintain an elongation value above 5% (actual average elongation value was 8.2%).

5. Technical chapter 2 – The effect of flash annealing (200°C/s heating rate) on lab-casted high-strength packaging grade steels for can-end applications.

5.1. Purpose of study

In this chapter, the effect of increasing the heating rate from a commercially feasible 20°C/s, to an unfeasible rapid heating rate of 200°C/s, was assessed. Whilst doing so, all other annealing parameters were kept the same, i.e., set at commercial parameters, e.g., soak temperature was 650°C. See Figure 3.4 for a schematic of the annealing cycle used.

As mentioned in the literature review section, the use of an ultra-rapid heating rate during annealing heat treatment has been shown to increase yield and ultimate tensile strength of steel by causing insufficient time for carbide formation. The result is more interstitial atoms carbon and nitrogen atoms to remain in solid solution in the ferrite matrix, thus increasing the strength via interstitial solid solution strengthening. Furthermore, it was found that rapid heating to temperatures ~70°C below the ~Ac1 transformation temperature resulted in a peak in hardness, shear stress, and shear strain. This was attributed to recrystallisation not being accelerated at this temperature. Therefore, it was hoped that comparable effects could be achieved in the six lab casted chemistries studied in the previous chapter. Like the previous chapter, samples were tensile tested in their 5% temper rolled and aged condition. Moreover, if an ultra-rapid heating rate yielded favourable mechanical property results, it could provide justification for the sponsor company to invest in upgrading their CAPL to be capable of implementing rapid heating rates.

For information and details regarding the experimental procedures used in this chapter, please refer to Table which will direct you to the relevant sections within the Methods and Experimental Chapter (Chapter 3).

Table 5.1. Where to find information and details on the experimental procedures used in this chapter.

Procedure	Section number
Processing history	3.1
OES & ELTRA obtained chemistry	Table 4.6
Transformation temperatures	3.3
Annealing heat treatments performed	3.4.3
Temper rolling and Ageing	3.7
Tensile testing parameters	3.8.1
Optical microscopy	3.11
Hardness testing	3.14
Grain Size Analysis	3.12

5.2. Results

5.2.1. Tensile results

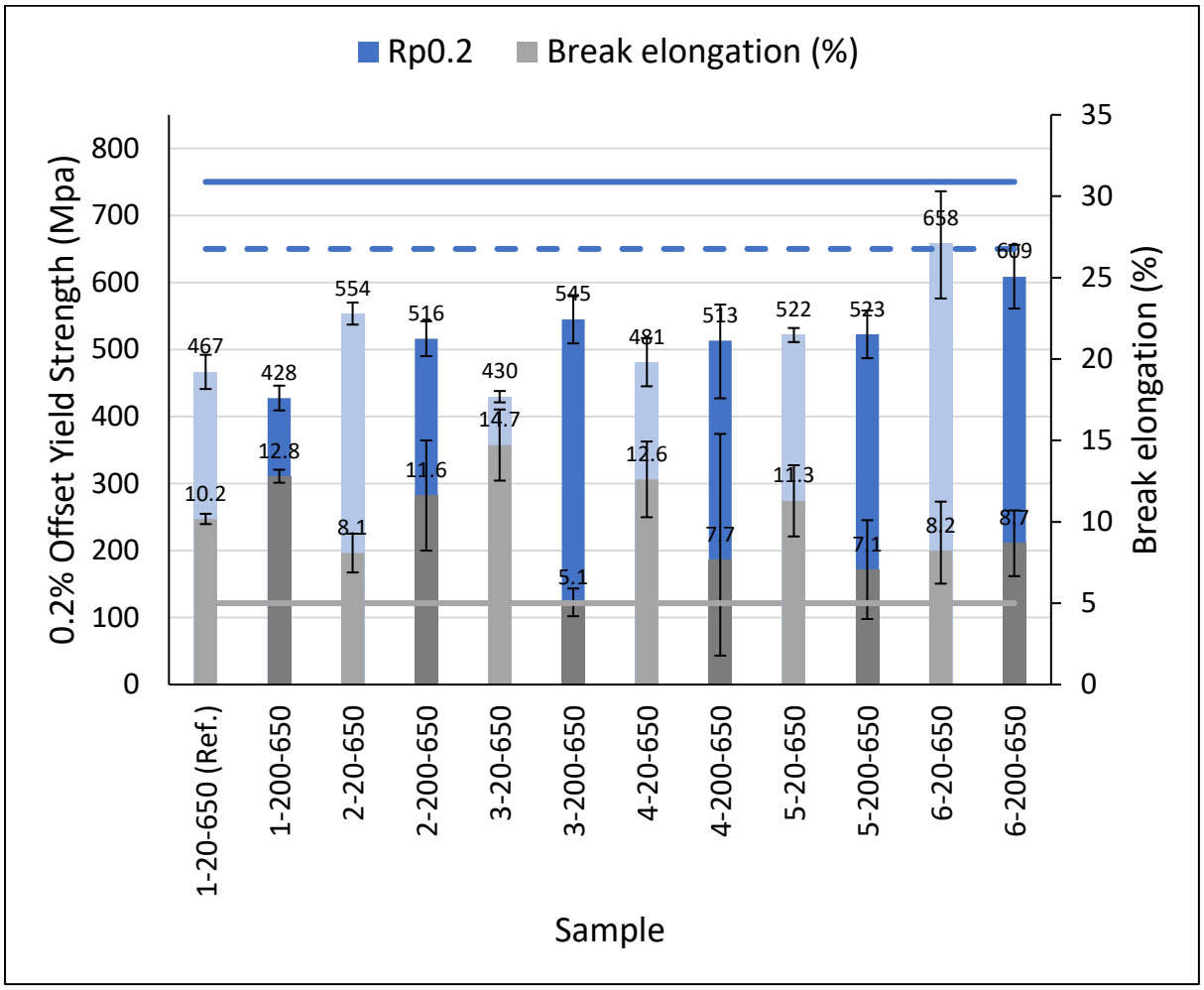

Figure 5.1. Bar graph comparing the yield strength and break elongations of alloys 1-6 when heating rate was increased to 200°C/s (darker shade bars). Yield strength minimum (dashed line) and maximum (solid line) targets are represented by the horizontal blue lines. 5% minimum total elongation is represented by the horizontal grey line. For reference, the tensile data when 20°C/s heating rate was used is included (lighter shade bars).

5.2.2. Grain size data

Table 5.2. As annealed grain size data (µm) for alloys 1-6 when heating rate was increased.

	Annealing condition							
	HR=20°C/s-ST=650°C				HR=200°C/s-ST=650°C			
Alloy	Average	Mode	Skew	S. D.	Average	Mode	Skew	S. D.
#1	3.6	2.0	1.5	1.7	4.2	2.5	1.2	1.9
#2	4.9	2.3	1.7	2.9	4.4	3.0	0.8	1.6
#3	3.7	2.2	1.5	1.7	3.6	2.1	1.4	1.5
#4	3.8	2.4	1.0	1.5	3.7	2.5	1.4	1.6
#5	4.0	2.3	1.6	2.0	3.5	2.1	1.2	1.3
#6	4.3	2.6	1.2	1.8	4.2	2.1	1.2	2.0

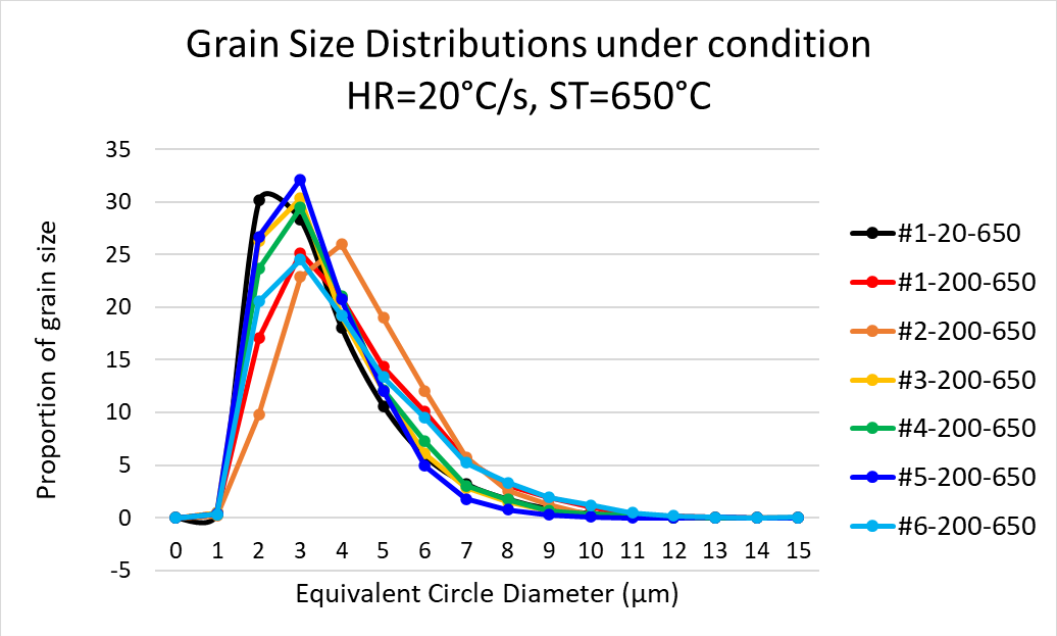

Figure 5.2. Effect of increasing heating rate from 20°C/s to 200°C/s on grain size distributions. Grain size distribution of reference sample 1-20-650 is included for comparison purposes.

5.2.3. Analysis of results

Figure 5.1 shows the effect on tensile properties when heating rate was increased from 20°C/s to 200°C/s. The offset yield strengths of alloys 1, 2, and 6 decreased when heating rate was increased, and were accompanied with an increase in break elongation. On the other hand, alloys 3, 4, and 5 (although average yield didn't change much) increased in yield strength and break elongation decreased.

Table 5.3 shows the effect of heating rate on yield strength and break elongation for alloys 1-6.

Table 5.3. Table showing the effect of increasing heating rate from 20°C/s to 200°C/s at sub-critical 650°C soak temperature, on tensile properties.

Alloy	Heating rate	Soak temperature	Offset yield strength (MPa)	Change in offset yield strength (MPa)	Break elongation (%)	Change in Break elongation (%)
1	20	650	467		10.2	
	200	650	428	-39MPa	12.8	+2.6%
2	20	650	554		8.1	
	200	650	516	-38MPa	11.6	+3.5%
3	20	650	430		14.7	
	200	650	545	+115MPa	5.1	-9.6%
4	20	650	481		12.6	
	200	650	513	+32MPa	7.7	-4.9%
5	20	650	522		11.3	
	200	650	523	+1MPa	7.1	-4.2%
6	20	650	658		8.2	

	200	650	609	-49MPa	8.7	+0.5%

In the previous chapter, sample 6-20-650 was highlighted as a potential candidate to fulfil the project aim. However, increasing the heating rate to 200°C/s has reduced the average yield strength from 658MPa to 609MPa which is below the target range for yields strength. Moreover, the break elongation value appears to have been insignificantly affected, increasing from an average of 8.2% to 8.7%.

5.3. Discussion

5.3.1. Alloy 6

It was expected that the yield strength of alloy 6 would have increased, and not decreased from 658MPa to 609MPa. This was expected because, as mentioned in the literature review section, work by (M. A. Mostafaei and Kazeminezhad, 2016) showed that the hardness of samples annealed with a 200C/s heating rate increased with soak temperature up to a maximum around ac1 temperature, whereas the hardness of samples furnace annealed with a 0.3C/s heating rate decreased with soak temperature even as soak temperature passed the ac1. The increase in hardness in that work was credited to **insufficient time for carbides** to form, therefore a greater amount of carbon was in solid solution. Therefore, nitrogen being an interstitial element, it was presumed it behave similarly to carbon in that study, in that it can also form precipitates, and because this work used a temperature below the Ac1 for this alloy, nitrogen precipitation would be retarded, and thus the sample would display a higher hardness and thus exhibit a higher yield strength.

Due to the sub-critical soak temperature 650°C and short soak time used, it was unlikely that substantially visible second-phase particles were generated in these samples, and therefore ‘Zener Pinning’ can be discredited for refining the microstructures.

Looking at the microstructures below for samples 6-20-650 and 6-200-650, the presence of carbides (darker areas) can be seen to be less in sample heated at

200°C/s heating rate. Therefore, this leads me to believe the high heating rate has retarded carbide formation and presumably nitride formation. Therefore, the reduction in yield strength is not due to solute atoms carbon and nitrogen precipitating.

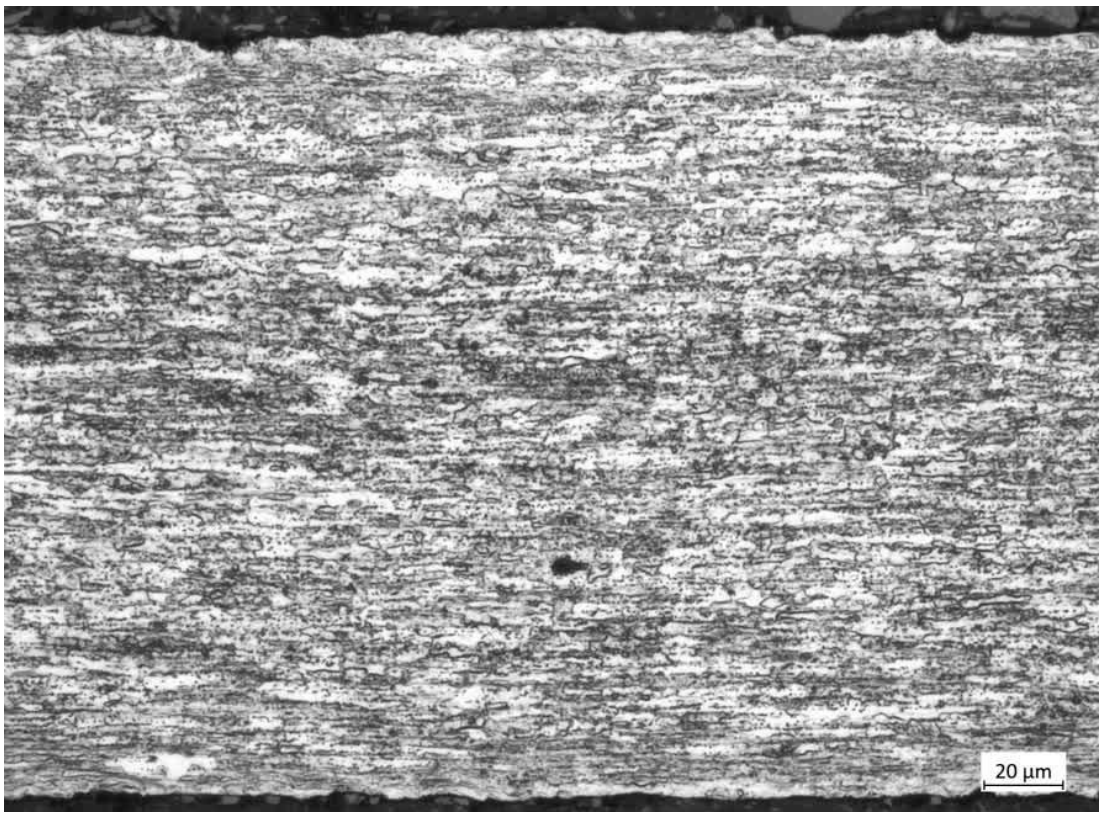

Figure 5.3. Optical microstructure of sample 6-20-650

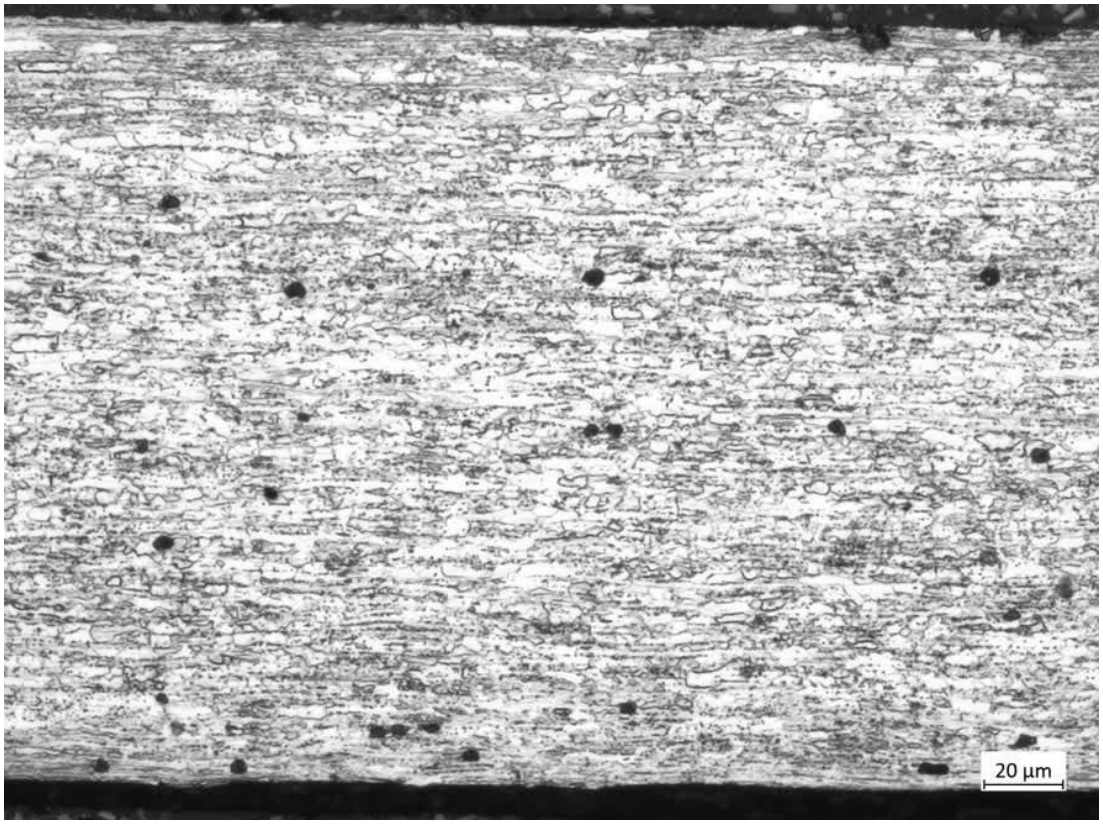

Figure 5.4. Optical microstructure of sample 6-200-650.

Another reason for using the high heating rate is because the expectation of **increased nucleation rate and reduce time for grain growth** (Wang *et al.*, 2011), and thus would exhibit a slightly refined microstructure as measured by average grain size. However, the average grain size of sample 6-200-650 decreased by an insignificant amount from **4.3µm to 4.2µm.** Such a reduction is expected not expected to change the yield strength significantly, and therefore, **change in yield strength is not due to grain size changes**.

It could be argued that sample 6-200-650 underwent more recrystallisation when heating rate was increased from 20°C/s to 200°C/s, which in turn lowered the dislocation density, and thus yield strength. This could also explain the relatively insignificant increase in break elongation from 8.2% to 8.7%. Perhaps the yield strength reduction was **due to more recrystallisation occurring**. However, there isn't a strong justification for this as a slower heating rate will overall provide a larger time-temperature response compared to a faster one. As break elongation should be significantly affected by dislocation content (even more so than yield

stress) dislocation content should be higher in the 200°C/s heating rate sample, thus yielding a lower break elongation value.

The higher nitrogen content in alloy 6 is responsible for its reduction in yield strength. This is because alloy 5, which contains 175ppm less nitrogen, didn't change in yield strength but did decrease in break elongation. Therefore, there is a weakening mechanism associated with nitrogen, particularly when levels are high (like those in alloy 6, i.e., 283ppm), and when a rapid 200°C/s heating rate was used. At slower heating rates, where the time at temperature is greater, you could get more precipitation if there is a lot of carbon still in solution prior to the start of annealing. Therefore, it could be presumed that under conditions of rapid 200°C/s heating rate, whilst carbon precipitation is reduced, more nitrogen precipitation occurs instead. Furthermore, because the stress-strain graph for rapidly heated sample exhibits longer discontinuous yielding, it's implied that a greater amount of atmosphere of nitrogen around dislocation cores took place. See Figure 5.5 for examples of stress-strain curves showing the difference between discontinuous yielding behaviour length for samples 6-20-650 and 6-200-650.

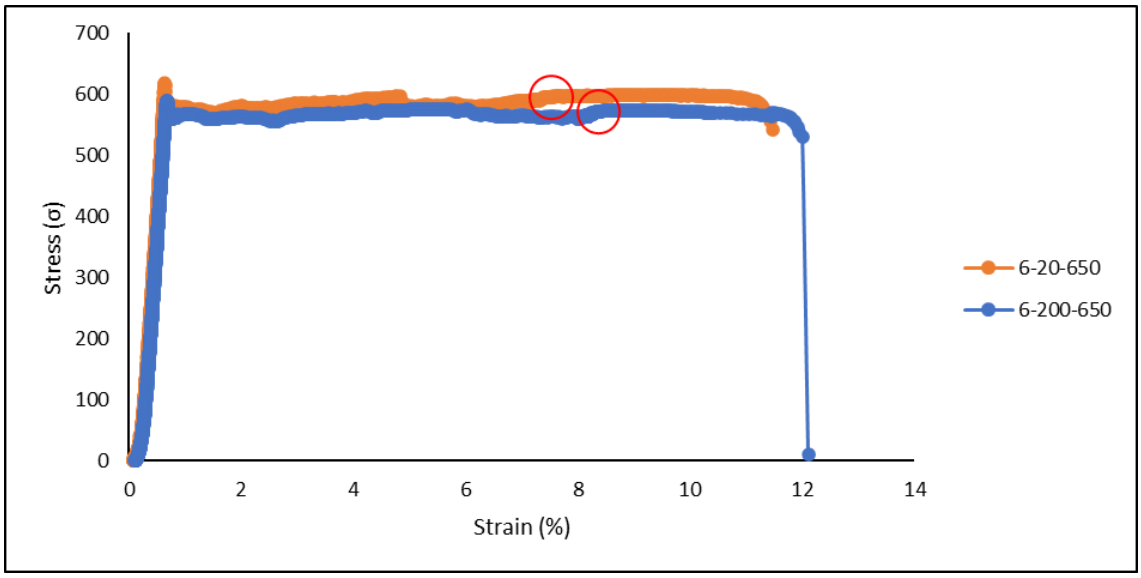

Figure 5.5. Example of stress-strain curves for samples 6-20-650 and 6-200-650. Note the end of the discontinuous yielding sections (circled in red).

5.3.2. Reference Alloy 1

It was interesting to see that the average grain size of alloy 1 increased. This is because an expectation of increasing the heating rate from 20°C/s to 200°C/s is to increase nucleation rate and reduce time for grain growth (Wang *et al.*, 2011), and thus would exhibit a slightly refined microstructure as measured by average grain size. Therefore, it can be implied that the lower silicon and phosphorus contents in alloy 1 were a cause of the higher grain size by suppressing recovery and recrystallisation and encouraging grain growth. The larger average grain size of alloy 1 would have contributed to the reduction in yield strength.

Alloys 2-6 did exhibit a smaller average grain size which implies that higher silicon and phosphorous contents of alloys 2-6 were responsible for the finer ferrite grain size. It is said that higher heating rates cause an **increase in the recrystallisation start temperature** close to Ac1 temperature, therefore which may have the effect of **producing a partial recrystallised and refined microstructure**. Furthermore, the skew values of alloys 2-6, as shown in Table 5.2, are less positive when heating rate was increased, showing that the distribution of grain sizes is becoming more symmetrical. This is indicative of incomplete recrystallisation, and silicon and phosphorus encourage the partial recrystallisation and grain refinement to occur.

5.4. Conclusion

Overall, using a rapid heating rate of 200°C/s has had a mixed effect on tensile properties, depending on the chemistry used. For example, in some samples. i.e., alloys: 1, 2, and 6, proof stress decreased, and break elongation increased, whereas alloys 3 and 4 saw increases in proof stress and reductions in break elongation value. Alloy 5 saw no change in average proof stress but did exhibit a reduction in break elongation. Furthermore, the higher heating rate had a less significant effect when compared to the compositional effect seen in alloys 5 and 6 noted in the previous chapter.

Increasing the heating rate from 20°C/s to 200°C/s resulted in:

- The yield strength of high nitrogen sample alloy 6 to have decreased from 658MPa to 609MPa possibly because more recrystallisation occurred. It is unlikely nitride precipitation occurred because the microstructures of higher heating rate samples show fewer carbides. Average grain size decreased insignificantly so effect of grain size can be ruled out. It was noted that the grain size distribution of alloy 6 had a longer tail compared to alloy 5. This implies that the higher nitrogen in sample alloy 6 resulted in more recrystallisation/instability at higher heating rate.
- Higher heating rates decreased average grain size by an insignificant small amount. Therefore, this was determined to have had an insignificant influence on the strength properties seen in the context of the Hall-Petch relationship.

6. Technical chapter 3 – The effect of intercritical soak temperature 850°C on lab-casted high-strength packaging grade steels for can-end applications.

6.1. Purpose of study

This chapter will look at increasing the yield strength of six lab casted packaging grade steels for can-end applications, by using an inter-critical soak temperature of 850°C during the annealing process. The reason for using an inter-critical soak temperature is so that small amounts of austenite phase forms during the soak stage, where upon cooling, then transforms to a harder secondary phase. It is the formation of this harder secondary phase that will be exploited to achieve greater yield strength values. If subjecting packaging grade steel compositions to inter-critical soak temperatures (temperatures which the sponsor company's CAPL cannot currently achieve) yield favourable results (i.e., mechanical properties), then this could provide justification for investment to upgrade the CAPL to allow it the capability.

6.2. Experimental procedure

For information and details regarding the experimental procedures used in this chapter, please refer to Table which will direct you to the relevant sections within the Methods and Experimental Chapter (Chapter 3).

Table 6.1. Where to find information and details on the experimental procedures used in this chapter.

Procedure	Section number
Processing history	3.1
OES & ELTRA obtained chemistry	Table 4.6
Transformation temperatures	3.3
Annealing heat treatments performed	3.4.4
Temper rolling and Ageing	3.7
Tensile testing parameters	3.8.1
Optical microscopy	3.11
Hardness testing	3.14
Grain Size Analysis	3.12

For details on the annealing heat treatment procedure carried out in this chapter, please see chapter 3.4.4.

6.3. General remarks

As mentioned earlier, the use of an inter-critical soak temperature enables the formation of austenite, which upon cooling, transforms to a harder secondary phase. It is this transformation that is to be exploited to increase the yield strength of these steels. It is expected that each chemistry will have a higher yield and tensile strength compared to the values seen in the two previous chapters.

Given that the chemistries of alloys 1-5 only vary in silicon and phosphorous contents, and the two elements are known to have a smaller effect on strength properties when compared to nitrogen, it is expected that the mechanical properties of these alloys will change by a smaller amount when compared to the high nitrogen sample alloy 6. Looking at how the yield strength of alloy 6 decreased by a relatively large amount in the previous chapter due to the high heating rate, a reason put down to a higher amount of nitrogen precipitation occurring, it is expected that an inter-critical soak temperature will lead to a greater amount of nitrogen precipitation occurring, and thus a lowering of yield strength due to loss of nitrogen's solid solution strengthening effect. However, it is unknown whether this loss in solid solution strengthening can be compensated with and reversed via the formation of harder secondary phase.

6.3.1. JMatPro TTT diagram

Figure 6.1 shows the predicted TTT diagram for the lab casted alloy 1 (with the cooling sections of annealing cycle superimposed). This diagram was generated using JMatPro version 10.2 software with settings of 850°C austenitisation temperature and 5µm prior austenite grain size. Figure 6.1 shows that the soak temperature 850°C was with in the Ac1 and Ac3 transformation temperatures for this grade, and therefore inter-critical annealing was conducted. Furthermore, the TTT diagram predicts that upon cooling, the microstructure will cool through the ferrite nose and then through the pearlite nose. It is therefore, expected that some volume fraction of pearlite will form.

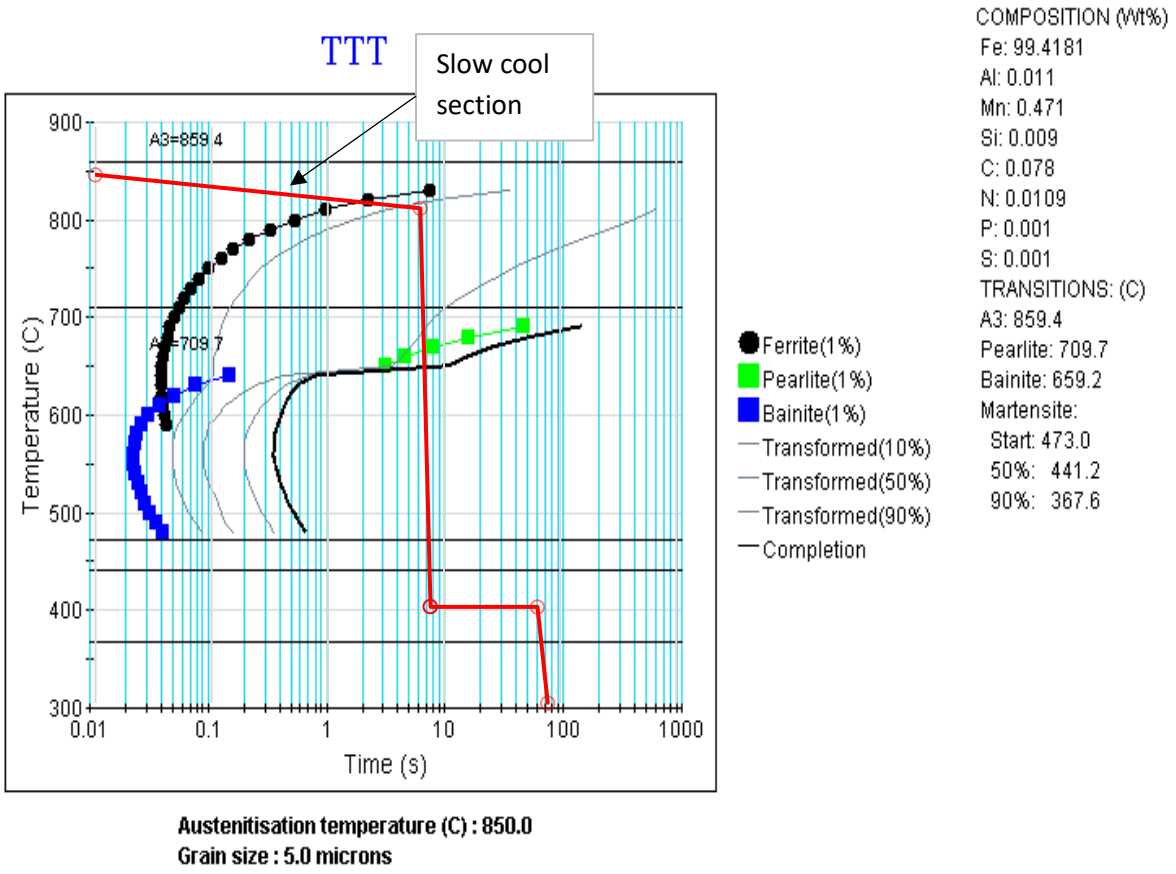

Figure 6.1. JMatPro generated TTT diagram for alloy 1 with annealing cycle superimposed with slow cool section highlighted.

6.4. Results

6.4.1. Tensile data

The average tensile results for alloys 1-6 annealed at intercritical 850°C soak temperature is given in Table 6.2. Figure 6.2 shows a bar chart of the most relevant parameters i.e., average Rp0.2 offset yield strength, tensile strength, and average break elongation of each sample, with targets for yields strength (650-750MPa) and break elongation (minimum of 5%) shown.

Table 6.2. Table showing the average mechanical properties of alloys 1-6 in their 5% temper rolled condition.

Sample	Heating rate (°C/s)	Soak temperature (°C)	offset yield, 0.2% (MPa)	Tensile strength (MPa)	Break elongation (%)
1-20-650	20	650	467	486	10.2
1-20-850	20	850	374	437	9.8
2-20-650	20	650	554	574	8.1
2-20-850	20	850	546	560	9.2
3-20-650	20	650	430	459	14.7
3-20-850	20	850	585	586	4.6
4-20-650	20	650	481	507	12.6
4-20-850	20	850	508	510	3.6
5-20-650	20	650	522	542	11.3
5-20-850	20	850	561	565	5.7
6-20-650	20	650	658	707	8.2
6-20-850	20	850	604	620	7.6

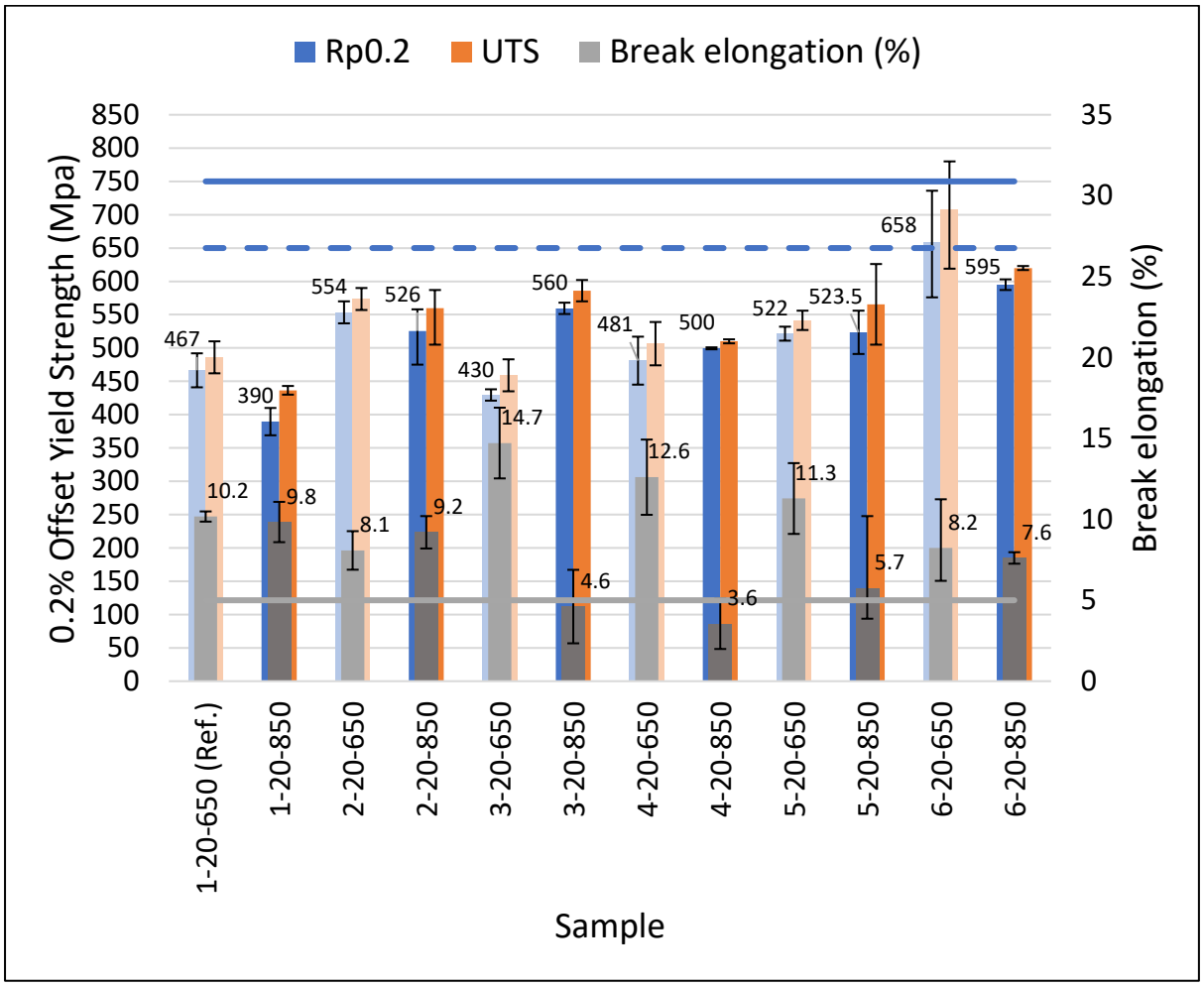

Figure 6.2. Bar chart showing the effect of increasing the annealing soak temperature from 650°C to 850°C on alloys 1-6 (darker shade bars). For reference, tensile values of alloys 1-6 when annealed using commercial cycle (lighter shade bars) are included for reference.

Table 6.3 shows the change in mechanical properties when soak temperature was increased from 650°C to 850°C.

Table 6.3. Table showing the changes in mechanical properties when soak temperature was increased from 650°C/s to 850°C/s.

Alloy	Heating rate	Soak temperature	Offset yield strength (MPa)	Change in Offset yield strength (MPa)	Break elongation (%)	Change in Break elongation (%)
1	20	650	467		10.2	
	20	850	390	-77	9.8	-0.4
2	20	650	554		8.1	
	20	850	526	-28	9.2	+1.1
3	20	650	430		14.7	
	20	850	560	+130	4.6	-10.1
4	20	650	481		12.6	
	20	850	500	+19	3.6	-9
5	20	650	522		11.3	
	20	850	524	+2	5.7	-5.6
6	20	650	658		8.2	
	20	850	595	-63	7.6	-0.6

6.4.2. Grain size data

Table 6.4 gives statistical information regarding the grain sizes of alloys 1-6 when soak temperature was increased from 650°C to 850°C. Grain size information on samples annealed using commercial parameters are inserted for comparison.

Table 6.4. Table showing statistical information regarding the grain sizes of each sample in as-annealed condition.

	Annealing condition							
	HR=20°C/s-ST=650°C				HR=20°C/s-ST=850°C			
Alloy	Average	Mode	Skew	S. D.	Average	Mode	Skew	S. D.
#1	3.6	2.0	1.5	1.7	4.4	2.3	1.6	2.2
#2	4.9	2.3	1.7	2.9	5.6	5.0	0.6	2.3
#3	3.7	2.2	1.5	1.7	4.9	2.0	1.1	2.3
#4	3.8	2.4	1.0	1.5	5.1	2.6	1.4	2.9
#5	4.0	2.3	1.6	2.0	4.3	2.1	0.9	1.7
#6	4.3	2.6	1.2	1.8	4.1	2.5	1.1	1.7

6.4.3. Grain size distributions

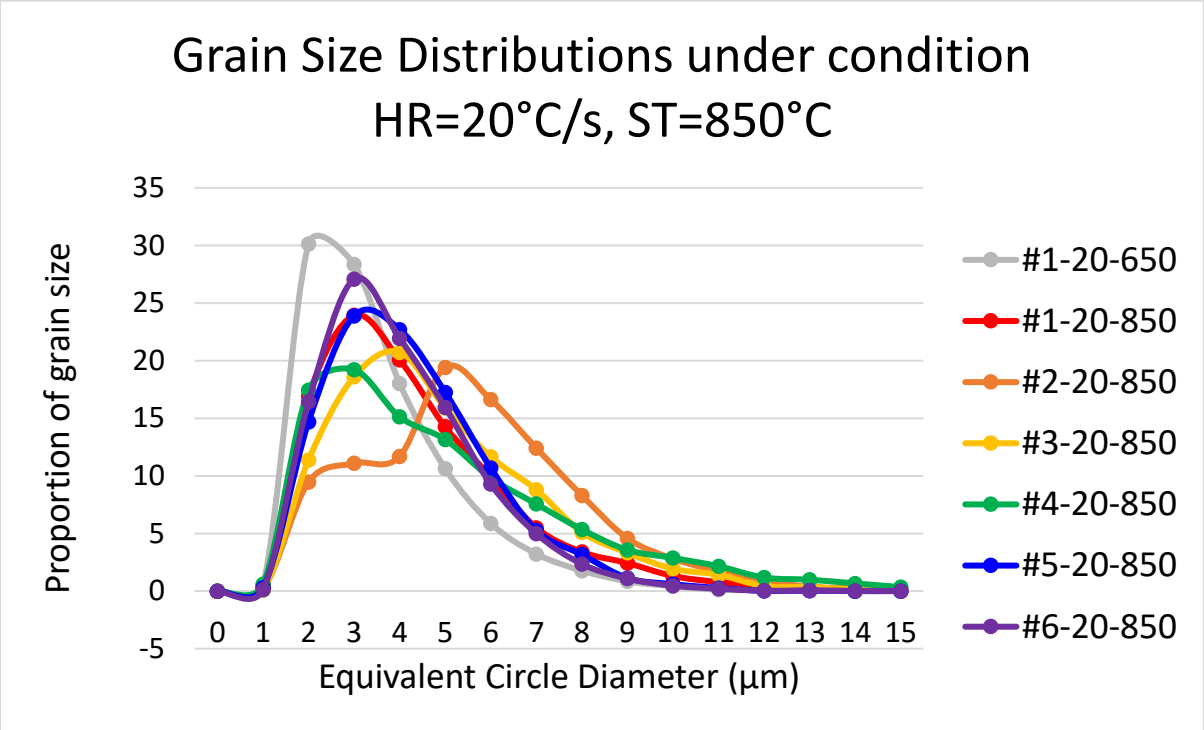

Figure 6.3. The effect of increasing the soak temperature from 650°C to 850°C on the grain size distribution of alloys 1-6. Baseline Sample, 1-20-650, is inserted for comparison.

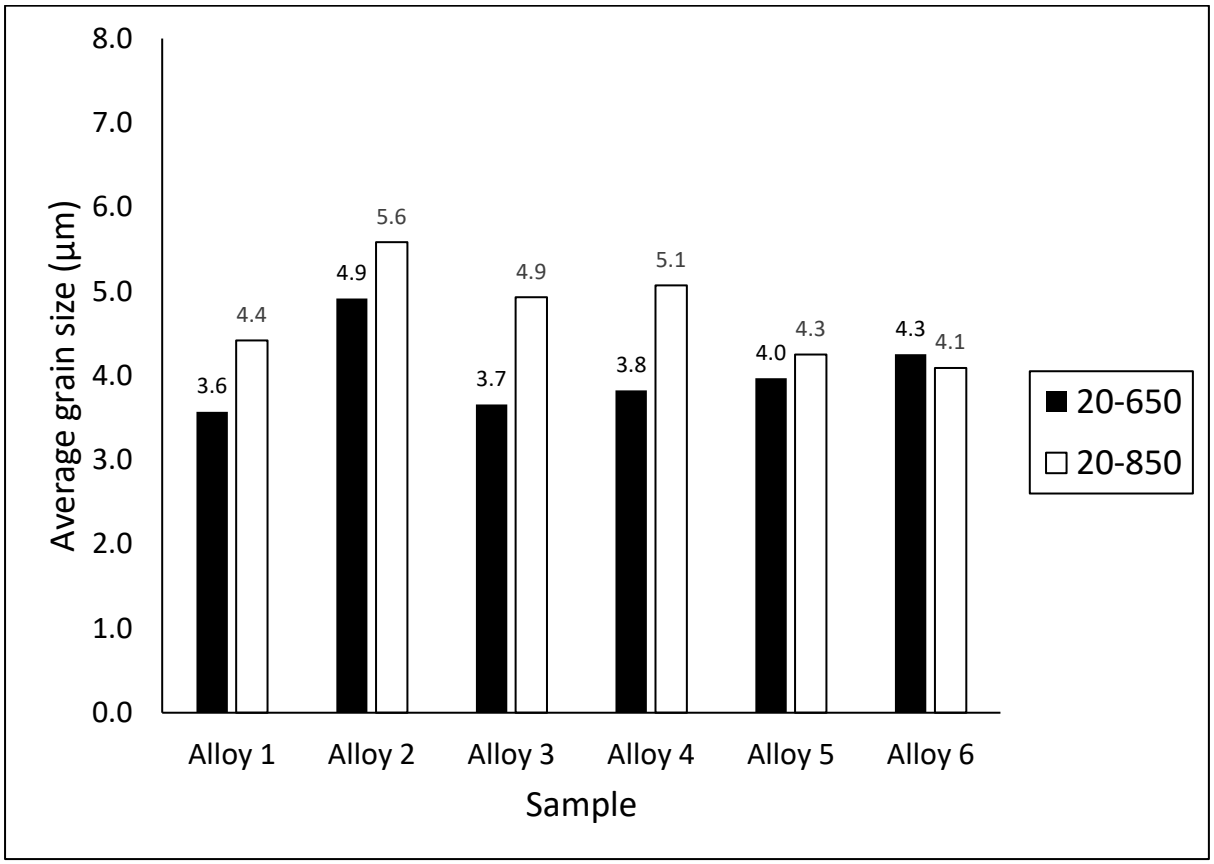

Figure 6.4. Average grain size of alloys 1-6 after annealing to intercritical 850°C. Average grain size under commercial annealing conditions is shown for comparison.

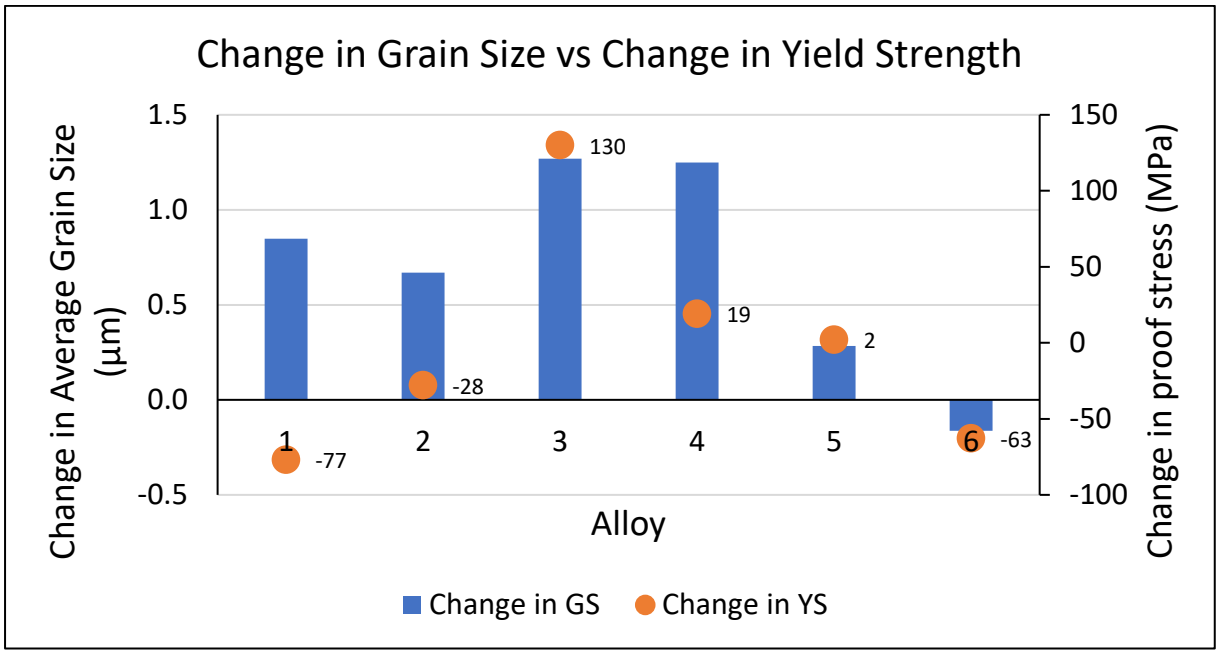

Figure 6.5. Change in average grain size vs change in average Yield strength of alloys 1-6.

Figure 6.5 shows the change in average grain size vs change in average proof stress. As shown, reference alloy 1, high silicon- medium phosphorous alloy 2, and high nitrogen alloy 6 decreased in yield strength by -77MPa, -28MPa, and -63MPa respectively. The yield strength of Low silicon-medium phosphorous alloy 4 increased by +19MPa but its break elongation decreased by 9%, from 12.6% to 3.6%, below the minimum 5% (as seen in Figure 6.2). Similarly, the yield strength of alloy 5 increased by an insignificant +2MPa but its break elongation value decreased by -5.6%, from 11.3% to 5.7%.

Finally, the yield strength of alloy 3 increased by an impressive 130Mpa, from 430MPa to 560MPa, but its break elongation decreased massively by 10.1%, from 14.7% to 4.6%. Therefore, neither of these alloys met the required mechanical properties when intercritical soak temperature 850°C was used. Overall, break elongation either decreased or stayed approximately the same for all samples.

Figure 6.4 shows the effect of intercritical annealing on average grain size. In general, average grain size increased by an insignificant amount in the regions of 0.3-1.2µm, except for alloy 6 which decreased by an insignificant 0.2µm. For alloys 2-6 there was a positive correlation between change in average grain size and change in average proof stress. For alloys 1 there was a negative correlation.

6.5. Discussion

The purpose of annealing to intercritical soak temperature 850°C was to generate secondary phase austenite which would then transform upon cooling to a harder secondary phase and increase the strength via secondary phase generation.

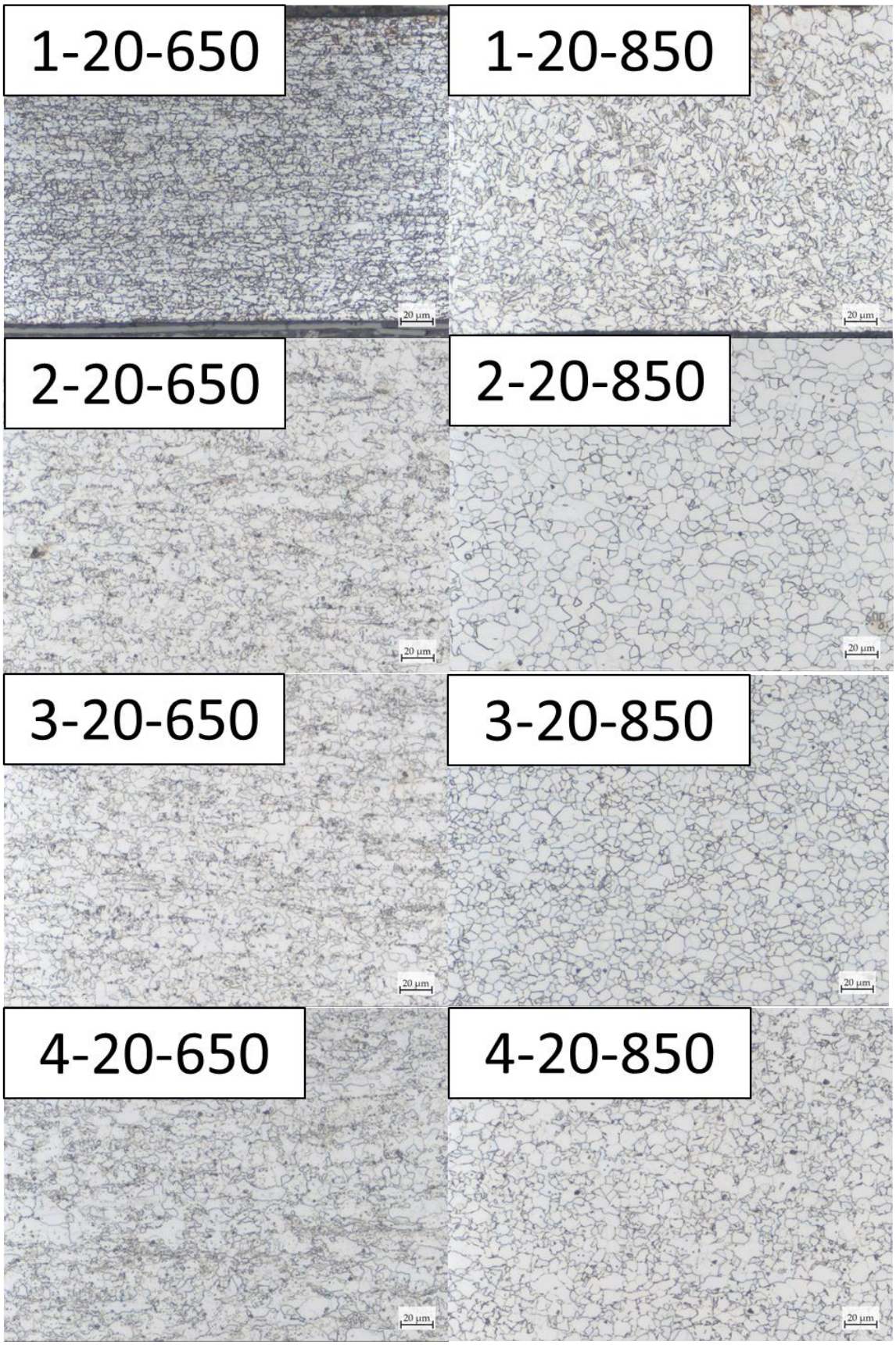

Figure 6.6. Optical microstructures of alloy 1-4.

Therefore, an explanation for some of the results where yield strength increased, in particular alloy 3, could be that secondary phase (e.g., pearlite) formed. However, when looking at the microstructure for alloy 3 (shown in Figure 6.6), there was no clear presence of secondary phase, and the microstructure appeared to be mostly ferrite.

In addition, the microstructures of all alloys 1-6 showed no secondary phase present. Instead, they show a fully recrystallised ferritic microstructure, with a larger average ferrite grain size, with fewer carbides (see Figure 6.6). Because the microstructures look very similar to each other i.e., not containing a secondary phase, it is likely that the change in mechanical properties seen in these alloys is not a result of secondary phase strengthening.

6.5.1. JMatPro

Furthermore, when plotting the annealing cycle on a TTT diagram for these alloys, it was difficult for pearlite to form given the fast cooling and no holding in the pearlite region. Furthermore, it was very unlikely that secondary phase bainite or martensite would be generated. This is due to the ‘slow cool’ section that took place after the soak section and prior to rapid cooling section. Figure 6.7 shows a JMatPro generated TTT diagram for alloy 1, which looks very similar to the TTT diagram of the other alloys, where all showed the same trend that during the slow cool section, the microstructure cooled through the ferrite nose, and then cooled through the pearlite nose during rapid cooling.

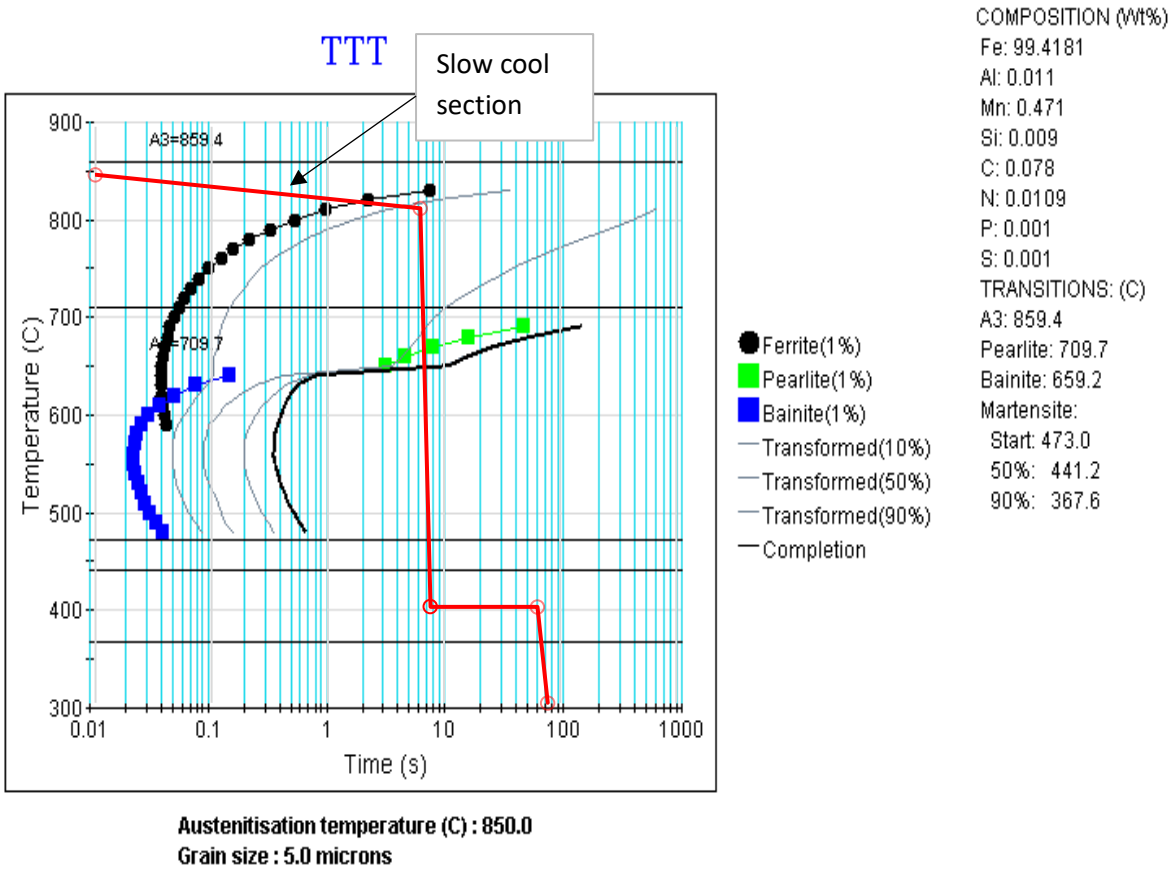

Figure 6.7. JMatPro generated TTT diagram for alloy 1 with annealing cycle superimposed with slow cool section highlighted.

The inclusion of a slow cool section in the simulated annealing treatment prevents these alloys from generating secondary phase bainite or martensite. Moreover, the effect of removing 'the slow cool section' was studied and discussed later.

If the average grain size for these alloys either increased or changed insignificantly, and secondary phase generation did not occur, another strengthening mechanism must have been responsible for the increase in yield strength for some alloys e.g., alloy 3 and the reduction of yield strength as seen in alloy 6. It could be argued that the strength increases, and reductions seen in alloys 2-5 are within measurement error. Perhaps precipitation of elements occurred in alloy 3 causing precipitation strengthening to have occurred. Given the high 0.0283wt%N content of alloy 6, precipitation of nitrogen containing precipitates may have reduced the yield strength by reducing the amount of free nitrogen dissolved in the ferrite matrix.

Given nitrogen's mobility at room temperature, natural room temperature aging could have occurred when samples were removed from the freezer and left out during periods of waiting

for external temper rolling, and machining of tensile specimens, and so must be considered as an influence on these tensile results. However, every batch of samples were subjected to broadly uniform storage conditions (time and temperature) between production and testing, and so is a factor that can be ignored.

6.5.2. Grain Size

The alloys that decreased in yield strength (as seen in alloys 1,2 and 6) could be due to the increase in average grain size that we see in Figure 6.4, which according to the Hall-Petch relationship (equation below) will decrease the grain size.

$$\sigma_y = \sigma_0 + \frac{k^y}{\sqrt{d}}$$

Table 6.5 shows the theoretical changes in yield strength for alloys 1-6 associated with their changes in average grain size.

Table 6.5. The difference in average grain size of alloys 1-6 after intercritical annealing, and the resulting effect on yield strength

Alloy	Average grain after commercial annealing (µm)	Average grain size after intercritical soak temperature annealing (µm)	Effect on yield strength (MPa)
1	3.6	4.4	-28MPa
2	4.9	5.6	-16MPa
3	3.7	4.9	-37MPa
4	3.8	5.1	-39MPa
5	4.0	4.3	-10MPa
6	4.3	4.1	+6MPa

However, the average grain size of alloy 6 decreased by a negligible 0.2µm, so for this sample it is likely another mechanism is responsible for the reduction in yield strength. Additionally, the average grain size of alloys 1 and 2 did increase by 0.8µm and 0.7µm respectively, which equates to yield strength decreasing by 28MPa for alloy 1, and 16Mpa for alloy 2. This leaves a 49Mpa unaccounted for alloy 1, and 12MPa for alloy 2. Whilst the unaccounted 12Mpa for alloy 2 could be put down to statistical variation, the unaccounted 49MPa in alloy 1 is too large to be ignored. Therefore, increases in average grain size cannot solely justify why yield strength decreased in alloys 1, 2 and 6. Moreover, alloys that experienced an increase in yield strength, i.e., alloys 3, 4, and 5, also experienced an increase in average grain size.

Alloys 4 and 5 which experienced large reductions in break elongations were accompanied by minor increases of yield strength by magnitudes of 19MPa for alloy 4, and 2Mpa for alloy 5. On the other hand, alloy 3 experienced a substantial reduction in break elongation value from 14.7% to 4.6%, but its yield strength increased by an appreciable 130Mpa.

Furthermore, the average grain size of alloy 3 and 4 increased by a similar magnitude of 1.2-1.3µm which is equivalent to decreasing the yield strength by 37-39MPa. Nevertheless, the yield strength increased, and at different amounts (+130MPa for alloy 3, +19MPa for alloy 4).

This implies that coarsening grain size is not significantly responsible for these results, and these intercritical annealing soak conditions are promoting another mechanism to act causing some grades (alloys 1, 2 and 6) to decrease in yield strength and not affect the average break elongation value much, and other grades (4 and 5) to substantially reduce in break elongation value whilst having negligible changes to yield strength, and thirdly for alloy 3 to largely increase in yield strength and reduce in break elongation value significantly. In the case for alloy 3, which has the highest carbon content of the alloys, it is plausible there is less well distributed second phase after heat treatment.

Precipitation of elements could be responsible for these results. In the samples where yield strength decreased, for example alloy 6, nitrogen precipitates could have formed thus taking free nitrogen out of solution, thereby reducing the interstitial strengthening effect due to interstitial form nitrogen. On the other hand, given that nitrogen has a higher solubility in austenite, nitrogen diffused from ferrite to austenite at intercritical temperature. Therefore, austenite areas would have seen higher nitrogen content and therefore less well distributed

upon cooling in the final microstructure, thus resulting in a reduction in strength as seen in a tensile test.

6.5.3. Thermo-calc

For an initial insight into what phases and precipitates might be present in these samples, Thermo-calc simulations were run. However, it must be noted that these predictions are based on equilibrium rather than industry conditions.

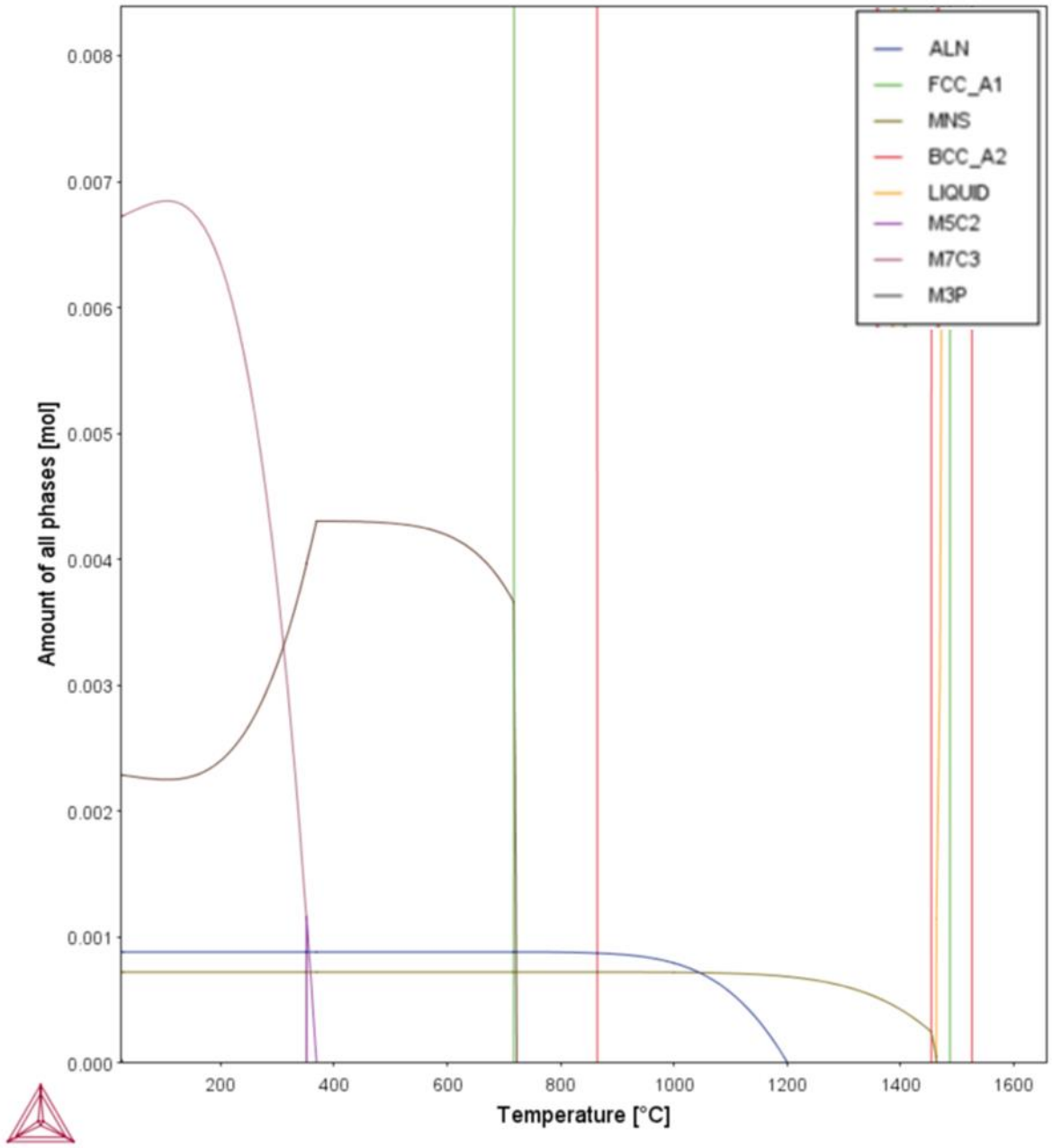

Figure 6.8: Phases formed in alloy 1

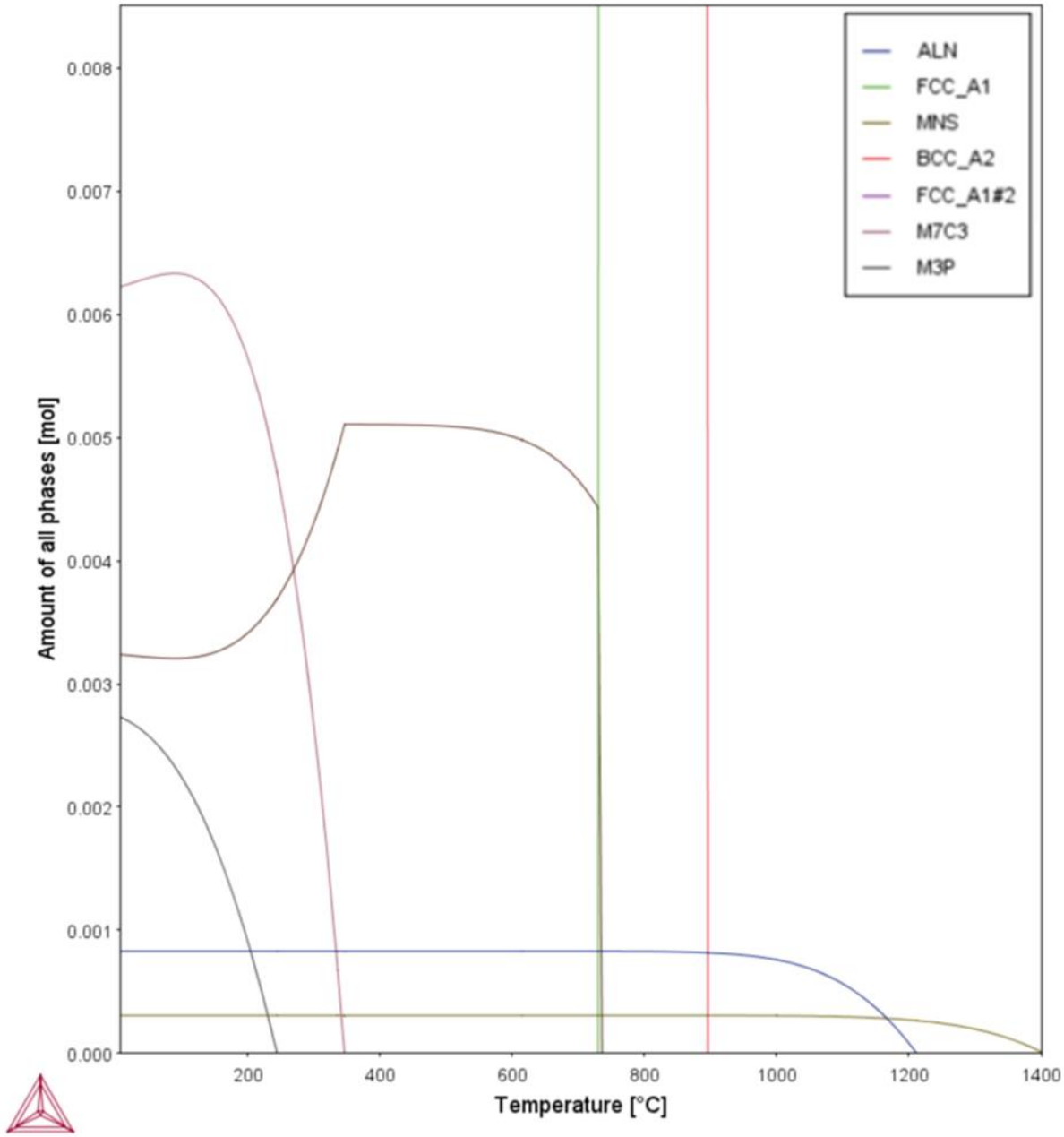

Figure 6.9: Phases formed in alloy 3

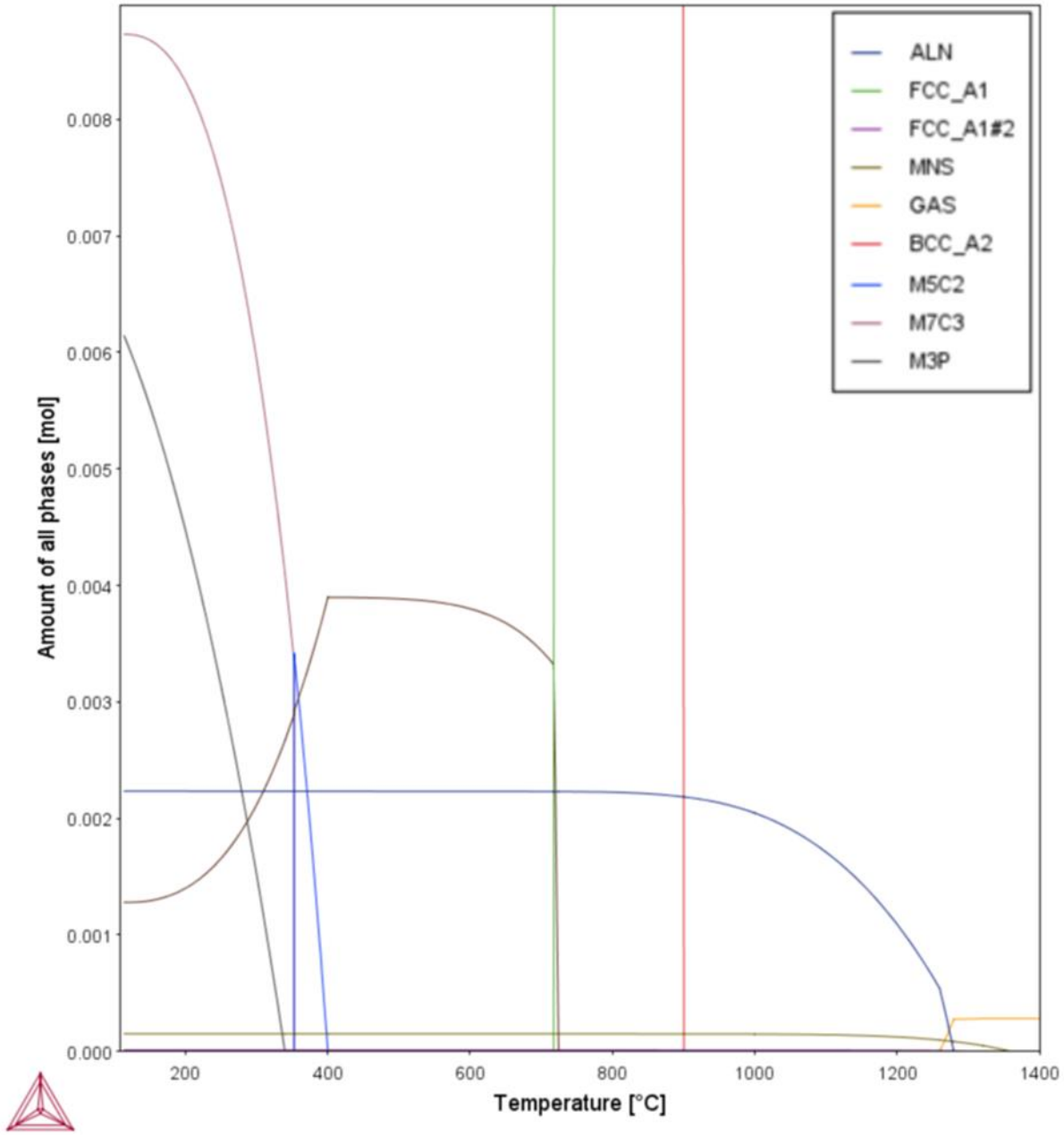

Figure 6.10: Second phases formed in alloy 6

Figure 6.8, Figure 6.9, and Figure 6.10 show the phases present under equilibrium conditions for alloys 1, 3, and 6. As is expected, phases Ferrite (BCC_A2) and Austenite (FCC_A1) form in this low-carbon steel. As seen in all alloys, Thermo-Calc predicts that manganese sulphide (MnS) is the first precipitate to form, with formation beginning at temperatures around 1300-1465°C, and reach full precipitation at temperatures 1100-1200°C. The next precipitate to form is AlN at temperatures 1200-1300°C, and reaches full precipitation at

~900°C. Given the hot-rolling conditions for these alloys included being reheated to 1250°C to be rough milled into slabs and subsequently reheated to 1220°C for at least 40 minutes, it could be expected that MnS was not fully in solution for all alloys. Thus, some amount of MnS may have been present by the time the slabs began to be reduced (from 30mm to 2.0mm) into hot-rolled sheets and entered the FRT(in) at 980°C (±30°C), transported for 3 seconds, and left FRT(out) at 950°C (±30°C). Although Thermo-Calc predicts that the FRT(in) temperature of 980°C (±30°C) should allow the precipitation of AlN to occur, it is unlikely it would have happened for two reasons:

1. There is evidence to say that MnS precipitates
2. Cooling began (Cooling(in)) at 910°C at a rate of 80°C/s and to a coiling temperature of 590°C ±20°C (Cooling(out)) which is a fast enough cooling rate, to a low enough coiling temperature to inhibit AlN formation

However, as mentioned previously, these thermo-Calc predictions are assuming theoretical conditions and not industrial conditions, so it is not immediately clear whether AlN could have precipitated and therefore responsible for the reduction in yield strength for alloy 6. Furthermore, AlN was fully in solutions for alloys 1-5 but not fully for alloy 6 during these hot-rolling conditions. Given the similar amount so aluminium in all alloys and the higher nitrogen concentration of alloy 6, it is possible that alloy 6 had a larger amount of nitrogen in precipitate form.

From these phase diagrams MnS forms first which may have prevented AlN from precipitating. Additionally, the volume fraction of austenite that was generated at 850°C was determined using single point equilibrium using Thermo-calc software. The results for alloys 1-6 are shown in Table 6.6.

Table 6.6. Predicted volume fractions of phases austinite and ferrite, and precipitates AlN and MnS at saok 850°C.

Alloy	Volume fraction of austenite (FCC) at 850°C	Volume fraction of ferrite (BCC) at 850°C	Mass percent of AlN	Mass percent of MnS
1	0.73702	0.26151	0.01791	0.03136
2	0.46325	0.53589	0.01650	0.00674
3	0.54425	0.45473	0.01688	0.01333
4	0.52111	0.47804	0.01759M%	0.00435
5	0.49720	0.50195	0.01711	0.00465
6	0.51979	0.47812	0.04534	0.00653

Again, it needs to be made aware these determined austenite volume fractions are when equilibrium conditions are used, not industry conditions. When, the simulated annealing cycle had a soak time of 50 seconds and included an overageing at 400°C for 56 seconds. This short soak section may have stopped the full transformation of ferrite to austenite from happening, therefore the actual generated volume fractions of austenite may have been much lower. This explains why some alloys, for example alloy 1, did not exhibit a ~74% secondary phase in its microstructure. However, after 50s it could be argued that 50s soak time is not far away from equilibrium, and a 74% austenite will not all transform into secondary phase anyway. Only with sufficient cooling (such as water quenching) coupled with sufficient carbon content would you get equivalent second phase percentages.

According to the single point equilibrium calculation, some TiC precipitate was predicted to have formed but was such small quantities, e.g., 9.31E-6, that it was ignored and assumed to have negligible effects towards mechanical properties. Furthermore, it was predicted that AlN would have formed at this temperature and could explain why some of the alloys decreased in strength, e.g., alloy 6, as nitrogen would have been taken out of solid solution. Therefore, it is

likely that nitrogen precipitated out of alloy 6 and is perhaps the reason why yield strength decreased.

6.5.4. Hardness tests

To test whether the reduction in yield strength of some samples was due to elements precipitating out, e.g., nitrogen in alloy 6, sample hardness was measured in their as-annealed condition.

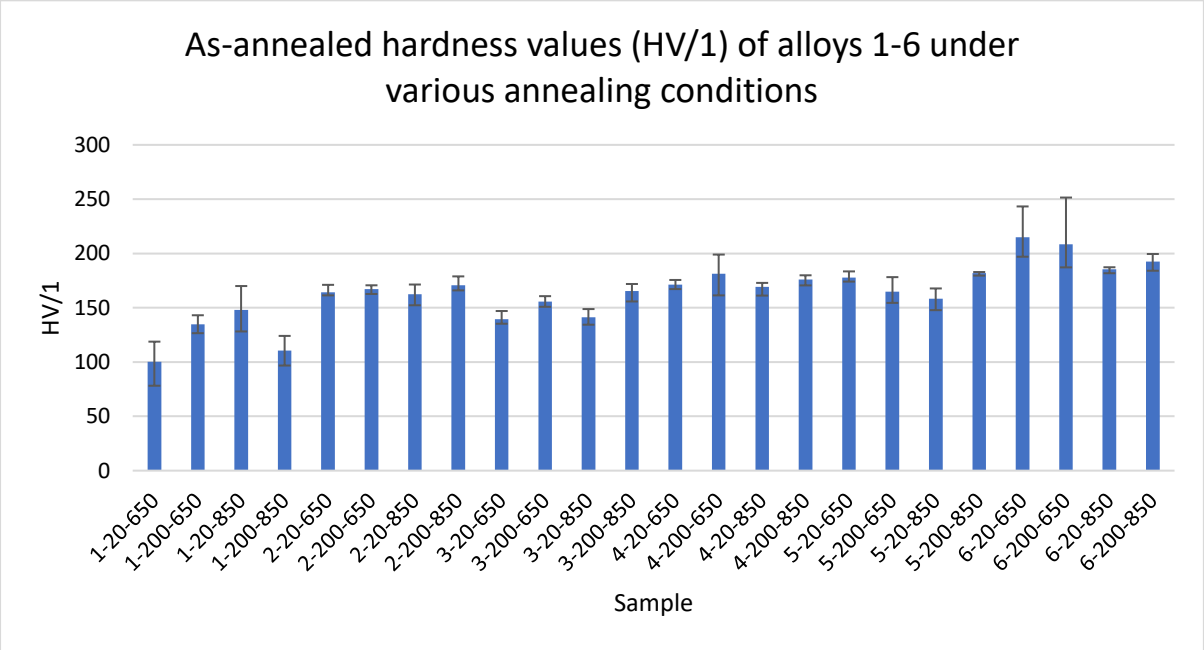

Figure 6.11. Hardness (HV/1) of alloys 1-6 under various annealing conditions.

Like the trend seen in the UTS values for alloy 6, the hardness of alloy 6 also decreased when an intercritical 850°C soak temperature was used. This implies nitrogen had precipitated out under this annealing condition. A reduction in hardness can also be seen in alloy 5. Alloys 2, 3, and 4 remain unchanged. Alloy 1 was the only sample to increase in hardness, which is opposite to what happened to the Rp0.2 and UTS of alloy 1.

The tensile results of alloy 3 show a significantly large 130MPa increase in yield strength, and 127MPa increase in UTS when the soak temperature was increased from 650°C to

850°C. However, interestingly the hardness value remains unchanged. Furthermore, the hardness of samples 1-20-850 and 3-20-650 are greater than the reference 1-20-650 sample but displayed lower Rp0.2 and UTS values in their tensile data. It could be that the tensile result for alloy 3 was anomalous.

6.5.5. Removing the slow cool section

As noted above, the slow cool section prevents these microstructures from generating bainite or martensite secondary phase. Therefore, simulated annealing was conducted without the slow cool section present, and instead, rapid cooling straight from the intercritical soak temperature to the overageing temperature was performed. The hardness was measured to gain quick insight into the mechanical properties. Figure 6.12 below shows the schematic of the annealing cycle performed when the slow cool section was removed.

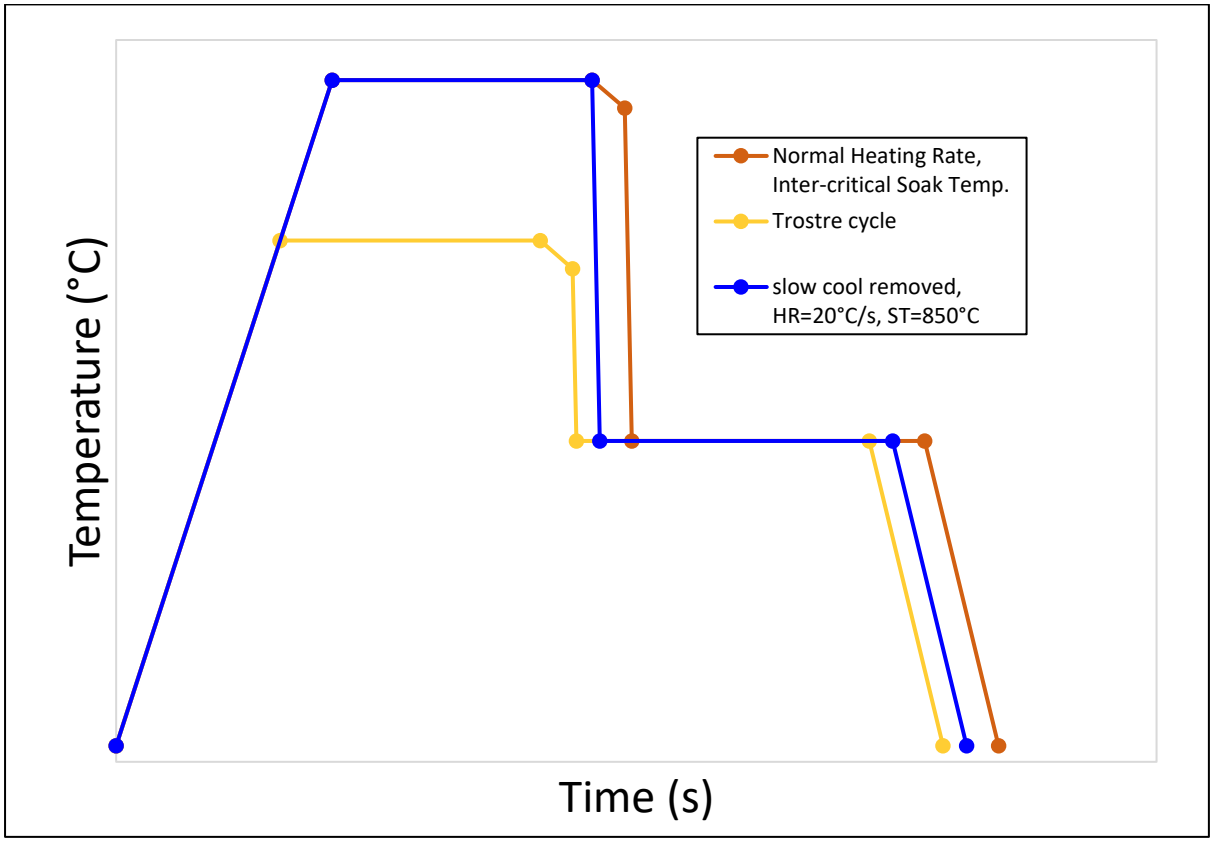

Figure 6.12. Schematic of the heat cycle performed where the slow cool section was removed. The commercial annealing cycle (yellow), and intercritical cycle with slow cool section (red) are included for reference.

The effect of removing the slow cool section on the hardness values of alloys 5 and 6 are shown in Figure 6.13.

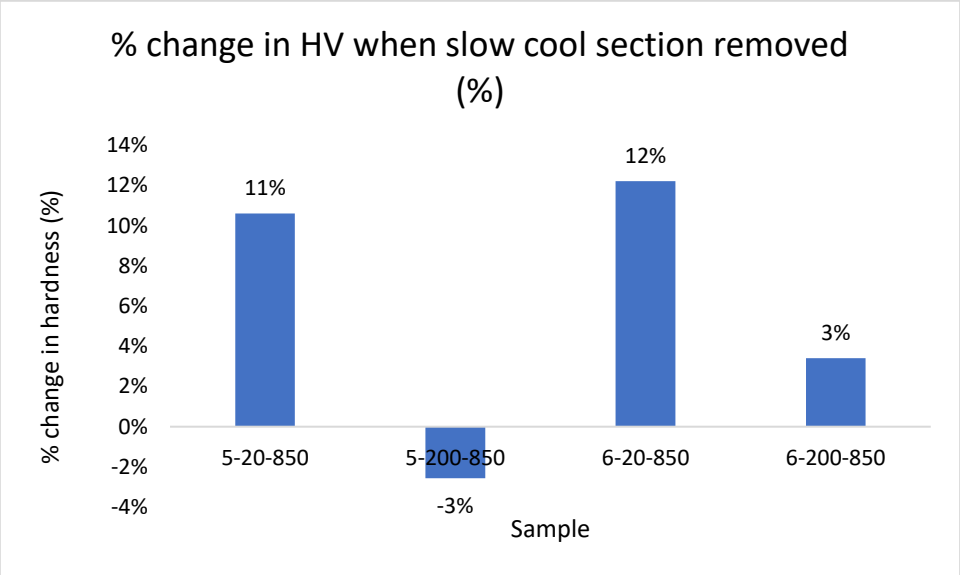

Figure 6.13. Change in Vickers hardness value when the slow cool section was removed from annealing simulations.

When the slow cool section was removed from the simulated annealing cycles, the hardness improved by around 11-12% for alloys 5 and 6 when 20°C/s heating rate was used. This implies that a harder secondary phase was generated and thus contributed to the rise in hardness values.

On the other hand, for samples annealed using a rapid 200°C/s heating rate, the hardness decreased by 3% in alloy 5, and increased by 3% in alloy 6. These small variations in hardness are small and insignificant and could just be natural variations brought about by the methodology. This implies that rapid heating rates bring about conditions that result in a softer material. Perhaps because rapid heating increases the nucleation kinetics of austenite resulting in finer austenite at soak temperature and potentially more inhomogeneous distribution of austenite compared to slower heating rates, this may be a reason why the percentage change in hardness is less for the 200°C/s heating rate samples.

However, examination of the microstructures showed no presence of secondary phase in the microstructure.

Information Sample 5-20-850 with slow cool section removed	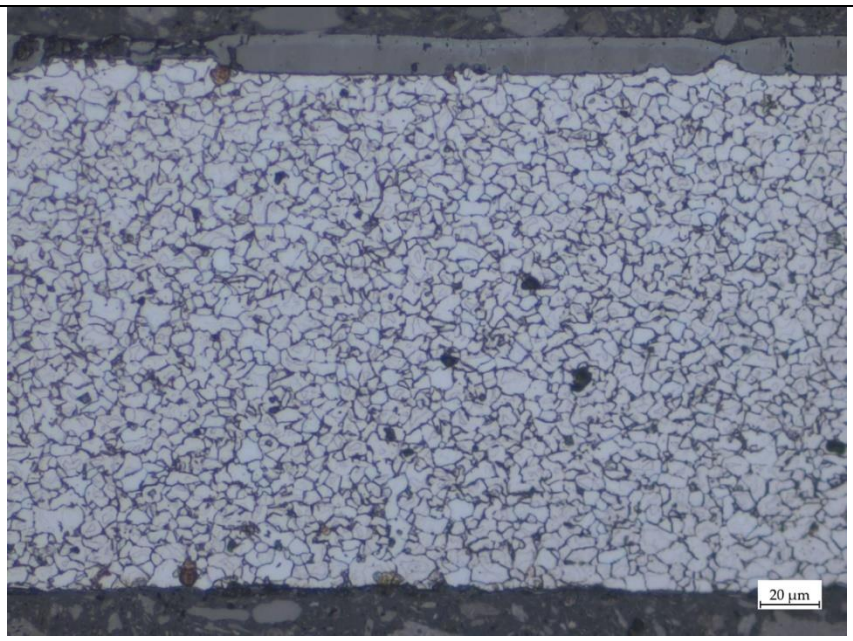
Information Sample 5-200-850 with slow cool section removed	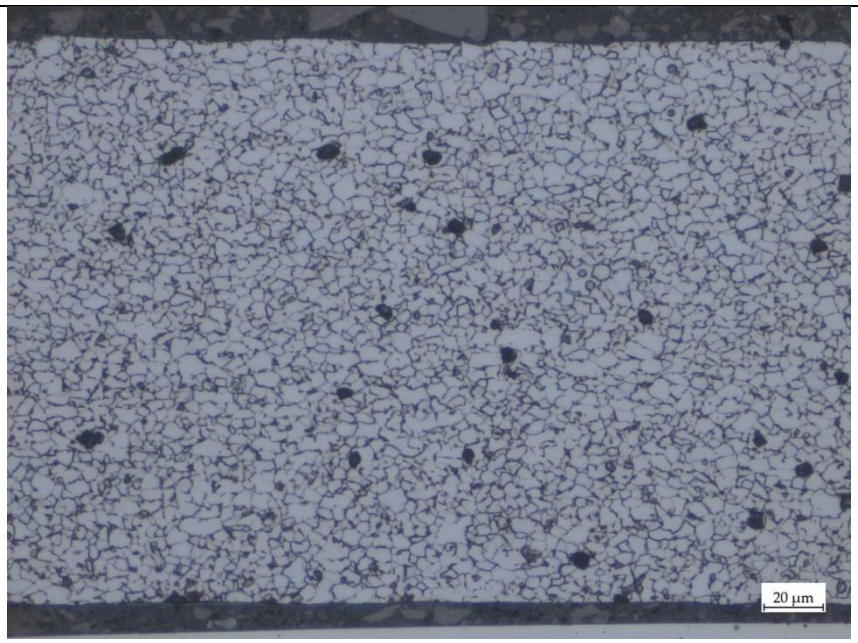

Information Sample 6-20-850 with slow cool section removed	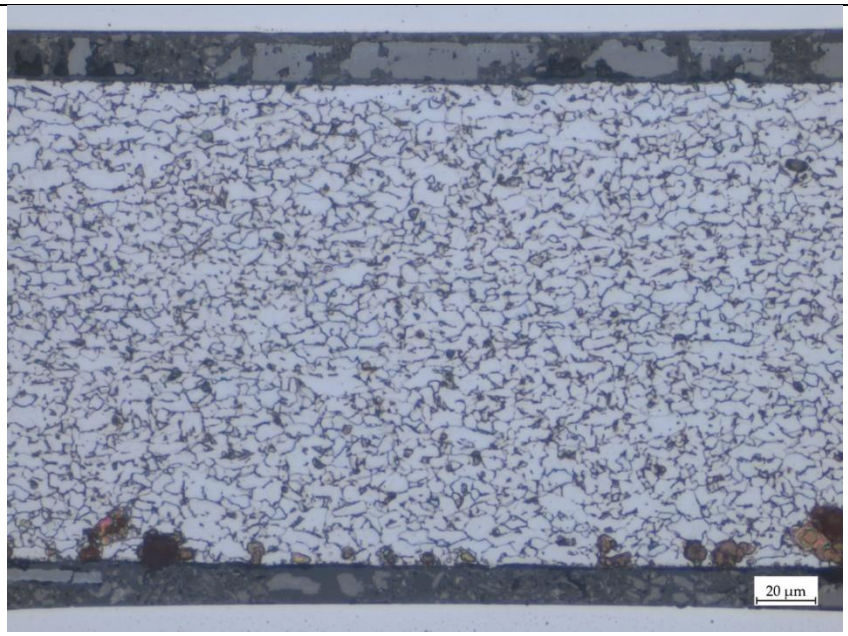
Information Sample 6-200-850 with slow cool section removed	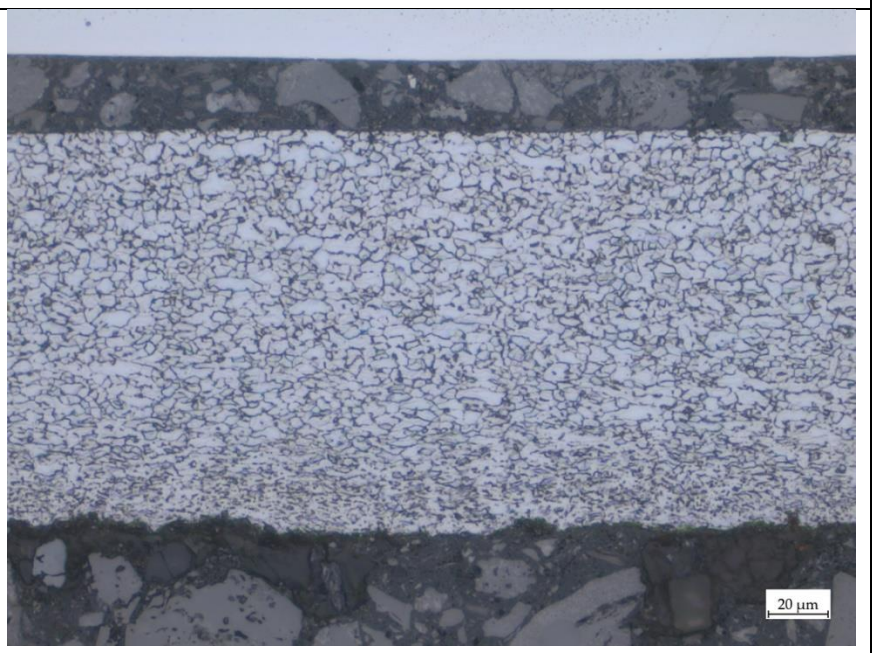

When looking at the optical microstructures of these samples, many nitrides can be seen in the high nitrogen sample annealed with the slow heating rate (6-20-850). Compare this microstructure to the rapidly heated high nitrogen chemistry sample, which shows very few. Both microstructures of alloy 5 show very little nitrides.

6.6. Conclusions

- Intercritical annealing at 850°C does **not** lead to generation of significant amounts of **secondary phase** and does not lead to strength improvements in packaging steels for can-end applications (except for alloy 3).
- Moreover, the **strengths** are often **reduced** or do not change by a significant amount because of intercritical annealing. The yield strength of Alloy 3 (containing high silicon 0.534wt%Si and low phosphorous 0.04wt%P) increased the most by an impressive 130MPa but had a break elongation value below the recommended 5%. This implies packaging steels for can-end applications are **not suitable** for **intercritical annealing** at 850°C, and there is not a strong business case investment for increased capability on the basis of this metallurgical approach to increase strength.
- Intercritical annealing at 850°C results in the **average grain size increasing slightly** between 0.3-1.2µm, apart from alloy 6 which was relatively unaffected (decreasing by 0.2µm).
- Removing the slow cool section increases the hardness of heavier alloyed packaging grade steel for can-end application, when an intercritical soak temperature was used. The effect is less dramatic (or reduced hardness) when a rapid heating rate is also used.

6.7. Recommended Future work

- Broadly, intercritical annealing appears to have had a negligible effect on these six lab casted chemistries with the potential exception of alloy 3. However, no appreciable amounts of second phase were obvious in any of the microstructures. As with chapter 2, the high nitrogen grade (alloy 6) appeared to show a reduction in strength when intercritical annealed. This could be due to the nitrogen partitioning to the austenite phase formed during intercritical temperature, resulting in depleting the ferrite and subsequent higher local driving forces for AlN precipitation that was shown to be thermodynamically favoured through Thermocalc simulations.
- To verify that nitrogen has precipitated out in alloy 6, it is advised to perform TEM work to confirm what these precipitates are in the intercritical annealed high nitrogen

sample (6-20-850). Additionally, thermoelectric power (TEP) measurements could be attempted to determine levels of carbon and nitrogen in solid solution after annealing.

- The use of an interstitial analyser would be great at determining the amount of nitrogen in solution. However, the instrument only accepts samples in cylindrical block form and not thin sheet form. Unfortunately, all material was hot-rolled and cold rolled. Perhaps it is worthwhile to cast the material again and machine two cylindrical blocks from it and subject one to commercial heat treatment conditions, and the other to the intercritical soak temperature cycle and compare the nitrogen contents in both.

7. Technical chapter 4 – The effect of rapid 200°C/s heating rate to intercritical annealing soak temperature 850°C on lab-casted high-strength packaging grade steels for can-end applications.

7.1. Purpose of study

This chapter will be assessing whether the mechanical properties of six lab casted packaging grade steels can be improved via further grain refinement, generation of secondary phase (e.g., bainite, pearlite islands), and secondary ferrite, by using a 200°C/s rapid heating rate to intercritical soak temperature 850°C. See Figure 3.6 for the annealing cycle performed on the six lab casted chemistries.

As mentioned in the literature review section, a combination of a 200°C/s rapid heating rate to an 850°C intercritical annealing soak temperature has been shown to increase the tensile properties of steel to maximum levels. It is stated this occurs because the rapid heating rate increases the ferrite recrystallisation temperature to a level that results in some volume fraction of non-recrystallised ferrite to be present during the soak stage of the intercritical annealing process. The presence of non-recrystallised ferrite during the soak stage provides preferential sites for austenite to form. This austenite then enhances the kinetics of recrystallization of this non-recrystallised ferrite, and inhibits the recrystallised ferrite growth, thus refining the average ferrite grain size. In addition to ferrite refinement, presence of secondary phase is expected. In general, it is then expected that the six lab casted chemistries will exhibit higher strength levels due to a smaller average ferrite grain size (compared to average ferrite size in previous chapters) and presence of secondary phase. If rapid heating rate to intercritical soak temperature yields desirable mechanical properties, then this could provide investment justification to upgrade the sponsor company's CAPL to enable it the capability to perform rapid heating rates and to reach intercritical soak temperatures.

For information and details regarding the experimental procedures used in this chapter, please refer to Table which will direct you to the relevant sections within the Methods and Experimental Chapter (Chapter 3).

Table 7.1. Where to find information and details on the experimental procedures used in this chapter.

Procedure	Section number
Processing history	3.1
OES & ELTRA obtained chemistry	Table 4.6
Transformation temperatures	3.3
Annealing heat treatments performed	3.4.5
Temper rolling and Ageing	3.7
Tensile testing parameters	3.8.1
Optical microscopy	3.11
Hardness testing	3.14
Grain Size Analysis	3.12

For details on the annealing heat treatment procedure carried out in this chapter, please see chapter 3.4.5.

7.2. Results

7.2.1. Tensile Results

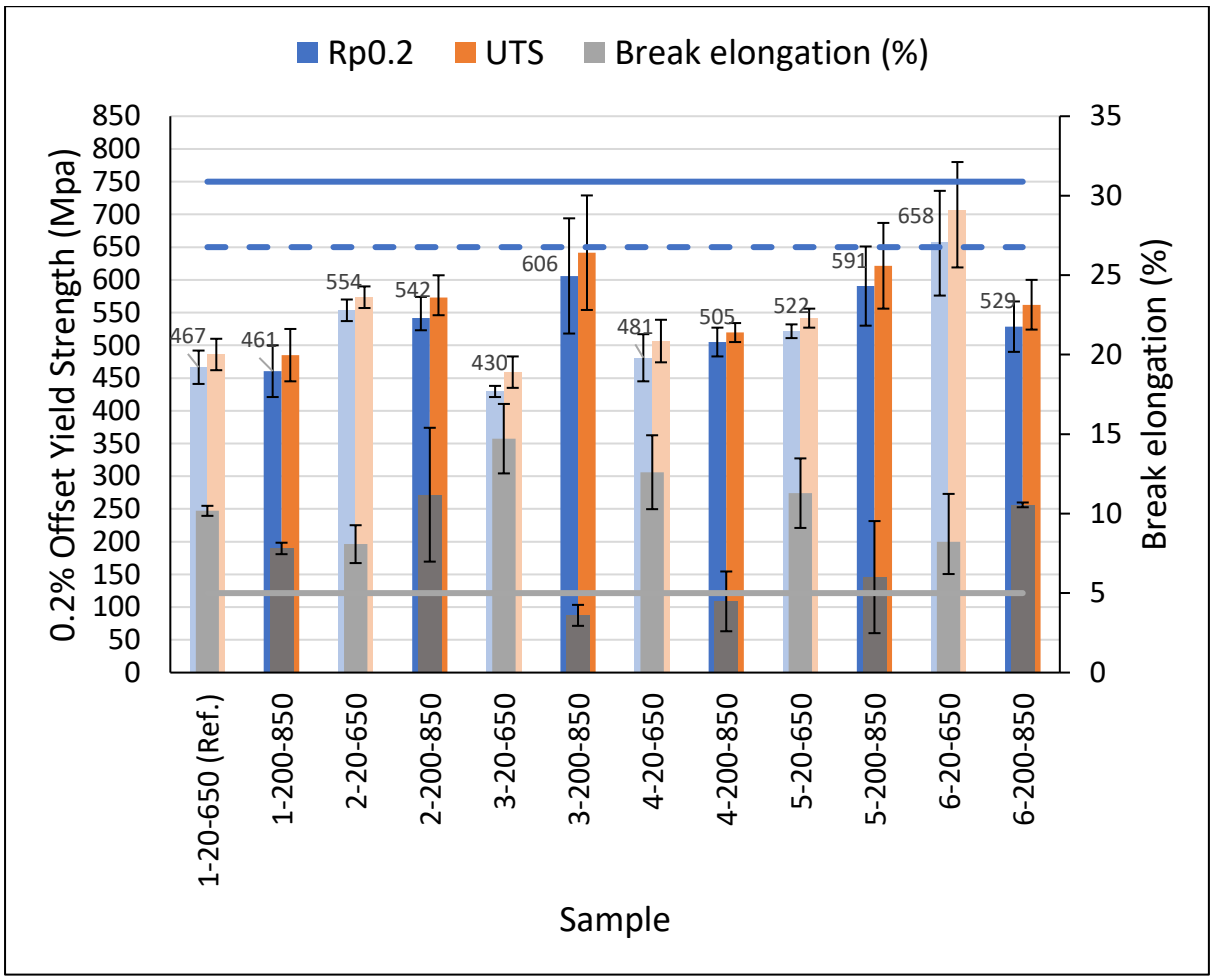

Figure 7.1. Bar chart showing the mechanical properties of alloys 1-6 when the heating rate and soak temperature were increased.

7.2.2. Grain size data

Table 7.2. Table showing statistical information regarding the grain sizes of each sample in as-annealed condition.

	Annealing condition							
	HR=20°C/s-ST=650°C				HR=200°C/s-ST=850°C			
Alloy	Average	Mode	Skew	S. D.	Average	Mode	Skew	S. D.
#1	3.6	2.0	1.5	1.7	4.1	2.0	1.4	2.1
#2	4.9	2.3	1.7	2.9	4.5	3.2	1.2	2.1
#3	3.7	2.2	1.5	1.7	4.3	2.2	1.3	2.0
#4	3.8	2.4	1.0	1.5	4.3	2.0	1.4	2.3
#5	4.0	2.3	1.6	2.0	4.0	3.1	1.0	1.5
#6	4.3	2.6	1.2	1.8	4.1	2.5	1.2	1.6

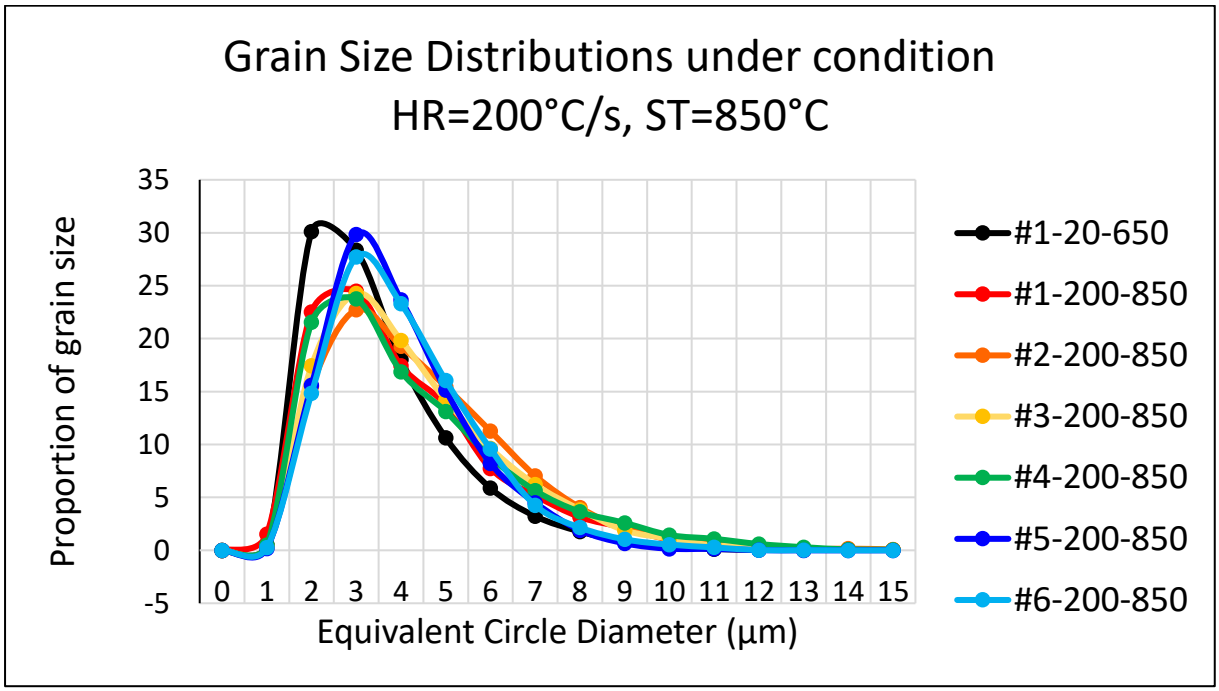

Figure 7.2. Grain size distribution of alloys 1-6 after rapid annealed to intercritical soak temperature. Distribution of reference sample and condition, 1-20-650, is included for reference (black line).

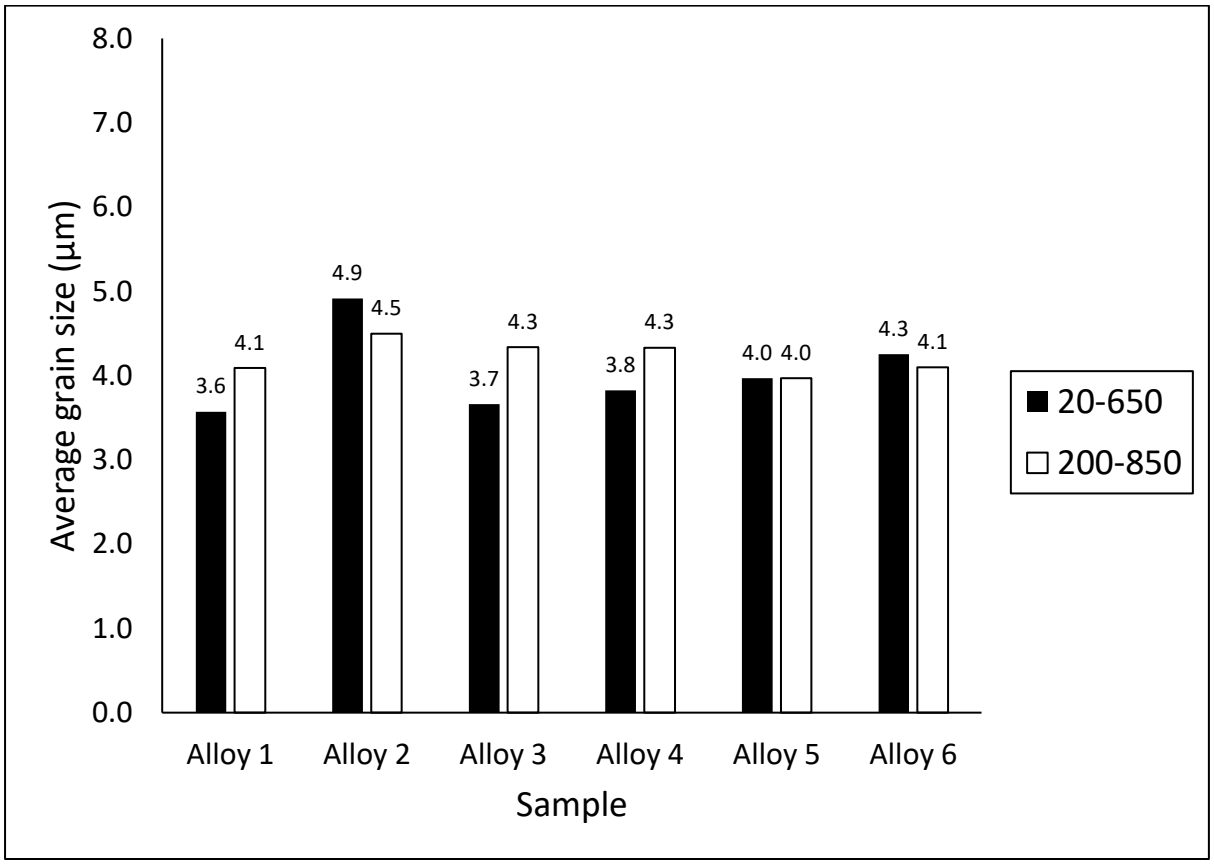

Figure 7.3. Average grain size of alloy 1-6 under different annealing conditions.

Table 7.3. Table showing the effect of increasing heating rate from 20°C/s to 200°C/s at sub-critical 650°C soak temperature, on tensile properties.

Alloy	Heating rate	Soak temperature	Offset yield strength (MPa)	Change in offset yield strength (MPa)	Break elongation (%)	Change in Break elongation (%)
1	20	650	467		10.2	
	200	850	461	-6MPa	7.8	+2.4%
2	20	650	554		8.1	
	200	850	542	-12MPa	11.2	+3.1%
3	20	650	430		14.7	
	200	850	606	+176MPa	3.6	-11.1%
4	20	650	481		12.6	
	200	850	505	+24MPa	4.5	-8.1%
5	20	650	522		11.3	
	200	850	591	+69MPa	6.0	-5.3%
6	20	650	658		8.2	
	200	850	529	-129MPa	10.6	+2.4%

7.2.3. Tensile results explained

The effect of increasing the heating rate from 20C/s to 200°C/s, and the soak temperature from 650°C to 850°C, on the mechanical properties of alloys 1-6 is shown in Figure 7.1.

The proof stress and ultimate tensile strength of alloy 1 were not affected by the increase in heating and soak temperature, with yield and tensile strengths decreasing by an insignificant 6MPa and 1MPa respectively. However, the break elongation decreased by a small 2.4%.

Whereas alloy 2 experienced a greater change in yield strength, decreasing from 554MPa to 542MPa (i.e., a reduction of 12MPa), however this is still an inconsequential change. Tensile strengths were also unaffected (decreasing by 1MPa). On the other hand, break elongation increased from 8.1% to 11.2%, a trend only seen elsewhere in alloy 6.

The yield strength and tensile strength of alloy 3 increased by an impressive amount, with yield strength increasing from 430MPa to 606MPa (an increase of 176MPa), and UTS increasing from 459MPa to 642MPa (an increase of 183MPa). However, the break elongation value decreased to a level below the minimum 5% target, from 14.7% to 3.6%, making it a non-feasible option as it is unsuitable for further can making processes. Similarly, alloy 4 sees some small increases in yield strength and UTS of 24MPa and 13MPa respectively but is accompanied by a substantial reduction of 8.1% in break elongation, bringing its break elongation value below the 5% target value.

Alloy 5 experienced an increase of 69MPa and 80MPa to yield and UTS respectively. Additionally, the break elongation reduces by 5.3%, from 11.3% to 6%. Alloy 6 saw a substantial reduction in yield strength from 658MPa to 529MPa (a reduction of 129MPa). Similarly, the UTS decreased by a significant amount, from 707MPa to 562MPa (a reduction of 145MPa). Moreover, the break elongation increases from 8.2% to 10.6% (an increase of 2.4%).

7.2.4. Tensile results summary

Alloys 1, 2, 4, and 5 do not experience any significant change in their strength values when higher heating rate and soak temperature were used. On the other hand, alloy 3 saw a large improvement in yield strength of 174MPa but suffered a substantial reduction in break elongation putting it below the 5% target. Alloy 6 is the only sample to experience substantial reductions in yield and tensile strengths.

7.3. Discussion

7.3.1. Grain refinement -Alloy 6

Looking at Figure 7.3, the average grain size of alloys 1-6 did not undergo significant grain refinement when rapidly heated to intercritical soak temperature, with some alloys insignificantly increasing or did not change. The effect of using a 200°C/s heating rate and an intercritical soak temperature of 850°C has resulted in the yield strength of alloy 6 decreasing by 129MPa, from 658MPa to 529MPa, the lowest yield strength seen in all annealing scenarios for this chemistry. This reduction in yield was accompanied by an increase in the break elongation from 8.2% to 10.6%. This result is surprising as it was expected that the behaviour would be like that documented in chapter 2 (The effect of flash annealing (200°C/s heating rate) on lab-casted high-strength packaging grade steels for can-end applications) but instead the yield strength would be 48MPa higher with improved ductility. These better properties would be expected to be the result of a **finer average grain size**, presence of **pearlite islands**, and **presence of secondary ferrite (α_2)**.

The reasons for greater yield strength expectation is because using a heating rate of 200°C/s is said to shift the recrystallisation temperature to near and below the Ac1 temperature (M.A. Mostafaei and Kazeminezhad, 2016). The effect of this is that recrystallisation is incomplete by the time the temperature of the steel reaches the intercritical 850°C temperature. The non-recrystallised ferrite inherently contains more stored strain energy, accelerating the kinetics of transformation of ferrite to austenite (Peranio *et al.*, 2010; Mohanty, Girina and Fonstein, 2011; Karmakar, Ghosh and Chakrabarti, 2013; Chbihi, Barbier and Germain, 2014). The formation of this austenite, which forms around the non-recrystallised and recrystallised ferrite grains, provides preferential site for non-recrystallised ferrite to recrystallise, whilst simultaneously pinning recrystallised ferrite from growing, thus refining the microstructure.

It should be noted however, that conflicting observations also appear in the literature indicating that rapid heating rates increase grain size via slowing down recrystallization by influencing the amount of carbon in solution (Ushioda *et al.*, 1989).

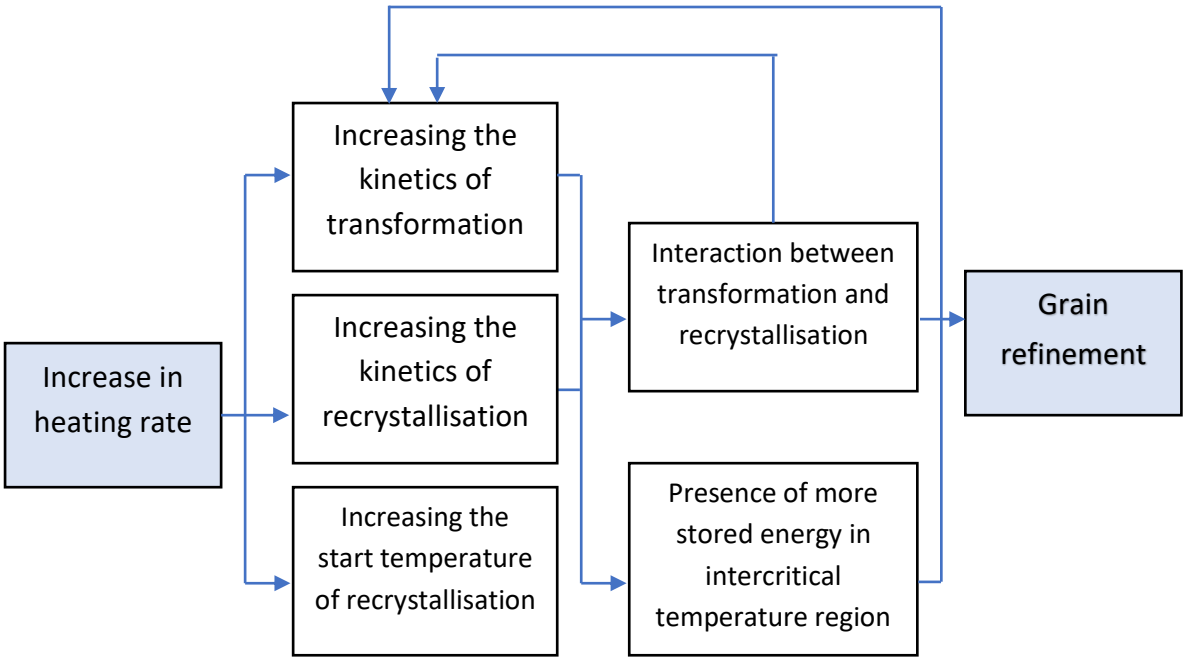

Figure 7.4. Relationships between the mechanisms involved in ultra-rapid annealing (URA) of low carbon steel.

However, the grain sizes for alloys 1-6 were largely unaffected, or increased slightly after rapid heating to intercritical temperature as shown in Figure 7.3. The small changes are not likely to have much effect on the yield strength or the break elongation value. Reasons why significant grain refinement didn't occur might be due two reasons:

1. Firstly, **appreciable amounts of austenite** didn't form and thus the kinetics of recrystallisation were not significantly improved. This could also explain why no visible amounts of pearlite islands could not be viewed using an optical microscope.
2. Secondly, the **high 90% cold reduction applied** to the material prior to annealing meant that the driving force for recrystallisation was so high that the rate of recrystallisation would not have been greatly enhanced via presence of austenite. This in combination with the small amounts of austenite formed could have meant no significant grain refinement could have occurred anyway.

Also, the other alloys didn't undergo significant grain size refinement either. This means that packaging grade steels do not undergo grain refinement via rapid heating rate to intercritical soak temperature. So, grain size effects are not likely responsible for the changes in yield strength and break elongation of alloys 1-6.

7.3.2. Did pearlite islands or secondary ferrite form in the chemistries?

Another expectation of rapid heating to intercritical soak temperature was the formation of pearlite islands. However, upon looking at some of the optical microstructures of each of the alloys, there seemed no evidence of pearlite island formation (see Figure 7.5).

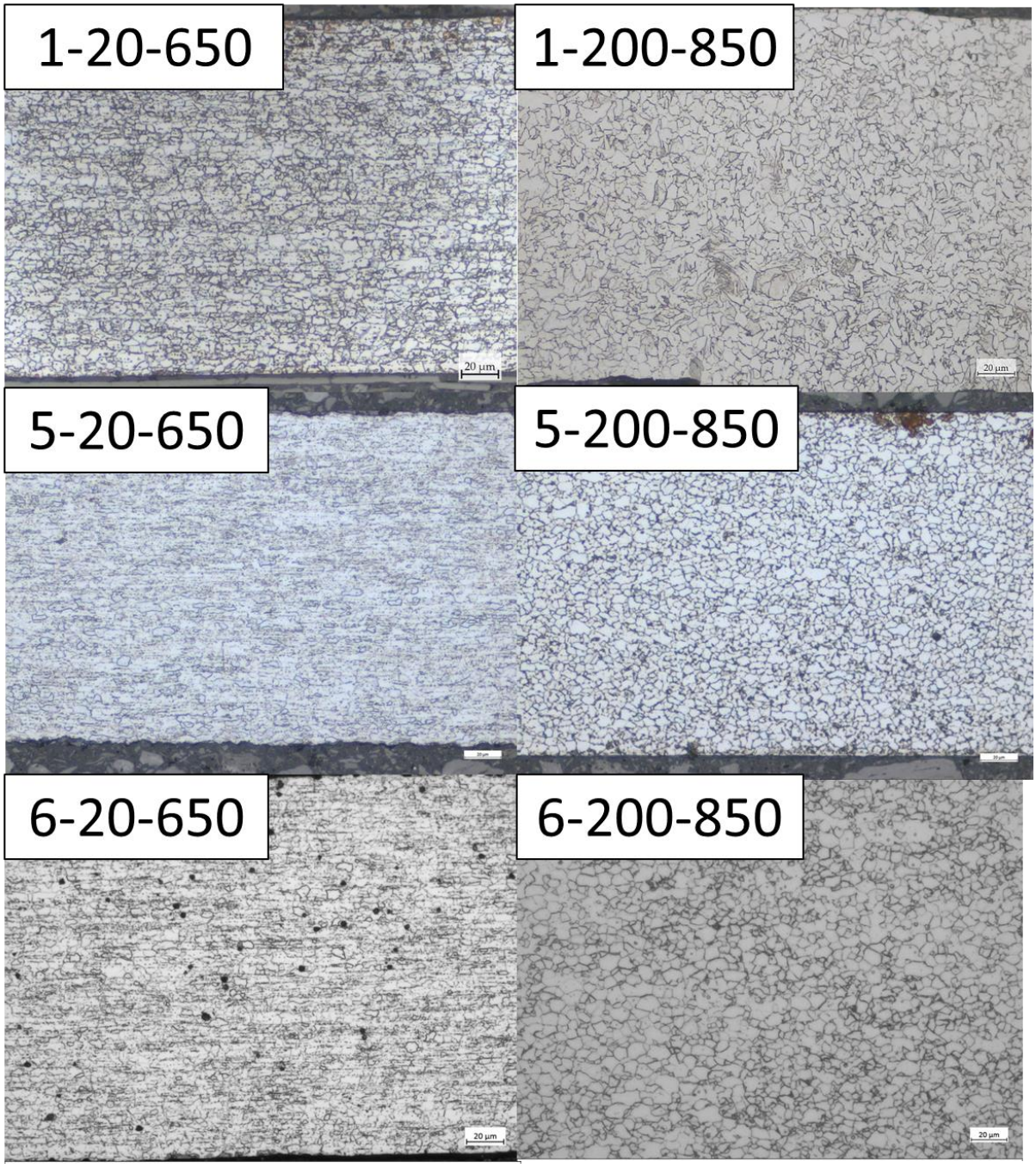

Figure 7.5. Note morphological difference between ferrite and secondary ferrite, especially in alloy 1.

Even when viewed under a scanning electron microscope, there were no clear signs of pearlite island formation (see Figure 7.6).

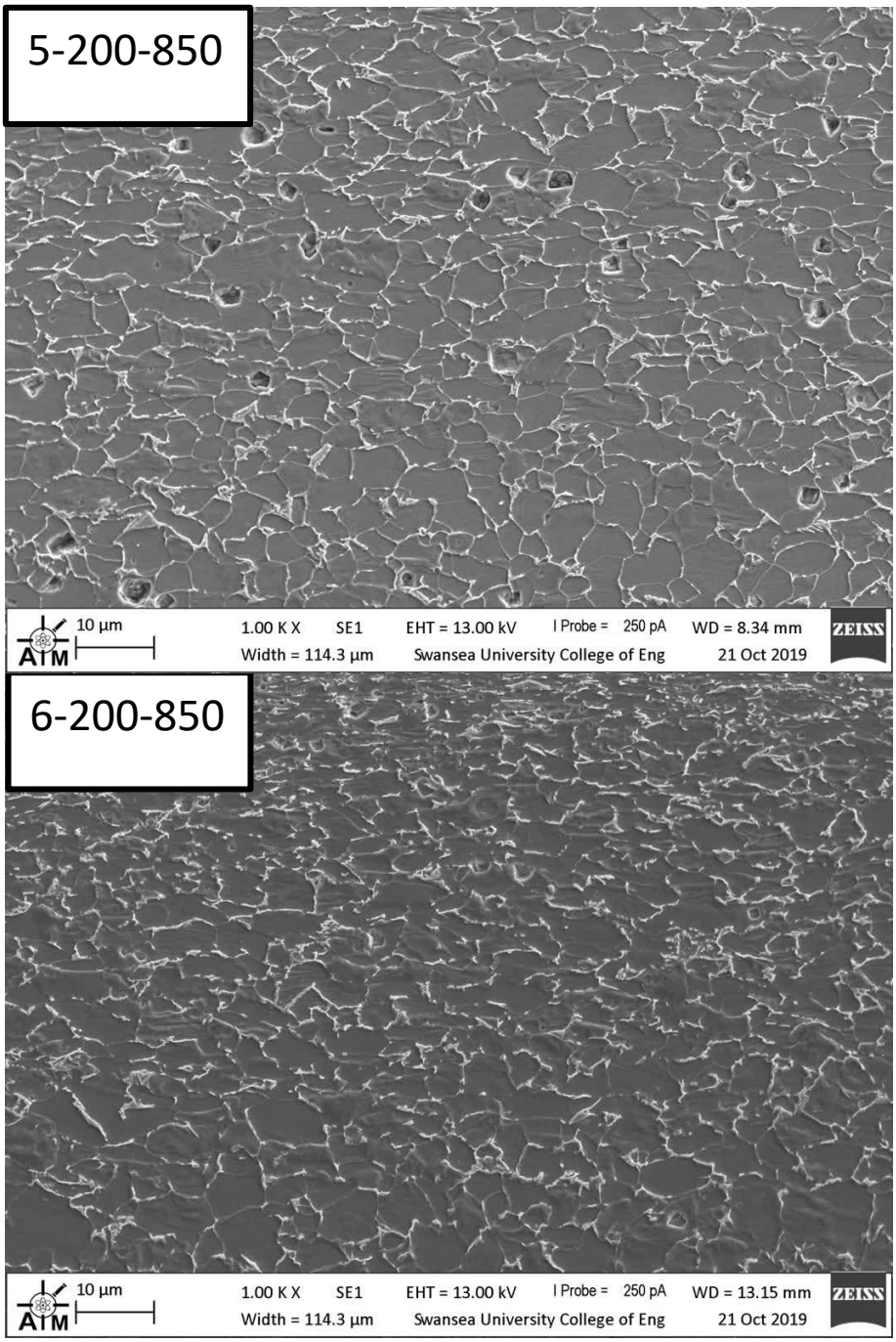

Figure 7.6. SEM images of alloys 5 and 6 under rapid heating and intercritical annealing conditions.

However, **the presence of secondary ferrite** (as shown by the irregular and sharp boundaries) **did form** and is especially noticeable in the optical microstructure of alloy 1.

These are likely to have originated from the transformation of austenite into secondary ferrite upon cooling.

However, it's unlikely the microstructures (including the presence of secondary ferrite) had any significant impact on the yield strength of these alloys. For example, the microstructures of alloys 5 and 6 look very similar, yet the yield strengths are different, and the way in which yield strength changed because of rapid heating to intercritical soak temperature was different. For example, alloy 5 increased in yield strength, whereas the opposite happened in alloy 6. Therefore, if grain size effect and microstructural effects (e.g., secondary phase hardening) didn't influence yield strengths, another mechanism must have occurred.

7.3.3. So why did yield strength increase/decrease in some chemistries?

Another explanation for the changes in yield strength might be due to **solid solution effects**. For example, Alloy 6's reduction in yield might be because nitrogen precipitated out of the matrix, thus reducing the solid solution strengthening effect of interstitial nitrogen. A reason for this is when looking at the mechanical properties of alloy 5 (which contains 175ppm less nitrogen), the yield strength increased from 522MPa to its highest 591MPa, whilst break elongation reduced from 11.3% to 6.0%. Also, like alloy 6, the average grain size did not change. Furthermore, the microstructure of alloy 5 looks identical to alloy 6 and shows no secondary phase e.g., pearlite islands. These rules out effects of grain size, secondary phase hardening, and suggests that the extra 175ppm nitrogen in alloy 6 is responsible for its reduction in yield. As mentioned previously, the difference in solubility of nitrogen in austenite and ferrite is potentially having an influence on properties.

Perhaps due to the high thermal energy provided by 850°C intercritical soak, diffusion of excess free nitrogen diffused to the small amounts of austenite, which lowered the lattice distortion of the ferrite. Additionally, due to rapid 300°C/s cooling, remained at those sites which became the boundaries between primary and secondary ferrite and precipitated out as atmospheric N_2 or aluminium nitrides, thus weakening grain boundary bonds or removing free nitrogen from solution. Alloy 6 does contain **0.012wt% more aluminium** (in addition to small titanium amount), and therefore has the potential to remove **120ppm** of nitrogen from solution and thus potentially reducing yield strength by **~96MPa** (using strengthening model from chapter 1 (Effect of chemistry at commercial annealing parameters) and tensile strength by 120MPa. However, no nitrogen precipitates were visible in the microstructure at the

optical level and no specific nitrogen agglomeration was detectable using EDX technique either. EDX showed a homogenous spread of all elements across the sample.

It is unexpected that the yield strength of alloy 6 is lower than alloy 5. This is because the higher concentration of nitrogen in alloy 6 meant that more nitrogen was available for dislocation pinning. Future work could involve using a Transmission electron microscope to scan the microstructure for nitrides or using an interstitial analyser to measure the amount of nitrogen in solution after different annealing cycles.

7.3.4. Role of silicon and phosphorus in Alloys 3 and 5

The presence of silicon and phosphorous, or the ratio of silicon and phosphorus, in addition to the conditions created by the rapid heating rate and intercritical soak temperature potentially enhancing the strengthening effects of silicon and phosphorus, are responsible for the large increases in yield strength seen in alloys 3 and 5. Phosphorus is said to retard recrystallisation and refine grain size, however Figure 7.3 shows that average ferrite grain size for alloy 3 and 5 increased and stayed the same respectively. However, looking at the SEM image of sample 5-200-850 in Figure 7.6, this is indicative that more grain misorientation is present, perhaps because of the phosphorous, and could explain why alloy 5 (and alloy 3) has a higher yield strength.

The hardness of samples 3-20-650 and 3-200-850 were measured to determine whether the solid solution effects were responsible for the large increase in yield strength seen. See Figure 7.7 for the results.

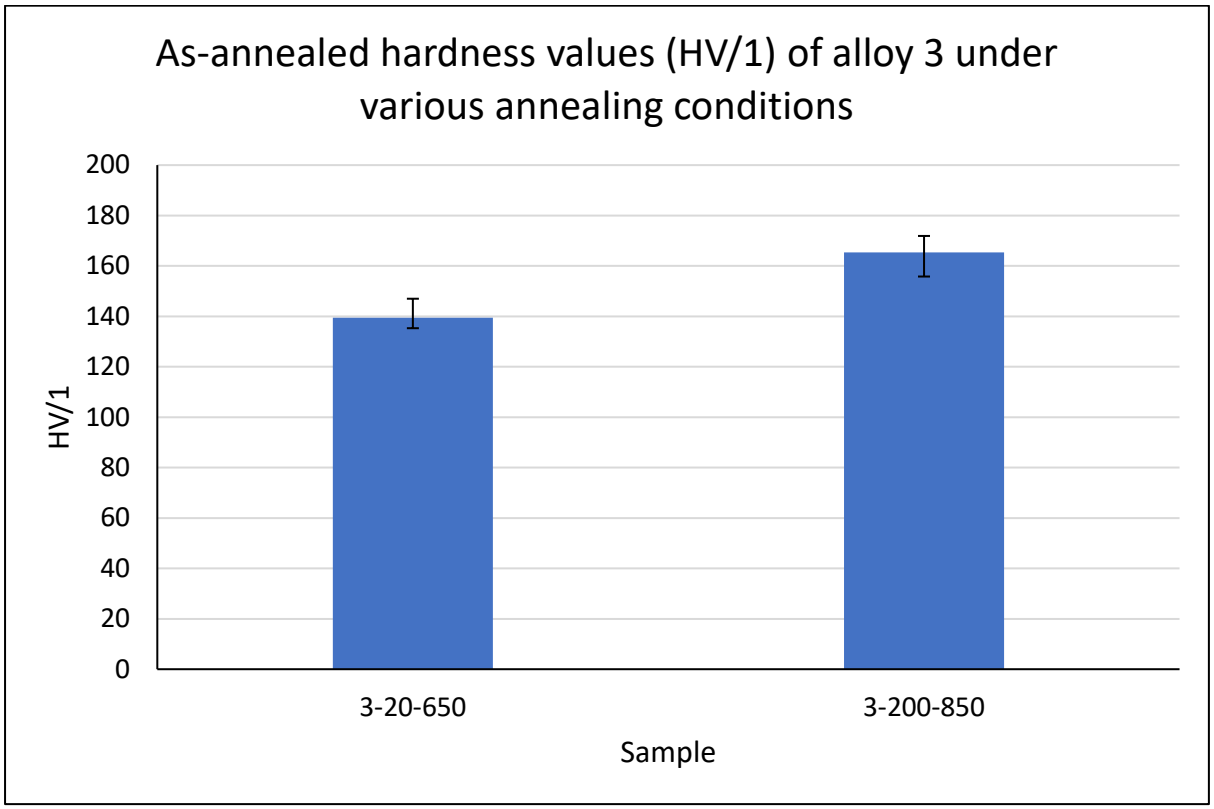

Figure 7.7. As-annealed hardness of alloy 3 after commercial annealing or rapid heating to intercritical annealing.

Figure 7.7 shows that the hardness value changed by an insignificant 26HV. Therefore, it leads me to think grain orientation spread within the grain is responsible.

If grain orientation spread is responsible, perhaps it is more prevalent in alloy 3 because silicon has been shown to increase recrystallisation in the intercritical zone (Drumond *et al.*, 2012), though phosphorus stabilises austenite, the lower amount in alloy 3 potentially reduced this effect.

7.4. Conclusion

- Ultra-rapid annealing to intercritical soak temperature **does not lead to significant grain refinement** in packaging grade steels, and in some alloys increases the average grain size. This implies packaging steels for can end applications **do not exhibit strong interaction between recrystallisation and transformation** at inter critical soak temperatures.
- Ultra-rapid annealing to intercritical soak temperature does not lead to the formation of pearlite islands in packaging grade steels, but does generate some secondary ferrite.
- Ultra-rapid annealing leads a **large reduction** in yield strength particularly when chemistry contains a **very high nitrogen content** way above current commercial capability. This is potentially due to precipitation of nitrogen from the ferrite matrix, reducing the solid solution strengthening effect.
- Other chemistries containing commercial levels of nitrogen either see negligible changes to yield strength or 70MPa-170MPa increase (alloys 3 and 5). The increase in yield strength values in alloys 3 and 5 are seen in other annealing conditions where only a rapid heating rate is used, or an intercritical soak temperature is employed, but not to such an extent as when a combination of both rapid heating and intercritical soak temperature are used. The high strength levels of alloys 3 and 5 are associated with their silicon and phosphorous contents.
- Yield strength improved in chemistries containing silicon and phosphorous but lead to break elongation values below the recommended 5% for can-ends.

8. Technical chapter 5 – The effect of removing the slow cool section from Trostre's continuous annealing production line on the microstructural and mechanical properties of packaging grade steel

8.1. Purpose of study

Regarding Tata steel's packaging competitors, ThyssenKrupp can manufacture a grade of steel for can-end applications with a yield strength of 650MPa ±50MPa. Additionally, ArcelorMittal can produce a grade of steel for can-end applications with a yield strength of 750MPa ±30MPa. It is presumed that ThyssenKrupp achieve their high strength product via increasing the amount of solution nitrogen above the theoretical solubility limit in steel, thus exploiting the effect that solution nitrogen has on the strength properties of steel. It is presumed they do this via nitriding steel coils during the continuous annealing process. On the other hand, ArcelorMittal achieve their high strength product through other means. Firstly, it has been identified that the microstructure of ArcelorMittal's high strength steel product contains a mixed phase of ferrite and presumably pearlite. Secondly, the composition of the steel used is similar to Trostre's commercial grade 3364 (see Table 8.1 below for 3364 chemistry).

Table 8.1. Table showing the composition of commercial grade 3364.

Steel	**C**	**Mn**	**Al**	**N**
Med.C – steel grade	0.04	0.23	0.02	0.002

Given that the chemistry of Arcelor's high strength product is like a Tata packaging grade, but the yield strength is much greater than Tata's current feasible product, it is presumed that the processing conditions ArcelorMittal use are different to Tata's and are responsible for the high strength. It is surprising that a ferrite-pearlite microstructure is responsible for giving the steel that ArcelorMittal manufacture the mechanical properties it has. However, in the previous chapter where an 850°C intercritical soak temperature has been used, the microstructure appears to be dominated by the ferrite phase only. Therefore, the work in this chapter has made efforts to try and determine the process required to make a mixed phase

microstructure in a packaging steel grade, and to generate bainite secondary phase. To achieve this, annealing simulations that remove the slow cool section from the CAPL were attempted in order to produce secondary phase bainite to form.

8.2. Materials and experimental procedure

For information and details regarding the experimental procedures used in this chapter, please refer to Table which will direct you to the relevant sections within the Methods and Experimental Chapter (Chapter 3).

Table 8.2. Where to find information and details on the experimental procedures used in this chapter.

Procedure	Section number
Processing history	3.1
OES & ELTRA obtained chemistry	Table 4.6
Transformation temperatures	3.3
Annealing heat treatments performed	3.4.6
Temper rolling and Ageing	3.7
Tensile testing parameters	3.8.1
Optical microscopy	3.11
Hardness testing	3.14
Grain Size Analysis	3.12

For details on the annealing heat treatment procedure carried out in this chapter, please see chapter 3.4.6. Alloys 5 and 6 were used in this chapter, with their compositions given in Table 8.3. Grade 3364 is given for comparison purposes.

Table 8.3. Chemical compositions of alloys 5 and 6. Grade 3364 is shown for reference.

Sample	C	Mn	Al	Si	S	P	Ti	N	Fe
3364	0.04	0.23	0.02	-	-	-	-	0.002	
Alloy 5	0.090	0.517	0.0550	0.255	0.003	0.111	0.001	0.0108	Bal.
Alloy 6	0.085	0.587	0.067	0.26	0.004	0.102	0.001	0.0283	Bal.

The compositions of alloys 5 and 6 were inserted into JMatPro® software, whereby respective Time Temperature Transformation (TTT) diagrams were generated (see Figure 8.1). Using these TTT diagrams, the 850°C intercritical soak temperature annealing cycle used in previous chapters was superimposed onto the diagrams to gain insight into the effect of the annealing section after the soak stage (i.e., slow cooling, rapid cooling and overageing) have on the prospect of generating a mixed phase microstructure.

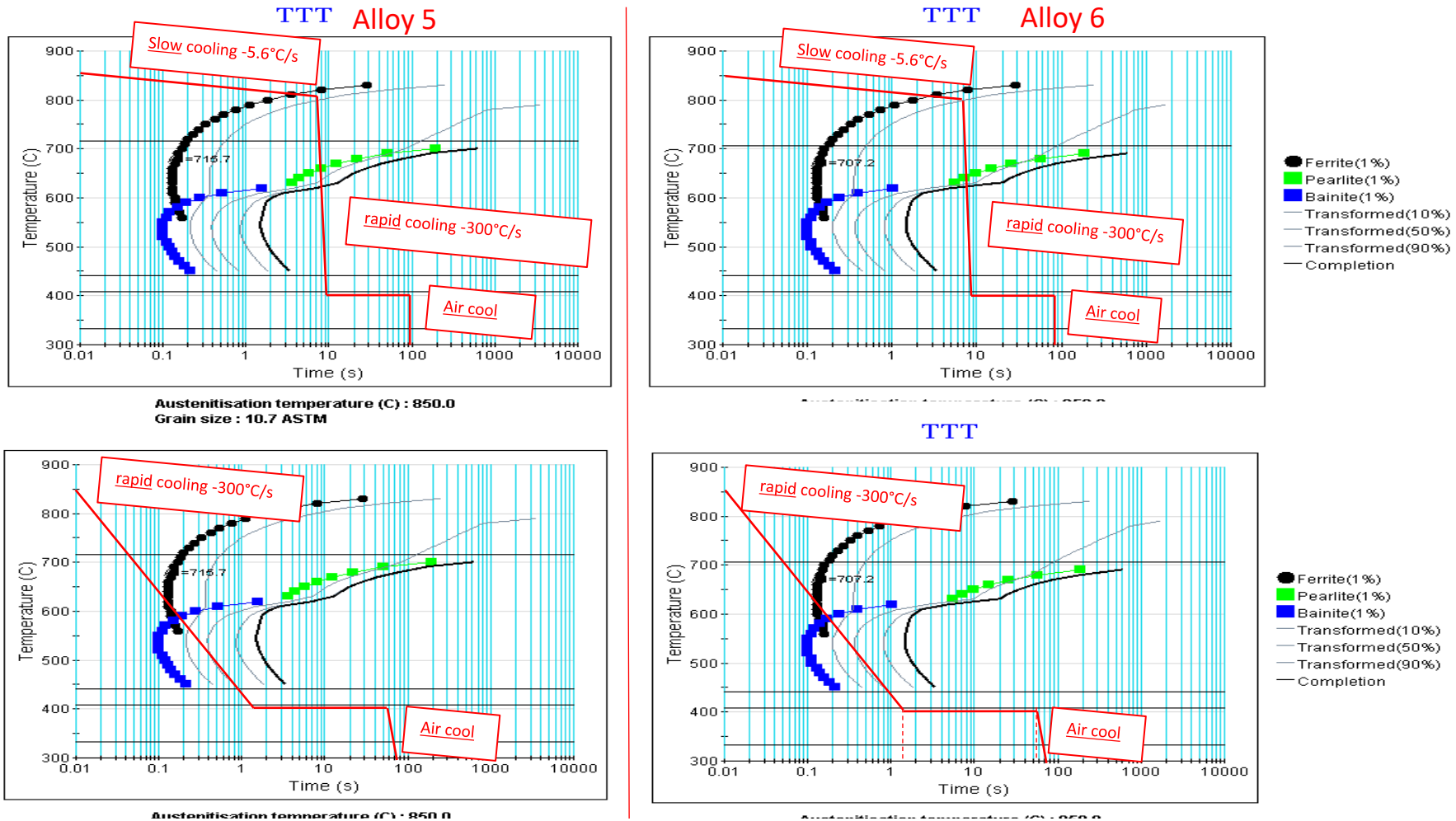

Figure 8.1. Composite image showing the intercritical annealing cycle with and without the slow cool section superimposed onto TTT diagrams for alloys 5 and 6.

Figure 8.1 shows a composite image of the temperature vs time diagram of the intercritical annealing cycle of sections that take place after the soak stage (i.e., Slow cooling, rapid cooling, overageing sections) superimposed onto the JMatPro® generated TTT diagrams for alloy 5 and 6. Additionally, it shows the effect of removing the slow cool section from the annealing procedure (see diagrams on bottom half)

For the annealing procedure that utilises the slow cool section, the cooling path intersects the Pearlite curve and does not intersect the Bainite curve for both alloys. On the other hand, when the slow cooling section is removed, the cooling curves then intersects the Bainite curve.

8.2.1. Why there a slow cooling section

The slow cool section represents a zone of the Trostre CAPL where the steel coil is transported from the soak section to the rapid cooling section. It has been mentioned by the industrial supervisor that it might be possible to remove, or shorten, this slow cooling section from the annealing line if it proves to enhance steel properties.

8.3. Results

8.3.1. Hardness

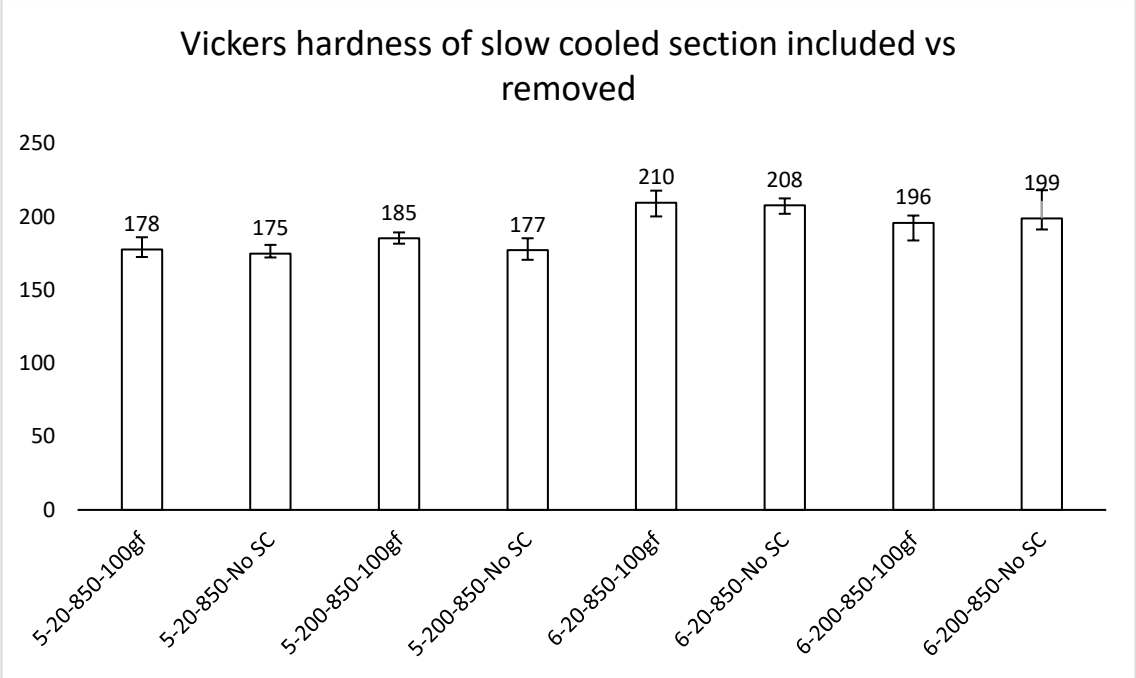

Figure 8.2. Graph showing the as-annealed hardness conditions of alloys 5 and 6 where the slow cool section was included and excluded.

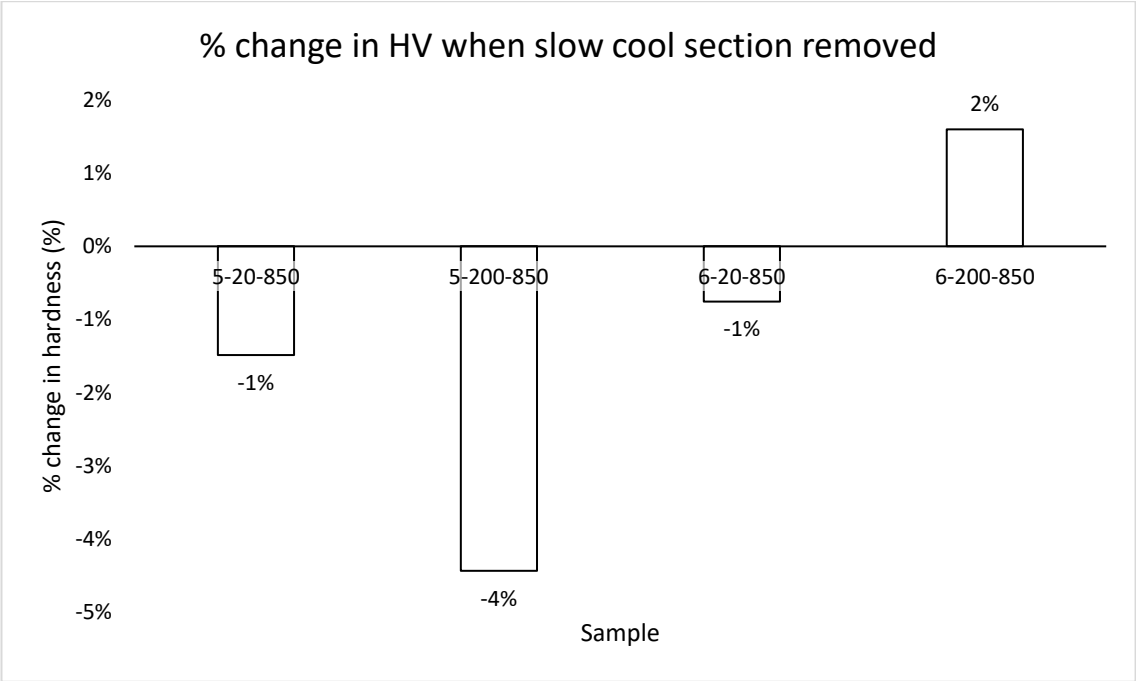

Figure 8.3. Percentage change in hardness of alloys 5 and 6 when slow cool section was removed.

Figure 8.2 shows the as-annealed hardness of alloys 5 and 6 where the slow cool section has been included and excluded from the simulated annealing heat treatments. When comparing the samples without the slow cool section to their respective samples where the slow cool section has been included, there seems to be negligible difference in hardness. The hardness of all slow cool removed samples is within the error margins of respective samples where the slow cool section was included. Therefore, it can be concluded that removing the slow cool section has negligible effect on the hardness values. Furthermore, this is indicative that second phase bainite did not form in the samples where the slow cool section was removed, because it would be expected that the formation of Bainite would have resulted in an increase in the hardness values. However, it's possible that Bainite did form, but at such small volume fractions that the hardness indenter did not register it, either because the size of the indenter was so large that the surrounding ferrite phase overwhelmed the contribution of bainite to hardness, or the indenter 'missed' areas of Bainite due to an inhomogeneous spacing of bainite. However, large areas of the sample were assessed.

8.3.2. Microstructures

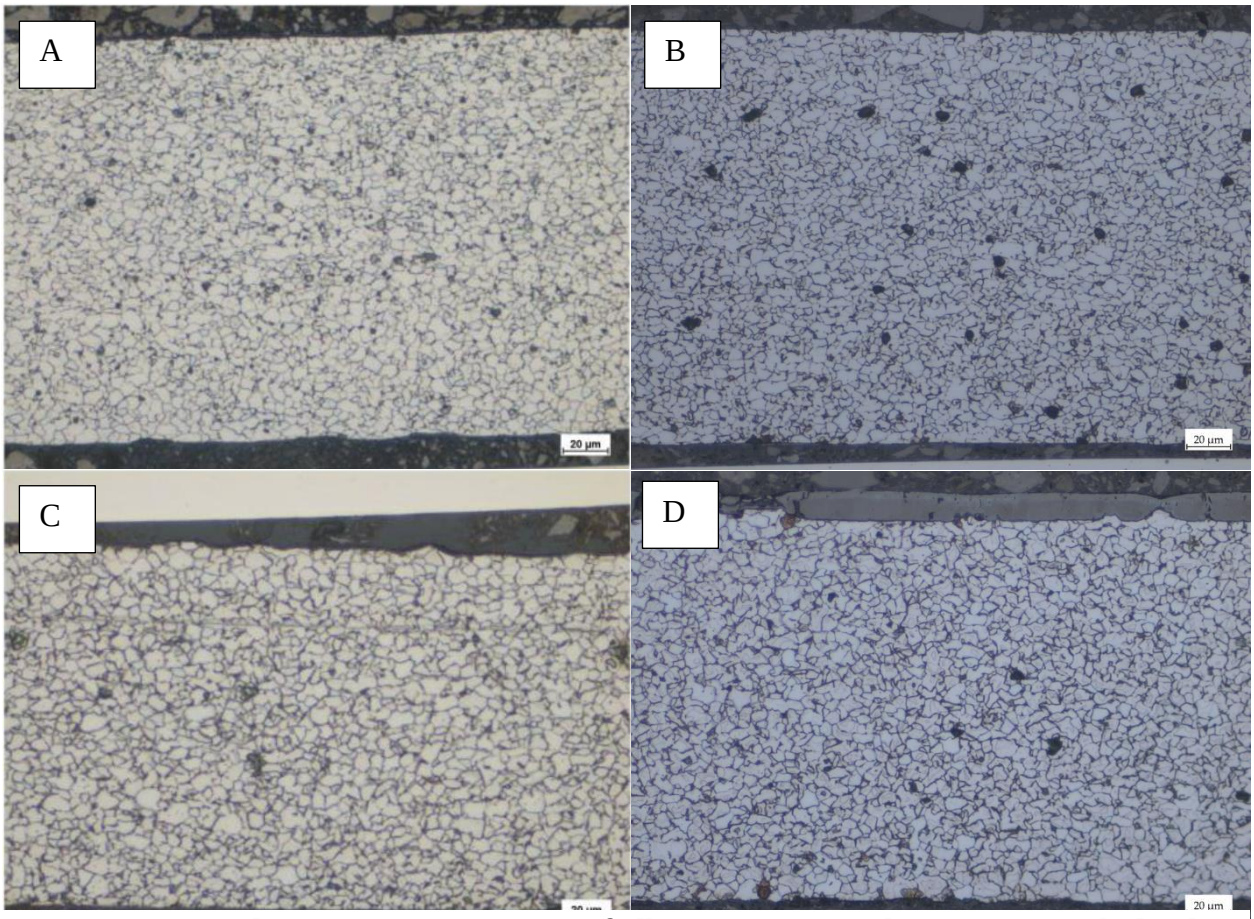

Figure 8.4. optical microstructure images of alloy 5; A) 200°C/s heating rate with the slow cool section B) 200°C/s heating rate without the slow cool section C) 20°C/s heating rate with the slow cool section D) 20°C/s heating rate without the slow cool section.

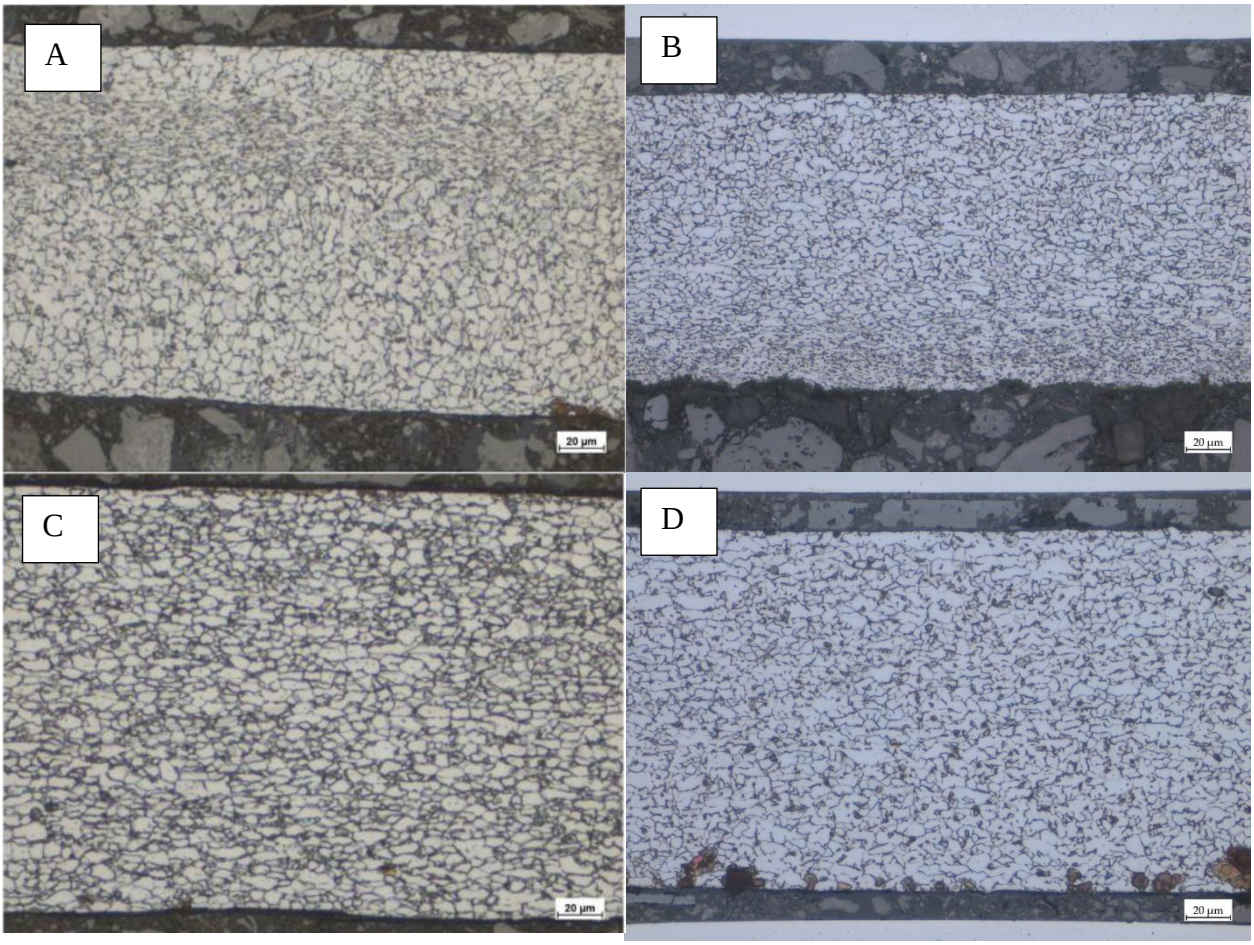

Figure 8.5. optical microstructure images of alloy 6; A) 200°C/s heating rate with the slow cool section B) 200°C/s heating rate without the slow cool section C) 20°C/s heating rate with the slow cool section D) 20°C/s heating rate without the slow cool section.

Figure 8.4 and Figure 8.5 show the microstructures of alloys 5 and 6 that have been annealed with the slow section included (A and C), and with the slow cool section excluded (B and D). The microstructures are very similar to each other and appear to be mostly a ferritic microstructure. This could explain the similarity in hardness seen in samples annealed with and without the slow cool section. Furthermore, the microstructure images show no presence of Bainite second phase.

8.4. Discussion

Perhaps the inclusion of the overageing section in the annealing cycles had an impact on the hardness results and microstructures of alloys 5 and 6, causing them to show no significant changes in hardness or microstructures. Given that bainite transformation is time dependant, and the cooling to the 400°C overageing temperature cuts across the bainite section to martensite formation (as seen in Figure 8.1), nevertheless any remaining austenite was likely to have transformed to martensite and bainite (more of the former).

8.5. Removing the slow cool section and overageing section

It is thought that the overageing section interferes with the generation of secondary phase. In one test run, it was discovered that there was an error in the cooling system of the Gleeble® 3500, for sample a 1-200-850 used in chapter 3. Instead of cooling from soak temperature 850°C to room temperature at a cooling rate of -300°C/s, the sample cooled to ~600°C before the cooling tailed off at -150°C/s to room temperature. As a result of this, the cooling profile of the sample went through the pearlite nose as seen in a TTT diagram.

Therefore, because rival ArcelorMittal produce a high strength steel with a similar microstructure, the experiment was repeated.

8.5.1. Results of no slow cool and no overage sections

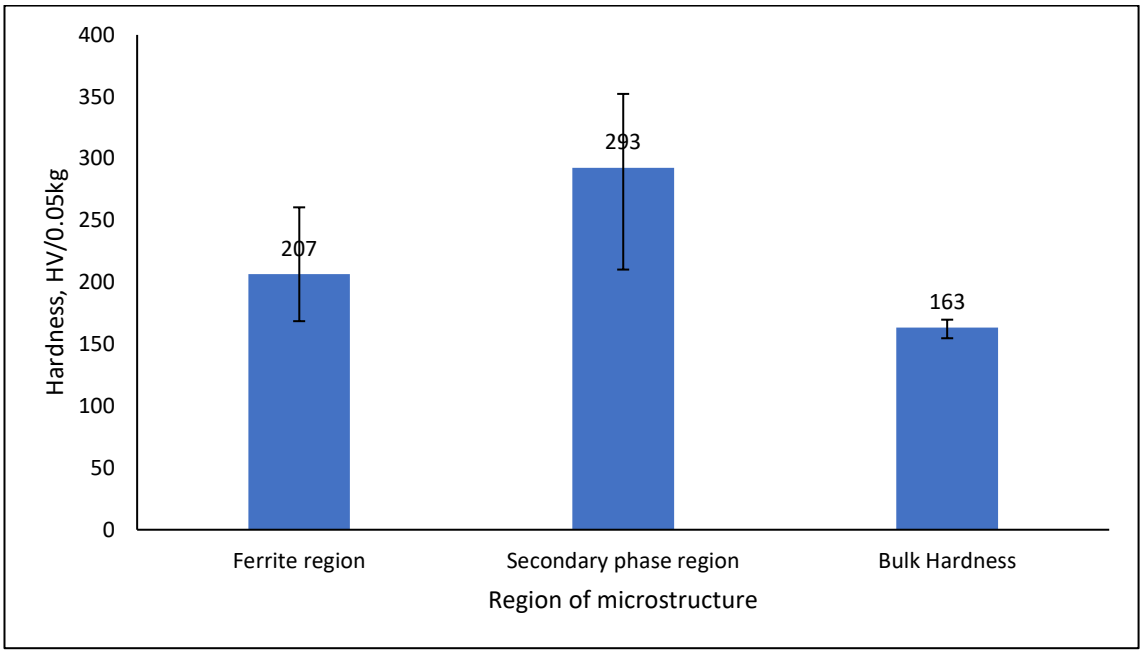

Figure 8.6. Hardness values of ferrite region and secondary phase region.

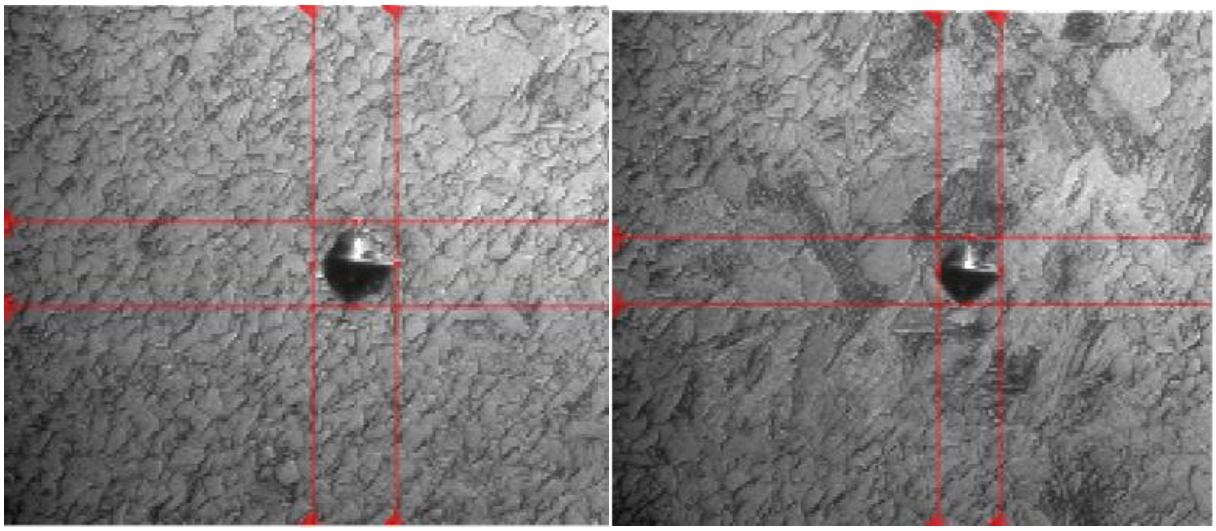

Figure 8.7. Microstructural image of hardness indent and area of microstructure measurement was taken from. Image on left shows ferrite region. image of right shows secondary phase region.

Removing the slow cool and overage section did result in small, localised area of harder secondary phase relative to the surrounding softer ferrite matrix phase when measured with a small hardness load of 50g load (see Figure 8.6 and Figure 8.7). Moreover, when bulk hardness was measured, the sample gave an average hardness value of 163HV, which equates to a similar ultimate tensile strength value seen in sample 1-200-850 (485MPa) in chapter 4, given ultimate tensile strength value is

approximately 3x greater than the hardness value (3x 163HV = 489MPa). Therefore, as this hardness measurement was conducted on material in its as-annealed state, it is reasonable to suggest that greater strength values would be seen if a 5% temper rolling, and aging were conducted.

8.6. Conclusions

- Removing only the slow cool section from simulated annealing cycles showed negligible difference in hardness values for alloys 5 and 6. Furthermore, there were no differences in the microstructures of alloys 5 and 6 when the slow cool section was removed. The similar microstructures could explain why there were no significant changes in hardness.
- Removing both the slow cool section and overageing sections from the CAPL cycles does result in presence of some harder secondary phase which increases the bulk hardness of packaging steel for can end applications. Therefore, there is potential that the tensile strength properties may also be increased to levels greater than those seen in chapter 4.

9. Technical Chapter 6 - Effect of rapid heating rates, soak temperatures, and cooling rates on the grain size and mechanical properties of a commercial nitrogenised packaging grade steel for can-end applications (impact activity)

9.1. Purpose of study

The purpose of this study was to determine the effect rapid heating rates have on the ferrite grain size of a commercial nitrogenised grade of packaging steel for can-end applications. This is so a rapid heating rate that gives the smallest ferrite grain size can be identified and used in later experiments (which assess effect of different soak temperatures and cooling rates) to ultimately minimise the number of total number of experiments. It is expected that using higher rapid heating rates will result in a smaller average ferrite grain size, but the size of the effect is unknown.

Based on previous chapter findings, it is evident across all chapters that there was most benefit to the nitrogenised approach whereby the presence of greater nitrogen contents meets the desired mechanical properties (see sample 6-20-640) or gets close to the desired properties. Therefore, assessment of an industrial nitrogenised grade will be used.

9.2. Introduction

There is a drive by the sponsoring company to develop a new grade of packaging steel for can-end applications, that can match or rival the products of competitors. This work will look at the effect of annealing cycle parameters (specifically heating rate, soak temperature, and rapid cooling rate) to determine the best approach to develop a grade of steel with a proof stress between 650-750MPa, a total elongation of at-least 5% in all directions after a double reduction rolling procedure. This implies that the total elongation must be at-least 35% in its as-annealed state.

The previous chapters looked at the effect of alloying elements Silicon, Sulphur, phosphorous, and nitrogen of lab-casted alloys, as well as effect of heating rate and soak temperature during the annealing cycle. This chapter focusses on the effect of sub-critical and intercritical **soak temperatures** and **cooling rate** on commercial nitrogenised 3465 grade. Additionally, the removal of some CAPL sections, i.e., the slow cooling and overageing sections were studied.

The goal of this body of work is to increase the strength of grade 3465 through **refinement** of the **ferrite grain** size and generation of harder **secondary phases** (mixed phase microstructure).

9.3. Experimental procedure

For information and details regarding the experimental procedures used in this chapter, please refer to Table which will direct you to the relevant sections within the Methods and Experimental Chapter (Chapter 3).

Table 9.1. Where to find information and details on the experimental procedures used in this chapter.

Procedure	Section number
Processing history	3.2
Composition	3.2
Transformation temperatures	3.3
Annealing heat treatments performed	3.5
Temper rolling and Ageing	3.7
Tensile testing parameters	3.8.1
Optical microscopy	3.11
Hardness testing	3.14
Grain Size Analysis	3.12

For details on the annealing heat treatment procedure carried out in this chapter, please see chapter 3.4.7. The material used in this chapter was cold rolled commercial packaging grade 3465 steel, with its chemical composition given in Table 3.2. The nitrogenised steel grade has applications in easy open ends where the thickness of the sheet is 0.18mm and below.

Figure 9.1 show the initial microstructure of grade 3465 in its cold reduced condition. The cold-rolled microstructure consists of ferrite grains aligned in the rolling direction with a uniform distribution of carbides in the ferrite matrix, as well as areas of remarkably high dislocation density.

Figure 9.1. Optical image of nitrogenised grade 3465, in its transverse orientation, in its cold rolled condition at a magnification of 500x.

For each tensile test, ASTM 25 specimens were machined from the centre of annealed samples with their lengths parallel to the rolling direction. Tensile testing was conducted at room temperature with strain rates of v1=0.00015sec^{-1}, v2= 0.00075sec^{-1}, v3= 0.00075sec^{-1}.

9.4. Heating rate selection

The 20°C/s was used because this is the Trostre steelworks highest heating rate possible. So, the effect of higher heating rates on the mechanical properties can be compared to it.

The 200°C/s heating rate was used because work done by (M. A. Mostafaei and Kazeminezhad, 2016) mentions that a 200°C/s heating rate was the best compromise between not increasing the start and finish recrystallization temperatures above the Ac1 temperature (for sub-critical annealing) but also allowing some un-recrystallised ferrite grains to be present during transformation of ferrite to austenite (above Ac1). For inter-critical annealing it was said that recrystallisation of ferrite will occur before the Ac1 temperature is reached,

but there still will be some present by the time intercritical temperatures are reached. It is the presence of this un-recrystallised ferrite during transformation which enhances the kinetics of transformation, which then enhances the kinetics of recrystallisation.

Increasing the heating rate from 200°C/s to 1,000°C/s is expected to increase the volume fraction of un-recrystallised ferrite when transformation starts (because recrystallisation start and finish temperature are now above Ac1 because of such a high heating rate). Therefore, it is expected this greater volume fraction of un-recrystallised ferrite at transformation temperatures will enhance the kinetics of transformation and thus recrystallisation further, consequently further refining the ferrite grain size. However, the magnitude of this refinement is not currently known (especially in packaging grade steels) or what the relationship between heating rate and grain refinement looks like in packaging steels.

I think that the 1,000°C/s heating rate will be more beneficial for the intercritical soak temperature cycles (more recrystallizations will occur and more refined ferrite grains) but less beneficial for the sub-critical soak temperatures (ferrite grains fail to recrystallize due to recrystallisation start and finish temperatures being pushed to higher temperatures above the Ac1). Therefore, the 200°C/s heating rate is seen as the better compromise.

9.5. Results

9.5.1. Grain size analysis

Table 9.2 and Figure 9.2 shows the average ferrite grain sizes of each test in table and graphic form respectively. Figure 9.3 displays the grain size distribution of each test.

Table 9.2. Effect of heating rate and soak temperature on average ferrite grain size.

Annealing condition	Average grain size (µm)
HR=20°C/s,ST=635°C	5.0
HR=200°C/s,ST=635°C	4.7
HR=1,000°C/s,ST=635°C	4.2
HR=20°C/s,ST=850°C	5.1
HR=200°C/s,ST=850°C	5.0
HR=1,000°C/s,ST=850°C	4.8

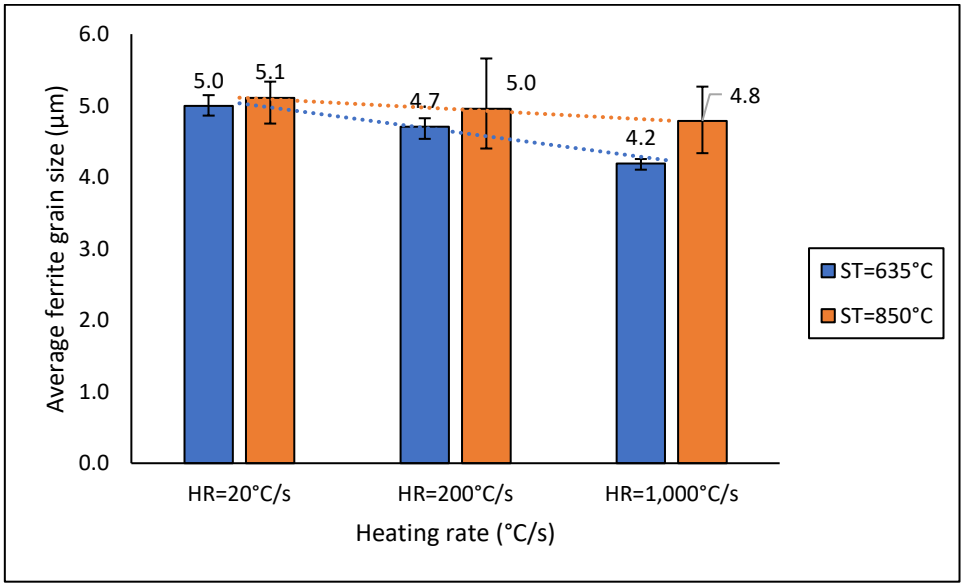

Figure 9.2. Effect of heating rate and 650°C (blue bars) and 850°C (orange bars) soak temperature on average ferrite grain size.

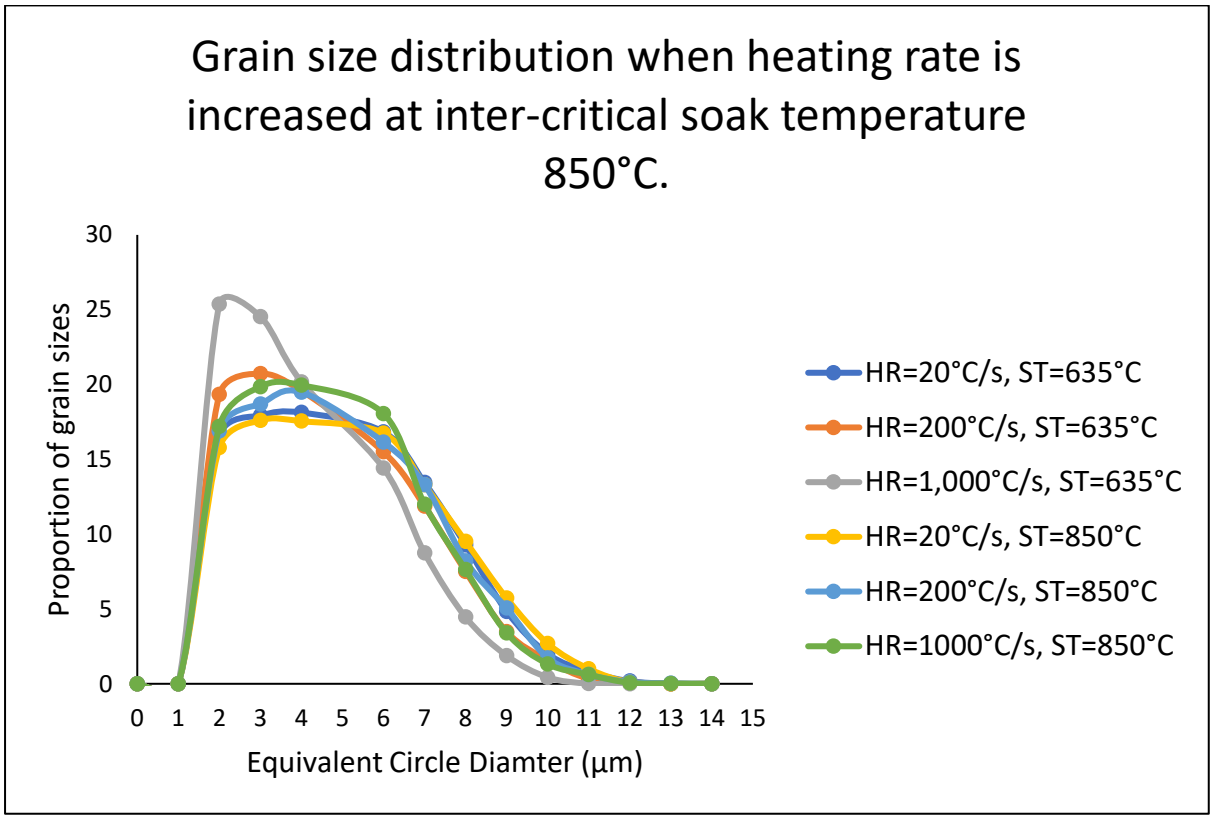

Figure 9.3. Average grain distribution of all samples.

From the Figure 9.2, the average grain size decreased as the heating rate increased. This grain refinement was seen at both soak temperatures. However, the **rate** of grain refinement with increasing heating rate is slightly greater at the sub-critical soak temperature **635°C**. When the heating rate is increased from 20°C/s to 200°C/s, average grain size number decreased by **0.3µm** (from 5.0µm to 4.7µm) at soak temperature 635°C, and by **0.1µm** (from 5.1µm to 5.0µm) at soak temperature 850°C. In addition, when heating is increased from 200°C/s to 1,000°C/s, average grain size number decreases by a further **0.5µm** (4.7µm to 4.2µm) at soak temperature 635°C, and by **0.2µm** (5.0µm to 4.8µm) at soak temperature 850°C. Therefore, at sub-critical soak temperature 635°C it appears that the rate of average grain refinement accelerates with heating rate, whereas at inter-critical soak temperature 850°C, the rate of average grain refinement with heating rate is less.

Furthermore, Figure 9.3 shows the **distribution** of grain sizes for all samples. In both soak temperatures as heating rate increases, the variation in grain size reduces, and the proportion of smaller grains increases. Samples annealed at soak temperature 635°C exhibit smaller variation in grain size and greater proportion of smaller grain sizes compared to samples

annealed to 850°C soak temperature (except for sample 20-635 which exhibits similar distribution curve to sample 20-850). This implies that grain growth at inter-critical soak temperature 850°C is less homogenous and preferential grain growth of certain grains occurs at the expense of others.

For comparison purposes, when Trostre anneal the nitrogenised grades (3464 and 3465) to soak temperature aim 635°C on the CAPL (line speed 400m/min), they expect the resultant grain size to be between 50,000-60,000 grains/mm^2 (equivalent to ASTM 12.8-13.2 or 3.7-4.3µm). The average grain size of 5µm for heating rate 20°C/s and soak temperature 635°C test sample is higher than expected, but perhaps the differences between laboratory methodology and the commercial manufacturing process were responsible for discrepancy. Knowing this, tensile results put forward later may be pessimistic with regards to property enhancements.

9.5.2. Statistical analysis of grain sizes

Table 9.3. Statistical information

Sample	Standard Deviation	ASTM grain size value	Median Skewness	Excel Skew
HR=20°C/s, ST=635°C	0.072	12.338	-0.689	-0.28
HR=200°C/s, ST=635°C	0.066	12.512	0.715	0.69
HR=1,000°C/s, ST=635°C	0.037	12.842	0.806	0.68
HR=20°C/s, ST=850°C	0.141	12.278	1.520	0.67
HR=200°C/s, ST=850°C	0.251	12.391	-0.519	-0.46

HR=1,000°C/s, ST=850°C	0.230	12.480	-0.775	-0.26

The calculated skewness, as shown in Table 9.3, can be used to describe how the distribution of grain sizes is influenced by the heating rates used. At sub-critical soak temperature 635°C, there is a negative skew (-0.28) when a heating rate of 20°C/s is used. However, the skew becomes positive at higher 200°C/s heating rate (0.69) and stays positive at a similar value (0.68) when heating rate is increased to 1,000°C/s. This means that at sub-critical soak temperature 635°C the distribution of grain sizes leans more towards the smaller grain sizes as heating rate is increased. This effect is shown in Figure 9.3 whereby the distribution is becoming narrower and exhibits a stronger peak towards the smaller grains. This could be explained by nucleation effects whereby a larger number of nuclei are growing, leading to smaller grains at the end of annealing.

In contrast, the opposite effect on skew is seen when inter-critical soak temperature 850°C is used. At heating rate 20°C/s, the skew is positive (0.67), but becomes negative at heating rate 200°C/s (-0.46) and stays negative (albeit decreasing in skewness) when heating rate is increased to 1,000°C/s (-0.26). This means that at inter-critical soak temperature 850°C the distribution of grain size leans more towards the larger grain sizes as heating rate is increased. This could be explained by the microstructure austenitising at the soak temperature. In those areas that have austenitised the ferrite grain size became dependant on the austenite grain size that is allowed to develop. This is likely to be larger based on the observation of grain coarsening seen in previous chapters so there will be a skew towards larger grains driven by that localised phenomenon. This can be seen in the distributions for the soak temperature 850°C tests in previous chapters too. In this case the effect probably predominates over nucleation effects. In the labs casted material, it’s a bit different as silicon and phosphorous are shown in the literature to influence the austenite behaviour.

9.5.3. Microstructural images

Figure 9.4. Microstructure of 3465 in its annealed condition when heating rate=20°C/s and soak temperature=635°C.

Figure 9.5. Microstructure of 3465 in its annealed condition when heating rate=200°C/s and soak temperature=635°C.

Figure 9.6. Microstructure of 3465 in its annealed condition when heating rate=1,000°C/s and soak temperature=635°C.

Figure 9.7. microstructure of 3465 in its annealed condition when heating rate=20°C/s and soak temperature=850°C.

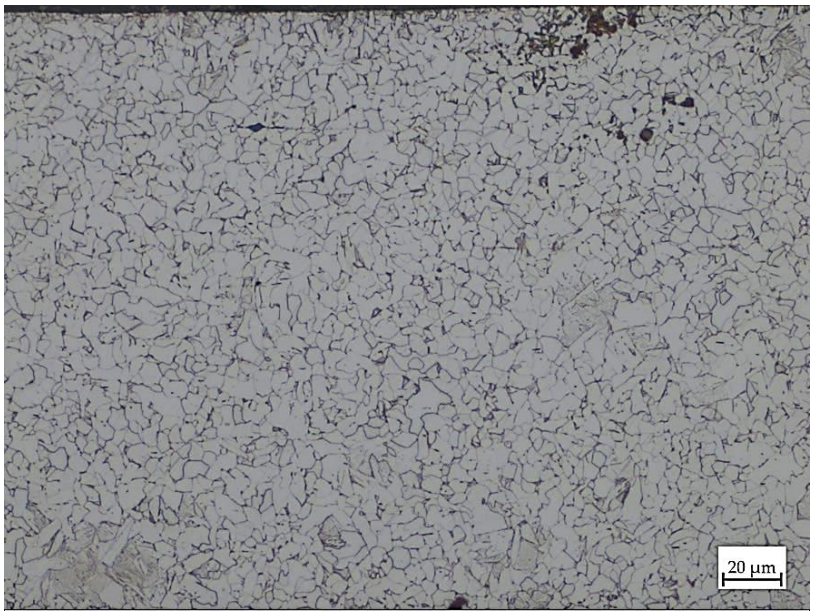

Figure 9.8. Microstructure of 3465 in its annealed condition when heating rate=200°C/s and soak temperature=850°C.

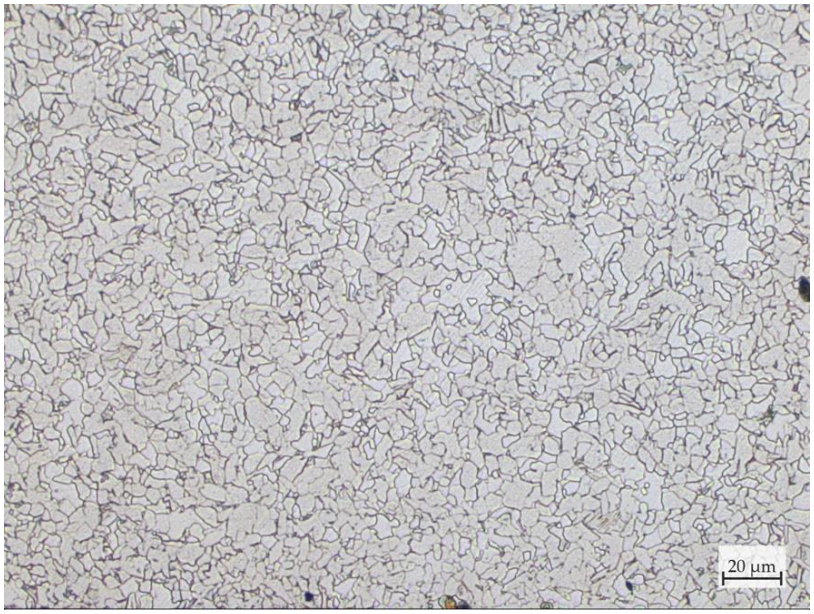

Figure 9.9. Microstructure of 3465 in its annealed condition when heating rate=1,000°C/s and soak temperature=850°C.

When comparing the microstructures of the cold rolled 3465 (Figure 3.1) to its as-annealed microstructures (Figure 9.4, Figure 9.5, Figure 9.6, Figure 9.7, Figure 9.8, and Figure 9.9), it is clear recrystallisation has occurred. The sub-critical 635°C microstructures exhibit ferrite grains (light areas) with a homogenous spread of carbides (dark). The inter-critical 850°C

microstructures also exhibit a microstructure predominantly ferrite, but also small amounts of secondary phase presumed to be Acicular ferrite (AF).

9.5.4. Hardness results

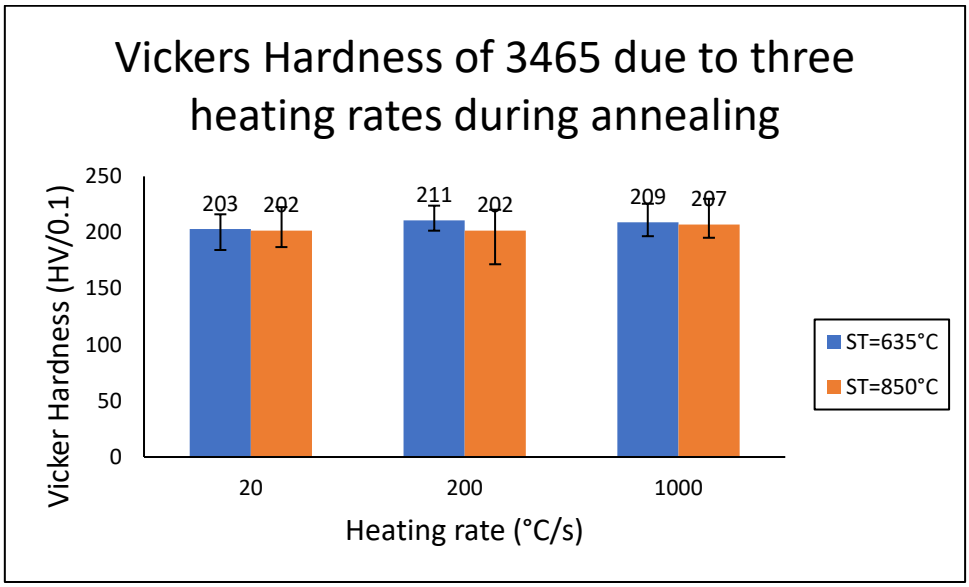

Figure 9.10. Effect of heating rates 20°C/s; 200°C/s; 1,000°C/s and soak temperatures 635°C and 850°C on vickers hardness.

For reference the HV/0.1 value of the material in its cold rolled condition is 309HV (±~20HV).

Figure 9.10 shows the effect of heating rate and soak temperature on the Vickers hardness of 3465 in its as-annealed condition. After annealing, the average hardness drops from its cold rolled average of 309HV to 202-211HV (a reduction of around 100HV) which is to be expected because the microstructures have shown recrystallization took place.

In general, the effect of heating rate and soak temperature is having insignificant influence on the Vickers hardness value. Given the small changes in average grain size due to heating rate and soak temperature, it is not surprising there is not significant difference in hardness value.

9.5.5. Summary of results

A heating rate of 200°C/s is to be selected for the next phase of this chapter because it produces a more refined ferrite grain size than the current industrial maximum capability value of 20°C/s. Although, the effect of heating rate on mechanical properties appears to contribute relatively little in terms of improving the mechanical properties of 3465 grade, it might have better results on more alloyed chemistries.

9.6. Conclusions

- The use of ultra-rapid heating rates, i.e., 200°C/s or 1,000°C/s did not lead to significant refinement of average ferrite grain size, either at sub-critical 635°C soak temperature, or an inter-critical 850°C soak temperature, for a commercial nitrogenised packaging grade steel. Although average ferrite grain size underwent slightly more refinement at sub-critical 635°C, it is practically insignificant. Therefore, it is not recommended that a heating rate above 200°C/s is used for the purposes of achieving further grain refinement in high-strength packaging steels for can-end applications. In addition, the feasibility of using a 1,000°C/s heating rate commercially may be unachievable and cost a lot in terms of running costs which will increase the cost of manufacturing of tinplate, a product that is required to be economical to produce.
- Use of ultra-rapid heating rates 200°C/s and 1,000°C/s resulted in the distribution of grain sizes to become less wide and increased the proportion of smaller grain sizes in the microstructure.
- Samples annealed at inter-critical 850°C soak temperature exhibited a larger variation in grain size compared to sub-critical 635°C soak temperature samples. IPF maps of sample 200-850 showed this larger variation is not attributed to the preferential growth of certain grain orientations because of the microstructure did not exhibit a preferred texture. This could explain why inter-critically annealed samples contained a larger range of grain sizes within the microstructure because of non-preferential grain growth.
- Vickers hardness value did not exhibit practically significant changes when ultra-rapid heating rates were used, possibly because the effect on average ferrite grain size

was minimal. This result was seen in both subcritical 635°C and inter-critical 850°C soak temperature samples. This implies that tensile properties such as yield, and tensile strength would also not be better when a heating rate above 200°C/s is used.

9.7. Phase 2 - Effect of annealing soak temperature and cooling rate

9.8. Purpose of study

This chapter aims to determine whether the strength properties of a commercial nitrogenised high-strength packaging grade steel for can-end applications can be increased via secondary phase generation (martensite) by utilising cooling rates that are higher than current CAPL capabilities (>300°C/s).

9.9. Experimental procedure

For information and details regarding the experimental procedures used in this chapter, please refer to Table which will direct you to the relevant sections within the Methods and Experimental Chapter (Chapter 3).

Table 9.4. Where to find information and details on the experimental procedures used in this chapter.

Procedure	Section number
Processing history	3.2
Composition	3.2
Transformation temperatures	3.3
Annealing heat treatments performed	3.4.7
Temper rolling and Ageing	3.7
Tensile testing parameters	3.8.1
Optical microscopy	3.11
Hardness testing	3.14
Grain Size Analysis	3.12

For details on the annealing heat treatment procedure carried out in this chapter, please see chapter 3.4.7. The material used in this chapter was cold rolled commercial packaging grade 3465 steel, with its chemical composition given in Table 3.2.

Furthermore, removing the slow cooling section enables martensite to be formed according to the TTT diagrams below.

9.10. Time Temperature Transformation (TTT) diagrams

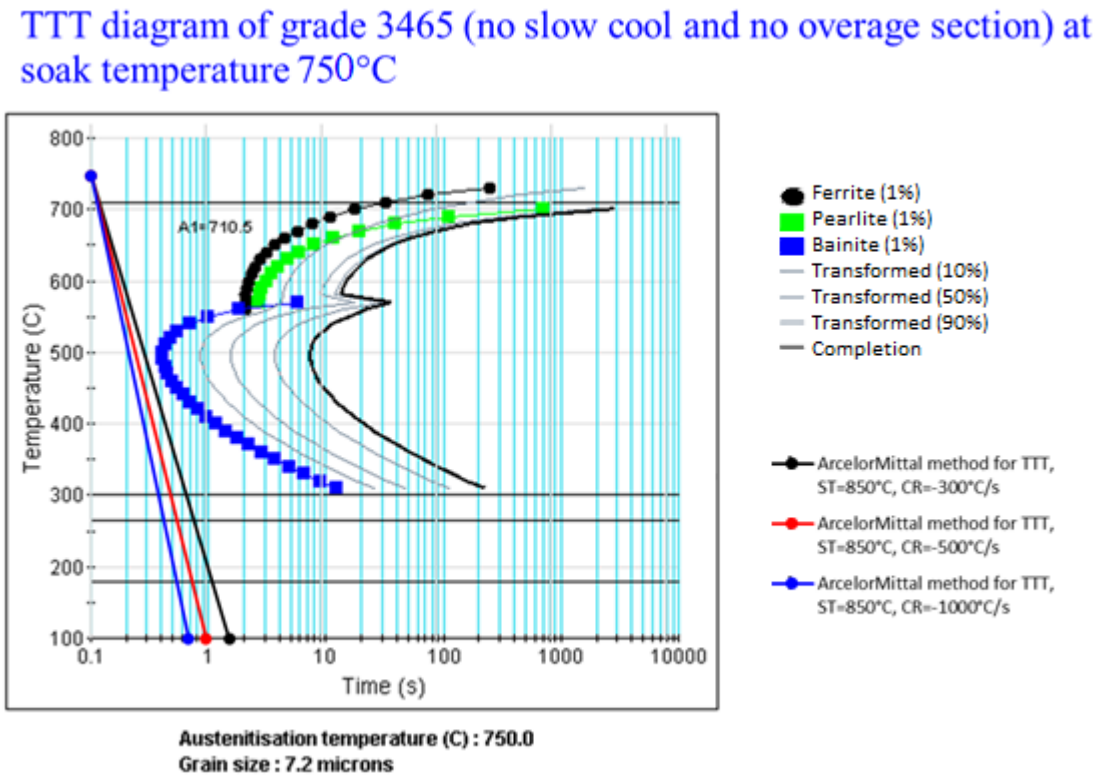

Figure 9.11. Composite image of a TTT diagram for commercial grade 3465, with rapid cooling from 750°C soak temperature to room temperatures curves superimposed where slow cooling and over ageing sections have been excluded from these heat treatments.

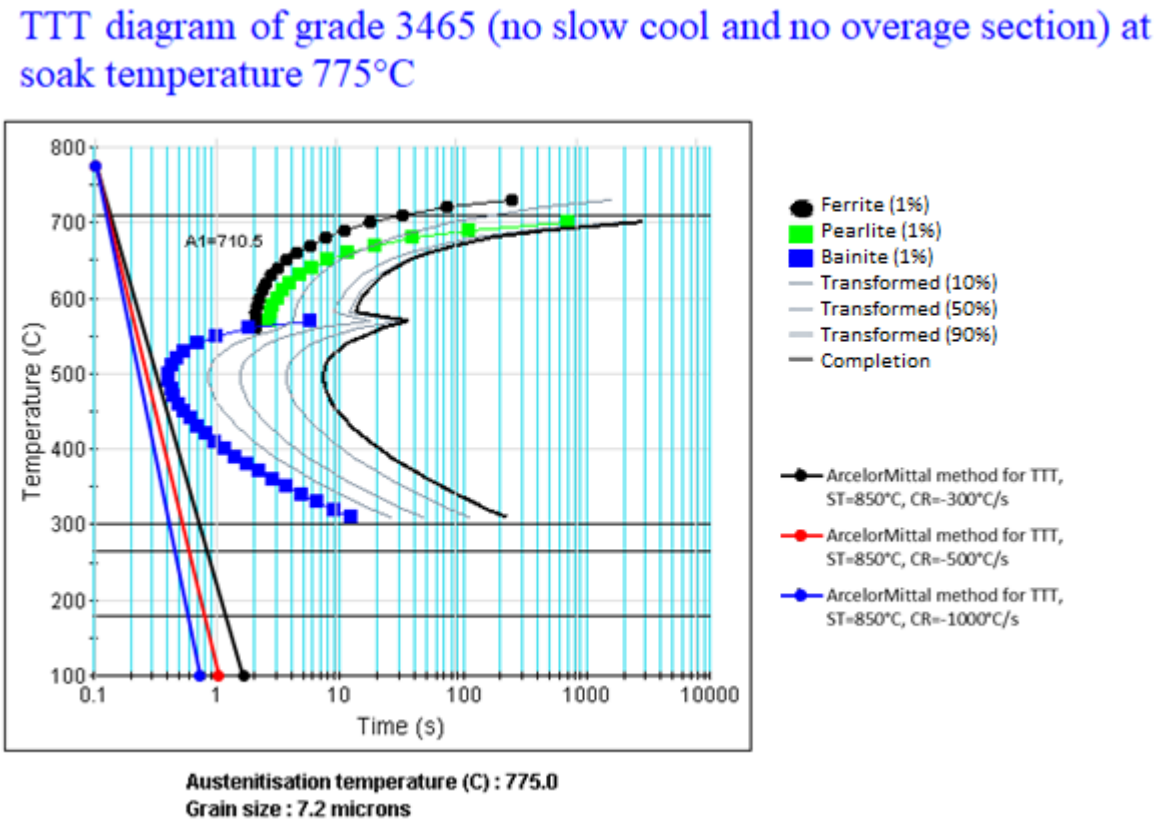

Figure 9.12. Composite image of a TTT diagram for commercial grade 3465, with rapid cooling from 775°C soak temperature to room temperatures curves superimposed where slow cooling and over ageing sections have been excluded from these heat treatments.

As Figure 9.11 and Figure 9.12 show, all cooling rates used in the intercritical annealed cycles should yield microstructures containing a martensite secondary phase upon cooling.

9.11. As-annealed tensile results

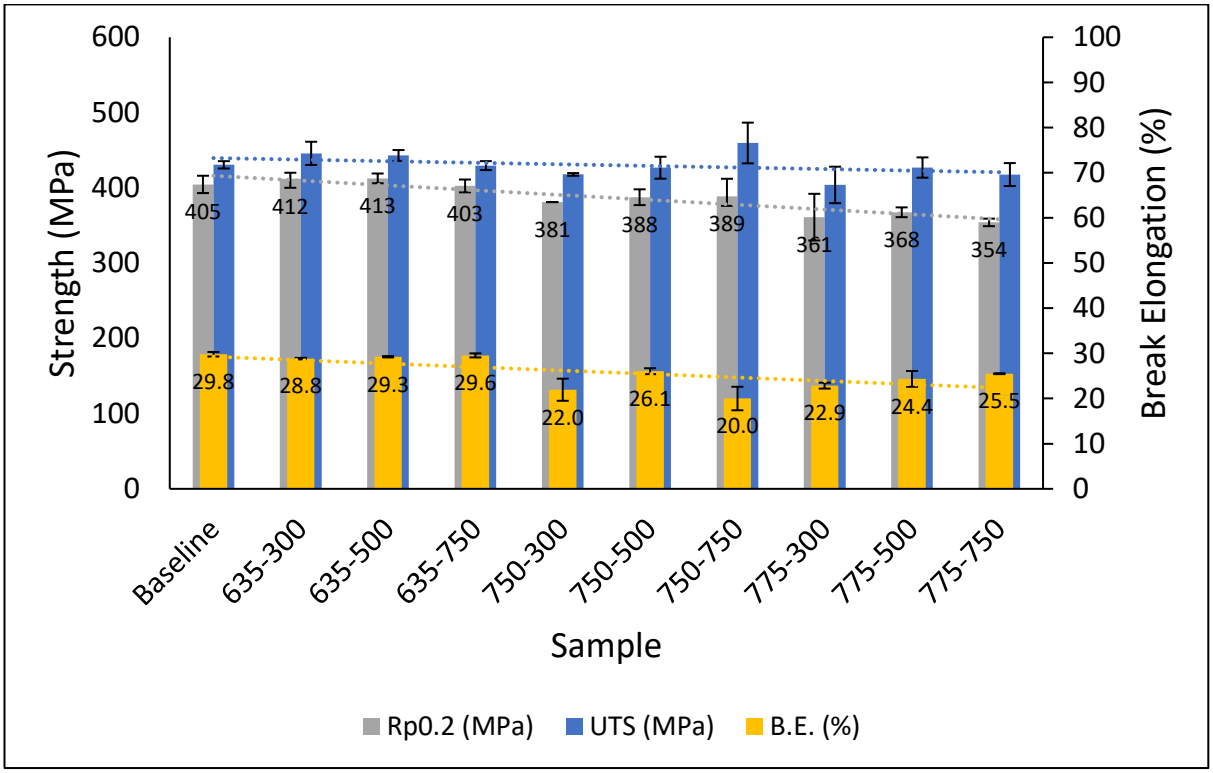

Figure 9.13. A graph showing the as-annealed properties of grade 3465 when annealed using soak temperature 635°C, 750°C, or 775°C, and cooled using cooling rate 300°C/s, 500°C, 750°C/s.

Figure 9.13 shows the mechanical properties yield strength, tensile strength, and break elongation values of samples in their as-annealed condition.

N.B. 'Reference' refers to when grade 3465 has been annealed using a heating rate, soak temperature, and cooling rate that the sponsor company can use, i.e., a heating rate of 20°C/s, a soak temperature of 635°C, and a cooling rate of 300°C/s. These levels for these parameters are also the maximum capabilities of the sponsor company's continuous annealing line.

First value in sample name refers to the soak temperature used, and the last number refers to the cooling rate used, for example sample 635-300 refers to a sample that was annealed at 635°C soak temperature and cooled using a 300°C/s cooling rate.

9.11.1. Effect of heating rate

The effect of increasing the heating rate from 20°C/s to 200°C/s and removing the slow cool and overageing sections has resulted in yield strength insignificantly increasing from an average of 405MPa to 412MPa (an increase of 7MPa), whilst break elongation remained unchanged (albeit a tiny reduction of 1%, from 30% to 29%).

9.11.2. Effect of increasing cooling rate after subcritical 635°C soak temperature

The effect of increasing the cooling rate from 300°C/s to 500°C/s after soaking at 635°C has resulted in insignificant changes to yield strength (and average increase of 1MPa) and break elongation. However, when the cooling rate was increased from 500°C/s to 750°C/s, the yield strength decreased from 413MPa to 403MPa (an average reduction of 10MPa), whilst break elongation remained unchanged. The average mechanical properties of samples of conditions soak=635°C and cooling rate=750°C/s gave very similar properties to the baseline sample.

9.11.3. Effect of increasing cooling rate after intercritical 750°C soak temperature

Overall, increasing the soak temperature from 635°C to 750°C has led to lower yield strengths and mostly lower tensile strengths. Furthermore, Break elongation values are also overall lower.

Whereas increasing the cooling rate at 635°C soak temperature causes yield and tensile strengths to on average decrease, the opposite effect is seen in 750°C soak temperature samples. For example, when cooling rate was increased from 300°C/s to 500°C/s, yield strength increased from 381MPa to 388MPa (an increase of 7MPa) whilst surprisingly break elongation increased from 22% to 24% (an increase of 4%). However, when cooling rate was increased from 500°C/s to 750°C/s the yield strength insignificantly changed (increased by an average of 1MPa) but tensile

strength increased from 427MPa to 460MPa (an increase of 33MPa). Furthermore, break elongation decreased from 26% to 20% (a reduction of 4%).

In summary, all samples annealed at soak temperature 750°C exhibited poorer mechanical properties (i.e., yield strength and tensile strength) compared to the baseline sample.

9.11.4. Effect of increasing cooling rate after intercritical 775°C soak temperature

Overall, samples annealed at soak temperature 775°C exhibited the poorest average mechanical properties compared to all other conditions, including the baseline sample.

9.12. 5% temper rolled tensile results

Figure 9.14 shows the 5% temper rolled properties of grade 3465 when annealed using three soak temperatures, i.e., sub-critical 650°C, intercritical 750°C or 775°C, and cooled using cooling rates 300°C/s, 500°C/s, or 750°C/s.

‘Baseline’ sample is the mechanical properties when commercial annealing conditions were used, i.e., heating rate=20°C/s, soak temperature = 635°C, and slow cool and overage section included.

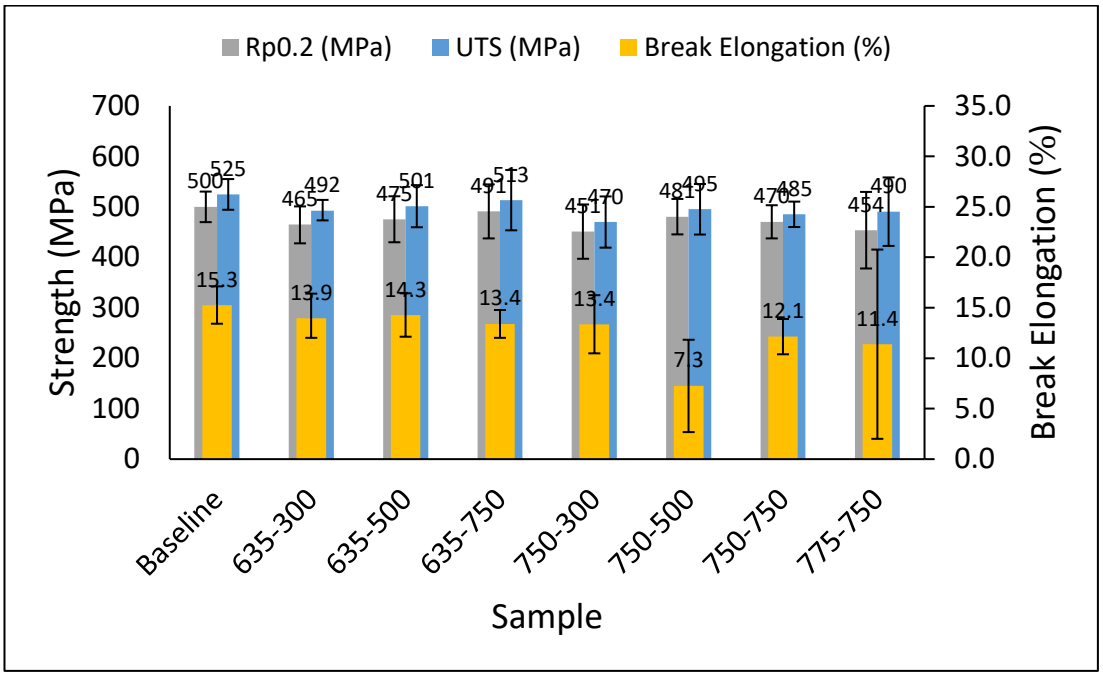

Figure 9.14. A graph showing the 5% temper rolled properties of grade 3465 when annealed using soak temperature 635°C, 750°C, or 775°C, and cooled using cooling rate 300°C/s, 500°C, 700°C/s.

9.12.1.Effect of cooling rate at soak temperature 635°C

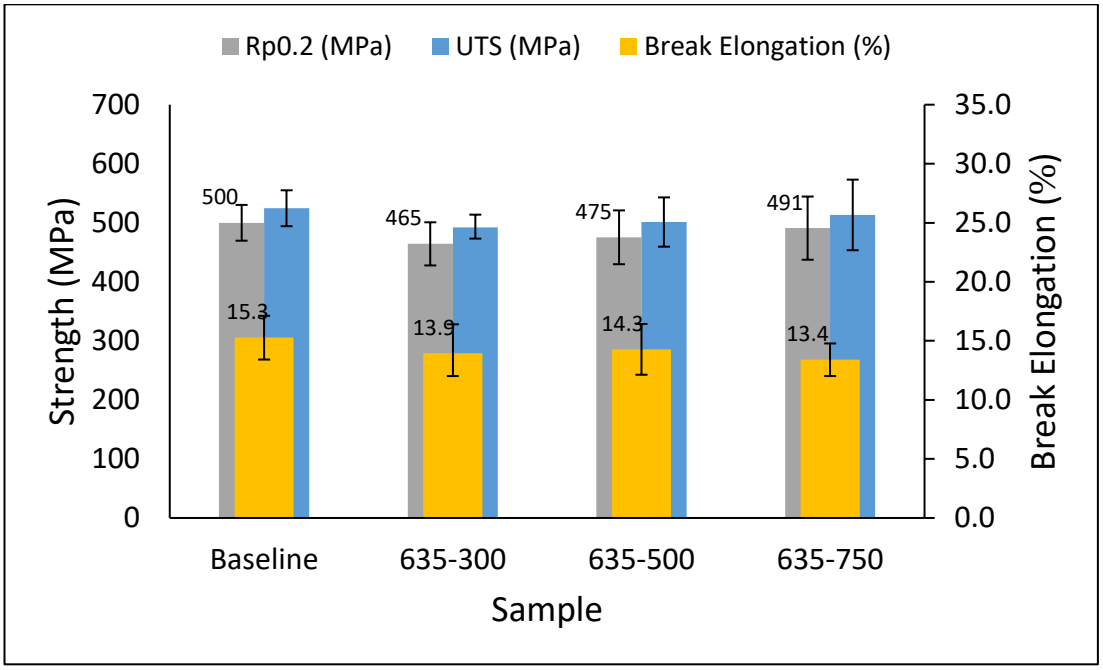

Figure 9.15. Effect of cooling rate on mechanical properties at soak temperature 635°C.

Figure 9.15 shows the effect of cooling rate at soak temperature 635°C. At soak temperature of 635°C, increasing the cooling rate also increased the Rp0.2 value.

Rp0.2 value increased by an average of 10MPa (from 465MPa to 475MPa) when cooling rate was increased from 300°C/s to 500°C/s, and increased by an average of 26MPa (from 465MPa to 491MPa) when cooling rate was increased from 300°C/s to 750°C/s. Like the Rp0.2 values, UTS also increased with cooling rate from 492MPa to 501MPa when cooling rate was increased from 300°C/s to 500°C/s, and from 492MPA to 513MPa when cooling rate was increased from 300°C/s to 750°C/s.

Whilst Rp0.2 and UTS increased with cooling rate, break elongation on average insignificantly changed, and remained the same, when cooling rate was increased from 300°C/s to 500°C/s, and to 750°C/s. However, the baseline annealing conditions gave superior mechanical properties where Rp0.2, UTS and break elongation were higher.

9.12.2.Effect of cooling rate at soak temperature 750°C

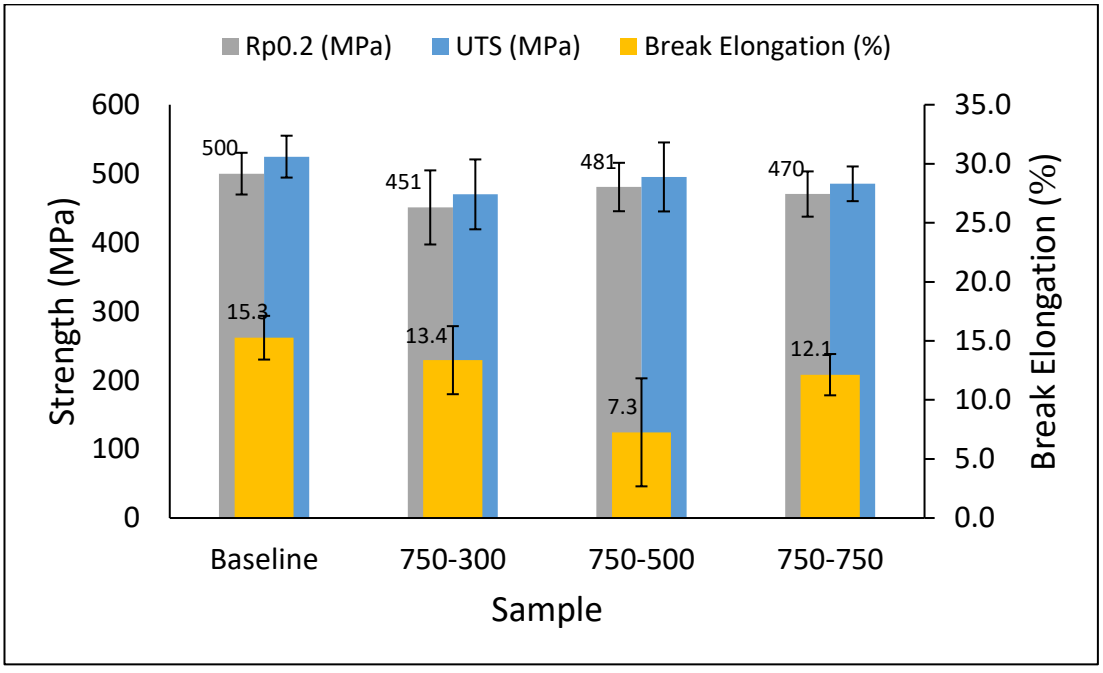

Figure 9.16. Effect of cooling rate at intercritical 750°C soak temperature.

Figure 9.16 shows the effect of cooling rate at intercritical soak temperature 750°C on the mechanical properties. Similarly, a trend of Rp0.2 (and UTS) value increasing when the cooling rate was increased was seen in samples annealed at soak temperature 750°C. For example, when cooling rate was increased from 300°C/s to

500°C/s, the average RP0.2 value increased by 30MPa (from 451MPa to 481MPa). When cooling rate was increased from 300°C/s to 750°C/s, average yield strength increased by 19MPa (from 451MPa to 470MPa). However, the highest Rp0.2 value, 481MPa, was seen in sample with cooling rate 500°C/s. This result was accompanied by the lowest break elongation value of ~7% for these soak temperature samples, a value that appears to be much lower than expected. Furthermore, when compared to the baseline, all samples had inferior values for all mechanical properties.

9.12.3.Effect of cooling rate at soak temperature 775°C

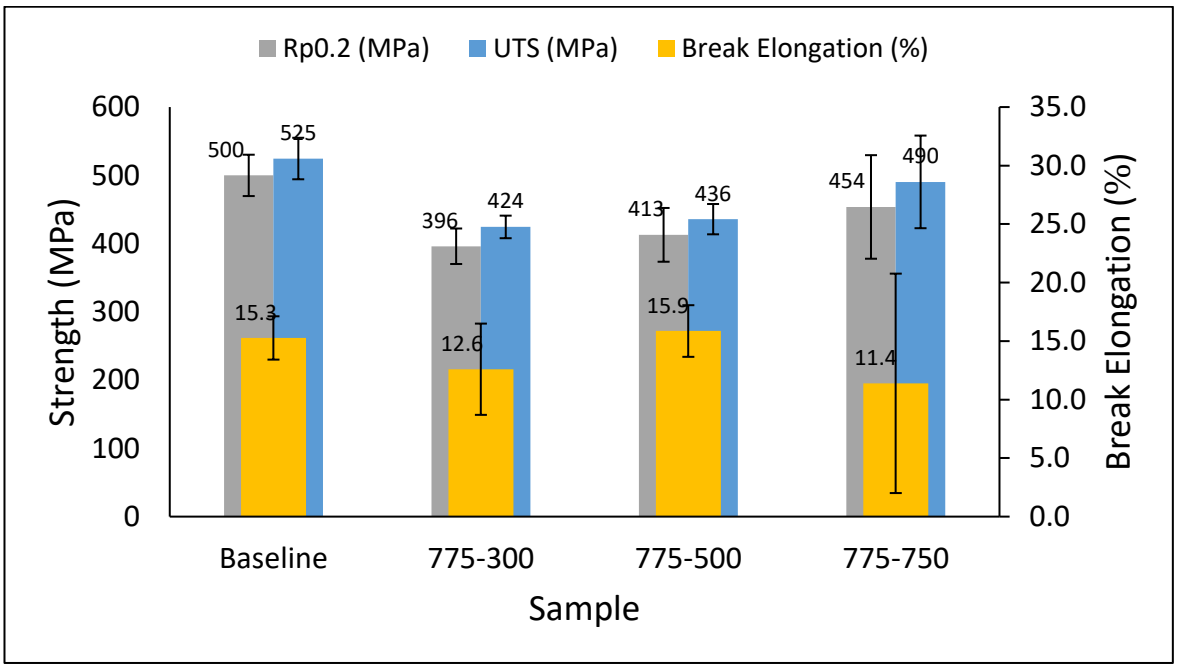

Figure 9.17. Effect of cooling rate at intercritical soak temperature 775°C.

As seen in Figure 9.17, the Rp0.2 and UTS values of samples annealed at soak temperature 775°C also exhibited a positive relationship with cooling rate. For example, Rp0.2 increased by 17MPa (from 396MPa to 413MPa) when cooling rate increased from 300°C/s to 500°C/s, and rose by 58MPa (from 396MPa to 490MPa) when cooling rate was increased from 300°C/s to 750°C/s. Interestingly, both Rp0.2 and break elongation value increased (by 17MPa and 3% respectively) when cooling

rate was increased from 300°C/s to 500°C/s. Simultaneous increases in both Rp0.2 and break elongation values are not seen in other samples.

Overall, increasing cooling rate generally increased the Rp0.2 and UTS values and mostly reduced the break elongation where the lowest average break elongation value is seen in sample cooled with a 750°C/s cooling rate. With cooling rate 750°C/s giving a better combination of Rp0.2 and break elongation values. However, all samples annealed at higher soak temperatures and/or higher cooling rates on average gave inferior mechanical properties when compared to the baseline sample (except for sample 775-500 which had a slightly higher 0.6% break elongation value, albeit an insignificant increase) .

9.12.4.Effect of increasing soak temperature

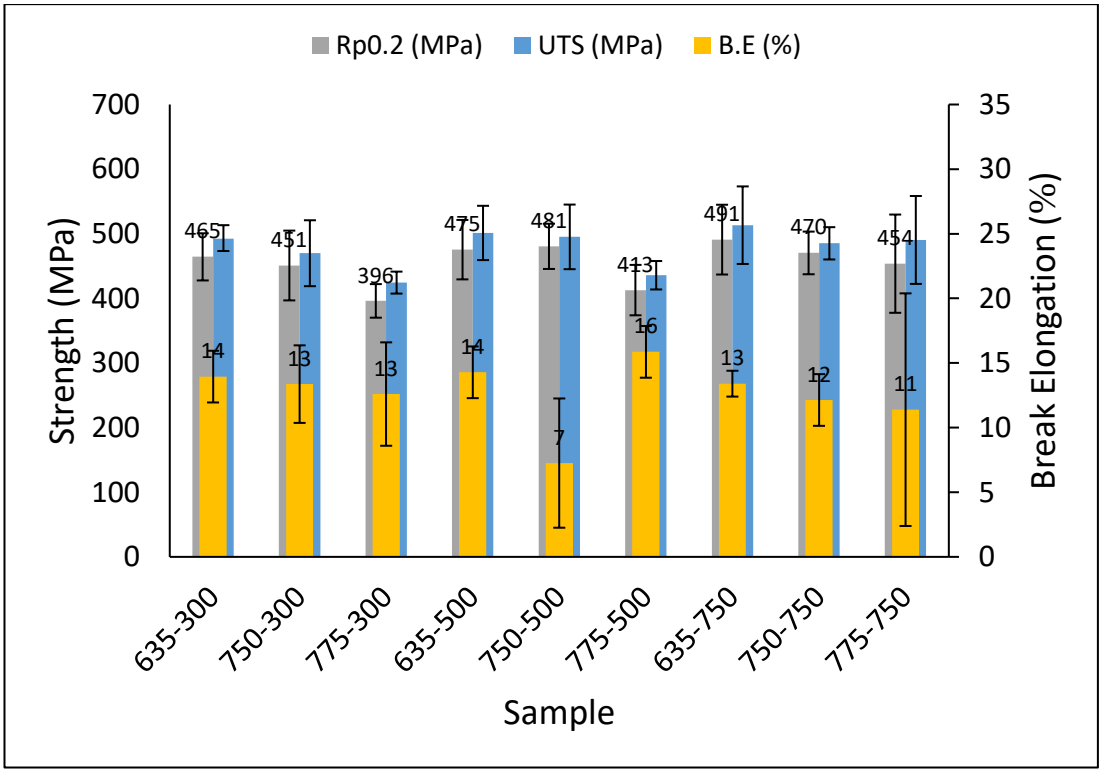

Figure 9.18. Effect of soak temperature on mechanical properties.

In general, for samples that were annealed using either a 300°C/s or 750°C/s cooling rate exhibited reductions in average Rp0.2 and UTS values, an insignificant reduction in break elongation, when the soak temperature was increased.

This trend is almost seen in samples cooled using a 500°C/s cooling rate, except for sample annealed at soak temperature 750°C, i.e., 750-500, which had almost the same level of Rp0.2 and UTS values as the lower soak temperature specimen 635-500. Additionally, sample 775-500 has the highest break elongation value of 16%. Overall, the lowest soak temperature of 635°C yields more favourable combination of Rp0.2 and break elongation values than the higher soak temperatures and cooling rates (see Figure 9.18).

9.12.5.Effect of 5% temper rolling

Table 9.5. Mechanical properties of grade 3465 in as annealed and 5% temper rolled conditions.

Condition										
As annealed				5% temper rolled						
Sample	***Rp0.2 (MPa)***	***UTS (MPa)***	***Break elongation (%)***	***Sample***	***Rp0.2 (MPa)***	***UTS (MPa)***	***Break elongation (%)***	***Δ Rp0.2***	***Δ UTS***	***Δ Break elongation***
Baseline	405	431	29.8	Baseline	500	525	15.3	+95	+94	-15
635-300	412	446	28.8	635-300	465	492	13.9	+53	+47	-15
635-500	413	443	29.3	635-500	475	501	14.3	+63	+58	-15
635-750	403	429	29.6	635-750	491	513	13.4	+88	+84	-16
750-300	381	418	22.0	750-300	451	470	13.4	+70	+52	-9
750-500	388	427	26.1	750-500	481	495	7.3	+93	+68	-19
750-750	389	460	20.0	750-750	470	485	12.1	+82	+26	-8
775-300	361	404	22.9	775-300	396	424	12.6	+35	+21	-10
775-500	368	427	24.4	775-500	413	436	15.9	+45	+9	-8
775-750	354	418	25.5	775-750	454	490	11.4	+100	+73	-14

9.13. Discussion

9.13.1. Microstructures

To help explain why increasing the cooling rate led to increases in Rp0.2 and UTS, and reductions in break elongation, it is sensible to first look at the microstructures for interesting features such as secondary phases. Below are optical images of the microstructures of samples from a range of soak temperatures and cooling rates. The rolling direction is in the left-right direction.

Figure 9.19. Optical microstructure of baseline sample.

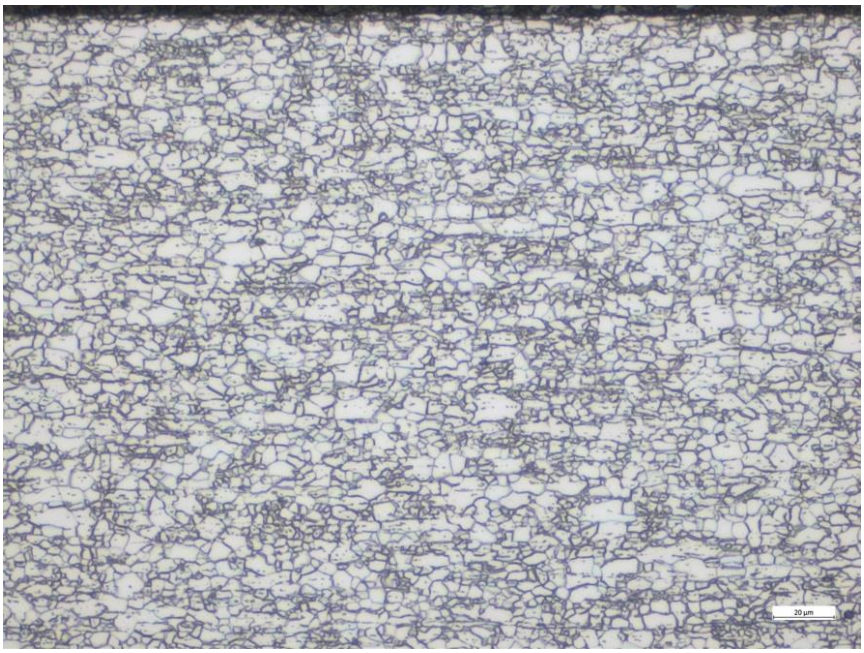

Figure 9.20. Optical microstructure image of sample 635-500.

Figure 9.21. Optical microstructure of sample 635-750.

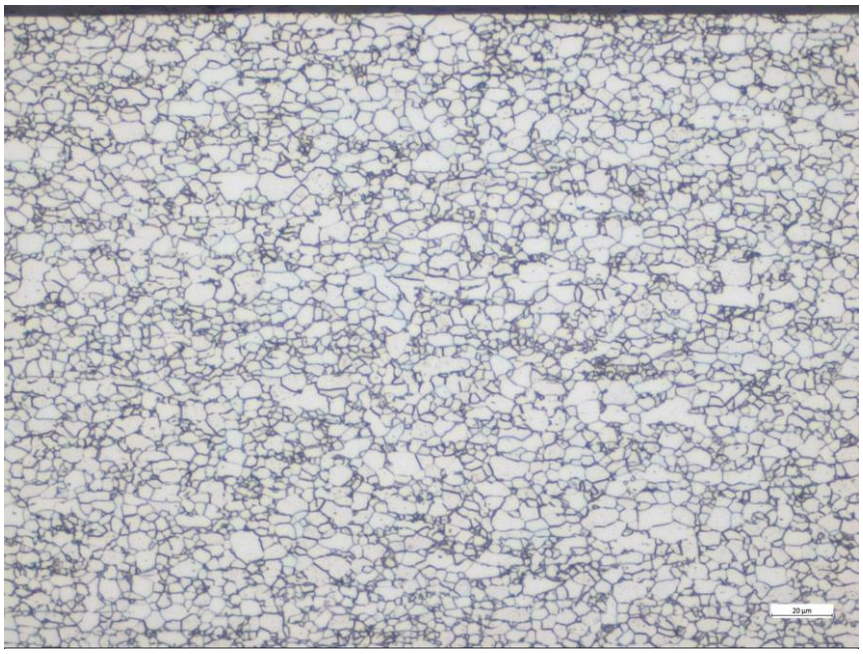

Figure 9.22. Optical microstructure of sample 750-500.

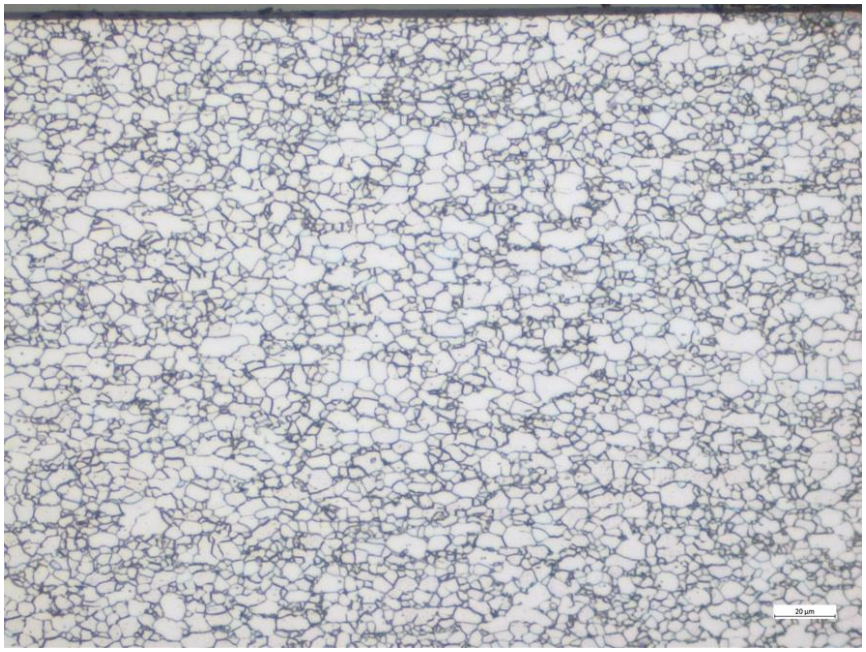

Figure 9.23. Optical microstructure of 750-750.

Figure 9.24. Optical microstructure of sample 775-500.

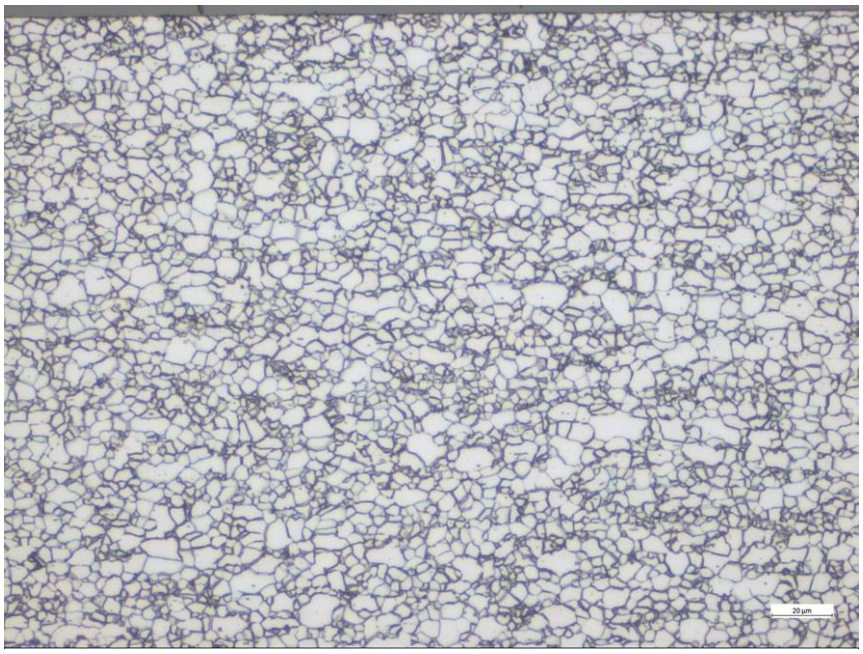

Figure 9.25. Optical microstructure of sample 775-750.

Firstly, the microstructures of sub-critically annealed (635°C soak temperature) samples show the presence of long trails of darker material throughout certain areas of the microstructure elongated along the rolling direction. These darker

trails could be carbides. Additionally, these features could also be poorly recrystallised grains. Rationale for this less recrystallised structure (remnants of the cold rolled microstructure) is that the 200°C/s heating rate increased the recrystallisation temperatures, and given 635°C is the lowest soak condition, these samples would be the most exposed to this effect.

These long dark features are not present in the microstructures of the intercritical annealed samples, giving them a lighter microstructure. It could be argued that the long dark trails are not carbides, but as mentioned previously, poorly recrystallised grains or residual dislocation strengthening from the cold rolling instead. Further rationale for this is that if carbides had the propensity to form, we would most likely see them in the intercritical soak temperature 750°C and 775°C samples. This is because the intercritical samples would have concentrated the carbon into the austenitised areas and thus we would see carbides within some grains, but none can be seen in the microstructures of intercritical samples (see Figure 9.22, Figure 9.23, Figure 9.24, and Figure 9.25). Perhaps then it is the presence of a greater amount of residual dislocations in the sub-critical 635°C annealed samples that is responsible for the greater strengths.

Secondly, all microstructures show a recrystallised microstructure of approximately similar ferrite grain size. Therefore, due to insignificant differences in size, it is unlikely that grain size strengthening is contributing much to the differences in mechanical properties seen in figures above. Moreover, grain size analysis was carried out to determine any statistical differences in grain sizes, which will be discussed later.

Thirdly, none of the microstructures show any visible presence of secondary phases such as bainite or martensite, when optically imaged at a magnification of 1,000x. Therefore, it can be presumed that the differences in tensile results cannot be accredited to the presence of secondary phases and their influences.

Therefore, the effect of grain size and/or number of interstitial atoms in solution could be responsible. Firstly, let’s consider grain size.

9.13.2.Grain sizes

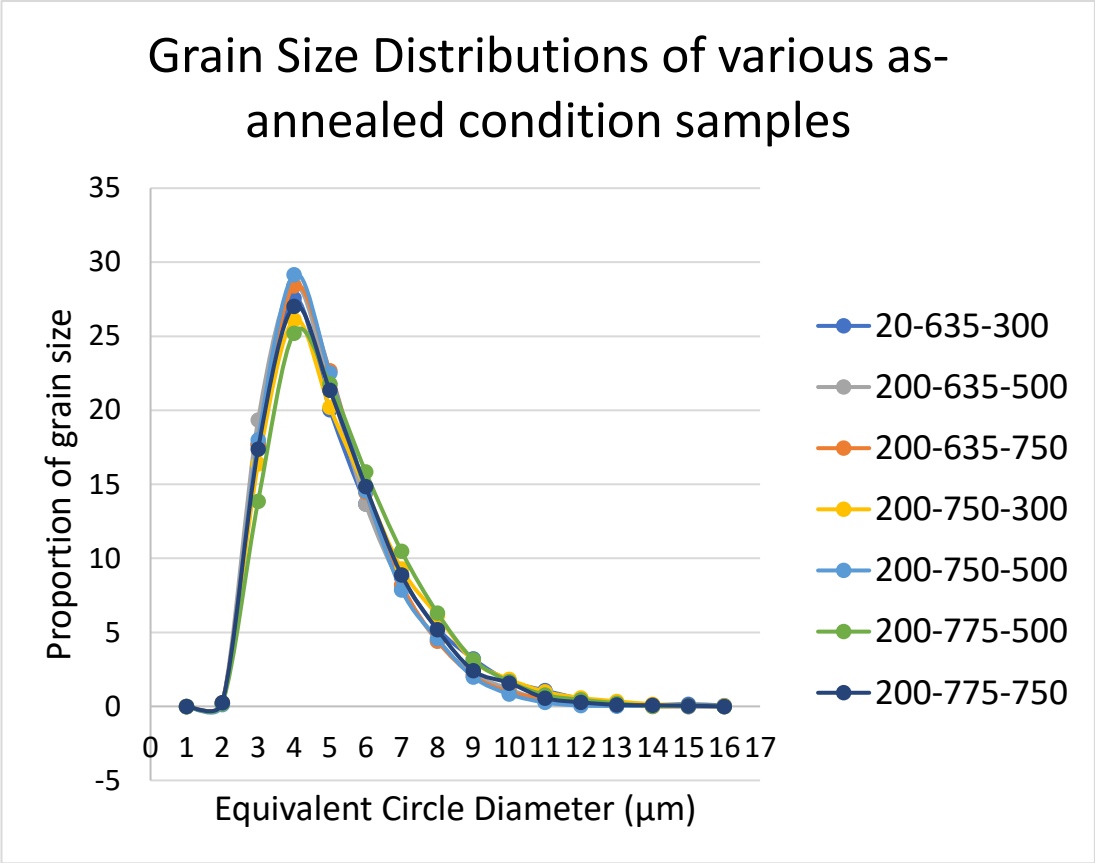

Figure 9.26. Grain size distributions for as-annealed samples

Table 9.6. Table showing statistical information regarding sample grain sizes.

Sample	Average	mode	Skew	S.D. P
20-635-300	4.2	2.5	1.5	2.0
200-635-500	4.0	2.1	1.2	1.7
200-635-750	4.0	2.2	1.2	1.6
200-750-300	4.3	2.1	1.4	2.0
200-750-500	3.9	2.1	1.1	1.6
200-775-500	4.3	2.2	1.1	1.8
200-775-750	4.1	2.1	1.2	1.8

Figure 9.26 shows the grain size distributions of a range of sample conditions in their as-annealed state. The distribution of grain sizes looks quite identical for all sample conditions shown, where all samples have a strong majority of grain size of 4µm. Because of the similarity in distribution, this implies that for this chemistry the grain

size distribution is not greatly influenced by soak temperatures ranging between 635-775°C, nor by cooling rates between 300-750°C/s.

Additionally, Table 9.6 shows extra statistical information regarding the grain sizes of samples such as mean and modal grain sizes. The average and modal grain size is very similar for all samples, which correlates with the similar distributions of samples shown in Figure 9.26. Therefore, based on the similarity in grain size distribution and statistical information shown in Figure 9.26 and Table 9.6, it can be presumed that the differences in mechanical properties of samples above are not the result of grain size influences.

9.13.3.Interstitial atoms

Because grain sizes characteristics are the same, and there's no presence of secondary phase, and all samples underwent the same level of 5% secondary reduction, we can presume that interstitial solution strengthening atoms are responsible, whereby different conditions are causing different effects. Looking at the stress vs strain curves below, we can see that each test gives varying yield point elongation characteristics.

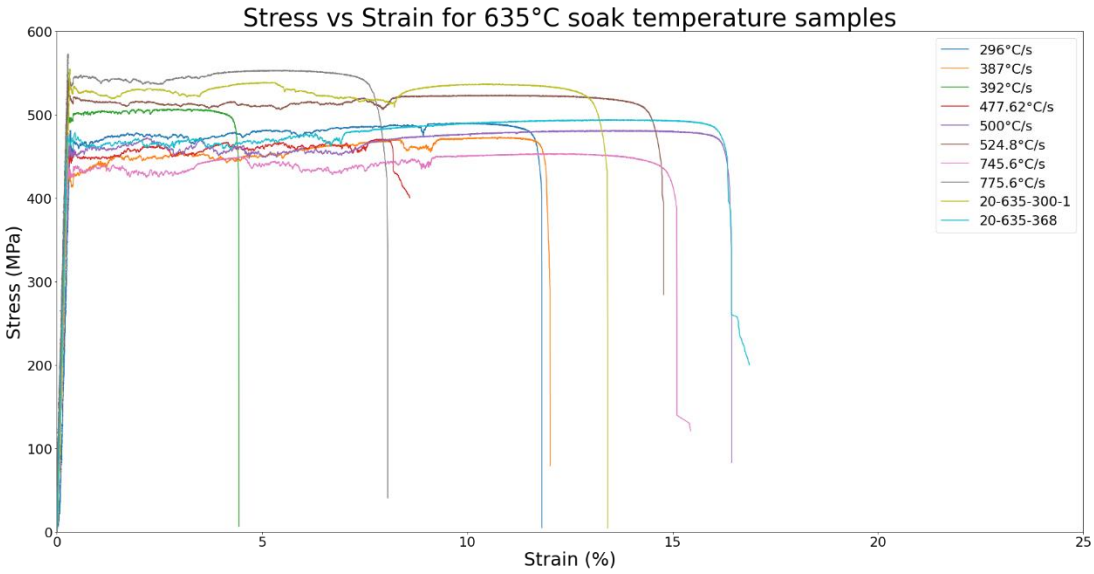

Figure 9.27. Stress vs strain curves for 635°C soak temperature samples.

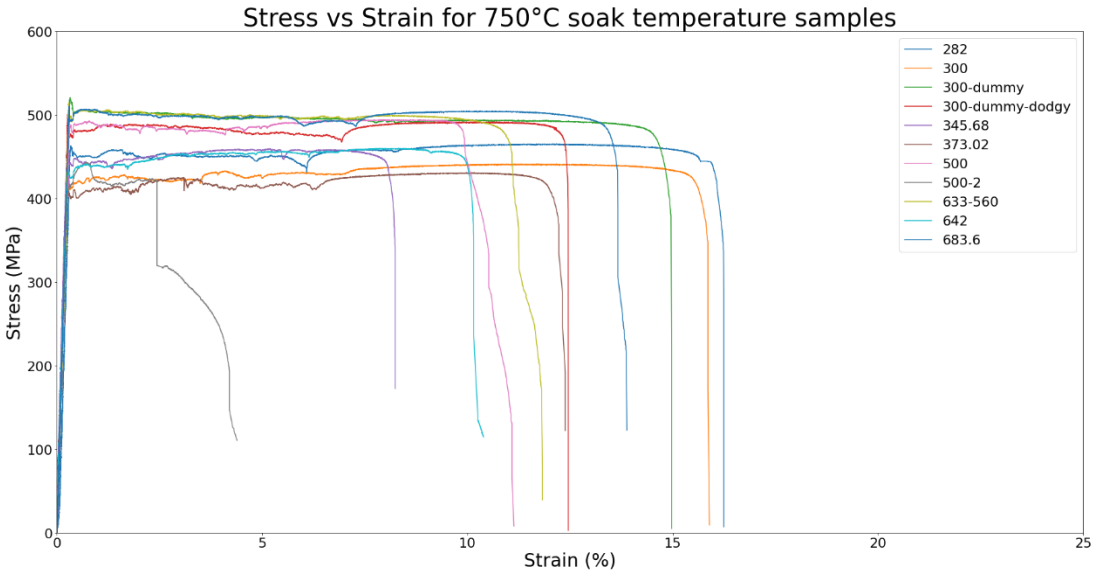

Figure 9.28. Stress vs strain curves for 750°C soak temperature samples.

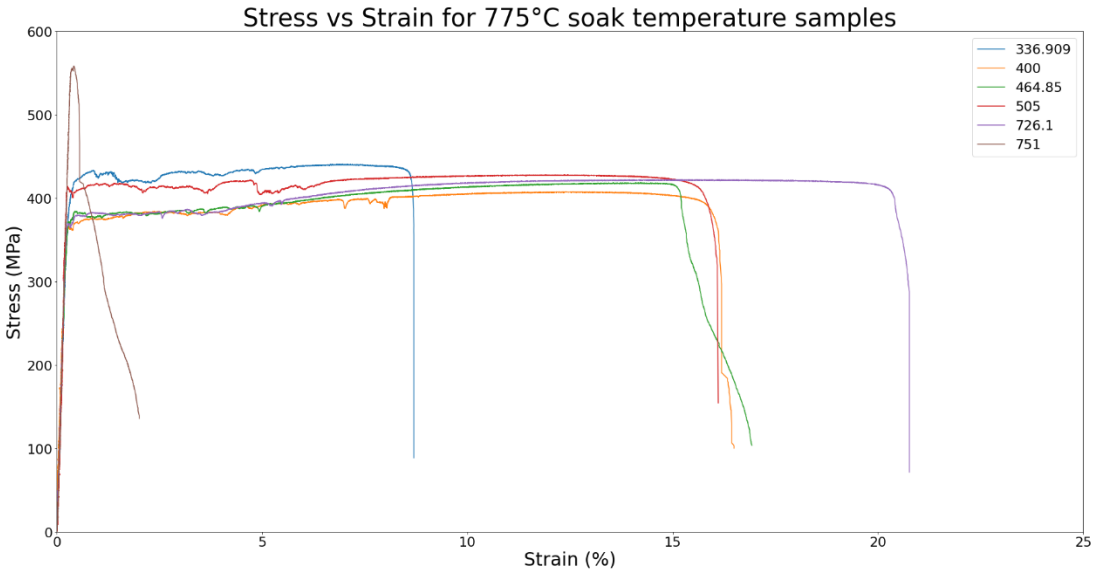

Figure 9.29. Stress vs strain curves for 775°C soak temperature samples.

9.13.4. Comparing the effect of soak temperature on the YPE characteristics

In general, when looking at the effect of soak temperature on the yield point elongation characteristics, we can see that when the soak temperature is increased from 635°C to 750°C, and then up 775°C, the YPE region relative to the overall width of the curve shrinks. See Figure 9.30 for the stress-strain curves for samples at different soak temperatures but cooled using 300°C/s cooling rate.

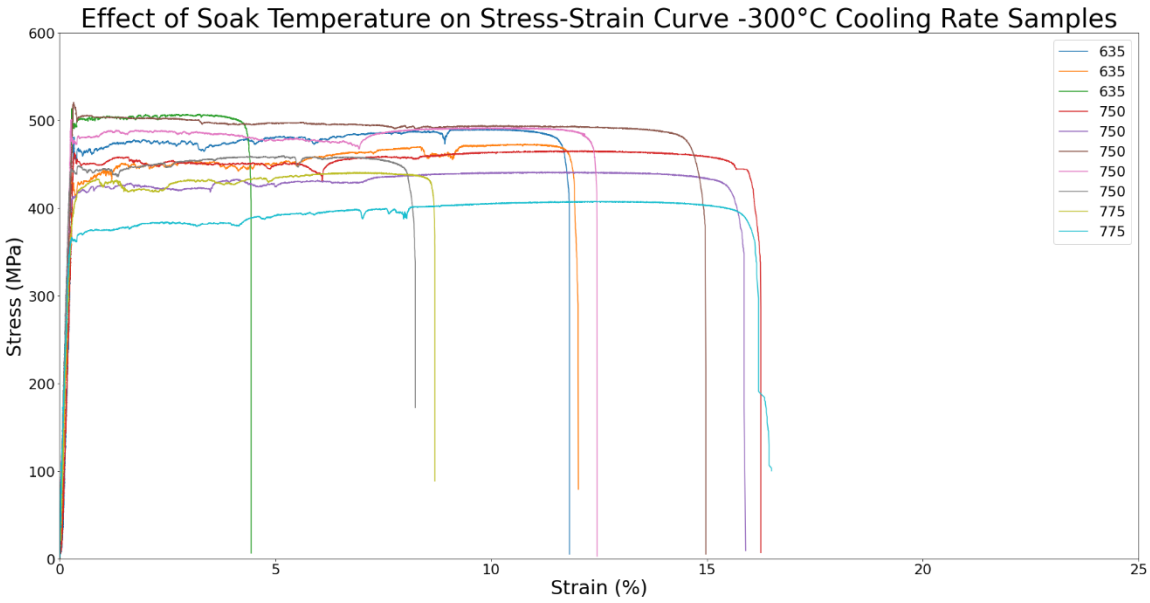

Figure 9.30. Effect of soak temperature on stress-strain curves for samples cooled at 300°C/s.

An explanation is intercritical treated samples contain a less homogenous distribution of carbon and nitrogen atoms. This is a result of the intercritical treated samples producing austenite phase during the soak stage, and because carbon and nitrogen have a greater solubility in austenite, there was a greater concentration of carbon and nitrogen atoms found in the austenite phase. Because the 300°C/s cooling rate is so fast, there is not enough time for carbon and nitrogen redistribution, resulting in less dislocation cores being trapped by carbon and nitrogen in all grains of intercritical treated samples. Locally, some grains that have reformed from austenite, will see a greater dislocation pinning effect but overall intercritical treated samples will experience less of a bulk effect, with the 775°C soak temperature samples experiencing even less.

9.14. Summary of results

Overall, when commercial nitrogenised packaging steel grade 3465 is subjected to simulated annealing cycle conditions that promote secondary phase martensite to form i.e., intercritical soak temperatures such as 750°C and 775°C, the result is poorer average mechanical properties (i.e., lower Rp0.2, UTS, and break elongation

values) compared to the current commercial cycle used for this grade. Therefore, it is not recommended that a combination of a 200°C/s heating rate, intercritical soak temperatures such as 750°C and 775°C, and cooling rates greater than 300°C/s, are used when annealing this grade of steel.

Secondary phase martensite did not form in this grade, which implies this grade is not able to generate any optically visible amounts of secondary phase martensite. Because secondary phase martensite did not form, and average mechanical properties were worse with increases in soak temperature, it is not recommended that this grade is intercritical annealed and thus modifications to the CAPL that permit intercritical temperatures are also not recommended.

9.15. Effect of aging temperature

It is not known what the effect of varying the aging temperature has on the mechanical properties in packaging steels.

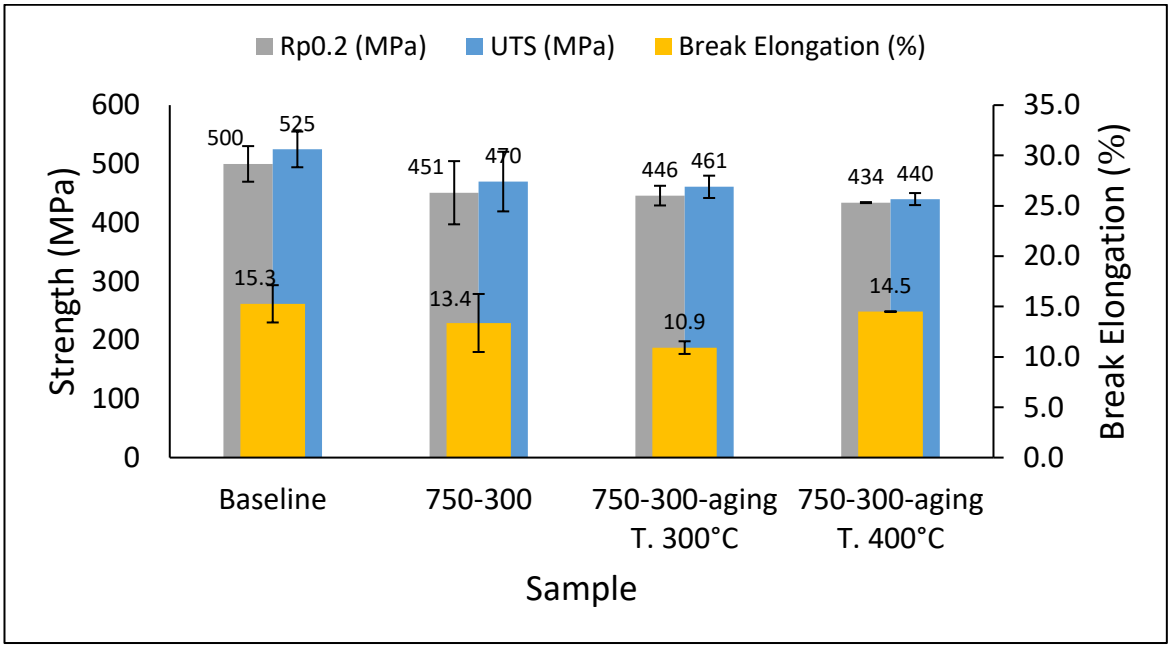

Figure 9.31. The effect of aging temperature on mechanical properties.

Figure 9.31 shows the effect of increasing the aging temperature used during the procedure outlined in the packaging standard EN10202, whereby samples must undergo an aging procedure of 200°C for 20 minutes prior to tensile testing. This experiment shows the effects on mechanical properties when the aging temperature was increased from the recommended 200°C, to 300°C and 400°C.

In general, increasing the aging temperature from 200°C to 300°C has resulted in insignificant reductions in average mechanical properties Rp0.2, UTS and break elongation values. For example, Rp0.2 reduced by 5MPa (from 451MPa to 446MPa), UTS reduced by 9MPa (from 470MPa to 461MPa), and break elongation reduced by 2.5% (from 13.4% to 10.9%). An explanation for these insignificant changes in results could be there were two competing mechanisms occurring. Because these samples were subjected to a 5% doubled-reduction procedure prior to aging, the dislocation strengthening would reduce strength because of mild recovery occurring at these low temperatures. However, the effect of interstitial strain aging would increase the strength (where carbon and nitrogen atoms migrated back to the dislocation cores). Therefore, it is possible that a balance of the two mechanisms occurred, which could explain the insignificant reductions.

Additionally, when aging temperature was increased further, from 200°C to 400°C, the strength values dropped even further. Rp0.2 value decreased by 17MPa (from 451MPa to 434MPa), UTS reduced by 30MPa (from 470MPa to 440MPa). Break elongation increased by 0.9% (from 13.4% to 14.5%).

9.16. Conclusions

- Increasing the soak temperature from a sub-critical 635°C to intercritical temperatures such as 750°C or 775°C resulted in a deterioration in all tensile properties. An explanation is the sub-critical 635°C treated samples contained a poorer recrystallised microstructure and thus a greater amount of retained dislocations which contributed to the higher strengths. This poor recrystallised grains and retained dislocations are possibly a result of the

rapid 200°C/s heating rate used, which increased the recrystallisation temperatures of this grade.

- The grain size distributions and statistical information of samples were not significantly affected by an intercritical soak temperature, and nor by increases in cooling rate.
- The effect of using higher aging temperatures was studied. It was found that increasing the proposed aging temperature from the recommended 200°C to 300°C, or 400°C, are detrimental and resulted in reductions to yield and tensile strengths.

9.17. Recommendations

It is recommended that the sponsor company should not use an aging temperature of 300°C or 400°C in the lacquering process, and the recommended packaging standard EN10202 value of 200°C should be continued to be used.

It is recommended that a body of work that investigates the effect of increasing the rapid cooling rate from its current commercial maximum setting be done. This is because yield and tensile strengths has been shown to increase in the magnitudes of 10-15MPa at sub-critical soak temperatures.

10. Final Conclusions and Recommendations

- The properties of the lab casted alloys are mainly dominated by chemistry effects such as solid solution strengthening, where the overall trend in some grades is broadly irrespective of the processing conditions applied. In some cases, processing condition can be used to positively enhance the strength properties especially the sub-critical soak temperatures through either retarded recrystallisation or some nucleation-based effects at the very highest heating rates.
- As seen in the tensile data for the lab cast chemistries, the use of nitrogen is most effective, and is a promising option in the solution to developing a new grade of high-strength packaging steel for can end applications. This is for several reasons.
    - Additional nitrogen has been shown to improve the strength values (yield and tensile) of steel, whilst accompanying losses in break elongation value have been relatively minimal.
    - Nitrogen is a relatively economic alloying element to add to packaging steel, compared to the likes of grain refining alloying elements such as niobium, titanium, and vanadium.
- Intercritical soak temperatures show no appreciable benefit, except in alloys of higher silicon and phosphorous concentrations. This could be linked to the reported effects of phosphorous and silicon on austenite stability, formation, and recrystallisation either in fully austenitic or intercritical states that are reported in the literature.
- Despite the higher carbon contents in some variants (particularly alloy 3) it appears that there is not a great deal of second phase to be produced. The TTT diagrams seem to suggest that very high cooling rates are required. However, when these cooling rates are imposed the structure does not seem to have appreciable transformation strengthening. This is unusual, but is suspected that the ferrite transformation kinetics are just too fast.
- It must be acknowledged that hot-rolled conditions are not explored here. Some elements in the lab cast chemistries could have an effect on the hot-rolling behaviour.

- Rapid heating rates are shown to decrease the average ferrite grain size. However, the influence on strength properties is mixed where certain grades increase in strength, or they decrease.

11. References

Cavendish Corporation Staff, M. (2003) *How it Works: Science and Technology, Volume 11*. Marshall Cavendish corporation.

The Can: Canmakers UK (1795) The Can │Canmakers UK. Available at: The Can | Canmakers UK (metalpackagingeurope.org). (Accessed: 17 March 2024).

Column: The delicious history of the tin can (2023) │Point/Plover Metro Wire.. Available at: Column: The delicious history of the tin can - Point/Plover Metro Wire (spmetrowire.com). (Accessed: 17 March 2024).

Abe, H. and Satoh, S. (1990) 'Abridged version Progress of Continuous Annealing Technology for Cold-Rolled Sheet Steels and Associated Product Development', 22(22).

Álvarez, P. *et al.* (2005) 'Grain Refinement by Rapid Transformation Annealing of Cold Rolled Low Carbon Steels', *Materials Science Forum*, 500–501, pp. 771–778. doi: 10.4028/www.scientific.net/MSF.500-501.771.

Azizi-Alizamini, H., Militzer, M. and Poole, W. J. (2011) 'Austenite Formation in Plain Low-Carbon Steels', *Metall and Mat Trans A*, 42, pp. 1544–1557. Available at: https://doi.org/10.1007/s11661-010-0551-5.

Callister, W. D. (1991) *Materials science and engineering: An introduction (2nd edition)*, *Materials & Design*. doi: 10.1016/0261-3069(91)90101-9.

Chbihi, A., Barbier, D. and Germain, L. (2014) 'Interactions between ferrite recrystallization and austenite formation in high-strength steels', *J Materi Sci*, 49, pp. 3608–3621. Available at: https://doi.org/10.1007/s10853-014-8029-2.

Chen, H. C., Era, H. and Shimizu, M. (1989) *Effect of Phosphorus on the Formation of Retained Austenite and Mechanical Properties in Si-Containing Low-Carbon Steel Sheet*.

Chowdhury, S. G., Pereloma, E. V. and Santos, D. B. (2008) 'Evolution of texture at the initial stages of continuous annealing of cold rolled dual-phase steel: Effect of heating rate', *Materials Science and Engineering A*. Elsevier BV, 480(1–2), pp. 540–

548. doi: 10.1016/j.msea.2007.07.060.

Drumond, J. *et al.* (2012) ‘Effect of Silicon Content on the Microstructure and Mechanical Properties of Dual-Phase Steels’, *Metallography, Microstructure, and Analysis*, 1(5), pp. 217–223. doi: 10.1007/s13632-012-0034-8.

Ferry, M., Muljono, D. and Dunne, D. P. (2001) ‘Recrystallization kinetics of low and ultra low carbon steels during high-rate annealing’, *ISIJ International*, 41(9), pp. 1053–1060. doi: 10.2355/isijinternational.41.1053.

Fox, A. G. and Mattes, V. R. (1990) ‘Microstructe and mechanical properties of HSLA 100 steel’.

Gorelik, S. S. (1981) ‘Recrystallization in Metals and Alloys’, *MIR Publishers*, p. 479.

Huang, J., Poole, W. J. and Militzer, M. (2004) *Austenite Formation during Intercritical Annealing*.

Hudd Hudd, R. C. and Llewellyn, D. T. (1998) *Steels: Metallurgy and Applications*.

Ivanisenko, Y. *et al.* (2003) ‘Annealing behaviour of nanostructured carbon steel produced by severe plastic deformation’, *Scripta Materialia*. Elsevier Ltd, 49(10 SPEC.), pp. 947–952. doi: 10.1016/S1359-6462(03)00478-0.

Karmakar, A., Ghosh, M. and Chakrabarti, D. (2013) ‘Cold-rolling and inter-critical annealing of low-carbon steel: Effect of initial microstructure and heating-rate’, *Materials Science and Engineering A*, 564, pp. 389–399. doi: 10.1016/j.msea.2012.11.109.

Khodabakhshi, F. and Kazeminezhad, M. (2011) ‘The annealing phenomena and thermal stability of severely deformed steel sheet’, *Materials Science and Engineering A*, 528(15), pp. 5212–5218. doi: 10.1016/j.msea.2011.03.024.

Lesch, C. *et al.* (2006) ‘Grain refinement of cold rolled microalloyed steels by rapid transformation annealing’, *EUR*, 22008, pp. 1–239.

Lesch, C. *et al.* (2007) ‘Rapid transformation annealing: A novel method for grain refinement of cold-rolled low-carbon steels’, in *Metallurgical and Materials*

Transactions A: Physical Metallurgy and Materials Science, pp. 1882–1890. doi: 10.1007/s11661-006-9052-y.

Lesch, C., Álvarez, P. and Bleck, W. (2007) 'Rapid Transformation Annealing: a Novel Method for Grain Refinement of Cold-Rolled Low-Carbon Steels.', *Metall and Mat Trans A*, 38, pp. 1882–1890. Available at: https://doi.org/10.1007/s11661-006-9052-y.

Li, P. *et al.* (2013) 'Effect of heating rate on ferrite recrystallization and austenite formation of cold-rolled dual phase steel', *Journal of Alloys and Compounds*, 578, pp. 320–327.

Madias, J., Moreno, A. and Genzano, C. (2015) 'Billet defects: pinhole and blowhole formation, prevention and evolution.'

Massardier, V. *et al.* (2010a) 'Identification of the parameters controlling the grain refinement of ultra-rapidly annealed low carbon Al-killed steels', *Materials Science and Engineering A*. doi: 10.1016/j.msea.2010.05.024.

Massardier, V. *et al.* (2010b) 'Identification of the parameters controlling the grain refinement of ultra-rapidly annealed low carbon Al-killed steels', *Materials Science and Engineering A*, 527(21–22), pp. 5654–5663. doi: 10.1016/j.msea.2010.05.024.

Meng, Q., Li, J. and Zheng, H. (2014) 'High-efficiency fast-heating annealing of a cold-rolled dual-phase steel', *Materials & Design*. Elsevier, 58, pp. 194–197. doi: 10.1016/J.MATDES.2014.01.055.

Mohanty, R. R., Girina, O. A. and Fonstein, N. M. (2011) 'Effect of Heating Rate on the Austenite Formation in Low-Carbon High-Strength Steels Annealed in the Intercritical Region', *Metall and Mat Trans A*, 42(3680). Available at: https://doi.org/10.1007/s11661-011-0753-5.

Mostafaei, M. A. and Kazeminezhad, M. (2016) 'Microstructure and mechanical properties improvement by ultra-rapid annealing of severely deformed low-carbon steel', *Materials Science and Engineering A*, 655, pp. 229–236. doi: 10.1016/j.msea.2016.01.005.

Mostafaei, M.A. and Kazeminezhad, M. (2016) 'Microstructure and mechanical

properties improvement by ultra-rapid annealing of severely deformed low-carbon steel', *Materials Science and Engineering: A*. Elsevier, 655, pp. 229–236. doi: 10.1016/J.MSEA.2016.01.005.

Muljono, D., Ferry, M. and Dunne, D. P. (2001) *Influence of heating rate on anisothermal recrystallization in low and ultra-low carbon steels, Materials Science and Engineering A303*. Available at: www.elsevier.com/locate/msea.

Narasimha-rao, Bangaru, V. and Sachdev, A. K. (1982) 'No Title', *Metall and Mat Trans A*, 13A, pp. 1899–1906.

Nutting, J., Wondris, E. F. and Wente, E. F. (2019) *Steel*. Available at: https://www.britannica.com/technology/steel.

Park, K. T. and Shin, D. H. (2002) 'Annealing behavior of submicrometer grained ferrite in a low carbon steel fabricated by severe plastic deformation', *Materials Science and Engineering A*, 334(1–2), pp. 79–86. doi: 10.1016/S0921-5093(01)01796-8.

Peranio, N. *et al.* (2010) 'Microstructure and texture evolution in dual-phase steels: Competition between recovery, recrystallization, and phase transformation', *Materials Science and Engineering A*, 527(16–17), pp. 4161–4168. doi: 10.1016/j.msea.2010.03.028.

PICKERING, F. B. P. (1978) *Physical Metallurgy and the Design of Steels, Applied Sciences Publishers*.

Ren, J. and Liu, Z. (2019) 'Mechanical Properties and Strength Prediction of Ti Microalloyed Low Carbon Steel with Different Ti Content', *IOP Conference Series: Materials Science and Engineering*, 611(1). doi: 10.1088/1757-899X/611/1/012010.

Rigsbee, J. M. and Vander Arend, P. J. (1979) 'Formable HSLA and Dual-Phase Steels', pp. 56–86.

SHAH, V. *et al.* (2020) 'Effect of silicon, manganese and heating rate on the ferrite recrystallization kinetics', *ISIJ International*, 60(6), pp. 1312–1323. doi: 10.2355/isijinternational.ISIJINT-2019-475.

Shin, D. H. *et al.* (2000) 'Microstructural changes in equal channel angular pressed

low carbon steel by static annealing', *Acta Materialia*, 48(12), pp. 3245–3252. doi: 10.1016/S1359-6454(00)00090-2.

Somani, M. C. *et al.* (2019) 'Static recrystallization characteristics and kinetics of high-silicon steels for direct quenching and partitioning', *International Journal of Materials Research*, 110(3), pp. 183–193. doi: 10.3139/146.111744.

Stockemer, J., Vanden Brande, P. and Brande, P. V. (2003) 'Recrystallization of a cold-rolled low-carbon steel by cold-plasma-discharge rapid annealing', *Metall and Mat Trans A*, 34, p. 1341. Available at: https://doi.org/10.1007/s11661-003-0245-3.

Teixeira, A. A. (2009) 'Conventional thermal processing (canning)', *Food engineering*, III.

Ushioda, K. *et al.* (1989) 'No Title', *Mats. Sci and Tech*, 2(807).

Wang, J. *et al.* (2011) 'Rapid heating effects on grain-size, texture and magnetic properties of 3% Si non-oriented electrical steel', *Bulletin of Materials Science*, 34(7), pp. 1477–1482.

Wright, R. N. (2011) 'Relevant Aspects of Carbon and Low Alloy Steel Metallurgy', in *Wire Technology*. Elsevier, pp. 199–228. doi: 10.1016/b978-0-12-382092-1.00014-2.

Xu, D. *et al.* (2014a) 'Effect of heating rate on microstructure and mechanical properties of TRIP-aided multiphase steel', *Journal of Alloys and Compounds*. Elsevier, 614, pp. 94–101. doi: 10.1016/J.JALLCOM.2014.06.075.

Xu, D. *et al.* (2014b) 'Effect of heating rate on microstructure and mechanical properties of TRIP-aided multiphase steel', *Journal of Alloys and Compounds*. Elsevier Ltd, 614, pp. 94–101. doi: 10.1016/j.jallcom.2014.06.075.

Zheng, C. and Raabe, D. (2013) 'Interaction between recrystallization and phase transformation during intercritical annealing in a cold-rolled dual-phase steel: A cellular automaton model', *Acta Materialia*. Elsevier Ltd, 61(14), pp. 5504–5517. doi: 10.1016/j.actamat.2013.05.040.

Abe, H. and Satoh, S. (1990) ‘Abridged version Progress of Continuous Annealing Technology for Cold-Rolled Sheet Steels and Associated Product Development’, 22(22).

Álvarez, P. *et al.* (2005) ‘Grain Refinement by Rapid Transformation Annealing of Cold Rolled Low Carbon Steels’, *Materials Science Forum*, 500–501, pp. 771–778. doi: 10.4028/www.scientific.net/MSF.500-501.771.

Azizi-Alizamini, H., Militzer, M. and Poole, W. J. (2011) ‘Austenite Formation in Plain Low-Carbon Steels’, *Metall and Mat Trans A*, 42, pp. 1544–1557. Available at: https://doi.org/10.1007/s11661-010-0551-5.

Callister, W. D. (1991) *Materials science and engineering: An introduction (2nd edition)*, *Materials & Design*. doi: 10.1016/0261-3069(91)90101-9.

Chbihi, A., Barbier, D. and Germain, L. (2014) ‘Interactions between ferrite recrystallization and austenite formation in high-strength steels’, *J Materi Sci*, 49, pp. 3608–3621. Available at: https://doi.org/10.1007/s10853-014-8029-2.

Chen, H. C., Era, H. and Shimizu, M. (1989) *Effect of Phosphorus on the Formation of Retained Austenite and Mechanical Properties in Si-Containing Low-Carbon Steel Sheet*.

Chowdhury, S. G., Pereloma, E. V. and Santos, D. B. (2008) ‘Evolution of texture at the initial stages of continuous annealing of cold rolled dual-phase steel: Effect of heating rate’, *Materials Science and Engineering A*. Elsevier BV, 480(1–2), pp. 540–548. doi: 10.1016/j.msea.2007.07.060.

Drumond, J. *et al.* (2012) ‘Effect of Silicon Content on the Microstructure and Mechanical Properties of Dual-Phase Steels’, *Metallography, Microstructure, and Analysis*, 1(5), pp. 217–223. doi: 10.1007/s13632-012-0034-8.

Ferry, M., Muljono, D. and Dunne, D. P. (2001) ‘Recrystallization kinetics of low and ultra low carbon steels during high-rate annealing’, *ISIJ International*, 41(9), pp. 1053–1060. doi: 10.2355/isijinternational.41.1053.

Fox, A. G. and Mattes, V. R. (1990) ‘Microstructe and mechanical properties of HSLA 100 steel’.

Gorelik, S. S. (1981) ‘Recrystallization in Metals and Alloys’, *MIR Publishers*, p. 479.

Huang, J., Poole, W. J. and Militzer, M. (2004) *Austenite Formation during Intercritical Annealing*.

Hudd Hudd, R. C. and Llewellyn, D. T. (1998) *Steels: Metallurgy and Applications*.

Ivanisenko, Y. *et al.* (2003) ‘Annealing behaviour of nanostructured carbon steel produced by severe plastic deformation’, *Scripta Materialia*. Elsevier Ltd, 49(10 SPEC.), pp. 947–952. doi: 10.1016/S1359-6462(03)00478-0.

Karmakar, A., Ghosh, M. and Chakrabarti, D. (2013) ‘Cold-rolling and inter-critical annealing of low-carbon steel: Effect of initial microstructure and heating-rate’, *Materials Science and Engineering A*, 564, pp. 389–399. doi: 10.1016/j.msea.2012.11.109.

Khodabakhshi, F. and Kazeminezhad, M. (2011) ‘The annealing phenomena and thermal stability of severely deformed steel sheet’, *Materials Science and Engineering A*, 528(15), pp. 5212–5218. doi: 10.1016/j.msea.2011.03.024.

Lesch, C. *et al.* (2006) ‘Grain refinement of cold rolled microalloyed steels by rapid transformation annealing’, *EUR*, 22008, pp. 1–239.

Lesch, C. *et al.* (2007) ‘Rapid transformation annealing: A novel method for grain refinement of cold-rolled low-carbon steels’, in *Metallurgical and Materials Transactions A: Physical Metallurgy and Materials Science*, pp. 1882–1890. doi: 10.1007/s11661-006-9052-y.

Lesch, C., Álvarez, P. and Bleck, W. (2007) ‘Rapid Transformation Annealing: a Novel Method for Grain Refinement of Cold-Rolled Low-Carbon Steels.’, *Metall and Mat Trans A*, 38, pp. 1882–1890. Available at: https://doi.org/10.1007/s11661-006-9052-y.

Li, P. *et al.* (2013) ‘Effect of heating rate on ferrite recrystallization and austenite formation of cold-rolled dual phase steel’, *Journal of Alloys and Compounds*, 578, pp. 320–327.

Madias, J., Moreno, A. and Genzano, C. (2015) ‘Billet defects: pinhole and blowhole

formation, prevention and evolution.'

Massardier, V. *et al.* (2010a) 'Identification of the parameters controlling the grain refinement of ultra-rapidly annealed low carbon Al-killed steels', *Materials Science and Engineering A*. doi: 10.1016/j.msea.2010.05.024.

Massardier, V. *et al.* (2010b) 'Identification of the parameters controlling the grain refinement of ultra-rapidly annealed low carbon Al-killed steels', *Materials Science and Engineering A*, 527(21–22), pp. 5654–5663. doi: 10.1016/j.msea.2010.05.024.

Meng, Q., Li, J. and Zheng, H. (2014) 'High-efficiency fast-heating annealing of a cold-rolled dual-phase steel', *Materials & Design*. Elsevier, 58, pp. 194–197. doi: 10.1016/J.MATDES.2014.01.055.

Mohanty, R. R., Girina, O. A. and Fonstein, N. M. (2011) 'Effect of Heating Rate on the Austenite Formation in Low-Carbon High-Strength Steels Annealed in the Intercritical Region', *Metall and Mat Trans A*, 42(3680). Available at: https://doi.org/10.1007/s11661-011-0753-5.

Mostafaei, M. A. and Kazeminezhad, M. (2016) 'Microstructure and mechanical properties improvement by ultra-rapid annealing of severely deformed low-carbon steel', *Materials Science and Engineering A*, 655, pp. 229–236. doi: 10.1016/j.msea.2016.01.005.

Mostafaei, M.A. and Kazeminezhad, M. (2016) 'Microstructure and mechanical properties improvement by ultra-rapid annealing of severely deformed low-carbon steel', *Materials Science and Engineering: A*. Elsevier, 655, pp. 229–236. doi: 10.1016/J.MSEA.2016.01.005.

Muljono, D., Ferry, M. and Dunne, D. P. (2001) *Influence of heating rate on anisothermal recrystallization in low and ultra-low carbon steels*, *Materials Science and Engineering A303*. Available at: www.elsevier.com/locate/msea.

Narasimha-rao, Bangaru, V. and Sachdev, A. K. (1982) 'No Title', *Metall and Mat Trans A*, 13A, pp. 1899–1906.

Nutting, J., Wondris, E. F. and Wente, E. F. (2019) *Steel*. Available at: https://www.britannica.com/technology/steel.

Park, K. T. and Shin, D. H. (2002) ‘Annealing behavior of submicrometer grained ferrite in a low carbon steel fabricated by severe plastic deformation’, *Materials Science and Engineering A*, 334(1–2), pp. 79–86. doi: 10.1016/S0921-5093(01)01796-8.

Peranio, N. *et al.* (2010) ‘Microstructure and texture evolution in dual-phase steels: Competition between recovery, recrystallization, and phase transformation’, *Materials Science and Engineering A*, 527(16–17), pp. 4161–4168. doi: 10.1016/j.msea.2010.03.028.

PICKERING, F. B. P. (1978) *Physical Metallurgy and the Design of Steels, Applied Sciences Publishers*.

Ren, J. and Liu, Z. (2019) ‘Mechanical Properties and Strength Prediction of Ti Microalloyed Low Carbon Steel with Different Ti Content’, *IOP Conference Series: Materials Science and Engineering*, 611(1). doi: 10.1088/1757-899X/611/1/012010.

Rigsbee, J. M. and Vander Arend, P. J. (1979) ‘Formable HSLA and Dual-Phase Steels’, pp. 56–86.

SHAH, V. *et al.* (2020) ‘Effect of silicon, manganese and heating rate on the ferrite recrystallization kinetics’, *ISIJ International*, 60(6), pp. 1312–1323. doi: 10.2355/isijinternational.ISIJINT-2019-475.

Shin, D. H. *et al.* (2000) ‘Microstructural changes in equal channel angular pressed low carbon steel by static annealing’, *Acta Materialia*, 48(12), pp. 3245–3252. doi: 10.1016/S1359-6454(00)00090-2.

Somani, M. C. *et al.* (2019) ‘Static recrystallization characteristics and kinetics of high-silicon steels for direct quenching and partitioning’, *International Journal of Materials Research*, 110(3), pp. 183–193. doi: 10.3139/146.111744.

Stockemer, J., Vanden Brande, P. and Brande, P. V. (2003) ‘Recrystallization of a cold-rolled low-carbon steel by cold-plasma-discharge rapid annealing’, *Metall and Mat Trans A*, 34, p. 1341. Available at: https://doi.org/10.1007/s11661-003-0245-3.

Teixeira, A. A. (2009) ‘Conventional thermal processing (canning)’, *Food engineering*, III.

Ushioda, K. *et al.* (1989) ‘No Title’, *Mats. Sci and Tech*, 2(807).

Wang, J. *et al.* (2011) ‘Rapid heating effects on grain-size, texture and magnetic properties of 3% Si non-oriented electrical steel’, *Bulletin of Materials Science*, 34(7), pp. 1477–1482.

Wright, R. N. (2011) ‘Relevant Aspects of Carbon and Low Alloy Steel Metallurgy’, in *Wire Technology*. Elsevier, pp. 199–228. doi: 10.1016/b978-0-12-382092-1.00014-2.

Xu, D. *et al.* (2014a) ‘Effect of heating rate on microstructure and mechanical properties of TRIP-aided multiphase steel’, *Journal of Alloys and Compounds*. Elsevier, 614, pp. 94–101. doi: 10.1016/J.JALLCOM.2014.06.075.

Xu, D. *et al.* (2014b) ‘Effect of heating rate on microstructure and mechanical properties of TRIP-aided multiphase steel’, *Journal of Alloys and Compounds*. Elsevier Ltd, 614, pp. 94–101. doi: 10.1016/j.jallcom.2014.06.075.

Zheng, C. and Raabe, D. (2013) ‘Interaction between recrystallization and phase transformation during intercritical annealing in a cold-rolled dual-phase steel: A cellular automaton model’, *Acta Materialia*. Elsevier Ltd, 61(14), pp. 5504–5517. doi: 10.1016/j.actamat.2013.05.040.

Quora. 2022. *What is the shear strength of mild steel?*. [online] Available at: <https://www.quora.com/What-is-the-shear-strength-of-mild-steel> [Accessed 22 September 2022].

Bibliography

(Hudd Hudd and Llewellyn, 1998)